National Library of Canada
Acquisitions and Bibliographic Services Branch
395 Wellington Street
Ottawa, Ontario
K1A 0N4

Bibliothèque nationale du Canada
Direction des acquisitions et des services bibliographiques
395, rue Wellington
Ottawa (Ontario)
K1A 0N4

Your file Votre référence

Our file Notre référence

NOTICE

The quality of this microform is heavily dependent upon the quality of the original thesis submitted for microfilming. Every effort has been made to ensure the highest quality of reproduction possible.

If pages are missing, contact the university which granted the degree.

Some pages may have indistinct print especially if the original pages were typed with a poor typewriter ribbon or if the university sent us an inferior photocopy.

Reproduction in full or in part of this microform is governed by the Canadian Copyright Act, R.S.C. 1970, c. C-30, and subsequent amendments.

AVIS

La qualité de cette microforme dépend grandement de la qualité de la thèse soumise au microfilmage. Nous avons tout fait pour assurer une qualité supérieure de reproduction.

S'il manque des pages, veuillez communiquer avec l'université qui a conféré le grade.

La qualité d'impression de certaines pages peut laisser à désirer, surtout si les pages originales ont été dactylographiées à l'aide d'un ruban usé ou si l'université nous a fait parvenir une photocopie de qualité inférieure.

La reproduction, même partielle, de cette microforme est soumise à la Loi canadienne sur le droit d'auteur, SRC 1970, c. C-30, et ses amendements subséquents.

Canada

UNIVERSITY OF ALBERTA

NOVEL SAMPLE INTRODUCTION TECHNIQUES
for
LASER IONIZATION
TIME-OF-FLIGHT MASS SPECTROMETRY

by

DAVINDER SINGH NAGRA ©

A thesis submitted to the Faculty of Graduate Studies and Research in partial fulfillment of the requirements for the degree of Doctor of Philosophy

IN

DEPARTMENT OF CHEMISTRY

EDMONTON, ALBERTA

FALL 1994

National Library
of Canada

Acquisitions and
Bibliographic Services Branch

395 Wellington Street
Ottawa, Ontario
K1A 0N4

Bibliothèque nationale
du Canada

Direction des acquisitions et
des services bibliographiques

395, rue Wellington
Ottawa (Ontario)
K1A 0N4

Your file Votre référence

Our file Notre référence

The author has granted an irrevocable non-exclusive licence allowing the National Library of Canada to reproduce, loan, distribute or sell copies of his/her thesis by any means and in any form or format, making this thesis available to interested persons.

L'auteur a accordé une licence irrévocable et non exclusive permettant à la Bibliothèque nationale du Canada de reproduire, prêter, distribuer ou vendre des copies de sa thèse de quelque manière et sous quelque forme que ce soit pour mettre des exemplaires de cette thèse à la disposition des personnes intéressées.

The author retains ownership of the copyright in his/her thesis. Neither the thesis nor substantial extracts from it may be printed or otherwise reproduced without his/her permission.

L'auteur conserve la propriété du droit d'auteur qui protège sa thèse. Ni la thèse ni des extraits substantiels de celle-ci ne doivent être imprimés ou autrement reproduits sans son autorisation.

ISBN 0-315-95238-5

Canada

UNIVERSITY OF ALBERTA
RELEASE FORM

NAME OF AUTHOR: DAVINDER SINGH NAGRA

TITLE OF THESIS: NOVEL SAMPLE INTRODUCTION TECHNIQUES FOR LASER IONIZATION TIME-OF-FLIGHT MASS SPECTROMETRY

DEGREE: DOCTOR OF PHILOSOPHY

YEAR THIS DEGREE GRANTED: 1994

Permission is hereby granted to the University of Alberta Library to reproduce single copies of this thesis and to lend or sell such copies for private, scholarly or scientific research purposes only.

The author reserves all other publication and other rights in association with the copyright in the thesis, and except as herein before provided neither the thesis nor any substantial portion thereof may be printed or otherwise reproduced in any material form whatever without the author's written permission.

Davinder Nagra

97 Edgeview Road N.W.,
Calgary, Alberta
Canada
T3A 4T8

August 29, 1994

UNIVERSITY OF ALBERTA

FACULTY OF GRADUATE STUDIES AND RESEARCH

The undersigned certify that they have read, and recommend to the Faculty of Graduate Studies and Research for acceptance, a thesis entitled NOVEL SAMPLE INTRODUCTION TECHNIQUES FOR LASER IONIZATION TIME-OF-FLIGHT MASS SPECTROMETRY submitted by DAVINDER SINGH NAGRA in partial fulfillment of the requirements for the degree DOCTOR OF PHILOSOPHY in CHEMISTRY.

Dr. Liang Li,
Associate Professor, Chemistry

Dr. Ron Kratochvil
Professor, Chemistry

Dr. Gary Horlick,
Professor, Chemistry

Dr. George Kotovych,
Professor, Chemistry

Dr. Charles Holmes
Assistant Professor, Biochemistry

Dr. James Reilly,
Professor, Chemistry

August 29, 1994

This work is dedicated to my parents and my sister. Without their full support and encouragement throughout the years, I would not have been able to come this far.

Abstract

Multiphoton ionization (MPI) mass spectrometry (MS) and supersonic jet spectroscopy (SJS) are powerful techniques for biochemical analysis. The combination of SJS/MPIMS provides high selectivity and high sensitivity for both molecular identification and structural analysis.

The first part of this thesis deals with SJS and MPIMS for the study of small molecules (MW < 1000). Chapter 2 demonstrates a method to enhance signal intensity without degradation in both the mass resolution and supersonic jet cooling by using a cylindrical lens instead of a spherical lens. Chapter 3 discusses MPIMS for the difficult isomer discrimination of substituted polycyclic aromatic hydrocarbons (PAH), anilines, and phenols.

Chapters 4-7 deal with alternative methods for introducing thermally liable and nonvolatile molecules into supersonic jets, as opposed to the more conventional laser desorption (LD). Chapter 4 describes fast atom bombardment (FAB) as a powerful means of desorption. Chapter 5 discusses pulsed rapid heating (PRH) for entraining nonvolatile molecules for SJS/MPIMS. Both FAB and PRH are simple and inexpensive methods, comparable in performance to LD.

In chapter 6 water and ammonia elimination from liable dipeptides is studied using PRH and LD. Chapter 7 deals with an application of PRH for obtaining gas phase UV-Visible absorption spectra. Finally, in order to have a better understanding of the mechanisms

involved in LD, chapter 8 describes the use of resonant two-photon ionization (R2PI) spectroscopy to examine the molecular cooling and supersonic jet formation in laser desorption.

In the second part of this thesis large molecules (MW > 1000) are studied with matrix-assisted laser desorption ionization (MALDI). In Chapter 9 we have coupled a continuous flow (CF) probe to MALDI for flow injection analysis of large peptides and proteins. In addition, a new data system was developed for transferring and storing mass spectra at high repetition rates, specifically for CF-MALDI. As a further extension to CF-MALDI, Chapter 10 describes the coupling of liquid chromatography (LC) with MALDI for the on-line separation and detection of peptides and proteins. And finally, chapter 11 discusses CF-MALDI with an improved parallel ion extraction geometry.

Acknowledgments

I would like to take this opportunity to express my deep appreciation to Professor Liang Li for his guidance, enthusiasm and encouragement. This work has been possible because of his enormous help with all my research projects. Dr. Li has always been available for questions and discussions about any aspect of my laser-based research. I strongly encourage anybody interested in analytical mass spectrometry to study under Dr. Liang Li.

I also wish to thank the members of my dissertation committee for their review of this thesis: Professor Ron Kratochvil, Professor Gary Horlick, Professor George Kotovych, Professor Charles Holmes, and Professor James Reilly (Indiana University).

I must also thank my fellow researchers during the initial 3 years: Jianyun Zhang (Robin), Alan Pui Ling Wang, and Xijian Guo (Steve). I deeply appreciate their knowledgeable and valuable assistance. I am also grateful to the other new members of my research group for the many helpful discussions we had during the last two years: Randy Whittal, Randy Purves, Dave Schriemer, Rafael Golding, and Yuqin Dai. It has been a privilege and a wonderful experience for me to have worked with all the above mentioned people. In particular, I like to thank Randy Whittal for helping me perform the parallel CF-MALDI experiments (chapter 11).

Much of this research work would not have been possible without the personnel in the machine shop and the electronics shop. Their expertise on building and modifying the pulsed rapid heating probe, continuous flow probe, as well as other skillful technical assistance is greatly appreciated.

In addition, I wish to acknowledge the following persons, departments, and agencies:

1. Department of Chemistry, University of Alberta for providing the facilities.
2. Natural Science and Engineering Research Council (NSERC) of Canada for a 2 year Post-Graduate Scholarship (PGS B) in 1992-4.
3. Canadian Society of Chemistry for the D.E. Ryan Award in 1992.
4. University of Alberta for the Walter H. Johns Scholarship for 2 consecutive years (1992-4).
5. American Society of Mass Spectrometry (ASMS) for the John B. Fenn travel stipend to attain the San Francisco Conference in June 1993.
6. University of Alberta Mary Louise Imrie Graduate Student Award, Faculty of Graduate Studies and Research, and the Vice-President of Research (Martha Piper) for a travel grant (ASMS Chicago Conference in June 1994).
7. The Alberta Environmental Research Trust fund.
8. Larry Coulson (chemistry) for developing a data system used for CF-MALDI.
9. Dr. Norman Dovichi for the loan of the Waters Quanta 4000 capillary electrophoresis system.

And finally, I wish to acknowledge the extreme name confusion the three Randys have created for me: RANDY Whittal (research group), RANDY Purves (research group), and RANDY Benson (machine shop). I lost track of how many times I said " Randy ? Which one ? "

TABLE OF CONTENTS

DEDICATION.....

ABSTRACT.....

ACKNOWLEDGMENTS.....

LIST OF TABLES.....

LIST OF FIGURES.....

LIST OF SCHEMES.....

LIST OF ABBREVIATIONS.....

CHAPTER

1. INTRODUCTION TO LASER IONIZATION MASS SPECTROMETRY..... 1

1.1 Introduction 1
1.2 Multiphoton Ionization 4
1.3 Supersonic Jet Expansion 9
1.4 Pulsed Laser Desorption / Vaporization 13
1.5 Supersonic Jet / TOF Mass Spectrometry 14
1.6 Electrospray Ionization and MALDI 17
1.7 Instrumentation 20

2. SIGNAL ENHANCEMENT BY USING A PLANAR LASER BEAM FOR MULTIPHOTON IONIZATION IN A SUPERSONIC JET / REFLECTRON TIME-OF-FLIGHT MASS SPECTROMETER 24

2.1 Introduction 24
2.2 Experimental 25
2.3 Results and Discussion 27
2.4 Conclusion 31

3. ON THE CAPABILITY OF MULTIPHOTON IONIZATION MASS SPECTROMETRY FOR ISOMER DISCRIMINATION: MASS SPECTRA OF POSITIONAL ISOMERS OF AROMATIC MOLECULES 33

3.1 Introduction 33
3.2 Experimental 34
3.3 Results and Discussion 35
3.4 Conclusion 57

4. PULSED FAST ATOM BOMBARDMENT SAMPLE DESORPTION WITH MULTIPHOTON IONIZATION IN A SUPERSONIC JET / REFLECTRON TIME-OF-FLIGHT SPECTROMETER 59

4.1 Introduction 59
4.2 Experimental 61
4.3 Results and Discussion 63
4.4 Conclusion 76

5. PULSED RAPID HEATING FOR VOLATILIZATION OF AMINO ACIDS AND SMALL PEPTIDES IN MULTI-PHOTON IONIZATION MASS SPECTROMETRY 77

Part I Pulsed Rapid Heating for Sample Vaporization 77
5.1 Introduction 77
5.2 Experimental 79
5.3 Results and Discussion 83
5.4 Conclusion 93

Part II Pulsed Rapid Heating for Studying Thermal Decomposition vs Vaporization 94
5.5 Introduction 94
5.6 Results and Discussion 94
5.7 Conclusion 106

6. MULTIPHOTON IONIZATION STUDY OF WATER AND AMMONIA ELIMINATION FROM DIPEPTIDES WITH PULSED RAPID HEATING AND LASER DESORPTION FOR SAMPLE VAPORIZATION 108

6.1 Introduction 108
6.2 Experimental 109
6.3 Results and Discussion 111
6.4 Conclusion 127

7. MEASUREMENT OF GAS-PHASE ULTRA-VIOLET VISIBLE ABSORPTION SPECTRA OF THERMALLY LABILE MOLECULES WITH A PULSED RAPID HEATING TECHNIQUE FOR SAMPLE VAPORIZATION 129

7.1 Introduction 129
7.2 Experimental 131
7.3 Results and Discussion 134
7.4 Conclusion 143

8. MOLECULAR COOLING AND SUPERSONIC JET FORMATION IN LASER DESORPTION 147

8.1 Introduction 147
8.2 Experimental 149
8.3 Results and Discussion 152
8.4 Conclusion 169

9. SUBPICOMOLE DETECTION OF LARGE PEPTIDES WITH CONTINUOUS-FLOW MATRIX-ASSISTED LASER DESORPTION IONIZATION MASS SPECTROMETRY 171

9.1 Introduction 171
9.2 Experimental 173
9.3 Results and Discussion 180
9.4 Conclusion 198

10 INTERFACING ON-LINE CONVENTIONAL OR PACKED CAPILLARY LIQUID CHROMATOGRAPHY WITH CONTINUOUS-FLOW MATRIX-ASSISTED LASER DESORPTION IONIZATION FOR THE ANALYSIS OF PROTEINS 200

10.1 Introduction 200
10.2 Experimental 202
10.3 Results and Discussion 210
10.4 Conclusion 220

11 OPTIMIZATION OF CF-MALDI WITH AN IMPROVED ION EXTRACTION GEOMETRY 221

11.1 Introduction 221
11.2 Experimental 222
11.3 Results and Discussion 226
11.4 Conclusion 233

12 SUMMARY 234

PUBLICATIONS 237

BIBLIOGRAPHY 239

List of Tables

Table

1.1 Typical matrices for matrix-assisted laser desorption ionization 19

3.1 MPI mass spectra of substituted anthracene and phenanthrene 36

3.2 MPI mass spectra of substituted anilines 38

3.3 MPI mass spectra of substituted phenols 39

4.1 Compounds studied by the Fast Atom Bombardment/ Supersonic Jet Multiphoton Ionization Technique 66

6.1 Summary of the major ions observed in the mass spectra of dipeptides studied by PRH/MPI 117

6.2 Summary of the major ions observed in the mass spectra of dipeptides studied by LD/MPI 118

6.3 Mass spectra of amino acid derivatives studied by PRH/MPI and LD/MPI 122

11.1 Mass accuracy observed for peptides with CF-MALDI 232

12.1 Publications 237

List of Figures

Figure

1.1 Energy level diagram in MPI transitions: (A) nonresonant MPI (B) resonant two-photon ionization (R2PI) and (C) two-photon resonant ionization 5

1.2 The difference between (A) electron impact (EI) ionization and (B) multiphoton ionization (MPI) 7

1.3 Schematic diagram of a supersonic jet expansion 10

1.4 Schematic diagram of translational cooling process 12

1.5 (A) Linear and (B) reflectron time-of-flight mass spectrometers 15

1.6 Schematic diagram of the supersonic jet /multiphoton ionization time-of-flight mass spectrometer setup (drawing is not to scale) 21

2.1 Optics and laser ionization in a reflectron TOFMS 26

2.2 The relative intensity of the aniline molecular ion peak vs the laser beam size 29

2.3 The relationship between mass resolution and laser beam size for a planar and a circular beam with a reflectron TOFMS 30

3.1 Mass spectra of 2-ethylphenol obtained by multiphoton ionization at 266 nm. The ionization laser power density was (A) $1x10^6$ W/cm^2 (B) $4x10^6$ W/cm^2 (C) $8x10^6$ W/cm^2 and (D) $1x10^7$ W/cm^2 42

3.2 Mass spectra of 2-ethylphenol obtained by electron impact ionization. The electron beam intensity is (A) 15 eV (B) 30 eV (C) 70 eV and (D) 200 eV 44

3.3 Soft and hard ionization MPI mass spectra of 1-aminoanthracene obtained by using a 266 nm laser beam for ionization with a laser power density of (A) $1x10^6$ W/cm^2 and (B) $1x10^7$ W/cm^2 48

3.4 Soft and hard ionization MPI mass spectra of 9-aminoanthracene obtained by using a 266-nm laser beam for ionization with a laser power density of (A) $1x10^6$ W/cm^2 and (B) $1x10^7$ W/cm^2 49

3.5 MPI mass spectra of (A) 2-isopropylphenol and (B) 4-isopropylphenol obtained by using a 266 nm laser beam for ionization with a laser power density of $1x10^7$ W/cm^2 51

3.6 EI mass spectra of (A) 2-isopropylphenol and (B) 4-isopropylphenol. The electron beam intensity is 70 eV 52

4.1 Mass spectra of tryptophan obtained by the fast atom bombardment/ supersonic jet multiphoton ionization technique at 266 nm. The ionization laser power density was (A) $1x10^6$ W/cm^2 (B) $4x10^6$ W/cm^2 and (C) $8x10^6$ W/cm^2 64

4.2 Mass spectrum of rubrene (MW 532) obtained by FAB/SJMPI at 266 nm. The laser ionization power density was ~ $1x10^6$ W/cm^2 67

4.3 Comparison of MPI mass spectra of Gly-Trp at 266 nm obtained by (A) using the fast atom bombardment method and (B) using the CO_2 laser desorption method for sample introduction into the supersonic jet expansion. The ionization laser power density was about $1x10^6$ W/cm^2 69

4.4 Mass spectra of (A) 4-acetamidophenol and (B) Tylenol obtained by using the FAB/SJMPI technique. The ionization laser beam was a 266 nm radiation with a power density ~ $1x10^6$ W/cm^2 72

4.5 MPI mass spectra of a mixture at 266 nm obtained by FAB/SJMPI: (A) tryptamine (MW 160) and indole-3-acetic acid (MW 175) (P ~ $4x10^6$ W/cm^2) (B) tryptamine and indole-3-acetic acid plus NaOH (P ~ $5x10^6$ W/cm^2) (C) tryptamine and indole-3-acetic acid plus NH_4OH (P ~ $4x10^6$ W/cm^2) 75

5.1 Schematic of the pulsed rapid heating probe and part of the experiment setup for multiphoton ionization mass spectrometry and supersonic jet spectroscopy 81

5.2 The signal output from the measurement of the contact time between the heating probe and the sample substrate 85

5.3 Soft and hard MPI mass spectra of tryptophan obtained by using the pulsed rapid heating method for sample vaporization with laser ionization at 266 nm. The ionization laser power densities were (A) $1x10^6$ W/cm^2 and (B) $1x10^7$ W/cm^2 86

5.4 Soft and hard MPI mass spectra of tryptophan obtained by using laser desorption with laser ionization at 266 nm. The ionization laser power densities were (A) $1x10^6$ W/cm^2 and (B) $1x10^7$ W/cm^2. The CO_2 laser power density was about $1x10^6$ W/cm^2 87

5.5 Soft ionization mass spectra of (A) tyrosine and (B) phenylalanine obtained by using the pulsed rapid heating method for sample vaporization with laser ionization at 266 nm. The ionization laser power density is about $1x10^6$ W/cm^2 89

5.6 Soft and hard MPI mass spectra of Ala-Tyr obtained by using the pulsed rapid heating method for sample vaporization with laser ionization at 266 nm..... 91

5.7 Soft and hard MPI mass spectra of Ala-Tyr obtained by using the pulsed CO_2 laser for sample desorption with laser ionization at 266 nm 92

5.8 Mass spectra from the direct heating of (A) tryptophan and (B) tyrosine..... 96

5.9 % Decomposition of tryptophan vs temperature of the heated probe tip at various constant contact times 99

5.10 % Decomposition of tyrosine vs temperature of the heated probe tip at various constant contact times 100

5.11 % Decomposition of tryptophan vs (A) contact time between the heated probe tip and the sample and (B) heating rate..... 102

5.12 % Decomposition of tyrosine vs (A) contact time between the heated probe tip and the sample and (B) heating rate 104

5.13 % Decomposition of tryptophan at various constant heating rates. Both the temperature and contact time are varied so as to maintain a constant heating rate 105

5.14 % Decomposition of tyrosine at various constant heating rates. Both the temperature and contact time are varied so as to maintain a constant heating rate 107

6.1 MPI mass spectra of Trp-Gly obtained at different laser desorption pulses at the same sample spot: (A) the averaged spectrum from the initial two laser pulses (B) the averaged spectrum from the third and forth pulses and (C) the averaged spectrum from the fifth and sixth pulses..... 112

6.2 LD/MPI mass spectrum of Trp-Gly obtained by averaging over 50 pulses at the same sample spot with the use of a thick sample..... 114

6.3 LD/MPI mass spectrum of Trp-Gly. No supersonic jet cooling is empolyed and a linear TOFMS is used..... 115

6.4 MPI mass spectra of Trp-Gly obtained by using the pulsed sample introduction method for sample vaporization..... 119

7.1 Schematic diagram of the atmospheric pulsed rapid heating / UV spectrometer experimental setup 132

7.2 Gas-phase UV spectra of (A) tyrosine (B) Dopa (C) norepinephrine and (D) tryptophan obtained by using the pulsed rapid heating method for sample volatilization in a diode array spectrophotometer 136

7.3 MPI mass spectra of (A) the pure solid sample of tryptophan (MW 204), (B) the sample collected from the condensed vapor after tryptophan is volatilized in the atmosphere by using the pulsed rapid heating method and (C) the sample collected from the condensed vapor after tryptophan is volatilized by using the slow heating method 138

7.4 UV spectra of 3-amino-4-hydroxybenzoic acid in (A) the gas phase obtained by the PRH method and (B) methanol solvent 141

7.5 UV spectra of (A) 3-amino-4-hydroxybenzoic acid in the gas phase obtained by the slow heating method (B) 2-aminophenol in the gas phase obtained by the PRH method and (C) 2-aminophenol in methanol solvent 142

7.6 MPI mass spectra of (A) the pure solid sample of 3-amino-4-hydroxy-benzoic acid (MW 153) and (B) the sample collected from the condensed vapor after 3-amino-4-hydroxybenzoic acid is volatilized in the atmosphere by using the PRH method 144

7.7 MPI mass spectra of (A) the pure solid sample of 2-aminophenol (MW 109) and (B) the sample collected from the condensed vapor after 3-amino-4-hydroxybenzoic acid is volatilized in the atmosphere by using the slow heating method 145

8.1 Schematic of the continuous flow probe and the ionization region of the reflectron time-of-flight mass spectrometer used for resonant two-photon ionization spectroscopic studies of the laser desorption process 150

8.2 R2PI spectra of benzimidazole obtained (A) from background molecules at room temperature and (B) from molecules generated by using LD with a 7.0 cm expansion distance 153

8.3 R2PI spectra of benzimidazole obtained from molecules generated by using LD with glycerol concentrations of (A) 0% (B) 10% (C) 20% and (D) 50%. The sample expansion distance is fixed at 6.5 cm 156

8.4 R2PI spectra of benzimidazole obtained from molecules generated by using LD with the sample expansion distances of (A) 4.0 cm (B) 5.0 cm and (C) 6.0 cm. The solution sample contains 5% glycerol 158

8.5 Sample pulse profiles of the benzimidazole neutrals generated from LD. The ionization signal is monitored as a function of the time delay between the desorption laser and the ionization laser. The ionization laser wavelengths used are (A) 277.57 nm, corresponding to the origin transition of benzimidazole and (B) 278.10 nm, corresponding to a hot band transition 161

8.6 R2PI spectra of benzimidazole with LD at different spatial positions of the sample profile shown in figure 8.5. The delay time between the desorption laser and the ionization laser is (A) 67 μs (B) 80 μs (C) 110 μs and (D) 130 μs 162

8.7 R2PI spectra of a benzimidazole and resorcinol mixture. The molecular ion peaks of benzimidazole and resorcinol are independently monitored by a gated integrator while the wavelengths are scanned 166

8.8 R2PI spectra of a benzimidazole and bradykinin mixture. The molecular ion peak of benzimidazole is monitored by a gated integrator while the wavelengths are scanned 167

9.1 Schematic of the initial flow probe used for continuous-flow matrix-assisted laser desorption ionization 175

9.2 Single-shot mass spectrum of lysozyme obtained by flow injection CF-MALDI. The total sample injection is 2 picomoles 181

9.3 Flow injection ion profiles of repeated injections of 2 picomoles of lysozyme 183

9.4 Flow injection ion profiles of repeated injections of different amounts of cytochrome c: (A) 3 picomoles and (B) 9 picomoles 185

9.5 Single-shot mass spectrum of cytochrome c obtained by flow injection CF-MALDI with a total injection of 3 picomoles of the sample 186

9.6 Single-shot mass spectrum of chicken egg albumin with an injection of 9 picomoles. The experimental conditions are similar to those of Figure 9.4 187

9.7 (A) Unsmoothed and (B) smoothed flow injection ion profiles obtained from an injection of 9 picomoles of chicken egg albumin 188

9.8 Peak areas in ion profiles as a function of the sample amount injected for cytochrome c. Error bars are ± 1 standard deviation from 5 repeat injections 191

9.9 (A) Linear and (B) reflectron time-of-flight mass spectra of bacitracin under CF-MALDI conditions. The molecular ion region is shown 194

9.10 (A) Mass spectrum (average of 5 shots) of a protein mixture obtained by MALDI in a static mode with the orthogonal ion extraction configuration. 1 μL solution containing 8 picomoles of lysozyme, 6.5 picomoles of ß-lactoglobulin, and 6 picomoles of trypsinogen is placed on the probe and mixed with 1 μL 3-NBA matrix. (B) mass spectrum (average of 5 shots) of a protein mixture obtained by CF-MALDI 196

10.1 Schematic of CF-MALDI with post-matrix addition (no LC column)..... 204

10.2 Schematic of conventional column (2.1-mm ID) LC/MALDI system..... 205

10.3 Details of 3-port mixing tee for CF-MALDI with post-matrix addition 206

10.4 Schematic of packed capillary LC/MALDI system..... 208

10.5 Schematic of packed capillary LC with UV (214 nm) detection..... 209

10.6 CF-MALDI flow injection analysis with post-matrix addition (no LC column) of (A) 4 repeat injections of cytochrome c (8 pmol each) and (B) 5 repeat injections of lysozyme (7 pmol each)..... 211

10.7 On-line gradient separation of cytochrome c and lysozyme with conventional LC (2.1-mm ID) and MALDI/TOFMS detection. Chromatograms represent 5 nmol injection each with 0.2% (10 pmol) split to MS (A) raw data and (B) data smoothing..... 212

10.8 Comparison of an on-line gradient LC separation of cytochrome c and lysozyme with (A) MALDI/TOFMS detection and (B) UV detection (242 nm)..... 214

10.9 On-line gradient separation of cytochrome c, lysozyme, and myoglobin with conventional LC (2.1-mm ID) and MALDI/TOFMS detection. Chromatograms represent 5 nmol injection each with 0.2% (10 pmol) split to MS (A) raw data and (B) data smoothing..... 215

10.10 On-line isocratic separation of cytochrome c (9 pmol) and lysozyme (8 pmol) with packed capillary LC and MALDI/TOFMS detection (A) raw data and (B) data smoothing 217

10.11 Isocratic separation of cytochrome c and lysozyme with a packed capillary LC and 214 nm detection..... 218

11.1 Schematic diagram of the new linear time-of-flight mass spectrometer with parallel ion extraction and an electrically insulated probe heater..... 223

11.2 Modified CF-MALDI probe tip and the acceleration plates of the time-of-flight mass spectrometer..... 224

11.3 Orthogonal and parallel ion extraction for time-of-flight mass spectrometry..... 227

11.4 Static MALDI mass spectra of bovine insulin ß-chain with 3-NBA. Sample desorbed both orthogonal and parallel to the flight tube 229

11.5 Mass spectra of bradykinin (9 pmol) with continuous-flow MALDI..... 230

List of Schemes

Scheme

3.1 Fragmentation of anilines and phenols 54

3.2 Proposed fragmentation process for 4-isopropylphenol after the absorption of two or more laser photons 55

5.1 The vaporization and decomposition of tryptophan 97

5.2 The vaporization and decomposition of tyrosine 98

6.1 Proposed MPI fragmentation pattern for substituted aromatic amino acids 125

6.2 Fragmentation process for dipeptides having a N-terminal aromatic group 126

List of Abbreviations

CF	Continuous Flow
CI	Chemical Ionization
EI	Electron Impact
FAB	Fast Atom Bombardment
FIA	Flow Injection Analysis
FTICR	Fourier Transform Ion Cyclotron Resonance
FTMS	Fourier-Transform Mass Spectrometer
FWHM	Full Width at Half Maximum
HPLC	High Performance Liquid Chromatography
IP	Ionization Potential
IR	Infrared
LC	Liquid Chromatography
LD	Laser Desorption
LDMS	Laser Desorption Mass Spectrometry
LN2	Liquid Nitrogen
$M^{+\cdot}$	Molecular Ion
MALDI	Matrix Assisted Laser Desorption Ionization
MPI	Multiphoton Ionization
MS	Mass Spectrometry
MW	Molecular Weight
PAH	Polycyclic Aromatic Hydrocarbon
PRH	Pulsed Rapid Heating
PSI	Pulsed Sample Introduction
R2PI	Resona Two Photon Ionization
REMPI	Resonant Enhanced Multiphoton Ionization
RSD	Relative Standard Deviation
SIMS	Secondary Ion Mass Spectrometry
SJ	Supersonic Jet
SJS	Supersonic Jet Spectroscopy
TOF	Time-of-Flight
TOFMS	Time-of-Flight Mass Spectrometry
UV	Ultraviolet
Vis	Visible

Chapter 1

Introduction to Laser Ionization Mass Spectrometry

1.1 Introduction

Mass spectrometry (MS) is regarded as one of the most sensitive and powerful methods of chemical analysis. The heart of mass spectrometry involves the production of ions from neutrals. As a result, the development of new and more versatile ionization sources for both small and large molecules has become one of the most active research areas. In the past ten years there has been a great deal of interest in the development of laser ionization mass spectrometry. Laser-induced multiphoton ionization (MPI) mass spectrometry has already established itself as a powerful technique for chemical detection and structural analysis [1,2]. With the discovery of matrix-assisted laser desorption ionization (MALDI) in 1987 [3], the mass spectrometric analysis of biopolymers in the molecular mass range between a few thousand to a few hundred thousand Daltons is now possible.

In MPI, an intense laser beam is used to ionize sample molecules and the resulting ions are usually detected by a time-of-flight (TOF) [1,2,4] or Fourier-transform (FT) mass spectrometer (MS) [5-9]. MPI is a versatile ionization source in which mass fragmentation patterns can be readily controlled for molecular weight determination or structural information. Supersonic jet spectroscopy (SJS) has been combined with MPI mass spectrometry in a TOFMS to further enhance the sensitivity and selectivity of the MPI technique [1,10-12]. By incorporating SJS with MPI mass spectrometry, a two-

dimensional detection scheme based on mass spectra and jet-cooled wavelength spectra can now be employed for identification and detection of molecules.

In the past both MPI mass spectrometry and SJS were limited to the studies of volatile molecules, since MPI and SJS are generally used for probing gas phase molecules. In order to extend these two techniques to study thermally labile biochemicals, a method for desorption / vaporization without thermal decomposition is required. Several methods, including supercritical fluid injection [13] and thermospray/heating [14], have been attempted to introduce these molecules into the supersonic jet. More recently, laser desorption (LD) has been successfully used to introduce biological molecules into a supersonic jet (SJ) expansion [15,16].

The first part of this thesis is mainly focused on the development of SJS and MPI/MS for the study of small biological molecules (MW < 1000). We were interested in simple alternative methods to introduce thermally labile and nonvolatile molecules into supersonic jets. Methods that have been developed and applied in our labs are pulsed fast atom bombardment (FAB) [17] and pulsed rapid heating (PRH) [18]. Both FAB and PRH are simple and inexpensive methods, comparable in performance to LD.

Other work was also carried out in relation to SJ/MPI mass spectrometry. A method was developed to enhance signal intensity by using a cylindrical lens instead of a spherical lens, without degrading the mass resolution or the supersonic jet cooling [19]. MPIMS for the difficult isomer discrimination of substituted polycyclic aromatic hydrocarbons (PAH), anilines, and phenols was studied [20]. Water and ammonia elimination from labile dipeptides was looked at using PRH and LD [21]. As an application, the PRH technique was used for obtaining gas phase UV-Visible

absorption spectra of thermally labile compounds [22]. Finally, in order to have a better understanding of the mechanisms involved in LD, resonant two-photon ionization (R2PI) spectroscopy was used to examine the molecular cooling and supersonic jet formation in LD [23].

In the second part of this thesis, large molecules (MW > 1000) were studied with matrix-assisted laser desorption ionization (MALDI). A data system was developed for transferring and storing mass spectra at high repetition rates, specifically for MALDI [24]. Continuous flow (CF) was coupled to MALDI for flow injection analysis of large peptides and proteins [25,26]. In order to further extend CF-MALDI, the coupling of liquid chromatography (LC) to MALDI for the on-line separation and detection of peptides and proteins was carried out [27]. Finally, current research in our laboratory involving CF-MALDI with an improved ion extraction geometry is described [28].

In this chapter the fundamentals of the MPI and supersonic jet technique will be introduced. Pulsed laser desorption for sample introduction will be discussed. As well, the combination of supersonic jet with time-of-flight mass spectrometry will be presented, along with an overview of MALDI. In the last section, the main instrumentation used in this thesis will be briefly described: supersonic jet expansion, various desorption techniques for sample introduction, multiphoton ionization of sample molecules, and TOFMS for ion separation and detection. Specific apparatus and experimental procedures unique to each topic will be discussed in the appropriate chapters.

1.2 Multiphoton Ionization

In the multiphoton ionization (MPI) technique a molecule absorbs more than one photon upon irradiation with an intense ultraviolet or visible light source. This results in ionization if the multiphoton energy exceeds the ionization potential of the molecule. In general, the absorption of photons is a low efficiency process. If, however, the photon energy corresponds to the energy difference between the ground state and an excited electronic state, then the efficiency of the absorption process or the cross-section for ionization is increased by several orders of magnitude. This technique is known as resonance-enhanced multiphoton ionization (REMPI) [10-13,29].

In the simplest cases the absorption of two UV-photons leads to ionization of the molecule, since most organic species have ionization potentials between 7 and 13 eV [29]. As a result, the MPI method that has found most extensive application and is used throughout this work is resonant two photon ionization (R2PI) [10-13,30,31]. As shown in Figure 1.1B, the first photon excites a molecule to an excited electronic state, i.e. S_0-S_1, and a second photon ionizes the molecule. There are several other processes in which MPI can also be induced. Also shown in Figure 1.1A and 1.1C are nonresonant MPI and two-photon resonant MPI, respectively. However, because in these processes at least one photon is nonresonant and interacts with a very short-lived virtual state ($< 10^{-15}$ s), the efficiency for ionization is far less than that achieved in R2PI. In addition, in nonresonant MPI the wavelength selectivity is lost, whereas in MPI it is a unique property.

A molecule that undergoes multiphoton ionization becomes a radical cation. Radical cations can also result from conventional ionization methods such as electron impact (EI), charge exchange (CE), and single-photon ionization. The basic difference

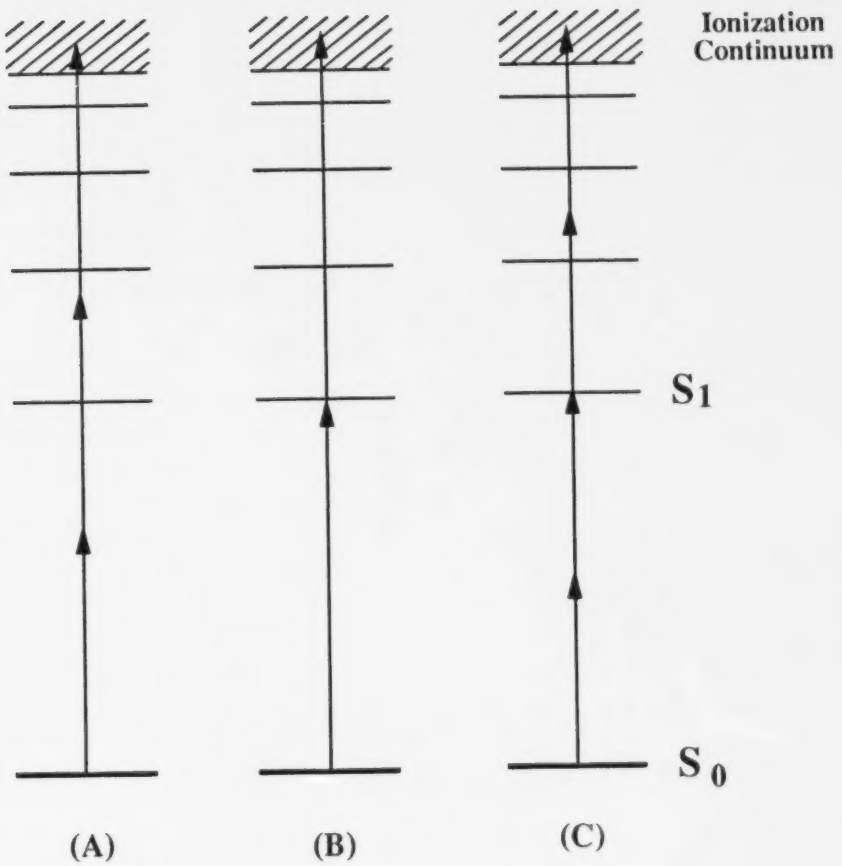

Figure 1.1 Energy level diagram showing MPI transitions: (A) nonresonant MPI (B) resonant two photon ionization (R2PI) and (C) two photon resonant ionization.

between conventional ionization methods and MPI is the mechanism of energy deposition into the reactant species. In conventional methods, energy that is greater than the ionization potential is supplied to the molecule in one step. As shown in Figure 1.2A, both ionization and fragmentation occur in the EI situation. In MPI, however, the energy deposition can be carefully controlled since the energy of a single photon is usually lower than the ionization potential (Figure 1.2B). Multiple absorption of photons is required to accumulate the necessary energy for ionization. Thus, the R2PI technique is extremely efficient for producing molecular ions. Frequently ionization in the several percent regime of the seeded molecules in a molecular beam can be achieved without fragmentation within the laser beam [2,30,31]. For several favorable cases, such as aniline and naphthalene, ionization efficiencies ranging from 10 to 100% have been estimated [2,30,31]. The high R2PI efficiency contrasts sharply with that of electron ionization, which typically ionizes less than 0.01% of the molecules that enter the ionization chamber of a mass spectrometer.

Soft Ionization: For identification purposes, soft ionization methods are often desirable because only the molecular ion with little or no fragmentation is produced. MPI can provide very efficient soft ionization for mass analysis [5,12,31-35]. In R2PI, soft ionization generally appears to occur at laser powers of ~ 10^6 W/cm^2 for a wide range of organic compounds. For small aromatic molecules such as aniline [30,33], benzene [2,36], and naphthalene [2,33,35], abundant molecular ions with little or no fragmentation can be routinely produced.

Hard Ionization: Extensive fragmentation for structural analysis can be obtained by either increasing the laser power density or changing the ionization wavelength. For instance, Zandee and co-workers [32,37,38] have shown that C^+ is the predominant ion

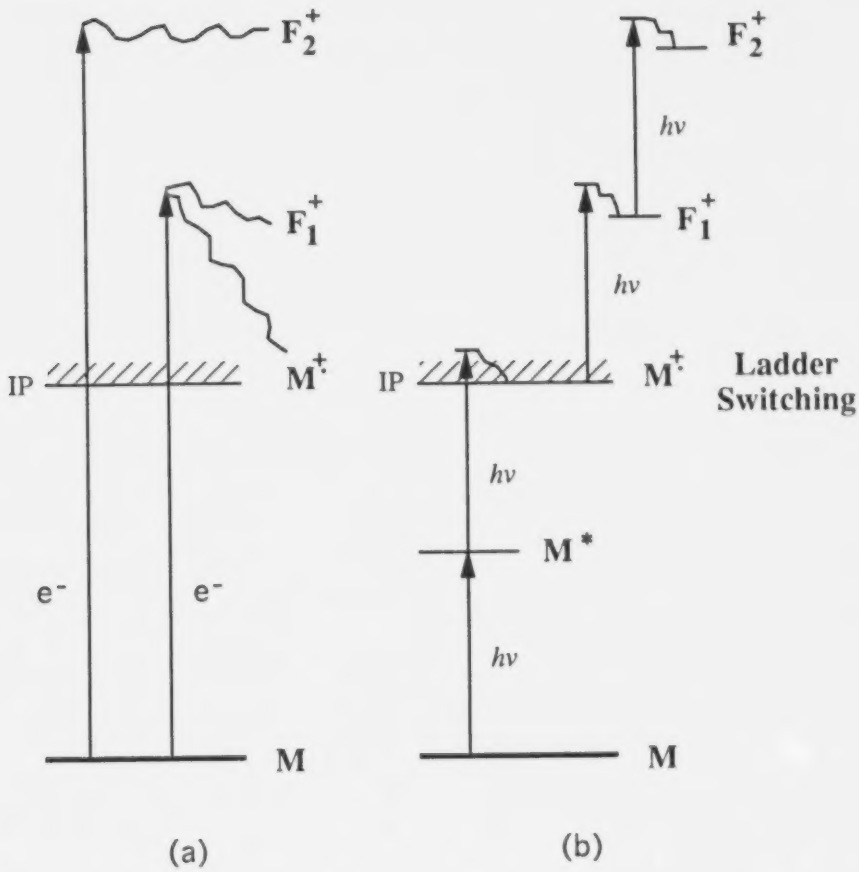

Figure 1.2 The difference between (A) electron impact (EI) ionization and (B) multiphoton ionization (MPI). IP = ionization potential; $M^{+\bullet}$ = molecular ion; F1+, F2+, ...= fragment ions. In contrast to EI, in MPI the molecular ions are formed with :

(1) a narrow energy distribution and

(2) little excess energy.

from REMPI of benzene with a laser power of 10^9 W/cm^2. With different laser power densities the fragmentation pattern will reflect different carbon cations, including such fragments as $C_6H_n^+$, $C_5H_n^+$, $C_4H_n^+$, $C_3H_n^+$, $C_2H_n^+$ and CH_n^+. The "ladder switching model" has been suggested to explain the MPI fragmentation process [39]. In this mechanism (see Figure 1.2B) either R2PI or one of the other MPI processes outlined previously is used to produce the molecular ion. The internal energy of the molecular ion is only slightly higher than the ionization energy. The subsequent absorption of additional photons will occur with increasing laser power, hence resulting in a "switching of ladders." When the rate of unimolecular decomposition exceeds the rate of photon absorption then fragmentation takes place. This occurs because of the excitation to a state that dissociates, producing ionic (neutral) fragments.

Wavelength Selectivity: In MPI, the wavelength of the laser light can also be varied [29]. The ionization probability will be low if the laser wavelength is not tuned to a real electronic intermediate state. Although the final detected product is ions, the ion current will depend on the absorption cross-section of the molecule at the chosen wavelength. Consequently, a plot of ion current versus the laser wavelength will reflect the absorption-excitation spectrum of the intermediate state. This is of great importance for a mixture analysis. The compound which is preferably ionized is the one which possesses an intermediate state in resonance with the wavelength being used. Therefore, it is possible to detect trace components in mixtures with increased sensitivity.

In conclusion, the MPI technique shows tremendous versatility as an ionization source for mass spectrometry in which either soft ionization or very extensive fragmentation can be produced. The MPI ionization cross-section reflects the absorption-excitation

spectrum of the intermediate state. This provides MPI mass spectrometry with a unique feature in mixture analysis, that is, identification and discrimination based on the spectral selection of compounds in mass analysis.

1.3 Supersonic Jet Expansion

The gas phase UV/Vis absorption spectra of polyatomic molecules at room temperature normally show broad and unresolved bands, since a large number of vibrational and rotational states are populated. To investigate molecules with resonance-enhanced MPI mass spectrometry, thermal excitation should be as low as possible, so that the broad absorption bands become sharp peaks and a selective excitation is possible. The supersonic jet (SJ) technique is used to enhance the selectivity of R2PI in molecular systems. A supersonic jet is formed by expanding a carrier gas (i.e. Ar) through a small orifice in a high pressure nozzle into a vacuum (see Figure 1.3) [31,40-42]. There are two essential requirements for generating a supersonic jet. Firstly, a large pressure gradient across the orifice/vacuum interface is required. The typical pressure in the nozzle is about 1 atm and the pressure in the vacuum is normally less than 10^{-4} Torr. Secondly, the orifice diameter must be larger than the mean free path of the gas so that many two-body collisions can take place during the expansion. To form a seeded molecular beam expansion, a small amount of sample is usually directly introduced into the nozzle and the mixture is allowed to expand through the orifice. For thermally labile nonvolatile compounds, a desorption technique such as LD [15,16], FAB (chapter 4) [17], or pulsed rapid heating (chapter 5) [18] is first used to vaporize the molecules, and the resulting gas phase neutrals are then entrained into the supersonic jet just outside the nozzle orifice.

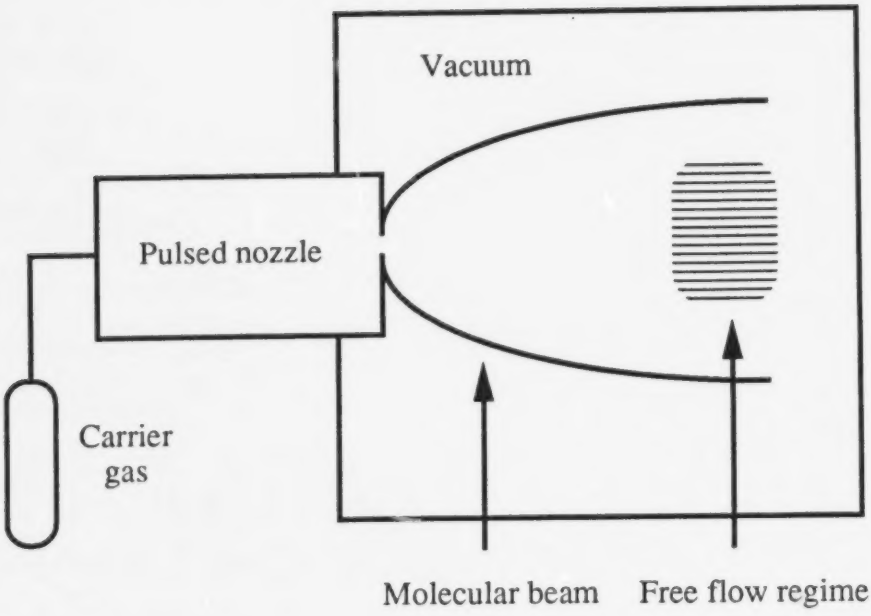

Features of Supersonic Jet Expansion:

1. Translation cooling
2. Free flow regime

Figure 1.3 Schematic of a supersonic jet expansion.

Several unique features can be provided by a supersonic jet expansion. The most important feature is the translational cooling which takes place during the jet expansion. A hydrodynamic process takes place during the early stages of the jet expansion in which the gas flows through the orifice and into the vacuum. This hydrodynamic expansion converts the random motion of the carrier gas into directed mass flow (Figure 1.4A). The carrier gas translational temperature decreases as a result of this conversion. This process can be understood by examining the velocity distribution of the carrier gas before and after the jet expansion. As shown in Figure 1.4B, inside the nozzle the velocity distribution of the gas can be expressed by the Maxwell-Boltzmann velocity distribution. Translational cooling takes place after the gas expansion, since the velocity distribution in the directed mass flow becomes very narrow (see Figure 1.4C). The typical translational temperature of a carrier gas such as Ar after expansion is 1°K [41,42].

Another important characteristic of the supersonic jet expansion is that a "free flow" collisionless regime is formed after the initial part of the expansion (see Figure 1.3). In the free flow regime, the molecules are isolated and free of any collisions.

To apply the supersonic jet technique to MPI mass spectrometry, a small amount of sample is seeded into the carrier gas, and the mixture is expanded through an orifice to form a molecular beam. As the expansion proceeds, there are a large number of two-body collisions between the light carrier gas and the heavy seeded species in which the internal energy of the large sample molecules is transferred to the carrier gas. Because the energy exchange between the molecular rotational motion and atomic translational motion is extremely fast, the rotational temperature of the molecules is similar to the translational temperature of the carrier gas, that is, 1°K. However, the energy transfer

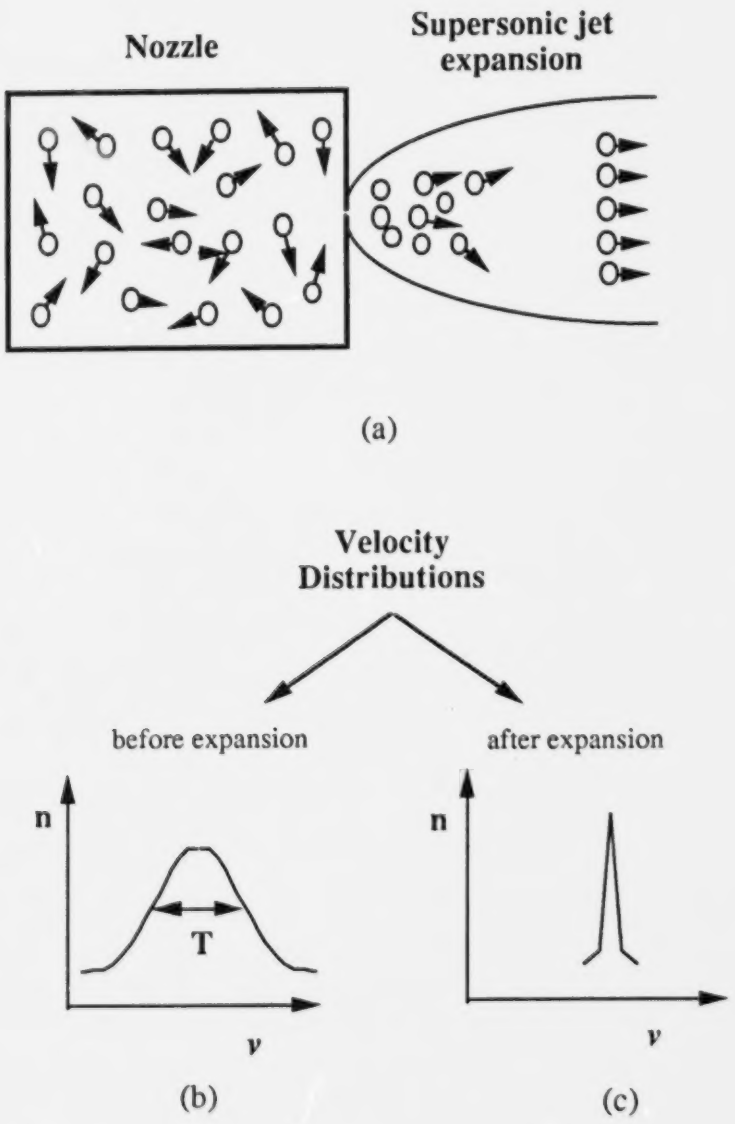

Figure 1.4 Schematic diagram of translational cooling process.

between the molecular vibrational motion and atomic translational motion is somewhat slow. Thus the vibrational temperature of the seeded molecules is usually above the translational temperature but well below the original temperature.

In summary, the supersonic jet expansion can be used to obtain ultra cold, isolated gas phase molecules with sharp spectral features. Thus R2PI spectroscopy with supersonic jets has the potential to provide enhanced selective ionization in MPI mass spectrometry.

1.4 Pulsed Laser Desorption / Vaporization

Lasers have been used since the 1960's to vaporize small amounts of solid inorganic material. More recently, lasers have been successfully used in vaporizing (desorbing) large thermally labile and nonvolatile biological molecules [43]. To extend the R2PI and supersonic jet technique to biological systems and other large molecules, it is essential to introduce these nonvolatile solid samples into the gas phase. It is difficult to volatilize biological molecules by traditional means (such as direct heating) without thermal degradation. The advantage of using lasers to generate gas-phase species is that the laser induces a rapid temperature increase, up to 10^8 K/s [43], which allows desorption to be favored over decomposition.

A high-powered pulsed infrared laser is typically used to perform laser desorption. The vaporizing laser imparts its energy to the sample, the substrate, or a suitable matrix. This form of rapid heating induces molecules to be desorbed from the surface before they have time to decompose. In the actual desorption process both ions and neutrals are formed, although the yield of neutral molecules is generally much larger than the ion yield. Typical values for the ratio of neutral molecules to ions are about 10^4:1 [44].

Nevertheless, most detection schemes for LD in the past were focused on the small percentage of ions produced during the desorption event.

To make use of the large ratio of neutral molecules to ions, a tandem arrangement of laser evaporation of intact neutral molecules into a supersonic jet followed by multiphoton ionization can be employed [45-48]. The result is a much larger sample available for ionization as compared to the generation of ions in direct laser desorption / ionization mass spectrometry. In addition, the desorption and ionization processes are now separated in time and space. Thus, the laser energies for desorption and ionization are now independent of one another. By controlling the output power of the ionization laser, R2PI can be used to produce mass spectral patterns that range from molecular ions to extensive fragmentation. In addition, the separation of desorption from the post ionization steps allows one to perform supersonic jet cooling of the desorbed molecules prior to ionization.

1.5 Supersonic Jet / Time-of-Flight Mass Spectrometry

The time-of-flight (TOF) method for mass analysis is exceedingly simple. Ions are accelerated through a known potential V, and the time t taken to reach a detector (in a field-free flight tube of length L) is measured (Figure 1.5) [49]. Assuming that all ions experience the same potential difference V, the arrival time of the ions will be proportional to the square roots of their masses. In our drift tube (1-meter length), a complete mass spectrum in the range 0-500 Da can be acquired in 50 μs. Thus, TOF requires rapid data acquisition, which has only been possible in the last few years. Nevertheless, the TOF mass spectrometer has many advantages such as high speed, high sensitivity, simplicity, low cost, and no mass limit.

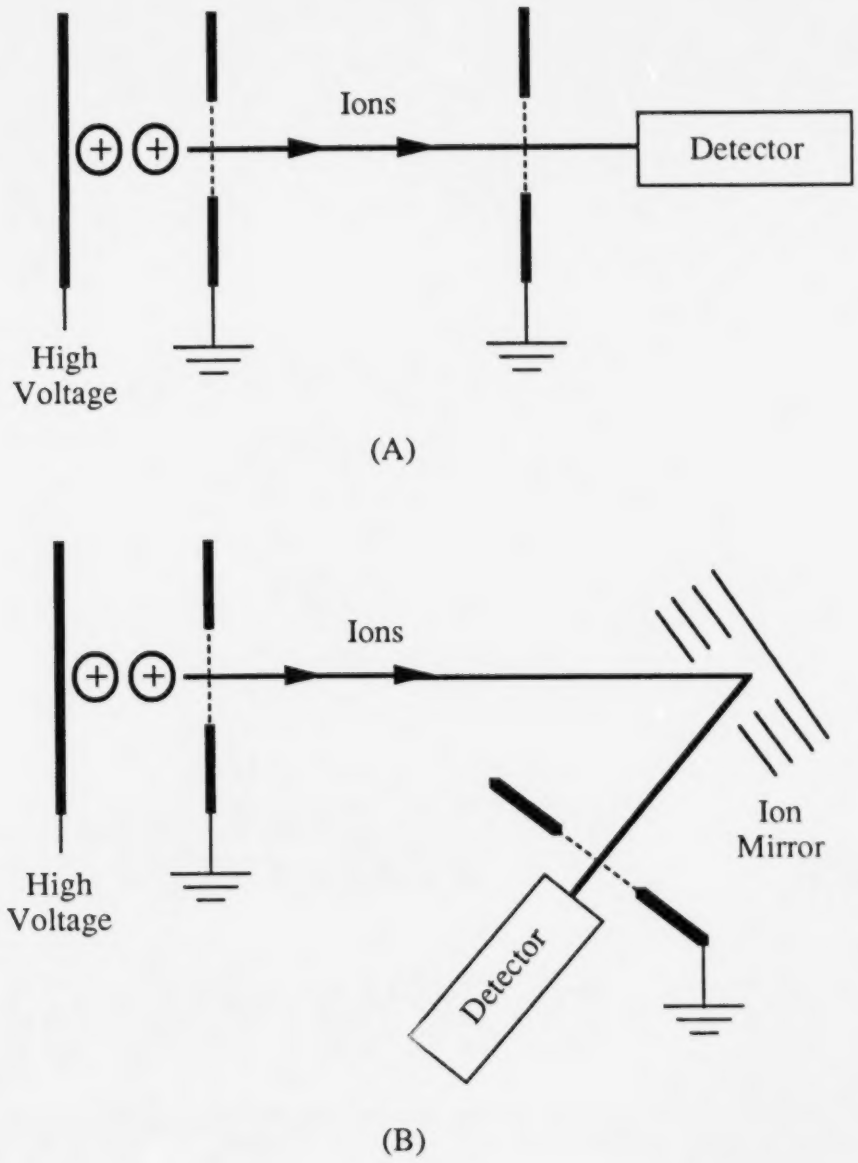

Figure 1.5 (A) Linear and (B) reflectron time-of-flight mass spectrometers.

It is first necessary to define mass accuracy and mass resolution when discussing mass spectrometer performance. Mass accuracy refers to the percent error involved in assigning a mass to a given ion signal. It is calculated by dividing the mass assignment error by the ion mass, and multiplying by 100%. On the other hand, mass resolution is a measure of an instruments' ability to produce separate signals from ions of similar mass. It is expressed as the mass m of a given ion signal divided by the full width at half maximum (FWHM) intensity of the signal Δm. The higher the mass resolution ($m/\Delta m$) the more superior the mass spectrometer in terms of discriminating ions of similar masses.

The simplest mass spectrometer system generally used in MPI experiments has been the linear time-of-flight (TOF) mass spectrometer. However, due to the initial energy and spatial spread in the ion-acceleration region, linear TOF mass spectrometry is generally a low resolution technique [29]. In an effort to compensate for this energy spread problem, the supersonic jet technique has been combined with TOF. As discussed in section 1.3, in an ideal supersonic beam all the molecules are traveling with the same velocity, thus minimizing the initial energy spread. Consequently, in a typical SJS/TOF mass spectrometer, a resolution of 500-1000 or higher can be achieved, since the resolution is limited only by the 5-10 ns width of the ionization laser pulse. This contrasts sharply to the more typical resolution of around 200 in a linear TOF instruments with no supersonic jet.

Another important technique which can substantially improve the resolution of TOFMS is known as the reflectron TOF (Figure 1.5) [50,51]. Mass resolution over 10,000 has been reported [52,53]. This device compensates for the difference in ion flight times of the same mass-to-charge by means of an ion reflector. A system of

electrostatic fields (i.e. the ion reflector) is placed at the end of the time-of-flight drift tube. The ion reflector allows ions with greater energies to penetrate a greater distance into the reflector region than ions with lower energies. The reflector scheme, therefore, compensates for the initial spread in ion velocities caused by the finite laser width used for ionization. If the total flight time in the drift and reflector region can be made the same for every ion of the same mass-to-charge ratio, then the ion packet widths will be narrow, as is necessary for the attainment of high resolution. Thus, by combining the supersonic jet with the reflectron technique the low resolution problem, which had limited TOF technology for many years, can now be overcome.

1.6 Electrospray Ionization and MALDI

Two recent developments, electrospray ionization (ESI) [54,55] and matrix-assisted laser desorption ionization (MALDI) [3,56], have made possible accurate and sensitive determination of molecular masses of large biopolymers such as proteins, carbohydrates, and polymers. Both techniques have overcome the main difficulties with MS methods, that is, the desorption and ionization of large and labile biomolecules. Although MALDI is exclusively used in this work, it should be noted that the techniques are not competitive, but rather complementary, since each exhibits unique features and characteristics.

ESI utilizes the highly charged droplets formed when a liquid is sprayed in a high electric field under atmospheric pressure. This process produces naked, intact protein molecules in ionized form from a dilute solution. Fenn and co-workers have found that ESI is a very efficient means for producing peptide and protein ions suitable for study by mass spectrometric analysis [55].

In 1987 Karas and Hillenkamp developed the MALDI technique [3]. A low concentration of analyte molecules, normally exhibiting low absorptivity, are embedded in a small, highly absorbing solid or liquid matrix. Typical matrices are listed in Table 1.1, along with applications. The mixture is subjected to intense, short duration bursts of ultraviolet (UV) laser light in the ion source of a mass spectrometer. This produces a rapid phase change of the matrix from a solid (or liquid) to a gas [57]. Since this takes place very quickly, a very dense gas is produced which will expand supersonically into the vacuum. This high gas density can carry the analyte molecules away from the surface and into the gas phase. Photoexcitation or photoionization of the matrix molecules most likely enhances ion formation of the analyte molecules. This results in proton transfer to the analyte molecules. In this respect the analyte molecules are shielded from the excessive laser energy that would ultimately lead to their decomposition.

Samples are prepared for mass analysis by adding the analyte sample to a concentrated aqueous solution containing a large molar excess of a matrix [56]. A small volume of this mixture containing 1-10 pmol of analyte is dried on a sample probe. The thin layer of matrix microcrystals containing the isolated analyte molecules is inserted into the mass spectrometer. Bombardment with short duration UV laser pulses (typically from a nitrogen laser or Nd:YAG laser) produces charged analyte molecules, which are subsequently analyzed in a time-of-flight mass spectrometer. Depending on the amount of sample loading, the mass spectrum will show peaks corresponding to singly and doubly protonated intact analyte molecules, as well as dimers and trimers.

In this work, we were interested in coupling MALDI to continuous flow (CF) methods. This is possible if a liquid matrix is employed, as opposed to the more traditional solid

Table 1.1

Typical matrices for Matrix-Assisted Laser Desorption Ionization (MALDI)

Matrix	Form	Applications
Nicotinic acid	Solid	Proteins
Succinic acid	Solid	Proteins
2-Amino-5-nitropyridine	Solid	Nucleotides
5-Chlorosalicylic acid	Solid	Nucleotides
trans-3-Indoleacrylic acid	Solid	Nucleotides Polymers
3-Hydroxypicolinic acid	Solid	Nucleotides
2,4,6-Trihydroxyacetophenone	Solid	Nucleotides Oligosaccharides
2,5-Dihydroxybenzoic acid	Solid	Polymers Oligosaccharides
3,5-Dimethoxy-4-hydroxycinnamic acid (sinapinic acid)	Solid	Proteins
3,4-Dihydroxycinnamic acid (caffeic acid)	Solid	Proteins Oligosaccharides
4-Hydroxy-3-methoxycinnamic acid (ferulic acid)	Solid	Proteins Oligosaccharides
α-Cyano-4-hydroxycinnamic acid	Solid	Peptides Proteins
2-Nitrophenyl octyl ether	Liquid	Polymers
3-Nitrobenzyl alcohol	Liquid	Proteins

matrices. We have exclusively concentrated on 3-nitrobenzyl alcohol (3-NBA) as the liquid matrix (Table 1.1). Chapters 9-11 discuss CF-MALDI for flow injection analysis, which is eventually extended to on-line LC-MALDI for detection of peptides and proteins.

1.7 Instrumentation

The supersonic jet time-of-flight mass spectrometer setup used in our research is shown in Figure 1.6 [17-21,58]. It consists of an angular reflectron TOFMS (R.M. Jordan Co., Grass Valley, CA) mounted vertically in a six-port cross pumped by a 6-in. diffusion pump (Varian Associates, Inc., Lexington, MA). A pulsed nozzle (R.M. Jordan Co., Grass Valley, CA) with a 50-μs pulse width is used to form a supersonic jet. CO_2 is used as the expansion gas throughout our work. The pulsed supersonic jet is oriented perpendicular to both the sample probe and TOF flight tube so that it can easily carry the desorbed sample to the ionization region. The distance between the nozzle and acceleration region is about 20 cm. The jet expands into the acceleration region of the TOF and a laser beam, perpendicular to both the jet and flight tube, ionizes the sample. The 1-meter-long flight tube is differentially pumped by a 4-in. diffusion pump (Varian Associates, Inc.). The pressure in the flight tube is usually below 2×10^{-7} Torr and the pressure in the ionization region is $< 10^{-6}$ Torr.

For the study of thermally labile and nonvolatile biomolecules, a desorption/ ionization scheme is generally used. In the experiments, samples are coated on a ceramic probe and placed very close to the nozzle orifice. A pulsed laser beam, a FAB gun (chapter 4), or a PRH probe (chapter 5) is first turned on to desorb the sample. Next, the pulsed nozzle opens to form a supersonic jet, and the sample is then entrained into the jet and carried into the ionization region of the TOFMS where the ionization proceeds.

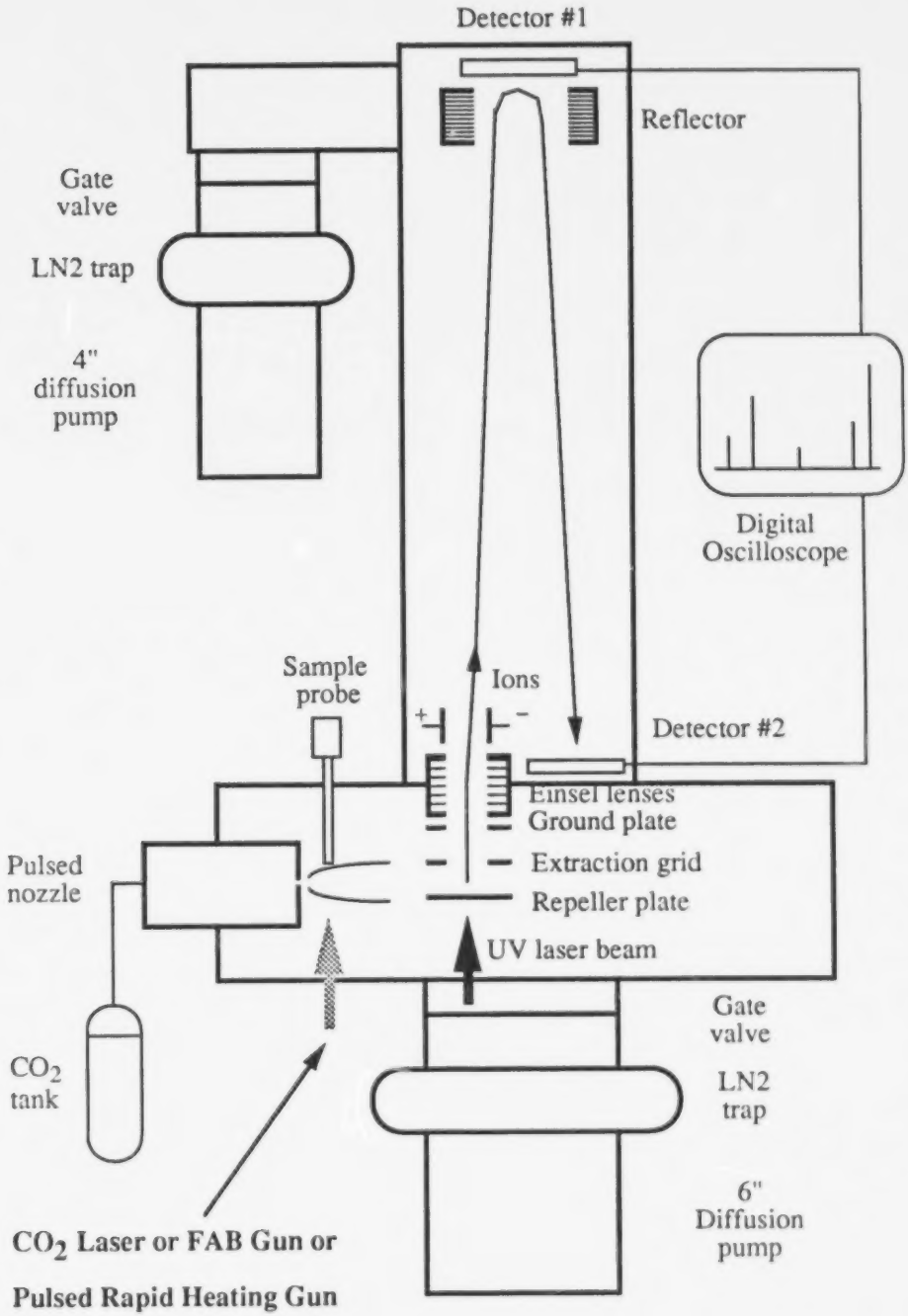

Figure 1.6 Schematic diagram of the supersonic jet / multiphoton ionization time-of-flight mass spectrometer setup (drawing is not to scale).

The R2PI mass spectrometry experiments are performed with a frequency-quadrupled neodymium:yttrium aluminum garnet (Nd:YAG) laser ionization source (GCR-3, Spectra-Physics, Mountain View, CA), which generates 266 nm radiation with a 7 ns pulse width. The laser is normally operated at a 10 Hz repetition rate. The diameter of the beam from the laser is about 7 mm. A 25.4 mm diameter cylindrical lens (ESCO, Oak Ridge, NJ) or combination of a concave and a convex lens is used to produce a 2-3 mm diameter beam for ionization. The laser power is measured with an Ophir Model 10A-MED-AN laser power/energy meter (Diamond Ophir Optics, Wilmington, MA). Laser ionization (R2PI) spectroscopy is performed using the frequency doubled dye output from a Quanta-Ray DCR-2A Nd:YAG pumped dye laser system.

In our SJS/TOFMS system, microchannel plate detectors are used for ion detection. Two detectors have been installed in the system. One is placed behind the reflecting field, which is at the end of the flight tube, so that this system will function as a linear TOFMS when the reflecting field is turned off. When the field is on, ions will be reflected. Thus, the other detector is placed near the extraction grid at the other end of the flight tube (see Figure 1.6).

The mass spectrum is recorded by a LeCroy 9400A digital oscilloscope. All mass spectra are then stored in either a IBM-compatible 386SX or 486DX33 PC for processing. In chapter 9 a data system is described for transferring and storing mass spectra at high repetition rates, specifically for MALDI.

The mass resolution of our reflectron SJS/TOFMS system is above 2000 for aniline at m/z 93. It is found that the resolution increases when the mass of the ion increases.

For instance, the mass resolution of the system is about 4100 for 1,3,5-triphenylbenzene at m/z 306. Thus isotope peaks can be easily resolved in our system.

The CF-MALDI experimental setup will be described in chapter 9.

Chapter 2

Signal Enhancement by Using a Planar Laser Beam for Multiphoton Ionization in a Supersonic Jet / Reflectron Time-of-Flight Mass Spectrometer

2.1 Introduction

Multiphoton ionization (MPI) mass spectrometry (MS) combined with supersonic jet spectroscopy (SJS) is a very powerful method for chemical analysis [1,10,11]. In this technique, sample molecules are generally introduced into a supersonic jet and carried into the ionization region of a time-of-flight mass spectrometer (TOFMS) where ions are produced through a resonant two-photon ionization (R2PI) process. Both a R2PI jet-cooled spectrum and a MPI mass spectrum can be obtained. It has been demonstrated that the two-dimensional detection scheme based on the jet-cooled spectrum and the MPI mass spectrum can provide a unique means of molecular identification and structural analysis of organic and biological molecules with high sensitivity and selectivity [1]. In addition, when SJS/MPIMS is combined with various desorption techniques such as laser desorption (LD), fast atom bombardment (see chapter 4), and pulsed rapid heating (see chapter 5) for sample vaporization, thermally labile and nonvolatile species can be studied. However, sample dilution, sample expansion, and jet expansion of the carrier gas are all unavoidable when using a supersonic jet. This ultimately reduces the sensitivity of the SJS/MPI technique. Therefore, in order to increase the overall sensitivity of SJS/MPI mass spectrometry, the extent of the sample expansion should be reduced and a larger laser beam size be used to ionize as large a proportion of molecules as possible.

In this chapter, a simple technique for signal enhancement is described. A cylindrical lens is used to produce a planar laser beam for ionization, instead of the more conventional circular laser beam. In the SJS/MPI system, a supersonic jet and a relatively high resolution reflectron TOFMS are used. Thus, a study is conducted on the effects of signal enhancement, mass resolution, and jet cooling by using a planar laser beam. It will be demonstrated that the use of a planar beam instead of a circular beam enhances the signal about 4 to 16 times depending on the laser beam sizes, i.e. the diameter of the beam for a spherical lens or the width of the beam for a cylindrical lens, without losing resolution. Even with a large planar beam (i.e. length = 15 mm, width = 5 mm), resolution above 2000 can be achieved. In addition, supersonic jet cooling can still be obtained.

2.2 Experimental

The experimental setup for SJS/MPI mass spectrometry is discussed in detail in section 1.7. In brief, it consists of an angular reflectron TOFMS mounted vertically in a six-port cross pumped by a 6-in diffusion pump. The pulsed supersonic jet expands into the acceleration region of the TOF and a laser beam perpendicular to both the jet and flight tube ionizes the sample. The flight tube is differentially pumped by a 4-in. diffusion pump. The pressure in the flight tube is usually below 6×10^{-7} Torr and the pressure in the ionization region is $< 10^{-6}$ Torr.

The ionization source is a frequency quadrupled Nd:YAG laser (GCR-3, Spectra-Physics) which generates 266 nm radiation with a 7-ns pulse width. The beam diameter directly from the laser is about 8 mm. This beam can be expanded up to 20 mm by using a combination of a convex and a concave lens (see Figure 2.1). The

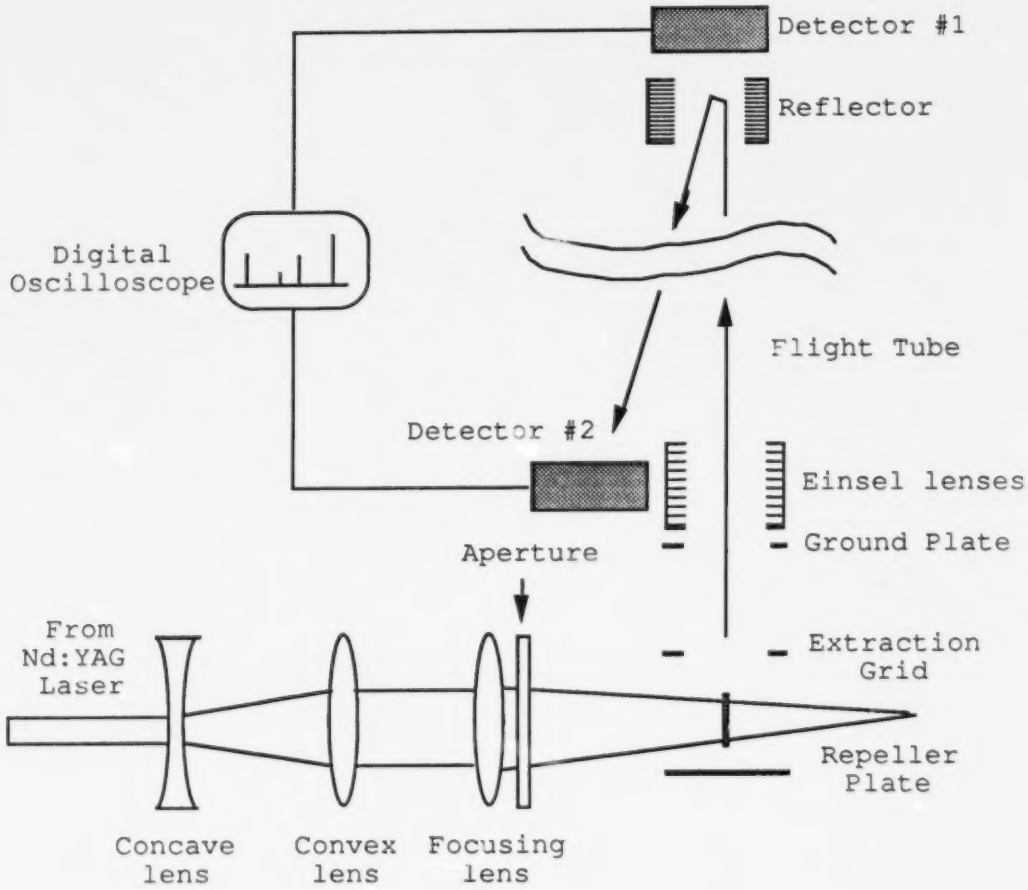

Figure 2.1 Optics and laser ionization in a reflectron TOFMS. The shaded area between the extraction grid and repeller plate is the position where the beam size is measured.

expanded laser beam is then focused into the ionization region of the TOFMS with either a cylindrical lens (focal length = 152 mm) to generate a planar beam or a spherical lens (focal length = 150 mm) to generate a circular beam. The 25.4-mm-in-diameter cylindrical lens is made of UV grade fused silica (ESCO, Oak Ridge, NJ) and can be easily mounted into a regular lens holder used for the spherical lens. Different rectangular aperture sizes or circular apertures are inserted in between the lens and the focal point to generate various laser beam sizes. The length of the planar beam is fixed at 15 mm while the width of the beam can be varied. The focal point is located about 30 mm away from the center of the repeller plate to avoid local excess ionization. The laser beam size can be measured by using heat-sensitive paper to display the beam profile. The beam size (i.e. cross section) given below refers to the size of the laser beam at the plane passing through the centers of the repeller plate and the extraction grid.

Argon is used as the expansion gas for the generation of the supersonic jet. Aniline is used in this study and introduced into the argon directly. The mass spectrum is recorded by a LeCroy 9400A digital oscilloscope. All mass spectra are obtained with signal averaging over 200 laser pulses.

2.3 Results and Discussion

Since the ionization signal intensity is directly related to the number of molecules within the interaction region between the laser beam and the molecular beam, any increase of the beam size will enhance the signal intensity. Indeed, we have found that the signal intensity increases with the increase of the diameter (D) of the circular beam for a spherical lens or the width (W) of the planar beam for a cylindrical lens. The use of a planar laser beam instead of a circular beam (when D = W) increases the ionization

area. Thus signal enhancement with a cylindrical lens is possible. Figure 2.2 shows the relative intensity between the aniline molecular ion peak when a cylindrical lens is used and when a spherical lens is used at different laser beam sizes (D or W). This figure is obtained at a laser power density of about 5 x 10^6 W/cm^2. When the laser power is slightly increased fragment ions are observed. As Figure 2.2 shows, signal enhancement from about 4 to 16 times can be achieved depending on the beam size by simply using a cylindrical lens.

Effect of Planar Laser Beam on Mass Resolution: It has been known that a TOFMS equipped with a reflectron field can improve mass resolution significantly over a simple linear TOFMS [50]. Mass resolution above 10,000 has been reported [52,53]. Our system consists of two ion detectors, as described in section 1.7. One is placed behind the reflecting field which is at the end of the flight tube so that this system will function the same as a linear TOFMS when the reflecting field is turned off. When the field is on ions will be reflected. Thus, the other detector is placed near the extraction grid at the other end of the flight tube. When the system is operated in a linear TOFMS mode, mass resolution is found to be about 300 for aniline at m/z 93 with a small size laser beam (1-mm). When the beam size is increased, the resolution is so dramatically reduced that a reliable mass identification becomes very difficult. However, with a reflectron TOFMS, mass resolution above 2000 can be obtained even with a 5-mm x 15-mm laser beam. Figure 2.3 shows the relation between mass resolution and laser beam size. This figure indicates that the use of a planar beam instead of a circular beam does not change the mass resolution. Thus, we can have net signal enhancement without losing resolution. Figure 2.3 also shows that the mass resolution decreases when the diameter or the width of the laser beam is increased. This suggests that our reflectron TOFMS can only partially compensate the initial spatial distribution.

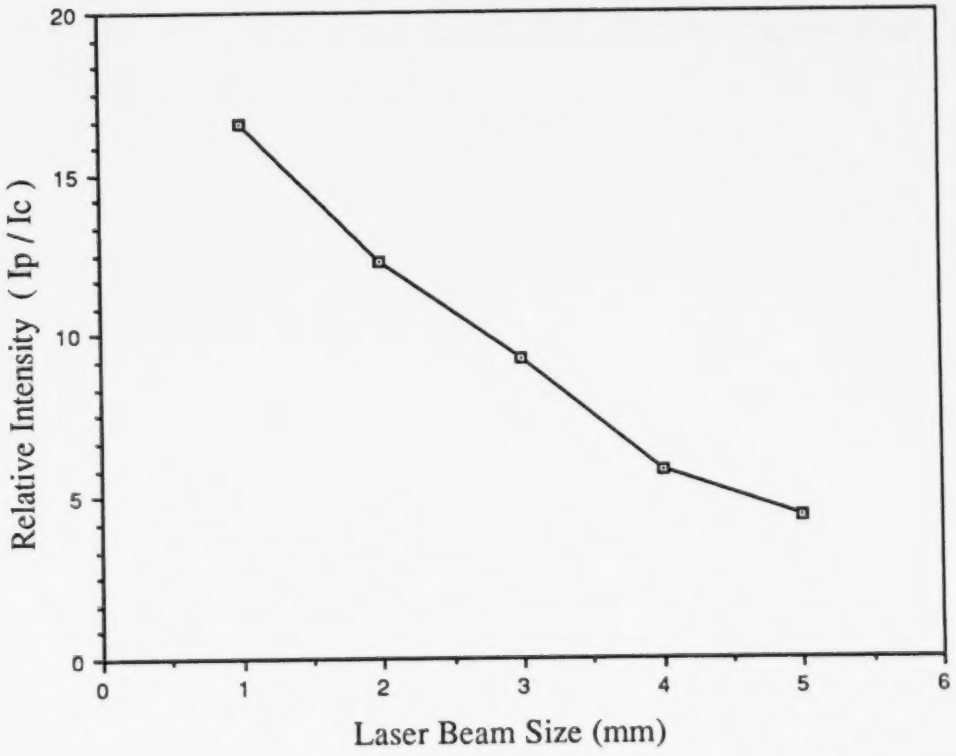

Figure 2.2 The relative intensity of the aniline molecular ion peak vs the laser beam size. I_p is the aniline signal intensity obtained using a planar beam. I_c is the aniline signal intensity obtained using a circular beam. Beam size refers to the diameter of the circular beam or the width of the planar beam (length = 15 mm). The laser power density is about 5×10^6 W/cm^2 and remains constant throughout the study.

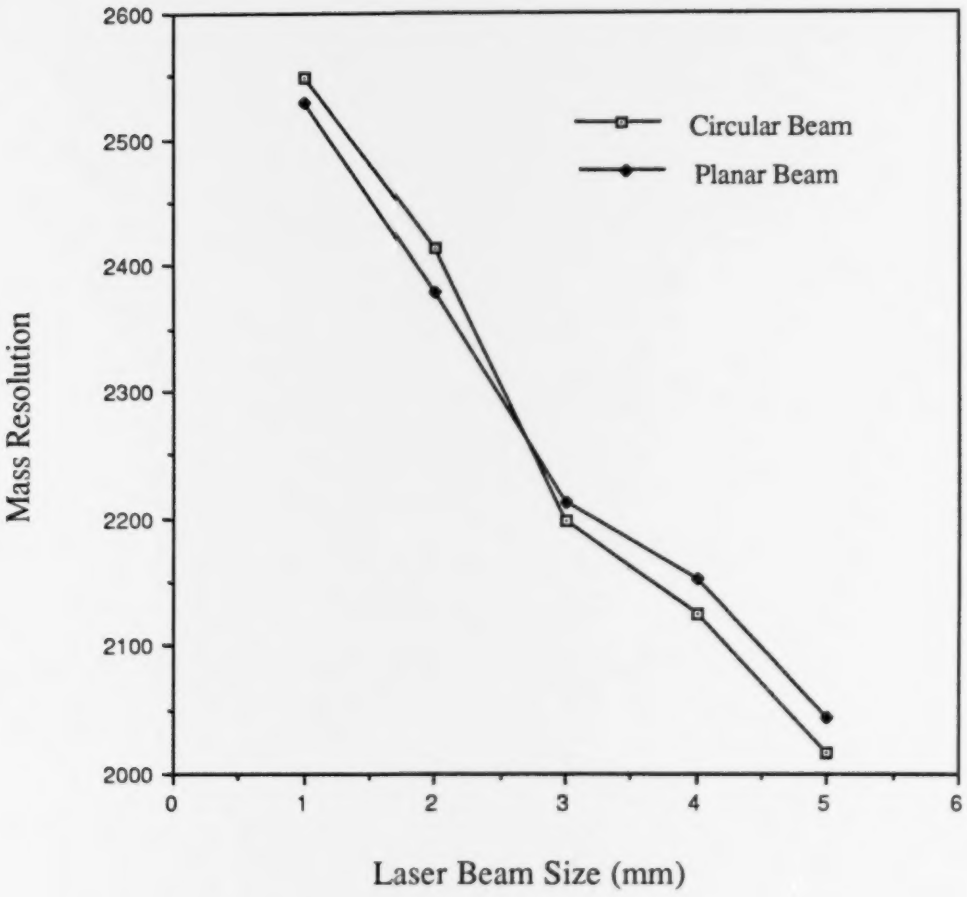

Figure 2.3 The relationship between mass resolution and laser beam size for a planar and a circular beam with a reflectron TOFMS.

Effect of Planar Laser Beam on Supersonic Jet Cooling: We have examined the cooling effect by examining the mass resolution in a linear TOFMS [34]. In a linear TOFMS, the mass resolution is directly related to the initial kinetic energy distribution of the sample molecules. The energy distribution will be very broad if there is no cooling or only partial cooling for the molecules in the jet [34], thereby resulting in low resolution. By running our system in a linear TOFMS mode the mass resolution remains the same when a circular laser beam is replaced with a planar beam. Thus, the signal can be enhanced by the use of a planar beam without affecting the jet cooling. This result is very significant for the R2PI supersonic jet spectroscopy studies of biological molecules [16,59,60]. For most biological molecules, the use of high laser power will have two effects, namely, severe fragmentation and spectral peak saturation of the wavelength spectrum. The signal enhancement from 4 to 16 times will allow one to reduce the ionizing laser beam power about 2 to 4 times for R2PI while the overall signal intensity remains the same. Note that thermally labile and nonvolatile biochemicals are usually introduced into the jet by LD [1]. In the LD experiment, it is very difficult to increase the signal intensity by desorbing a larger quantity of sample from a glycerol matrix per laser pulse. This is because the sample has to be desorbed gently for an extended period to allow the ionization laser scan through the whole wavelength region. In addition, increasing the desorption laser power sometimes decreases the pulse-to-pulse reproducibility.

2.4 Conclusion

Signal enhancement from 4 to 16 times in a SJS/MPI can easily be achieved by using a planar ionization laser beam. The use of a planar beam does not affect mass resolution and supersonic jet cooling. This method should be useful for sensitive detection of

organic and biological molecules, and for obtaining supersonic jet spectra of biochemicals.

Chapter 3

On the Capability of Multiphoton Ionization Mass Spectrometry for Isomer Discrimination: Mass Spectra of Positional Aromatic Isomers

3.1 Introduction

Multiphoton ionization mass spectrometry in combination with supersonic jet spectroscopy is a very powerful technique for chemical detection and structural analysis [1,11]. However, the capability of MPI for isomer discrimination based on mass spectral fragmentation patterns has not been fully addressed. For the analysis of organic pollutants, one of the most challenging problems is, indeed, isomer discrimination. The identification of different isomers in a mixture is very important. This is particularly true for the identification of polycyclic aromatic hydrocarbons (PAHs), since carcinogenic properties of PAHs depend strongly on isomeric structure and substitution. Although chromatography techniques can be used for the separation of isomers prior to the introduction of the sample into a mass spectrometer, the separation of isomers in a complicated matrix is often incomplete. Thus a selective detection method is required. It is well known that it is difficult to discriminate isomers based on electron impact (EI) mass spectra. MPI may be a more powerful technique for the elucidation of molecular structure in that the molecular ion peak can be readily obtained, while the molecular ion peak is sometimes absent in the EI mass spectrum.

Some studies suggest that isomer discrimination based on MPI mass spectra is difficult since almost identical mass spectra are obtained for specific isomer pairs [33,61-63].

However, Lubman has shown that although MPI mass spectra of azulene and naphthalene are identical, these molecules give different mass spectra at the same laser power in terms of relative intensity of peaks [62]. Thus isomer discrimination becomes possible. More recently, Johnston has shown that C_7H_8O and $C_8H_{10}O$ configurational isomers can be distinguished on the basis of their MPI mass spectra [64]. However, the EI mass spectra of these compounds also show different patterns and thus can be used for discriminating them. But one report demonstrated that MPI mass spectra of isomeric species such as n-butyl iodide and *tert*-butyl iodide are different although the EI mass spectra are almost identical [65,66]. McLafferty has shown that MPI mass spectra at 193 nm obtained with a Fourier transform mass spectrometer can be used to differentiate a number of isomers that have similar EI spectra [67].

In this chapter we report a study on the capability of MPI for the discrimination of aromatic positional isomers. In particular, this study is focused on interpreting the mass spectral fragmentation patterns of isomeric pairs of substituted PAHs, phenols, and anilines. These molecules are chosen mainly because they can be readily ionized by 266 nm photons and are environmentally significant. MPI mass spectra are compared with their EI spectra in an attempt to determine whether the MPI technique is more capable than EI for isomer discrimination for the compounds studied.

3.2 Experimental

The time-of-flight mass spectrometer setup has been described in section 1.7 [17-21,58]. In brief, it consists of an angular reflectron TOFMS (R.M. Jordan Co.) mounted vertically in a six-port cross pumped by a 6-in diffusion pump. A molecular beam is formed from a small leak in a glass tube connected to a sample reservoir. The

sample beam expands into the acceleration region of the TOF and a laser beam perpendicular to both the jet and flight tube ionizes the sample.

The ionization source is a frequency quadrupled Nd:YAG laser (GCR-3, Spectra-Physics, CA) which generates 266 nm radiation with a 7-ns pulse width. The laser is operated at 10 Hz repetition rate. A cylindrical lens is used to focus the laser beam to the mass spectrometer. The focal point is located about 30 mm away from the center of the repeller plate to avoid local excess ionization. A set of neutral density filters (Reynard Enterprises Inc., CA) is used to vary the laser power to study the relationship between ion intensity and laser power. All mass spectra are obtained with signal averaging over 200 laser pulses.

Chemicals were purchased from Aldrich Chemical Co., Milwaukee, WI and used without further purification.

3.3 Results and Discussion

Soft and Hard Ionization: Tables 3.1-3.3 show the MPI mass spectra of substituted PAHs and alkyl-substituted anilines and phenols. Only the major fragments are listed. Similar peaks in the sets of isomers less than 30% intensity of the base peak are not reported in the tables for clarity reasons. To compare the fragmentation patterns among these molecules, the laser power density is adjusted such that the most intense peak in the low-mass region ($m/z < 100$) has the same intensity as the most intense peak in the high-mass region (in most instances this is the molecular ion peak). In all cases studied the molecular ion can be obtained without any fragmentation at low laser power. When the laser power is increased, extensive fragment ions are generated.

Table 3.1 MPI spectra of substituted anthracenes and phenanthrenes.

Compound	MW	Major Fragments [m/z (% rel. int.)]
1-aminoanthracene	193	193 (97), 165 (56), 164 (25), 65 (18), 63 (82), 51 (58), 50 (40), 39 (100), 38 (47), 37 (50), 36 (10), 28 (31), 27 (28)
2-aminoanthracene	193	193 (100), 165 (32), 164 (18), 65 (51), 63 (64), 51 (51), 50 (50), 39 (96), 38 (47), 37 (72), 36 (31), 28 (59), 27 (34)
9-aminoanthracene	193	193 (100), 165 (29), 164 (33), 65 (11), 63 (53), 51 (44), 50 (29), 39 (90), 38 (32), 37 (35), 36 (13), 28 (10), 27 (16)
9-aminophenanthrene	193	193 (100), 165 (49), 164 (20), 65 (32), 63 (66), 51 (44), 50 (41), 39 (95), 38 (41), 37 (65), 36 (28), 28 (34), 27 (30)
9-bromoanthracene	258	258 (100), 256 (91), 178 (43), 176 (33), 150 (11), 75 (11), 74 (25), 63 (18), 51 (30), 50 (39), 39 (19), 38 (26), 37 (86), 36 (57), 12 (33)
9-bromophenanthrene	258	258 (98), 256 (100), 178 (60), 176 (79), 150 (42), 75 (35), 74 (35), 63 (40), 51 (61), 50 (68), 39 (26), 38 (30), 37 (86), 36 (58), 12 (12)
1-chloroanthracene	212	212 (100), 176 (36), 150 (30), 75 (25), 74 (43), 63 (34), 61 (29), 51 (37), 50 (62), 39 (40), 38 (32), 37 (95), 36 (96), 27 (36), 12 (82)
2-chloroanthracene	212	212 (100), 176 (42), 150 (31), 75 (30), 74 (45), 63 (42), 61 (31), 51 (60), 50 (65), 39 (39), 38 (36), 37 (100), 36 (78), 27 (31), 12 (56)
9-chloroanthracene	212	212 (100), 176 (15), 150 (11), 75 (16), 74 (29), 63 (22), 61 (24), 51 (38), 50 (51), 39 (29), 38 (29), 37 (82), 36 (76), 27 (29), 12 (87)

Table 3.1 (Continued) MPI spectra of substituted anthracenes and phenanthrenes.

Compound	MW	Major Fragments [m/z (% rel. int.)]
1-methylanthracene	192	192 (100), 63 (75), 62 (25), 61 (30), 51 (38), 50 (55), 39 (70), 38 (38), 37 (91), 36 (69), 27 (35), 12 (45)
2-methylanthracene	192	192 (97), 63 (69), 62 (30), 61 (27), 51 (47), 50 (68), 39 (65), 38 (53), 37 (100), 36 (54), 27 (26), 12 (43)
9-methylanthracene	192	192 (100), 63 (69), 62 (33), 61 (30), 51 (46), 50 (54), 39 (78), 38 (52), 37 (96), 36 (82), 27 (29), 12 (59)
1-methylphenanthrene	192	192 (87), 63 (55), 62 (24), 61 (21), 51 (62), 50 (61), 39 (77), 38 (46), 37 (100), 36 (60), 27 (21), 12 (37)
3,6-dimethylphenanthrene	206	206 (100), 192 (35), 189 (35), 63 (53), 62 (37), 51 (45), 50 (35), 39 (59), 38 (37), 37 (100), 36 (41), 27 (37), 12 (47)
9,10-dimethylanthracene	206	206 (100), 192 (17), 189 (14), 63 (43), 62 (22), 51 (51), 50 (49), 39 (56), 38 (42), 37 (93), 36 (54), 27 (31), 12 (13)

Table 3.2 MPI mass spectra of substituted anilines.

Compound	MW	Major Fragments [m/z (% rel. int.)]
2-methylaniline	107	107 (91), 106 (79), 77 (37), 53 (13), 52 (14), 51 (31), 50 (22), 41 (16), 39 (59), 38 (34), 37 (35), 30 (26), 28 (68), 27 (100)
3-methylaniline	107	107 (97), 106 (82), 77 (30), 53 (12), 52 (16), 51 (24), 50 (16), 41 (20), 39 (70), 38 (35), 37 (29), 30 (19), 28 (92), 27 (100)
4-methylaniline	107	107 (94), 106 (43), 77 (39), 53 (12), 52 (14), 51 (27), 50 (24), 41 (10), 39 (49), 38 (37), 37 (46), 30 (14), 28 (67), 27 (100)
2-ethylaniline	121	121 (88), 106 (74), 77 (45), 53 (12), 52 (12), 51 (32), 50 (19), 39 (50), 38 (24), 37 (20), 30 (32), 28 (65), 27 (100)
3-ethylaniline	121	121 (50), 106 (94), 77 (29), 53 (13), 52 (14), 51 (30), 50 (18), 39 (65), 38 (33), 37 (25), 30 (14), 28 (72), 27 (100)
4-ethylaniline	121	121 (85), 106 (95), 77 (99), 53 (21), 52 (14), 51 (31), 50 (15), 39 (59), 38 (25), 37 (15), 30 (18), 28 (75), 27 (100)
2-propylaniline	135	135 (67), 106 (93), 77 (87), 63 (11), 53 (25), 52 (14), 51 (37), 50 (16), 39 (54), 38 (21), 37 (14), 30 (46), 28 (64), 27 (100)
4-propylaniline	135	135 (61), 106 (95), 77 (67), 63 (13), 53 (22), 52 (16), 51 (32), 50 (20), 39 (57), 38 (27), 37 (24), 30 (18), 28 (69), 27 (100)
2-isopropylaniline	135	135 (92), 120 (28), 77 (32), 65 (9), 52 (44), 51 (50), 50 (8), 42 (14), 41 (14), 39 (45), 38 (28), 37 (38), 36 (13), 30 (11), 28 (45), 27 (100), 15 (15), 12 (20)
4-isopropylaniline	135	135 (95), 120 (75), 77 (19), 65 (11), 52 (10), 51 (26), 50 (26), 42 (18), 41 (15), 39 (45), 38 (33), 37 (56), 36 (25), 30 (10), 28 (68), 27 (100), 15 (19), 12 (31)

Table 3.3 MPI mass spectra of substituted phenols.

Compound	MW	Major Fragments [m/z (% rel. int.)]
2-methylphenol	108	108 (87), 107 (27), 90 (48), 79 (55), 77 (59), 53 (17), 51 (30), 50 (17), 39 (60), 38 (25), 37 (16), 27 (100)
3-methylphenol	108	108 (92), 107 (33), 90 (24), 79 (64), 77 (61), 53 (22), 51 (27), 50 (15), 39 (80), 38 (27), 37 (17), 27 (100)
4-methylphenol	108	108 (88), 107 (66), 90 (15), 79 (31), 77 (56), 53 (14), 51 (24), 50 (18), 39 (44), 38 (23), 37 (20), 27 (100)
2-ethylphenol	122	122 (94), 107 (58), 77 (58), 53 (15), 51 (22), 50 (12), 39 (29), 38 (12), 37 (9), 27 (100)
3-ethylphenol	122	122 (97), 107 (61), 77 (35), 53 (12), 51 (18), 50 (15), 39 (33), 38 (19), 37 (22), 27 (100)
4-ethylphenol	122	122 (65), 107 (94), 77 (27), 53 (10), 51 (15), 50 (15), 39 (25), 38 (17), 37 (26), 27 (100)
2-propylphenol	136	136 (99), 107 (93), 77 (65), 53 (15), 51 (22), 50 (13), 39 (28), 38 (14), 37 (12), 27 (100)
4-propylphenol	136	136 (53), 107 (100), 77 (25), 53 (7), 51 (13), 50 (13), 39 (20), 38 (15), 37 (27), 27 (100)

Table 3.3 (Continued) MPI mass spectra of substituted phenols.

Compound	MW	Major Fragments [m/z (% rel. int.)]
2-sec butylphenol	150	150 (67), 121 (81), 77 (98), 51 (88), 50 (57), 39 (48), 38 (30), 37 (44), 36 (16), 27 (100), 12 (10)
4-sec butylphenol	150	150 (49), 121 (88), 77 (30), 51 (38), 50 (40), 39 (64), 38 (46), 37 (83), 36 (47), 27 (100), 12 (27)
2-isopropylphenol	136	136 (91), 121 (39), 77 (61), 51 (49), 50 (27), 39 (28), 38 (16), 37 (28), 36 (10), 27 (100), 12 (13)
3-isopropylphenol	136	136 (81), 121 (42), 77 (34), 51 (26), 50 (23), 39 (56), 38 (34), 37 (52), 36 (20), 27 (100), 12 (15)
4-isopropylphenol	136	136 (58), 121 (79), 77 (19), 51 (32), 50 (38), 39 (49), 38 (35), 37 (86), 36 (45), 27 (100), 12 (33)

To compare isomer discrimination by MPI and EI based on the mass fragmentation patterns, we first examine the capability of MPI and EI for obtaining soft and hard ionization mass spectra for substituted aromatic molecules. As an example, Figure 3.1 shows the mass spectra of 2-ethylphenol as a function of ionization laser power density to illustrate the effect of laser power on the mass spectrum fragmentation pattern. The electron impact mass spectra of the same compound are shown in Figure 3.2. The signal intensity axes in Figures 3.1 and 3.2 are plotted as an actual scale (absolute intensity), rather than in a normalized percentage scale. As Figure 3.1 shows, the overall signal intensity decreases when the laser power is reduced. However, the intensity of the base peak (m/z = 122) does not change significantly when the ionization mode is changed from soft (Figure 3.1B) to hard (Figure 3.1C and 3.1D). In EI, the overall signal intensity is also reduced when the EI beam intensity is decreased, but at a much higher rate. The base peak (m/z = 122) in the soft ionization mass spectrum (Figure 3.2A) is 15 times less intense than the base peak (m/z = 107) in the hard ionization mass spectrum (Figure 3.2C). It should be noted that a high intensity fragment at m/z 107 is obtained along with the molecular ion peak in the EI mass spectrum even at very low electron beam intensity, as shown in Figure 3.2A. However, the MPI mass spectrum shows a molecular peak without any fragmentation at low laser power density (Figure 3.1A). These results suggest that (1) MPI can be used to obtain a soft ionization mass spectrum more readily than EI for this compound and (2) with MPI soft ionization can be obtained without significantly affecting the overall sensitivity, while the sensitivity is reduced significantly for EI soft ionization. Clearly, both EI and MPI soft ionization cannot be used for isomer discrimination due to the lack of fragmentation.

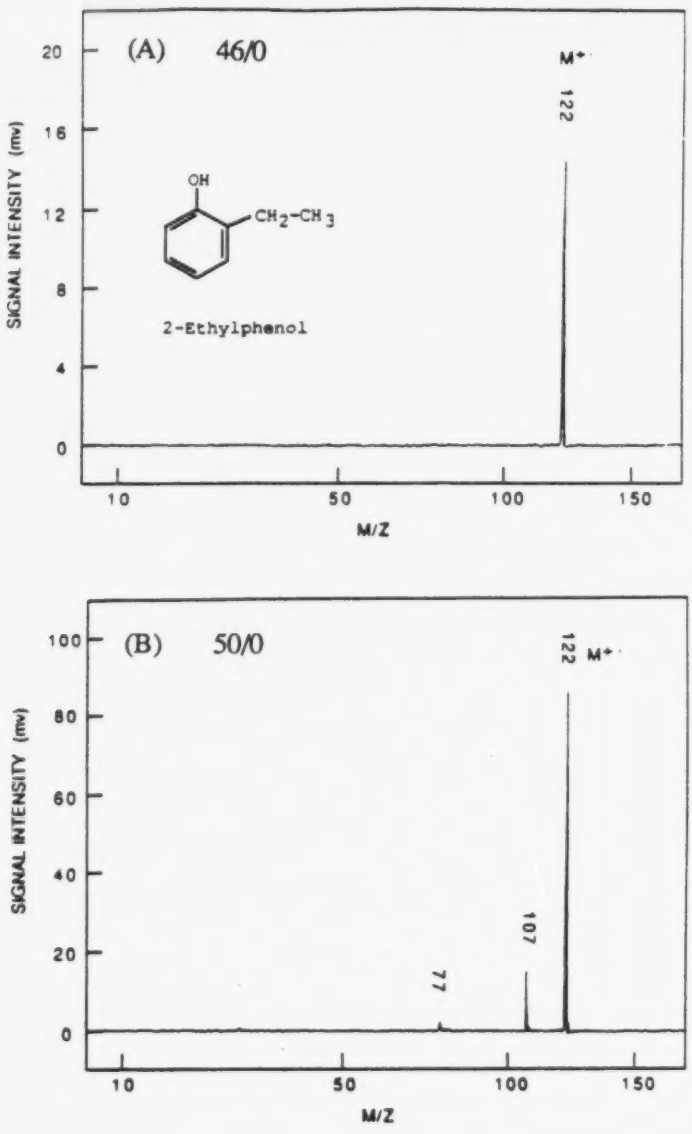

Figure 3.1 Mass spectra of 2-ethylphenol obtained by multiphoton ionization at 266 nm. The ionization laser power density was (A) $1x10^6$ W/cm^2 and (B) $4x10^6$ W/cm^2. The number such as 46/0 in (A) indicates the actual readings from the laser power panel for the oscillator (46 mJ/pulse at 1064 nm) and amplifer (0 mJ/pulse) from the Nd:YAG laser.

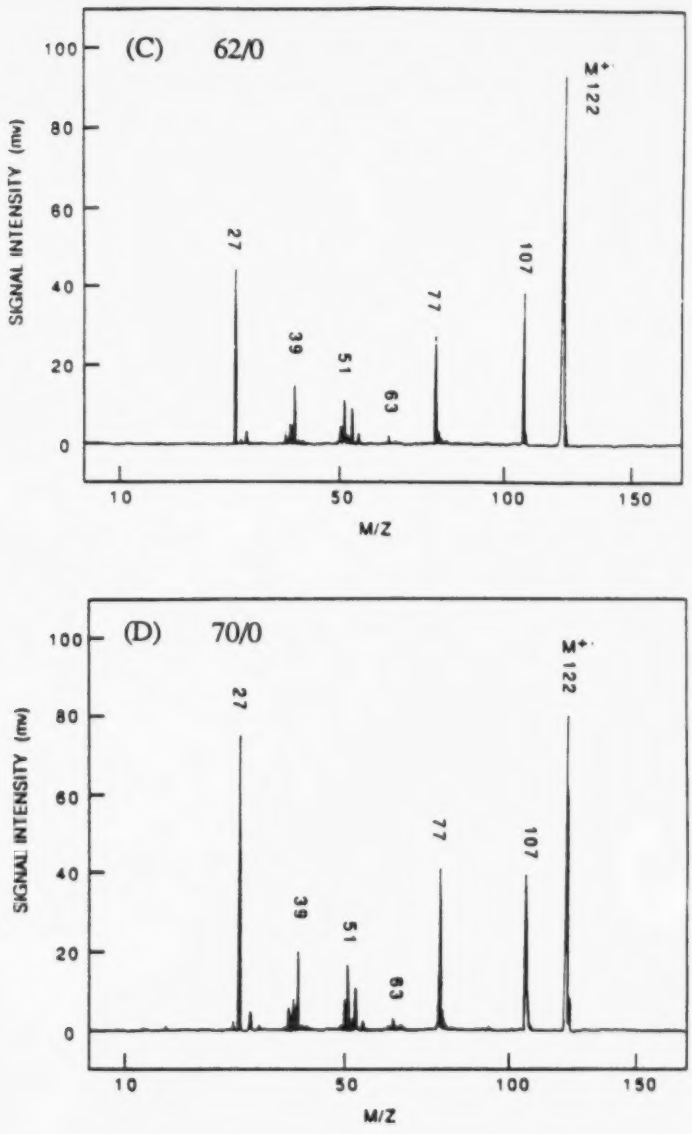

Figure 3.1 (Continued). Mass spectra of 2-ethylphenol obtained by multiphoton ionization at 266 nm. The ionization laser power density was (C) $8x10^6$ W/cm^2 and (D) $1x10^7$ W/cm^2. The number such as 62/0 in (C) indicates the actual readings from the laser power panel for the oscillator (62 mJ/pulse at 1064 nm) and amplifer (0 mJ/pulse) from the Nd:YAG laser.

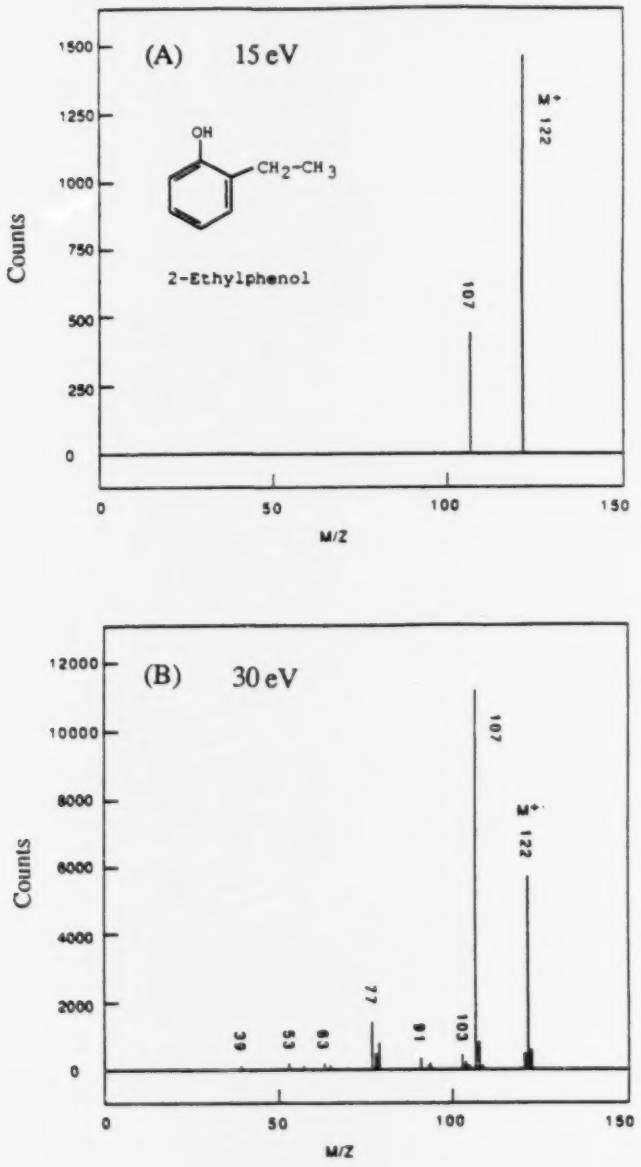

Figure 3.2 Mass spectra of 2-ethylphenol obtained by electron impact ionization. The electron beam intensity is (A) 15 eV and (B) 30 eV.

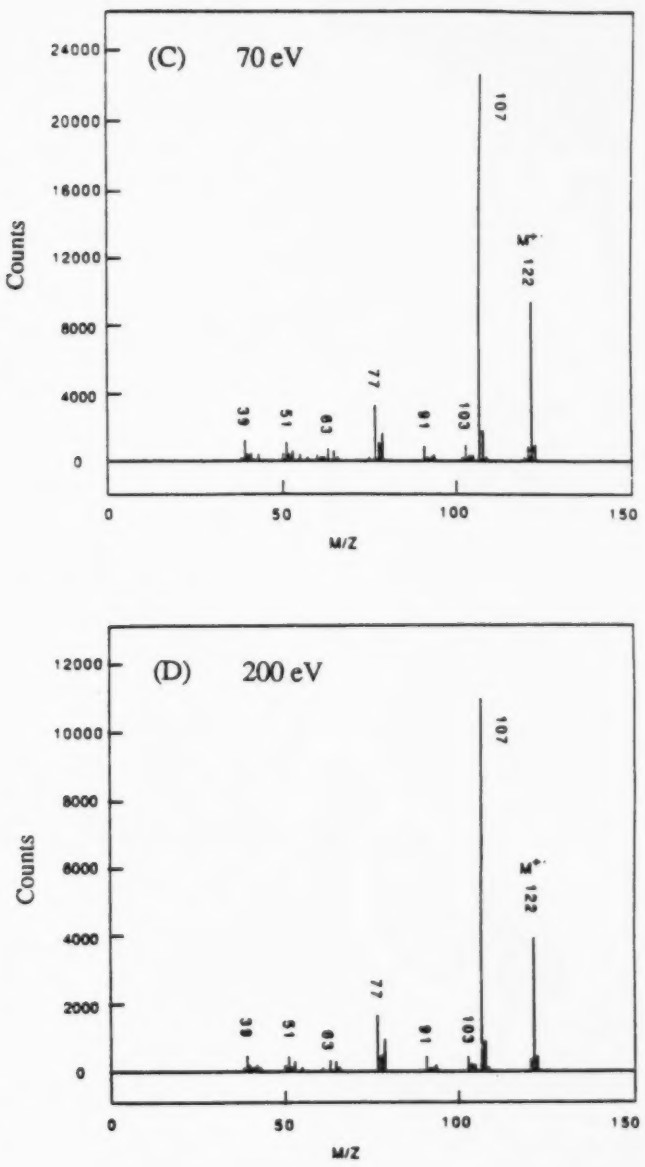

Figure 3.2 (Continued). Mass spectra of 2-ethylphenol obtained by electron impact ionization. The electron beam intensity is (C) 70 eV and (D) 200 eV.

However, as Figure 3.1 illustrates, MPI can generate extensive fragmentation not only in the high-mass region but also in the low-mass region (m/z < 100). Highly intense peaks corresponding to H^+, C^+ and $C_nH_n^+$ are observed at very high laser power density. This is different from the EI technique. As illustrated in Figure 3.2, even when the electron beam intensity is at 200 eV, the peak intensities of most fragments in the low-mass region are less than 5% of the base peak. In fact, when the electron beam intensity is increased above 70 eV, no significant increase in the intensities of the smaller fragments are found. Note that because resonant enhanced MPI is a very selective ionization method, background molecules such as pump oil and certain solvents do not ionize. Therefore, the MPI mass spectrum in the low-mass region is extremely reliable for the interpretation of molecular structure. Obtaining highly intense low-mass fragments is particularly important for isomer discrimination. However, the results shown in Tables 3.1-3.3 indicate that some isomer pairs (i.e. all substituted PAHs) have almost the same mass fragmentation patterns, whereas other isomer pairs (i.e. isobutylphenols) have different patterns in the low-mass region. This difference may be explained by examining the fragmentation process.

Isomerization and Fragmentation: For the generation of small fragments with MPI, there are at least two cases to be considered, depending on the rates of isomerization and fragmentation [66,68]. In the first case, the fragmentation process is faster than isomerization. The lack of isomerization allows one to identify the isomers based on the structure specific mass fragmentation patterns generated from different isomers. In the second case, isomerization of the parent ions precedes fragmentation. That is, immediately after being generated by the laser in the ionization region of the TOFMS, parent ions from isomers rearrange into some precursors. These then dissociate into small fragments either by the excess internal energy gained from the

initial ionization process or by the absorption of additional photons. If the precursors have a common structure, then the MPI mass spectra of the isomers will be indistinguishable. However, if the precursors have different structures, then the mass spectra generated from isomeric pairs may differ from each other. Consequently one may discriminate these isomers based on their mass spectra. This interesting result is examined more closely below.

In the first case, isomeric pairs are ionized and fragmented without random isomerization on the time scale (less than 10 ns) of interaction between molecules and the laser beam. This is the case for the isomeric n-butyl and isobutyl iodides (C_4H_9I) studied by Bernstein [65] and Neusser and Schlag [66]. They have shown that although the EI mass spectra for these two compounds are almost the same, the MPI mass spectra are different. It is believed that during the MPI process a larger amount of energy with a narrower energy distribution can be deposited in an ion than in the case of EI excitation.

In the second case, isomerization of the parent ion takes place before fragmentation during the MPI process. Studies of MPI mass spectra of polycyclic aromatic hydrocarbons (PAHs) show that isomers of PAHs give almost identical fragmentation patterns [33]. We have studied several pairs of substituted PAH isomers (see Table 3.1) at various conditions. In our system, samples can be introduced into the TOFMS by laser desorption [1,11], fast atom bombardment (see chapter 4) [17], pulsed rapid heating (see chapter 5) [18], or directing heating with or without a supersonic jet. We found that the MPI mass spectra for the above mentioned isomers were the same no matter what sample volatilization technique was used and whether or not the supersonic jet technique was employed. An example is given in Figures 3.3 and 3.4 for the soft

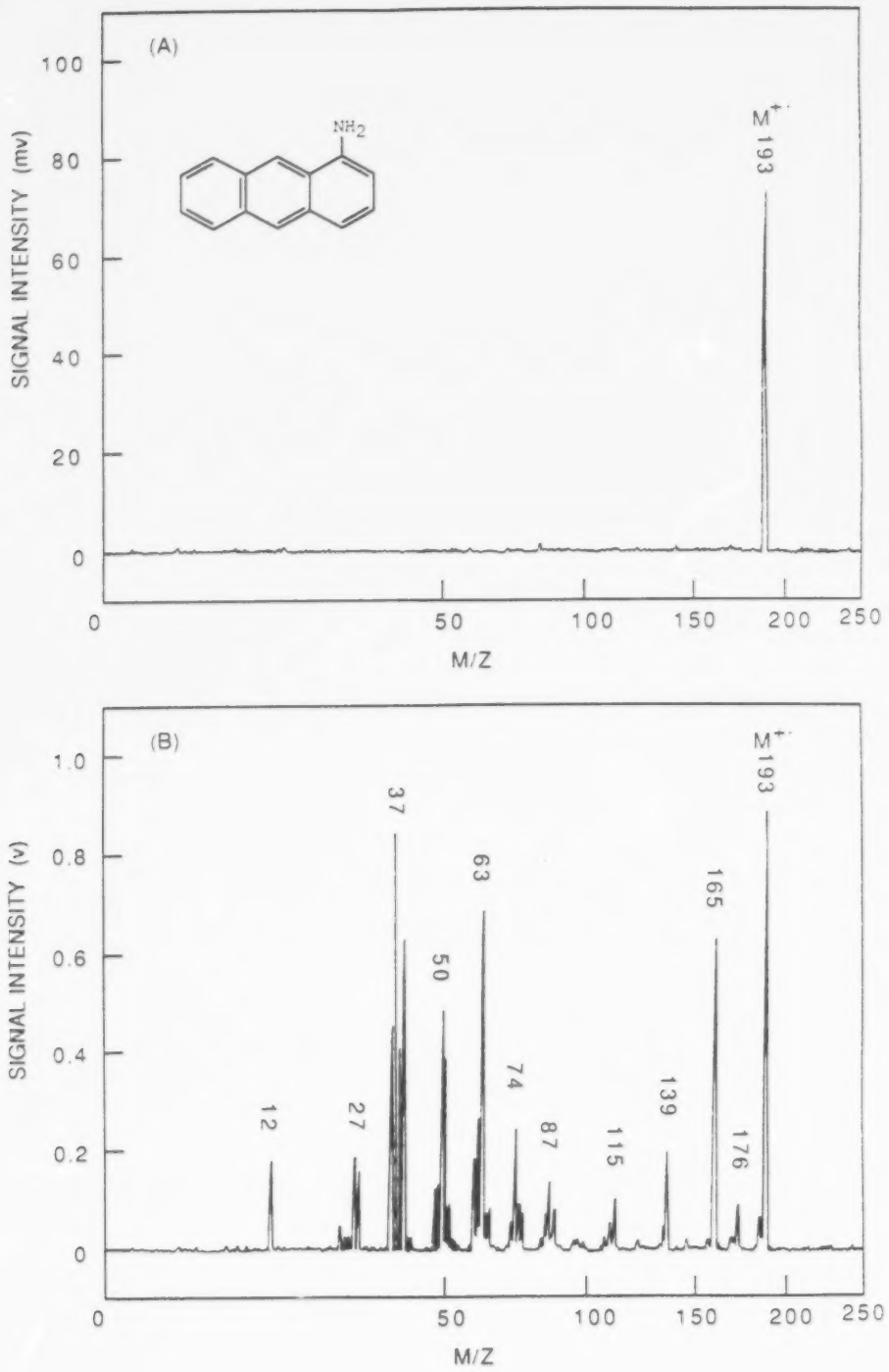

Figure 3.3 Soft and hard ionization MPI mass spectra of 1-aminoanthracene obtained by using a 266-nm laser beam for ionization with a laser power density of (a) $1x10^6$ W/cm^2 and (b) $1x10^7$ W/cm^2.

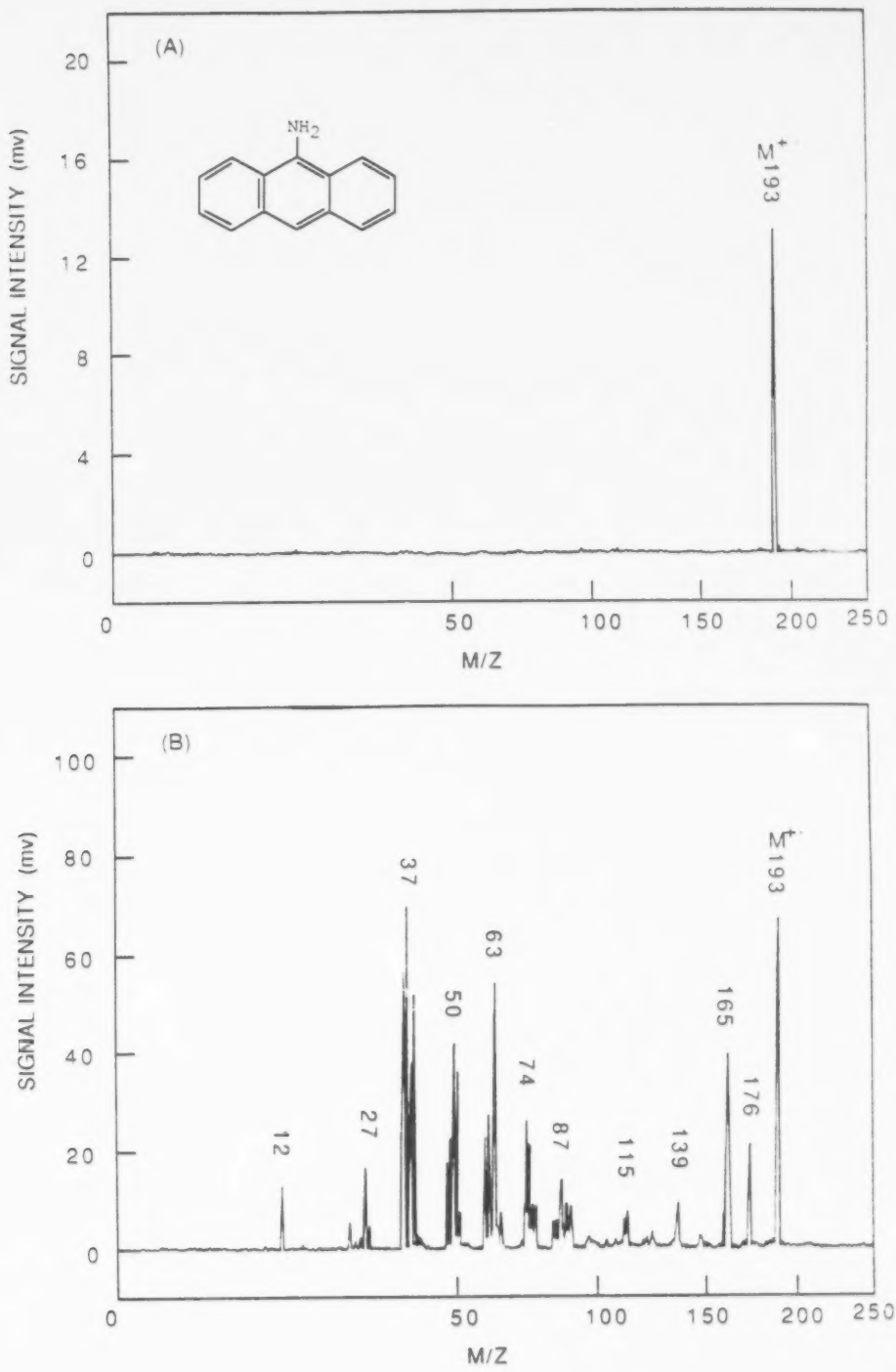

Figure 3.4 Soft and hard ionization MPI mass spectra of 9-aminoanthracene obtained by using a 266-nm laser beam for ionization with a laser power density of (a) $1x10^6$ W/cm^2 and (b) $1x10^7$ W/cm^2.

and hard ionization mass spectra of amino-group substituted anthracenes. As Figures 3.3 and 3.4 show, the MPI mass spectra of 1-aminoanthracene and 9-aminoanthracene are almost the same. The reason for obtaining almost identical mass spectra for these isomer pairs is believed to be that isomerization of the parent ions into a common structure takes place prior to fragmentation in the same manner as in the cases of unsubstituted PAHs [33,69].

Now, if the precursors generated by isomerization from isomer pairs are structurally different, then isomer identification may become possible. The precursors can be the ions with the same mass as the parent ions. The precursors can also be intermediate fragment ions which are generated from the molecular ions with the loss of neutral/radical species either during the isomerization process or prior to the isomerization process. Figure 3.5 shows the MPI mass spectra of one isomeric pair: 2-isopropylphenol and 4-isopropylphenol. The EI mass spectra for the same compounds are shown in Figure 3.6. Figures 3.5 and 3.6 illustrate that, unlike EI, MPI is capable of generating a large number of small fragments. The EI mass spectra for these two pairs of isomers are very similar. However, the MPI mass spectra for these isomers are different. We believe that different isomeric precursors (see below) are produced during the MPI and EI process from these ortho and para alkyl-substituted phenols and anilines. Due to the lack of high-intensity small fragments from the precursors in the EI mass spectra, it is difficult to reveal the structure difference between these isomeric precursors. However, in MPI, the large number of small fragments with relatively high intensities can provide sufficient difference in the mass fragmentation pattern to permit the distinction of isomeric molecules.

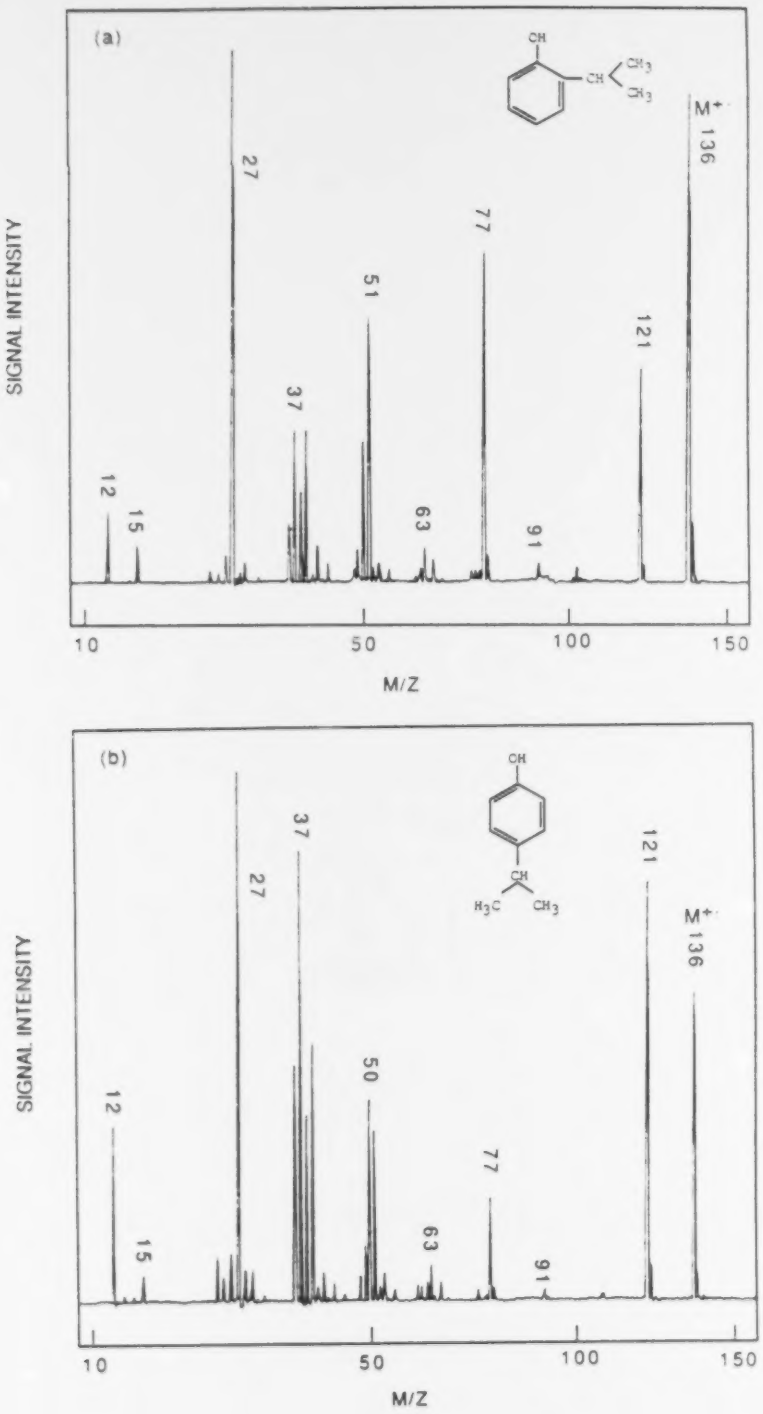

Figure 3.5 MPI mass spectra of (a) 2-isopropylphenol and (b) 4-isopropylphenol obtained by using a 266-nm laser beam for ionization with an approximate laser power density of 1×10^7 W/cm^2.

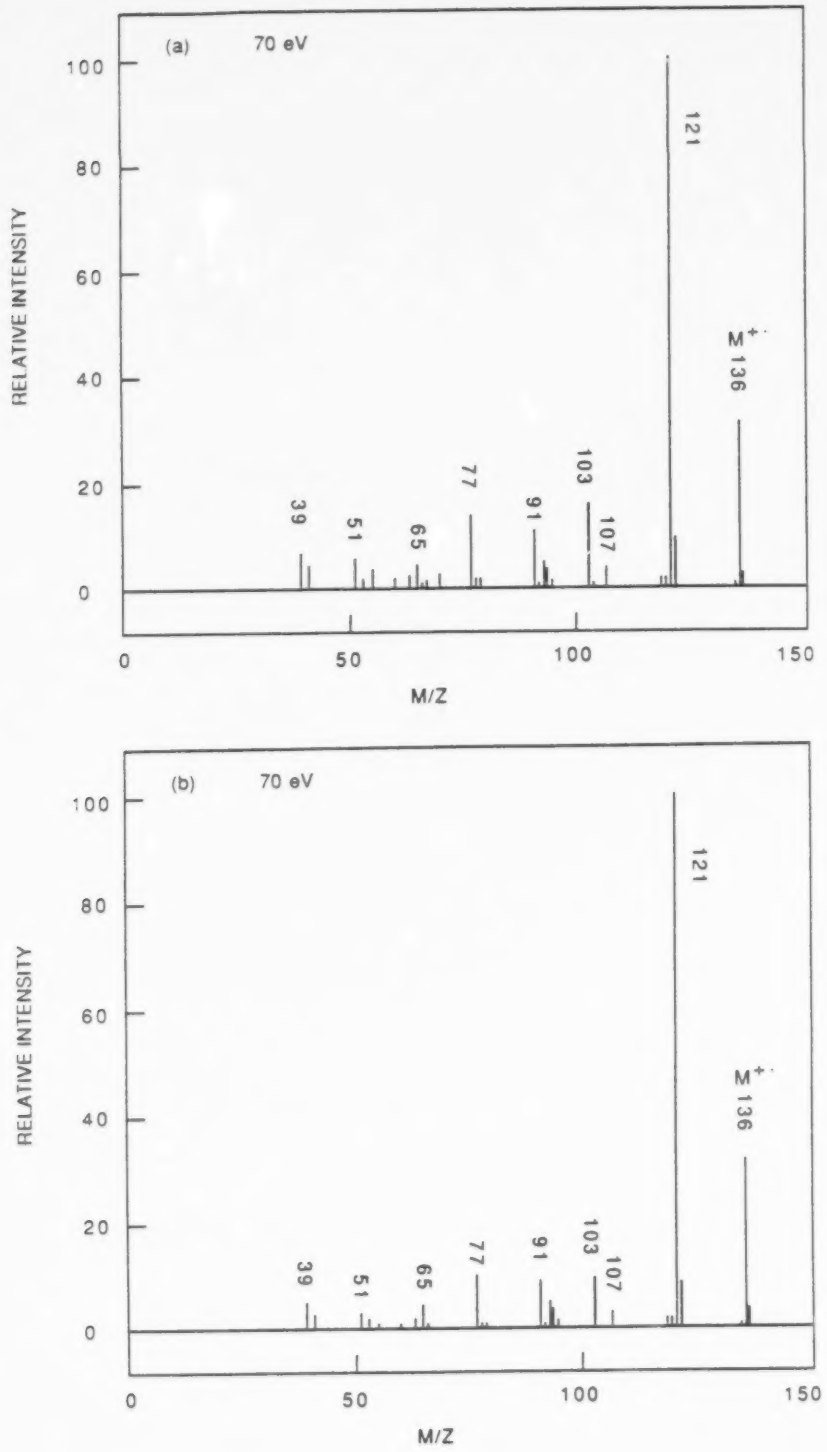

Figure 3.6 EI mass spectra of (a) 2-isopropylphenol and (b) 4-isopropylphenol. The electron beam intensity is 70 eV.

Fragmentation of Anilines and Phenols: Scheme 3.1 shows the ionization processes for the generation of tropyliums from alkyl-substituted anilines and phenols. Here we propose that tropylium is the precursor for further fragmentation. In our study, the formation of tropylium can be used to account for the mass spectral differences between some isomeric pairs. As Scheme 3.1 shows, if Y is a hydrogen such as in the cases of methyl-, ethyl-, propyl-, and butyl-substituted anilines and phenols, then the structures of the three tropyliums (A,B,C in Scheme 3.1) are the same. Consequently, the mass spectra in the low-mass region for ortho, meta, para alkyl-substituted phenols or anilines would be the same. Indeed, the mass fragmentation patterns for these isomeric pairs shown in Table 3.2 and 3.3 are almost the same. Now, if Y is an alkyl group such as a methyl- or ethyl- group, then one should expect that isomeric tropyliums have different structures. Thus the fragments from these isomeric tropyliums may be different in terms of relative intensity and/or type of fragments. This is the case for isopropyl phenols (see Figure 3.5), isopropyl anilines, and sec-butyl phenols shown in Table 3.2 and 3.3. The mass fragmentation pattern for these isomeric pairs are different.

Scheme 3.2 illustrates the proposed fragmentation processes of 4-isopropylphenol after it absorbs two or more laser photons. The number of photons involved in the generation of a particular ion can be found by studying the relationship between the ion signal intensity and the laser power [70-72]. The molecular ion (m/z = 136) is generated from a two-photon process. Although the ionization potential (IP) for 4-isopropylphenol is unknown, it is reasonable to assume that this molecule's IP is close to that of p-cresol (IP = 8.92 eV) [12] due to their structural similarity. Thus, it is not surprising that the molecular ion is generated by resonant two-photon ionization process at 266 nm (two photon energy = 9.2 eV). The peak at m/z 121 is generated

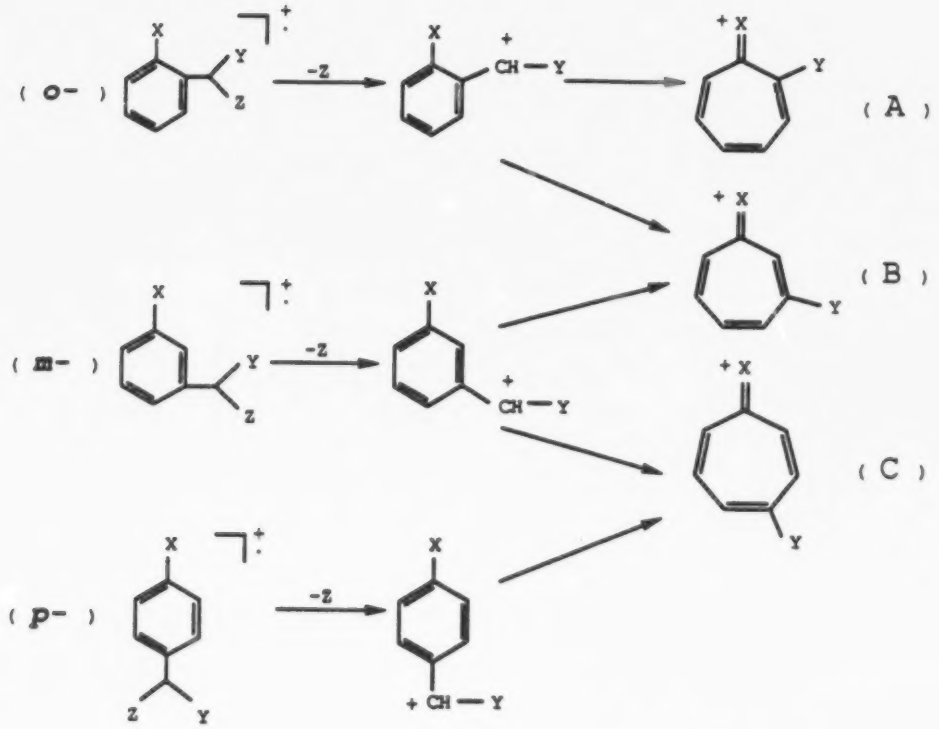

Scheme 3.1

Fragmentation of anilines and phenols.

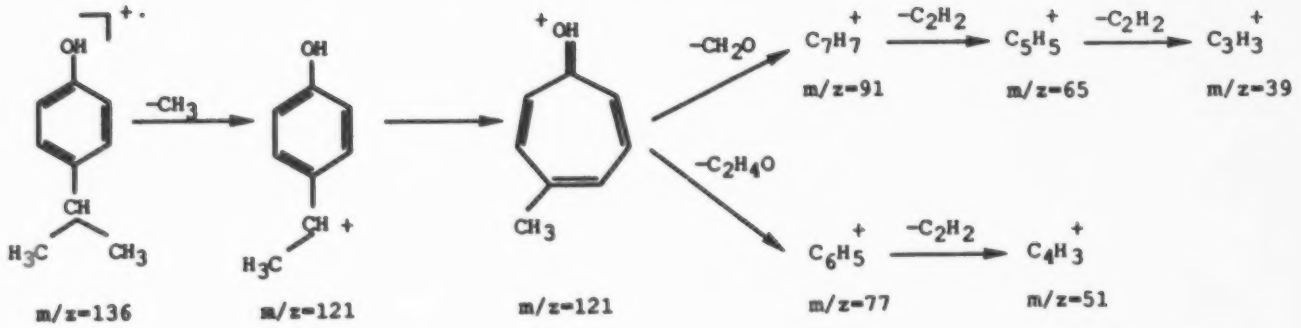

Scheme 3.2

Proposed fragmentation process for 4-isopropylphenol after the absorption of two or more laser photons.

from the molecular ion by absorbing one additional photon. This indicates that the appearance energy of this species is in between 9.2 to 13.8 eV. The fragment ions at m/z 91 and 77 are generated from a four-photon process. Major fragments from the five-photon process include ions at m/z 65, 51 and 39. The peak at m/z 27 is from a six-photon process. By replacing the hydrogen in the OH group of 4-isopropylphenol with deuterium, it is found that the m/z 121 peak shows the deuterium effect while smaller fragments such as m/z 77, 51, 39, etc. remain the same. Thus it is believed that the hydrogen atom from the OH group does not rearrange to the benzene ring and the smaller fragments do not contain the OH group.

Power dependence of the fragments and the deuterium effect are also studied for 2-isopropylphenol and the same results as that for 4-isopropylphenol are obtained. Thus, the isomer pair of isopropylphenol may have similar fragmentation pathways. Since the structures of the tropyliums for these two isomers are different, the generation of smaller fragments from the tropylium is also different. As Figure 3.5 shows, the ratio of the intensities of the peaks at m/z 37 and 39 to those of m/z 50 and 51 is significantly different for 2-isopropylphenol and 4-isopropylphenol. Although the relative intensity of the molecular ion peak (m/z 136) and M-15 peak can be changed by varying the ionization laser power density, the peaks at m/z 37 and 39 are always more intense than the peak at m/z 50 and 51 for 4-isopropylphenol and less intense than m/z 51 for 2-isopropylphenol. Thus, based on the relative intensity of peaks at m/z 37 and 39 and m/z 50 and 51, we can differentiate these two isomers. Note that the mass fragmentation pattern for 3-isopropylphenol (see Table 3.3) appears to be a combination of the patterns of 2- and 4-isopropylphenol. This supports our assumption that tropylium may be the intermediate precursor for further fragmentation. However,

more studies including the use of ^{13}C labeled compounds are needed to conclusively elucidate the fragmentation processes.

3.4 Conclusion

From studies of the MPI and EI mass spectra of positional aromatic isomers, we can conclude the following points:

(1) Soft ionization can readily be obtained with MPI at low laser power density for the above mentioned positional isomers. Although the base peak intensity generally increases when the laser power increases, the change is not very significant. Although the EI technique can also produce relatively soft ionization conditions, the intensity of the base peak is reduced significantly when the electron beam intensity is reduced from 70 to 15 eV.

(2) MPI can generate extensive fragmentation for structural analysis. Compared with EI, MPI is capable of producing fragment ions in the low-mass region with much higher intensity. These fragments are found to be valuable for isomer discrimination. We show that some isomeric pairs of alkyl-substituted anilines and phenols can be differentiated based on differences in the fragmentation patterns in the low-mass region. Although the type of fragments generated by EI and MPI appear to be similar because both produce molecular radical cations ($M^{+\cdot}$), the difficulty in generating a sufficient number of small fragments by EI limits its use for revealing the small structural differences present in isomeric pairs.

(3) For the positional isomers studied in our experimental setup, isomerization of the ring structure may occur during the fragmentation process. This isomerization is either from the parent ion itself or some fragment from the parent ion with the loss of all or part of the substituted group. For most positional isomers, the isomerization process generates a common precursor for further fragmentation, resulting in the same fragmentation pattern. Thus it is difficult to discriminate the isomers based on the mass fragmentation pattern. However, if the aromatic ring isomerization process produces a different precursors from the isomer pair, then it is possible to use MPI to discriminate the isomers based on the mass fragmentation patterns in the low-mass region.

(4) Fragmentation processes of alkyl-substituted anilines and phenols are based on the number of photons involved during the generation of fragment ions and the isotope effect. Tropyliums are proposed as intermediate fragments. Positional isomers of linear-alkyl substituted anilines and phenols generate the same tropylium structure. Because these compounds have the same fragmentation pattern in the low-mass region, it is difficult to discriminate these isomers. However, the aromatic ring isomerization of some positional isomers such as isopropylaniline generates structurally different tropyliums from the isomeric pair. The fragmentation of the tropyliums results in different patterns in the low-mass region. Thus isomers can be differentiated in this case.

Chapter 4

Pulsed Fast Atom Bombardment Sample Desorption with Multiphoton Ionization in a Supersonic Jet / Reflectron Time-of-Flight Mass Spectrometer

4.1 Introduction

A two-dimensional detection scheme based on jet-cooled R2PI wavelength (optical) spectra and multiphoton ionization (MPI) mass spectra can provide a powerful means of molecular identification and structural analysis with high sensitivity and selectivity, as already discussed in chapter 1. However, in the past MPI and supersonic jet (SJ) spectroscopy were generally used for probing gas phase molecules, hence studies were limited to volatile molecules. In order to extend these two techniques to the study of thermally labile biochemicals, a method for desorption/vaporization without thermal decomposition is required. Among the many techniques, laser desorption (LD) has been successfully used to entrain biological molecules into jet expansions [15,16]. In LD, a pulsed laser (i.e. CO_2 laser) is used to desorb molecules from a substrate placed close to the supersonic nozzle orifice. The molecules are then entrained into a pulsed supersonic jet and carried into a time-of-flight mass spectrometer (TOFMS) where the ionization takes place. The LD/SJMPI technique has been used for the study of biological molecules [1,11] such as catecholamines, indoleamines and their metabolites, drugs, amino acids, small peptides, and nucleosides.

In this chapter an alternative method is described for introducing thermally labile and nonvolatile molecules into supersonic jet expansions. The technique used herein is fast

atom bombardment (FAB) [73]. Instead of using photons from a high-power laser, we have used a FAB gun to generate fast atoms to desorb sample molecules. We demonstrate here that, as in LD, small biological molecules can be readily desorbed and entrained into a supersonic jet without significant thermal decomposition by using FAB. However, one of the advantages of this FAB method is that the FAB gun can be easily constructed and maintained at a small fraction of the cost of the desorption laser used in the LD method.

Although one may directly combine FAB with MPI post ionization without the use of a supersonic jet, there are several advantages to the use of a supersonic jet for sample delivery. One of the important advantages is that it provides a means to cool the gas-phase molecules [41] so that a high resolution jet-cooled wavelength (optical) spectrum can be obtained. The rapid cooling of molecules also prevents gas-phase biological molecules from thermal decomposition before they are ionized [29]. Another advantage is that the desorption region in which gas-phase molecules are generated can be spatially separated from the ionization region. This is particularly important for the FAB experiment described here. In the FAB method, glycerol or other liquid matrices are often used for sample deposition on a substrate for the desorption [73]. If the sample along with the matrix is directly placed between the high voltage repeller plate and extracting grid in a TOFMS, the matrix may cause some problems such as arcing [74,75]. A design by Cotter using a grounded source, called pulsed extraction TOFMS, can eliminate these problems and has been successfully used for biological molecule detection and for the study of the desorption mechanism [74]. However, if the desorption and post ionization are performed in the same extraction region, then the ions directly formed from the desorption process may interfere with the ions generated from the neutrals. This is especially true if a high flux ion or FAB gun is used in order

to generate enough sample vapor for obtaining a whole mass spectrum from one pulse. Hence, in this work the desorption and ionization are separated in space and time.

In this chapter, the experimental setup for the FAB/SJMPI technique is described. The capabilities of this method for the detection of thermally labile and nonvolatile molecules are examined. In addition, the analytical power of this technique is demonstrated by studying sensitivity and selectivity. The ability of this technique for the selective detection of the active substance in a drug tablet is also demonstrated. Finally, the effect of sample chemical properties on the desorption and ionization processes is discussed.

4.2 Experimental

The experimental setup for fast atom bombardment/supersonic jet multiphoton ionization (FAB/SJMPI) is discussed in section 1.7. In brief, it consists of an angular reflectron time-of-flight mass spectrometer [17-21,58], a pulsed nozzle, a pulsed saddle-field FAB gun [76,77], and 266 nm laser ionization.

A saddle-field FAB gun is so constructed that it can fit into the test chamber through a 2" flange and placed close to the nozzle orifice. The distance between the FAB gun outlet and the nozzle orifice is about 40 mm. The distance between the FAB gun and the center axis of the jet is also about 40 mm. A 5 mm or 10 mm-in-diameter sample probe made of machinable Macor ceramic is located at about 20 mm away from the center axis of the jet. About 100 μg sample is generally used and placed on the sample probe directly by either wetting or dissolving the compound in a solvent (i.e. methanol) and coating on the surface with the use of a spatula. Although glycerol can be used as a matrix, we have found that in this study sample desorption can be performed and mass

spectra obtainable over a short period of time (more than 100 pulses) without the use of glycerol. Thus, for the compounds studied herein, glycerol was not used.

Argon or xenon is used in the saddle-field discharge for the FAB gun. The anode potential is fixed at 10 kV and, by adjusting the pressure in the gun, the discharge current varies from 1 to 5 mA. We have found that for chemicals with a high melting point it is necessary to use a higher discharge current in order to desorb a sizable amount of neutrals for laser post desorption ionization. The size of the FAB beam is approximately 1.5 mm in diameter as determined by examining the dark image created on thermal-sensitive paper after the paper has been briefly exposed to the FAB beam. The high voltage power supply for the FAB gun, a Spellman Model RHSR15PN60, can be operated in a continuous mode or a pulsed mode using an external trigger system.

The actual sequence of events is controlled by several delay generators. The FAB gun is first turned on to desorb the sample, the pulsed nozzle opens to form a supersonic jet, and then the sample is entrained into the jet and carried into the ionization region of the TOFMS. The selection of the experimental repetition rate (0.1-20 Hz) is mainly dependent on the pulse width of the FAB power supply. For most of the compounds reported herein, the pulse width is adjusted to be 300 ms with a 100-μs rise-time and 100-μs fall-time. Thus the repetition rate of the experiment is optimized at 3 Hz.

One of the parameters which we have not optimized for the current system is the duty cycle. There are several factors affecting the overall duty cycle. With a TOFMS, the ion detection duty cycle is very high since all ions can be detected in one single pulse. However, the duty cycle for the generation of ions is dependent on the pulse widths and repetition rates of the FAB desorption and the ionization laser beam. It also depends on

the pulse profile of the neutral molecules desorbed by FAB. One of the major factors limiting the duty cycle of our current system is the pulse width (~ 300 ms) of the FAB gun. To study the feasibility for the generation of a short pulsed neutral beam from the saddle-field FAB gun, we constructed a pulsed power supply which can generate a 10 kV pulse with a 10-μs pulse width and 5-μs fall and rise time to drive the FAB gun. In a double-sector MS, this FAB gun is used to desorb CsI and an ion signal profile is obtained by monitoring the signal intensity of Cs^+. We have found that the ion signal profile is almost exactly the same as the pulse shape of the voltage applied to the gun. However, we have found that this power supply with pulse peak current less than 1 mA is unable to generate enough power to drive the FAB gun to desorb enough neutrals for MPI/SJS experiments. Design and construction of a high power, short-pulsed power supply is planned. Nevertheless, this result demonstrates that a short (< 20 μs) pulsed FAB beam can be obtained with a saddle-field FAB gun. Thus it seems possible to obtain a short pulsed neutral beam to desorb molecules from insulators such as polymers without charge build-up on the surface, which is believed to be a problem generally found in ion beam desorption experiments [78].

All chemicals were purchased from Sigma Chemical Co., St. Louis, MO or Aldrich Chemical Co., Milwaukee, WI and used without further purification.

4.3 Results and Discussion

The mass spectra of tryptophan obtained by using fast atom bombardment sample desorption with multiphoton ionization at different laser power densities are shown in Figure 4.1. Tryptophan is known to be thermally labile [79]. However, Figure 4.1 demonstrates that a molecular ion peak can be readily obtained with no thermal decomposition products. Although the actual mechanism for the generation of neutrals

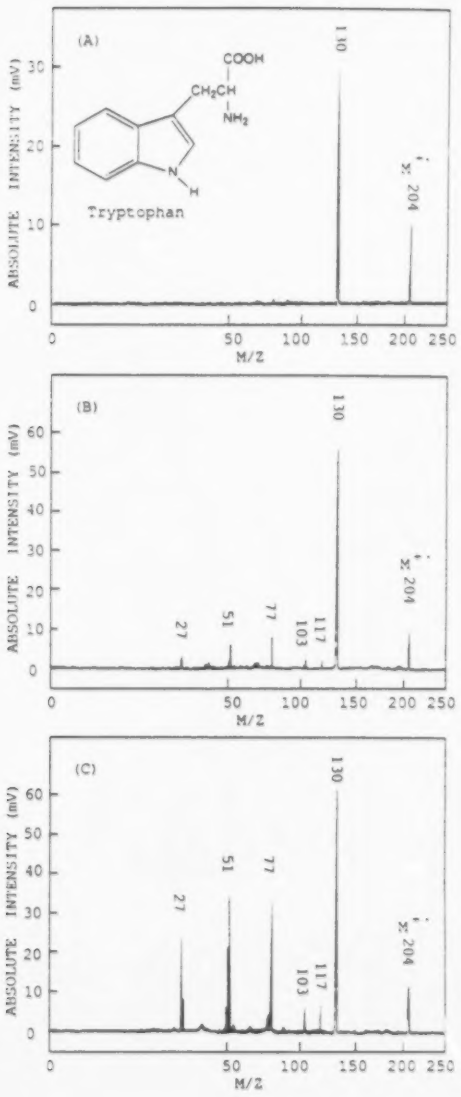

Figure 4.1 Mass spectra of tryptophan obtained by the fast atom bombardment/ supersonic jet multiphoton ionization technique at 266 nm. The ionization laser power density was (A) $1x10^6$ W/cm^2 (B) $4x10^6$ W/cm^2 and (C) $8x10^6$ W/cm^2.

is not completely understood, the rapid heating/sputtering induced by FAB can be used to introduce thermally labile biological molecules into a supersonic jet for multiphoton ionization. Other molecules, including amino acids, carboxylic acids, catecholamines, neuroleptic drugs, pineal indoles, small peptides and polycyclic aromatic hydrocarbons (PAHs), studied by this technique are shown in Table 4.1. In these experiments, sample molecules are desorbed by a pulsed FAB beam in a 1.5 mm diameter spot and post desorption ionization is performed with a 266 nm laser beam. The pulsed power supply for the FAB gun is adjusted so that the potential is 10 kV and the discharge current ranges from 1 to 5 mA. Although the actual power density of fast atoms impinging on the sample probe is unknown, we believe that the atom flux is very intense (> 10 $\mu A/cm^2$) [77]. As Figure 4.1 illustrates, the molecular ion, with no or little fragmentation, can be observed if the ionizing laser power is low. When the laser power density is increased, a mass spectrum with fragment ions can be obtained, which can be used for structural analysis. This important feature of MPI is also observed for most of the other compounds studied herein. Note that the axis of signal intensity in Figure 4.1 is plotted as an actual scale in mV, rather than as a normalized percentage scale. This shows that the overall signal intensity decreases when the laser power is reduced, a common characteristics of MPI.

Another key result is that, as shown in Table 4.1, PAHs can readily be studied by FAB/SJMPI. Figure 4.2 shows the MPI mass spectrum of rubrene (MW 532; mp > 315°C) obtained by using about 100 μg sample with FAB desorption sample introduction. The ionization laser power density is about $1x10^6$ W/cm^2 at 266 nm. Since the mass resolution is generally above 2000, the isotope composition can be easily revealed (see the insert in Figure 4.2). The peak at m/z 455 is the fragment from the molecular ion minus one benzene radical $(M-77)^+$. The fragment ion peak at m/z

Table 4.1 Compounds Studied by the Fast Atom Bombardment/ Supersonic Jet Multiphoton Ionization Technique

1. **Amino acids:**
   (1) Phenylalanine
   (2) Tryptophan
   (3) Tyrosine

2. **Carboxylic acids:**
   (1) Anthranilic acid
   (2) 3-Amino-4-hydroxybenzoic acid
   (3) Indole-3-acetic acid

3. **Catecholamines:**
   (1) Dopa
   (2) Dopamine
   (3) Synephrine

4. **Neuroleptic drugs:**
   (1) Chlorpromazine
   (2) Desipramine
   (3) Imipramine

5. **Pineal indoles:**
   (1) Harmaline
   (2) Melatonin
   (3) Tryptamine

6. **Peptides:**
   (1) Trp-Ala
   (2) Trp-Gly
   (3) Trp-Leu
   (4) Gly-Trp
   (5) Tyr-Ala
   (6) Tyr-Gly
   (7) Tyr-Leu
   (8) Phe-Gly
   (9) Trp-Gly-Gly
   (10) CBZ-Gly-Leu
   (11) CBZ-Ala-Gly
   (12) Gly-Tyr-amide

7. **PAHs:**
   (1) 2-Aminoanthracene
   (2) 9-Aminophenanthrene
   (3) Benzo[e]pyrene
   (4) Carbazole
   (5) 2-Chloroanthracene
   (6) Chrysene
   (7) Decacyclene
   (8) Perylene
   (9) Rubrene
   (10) Triphenylene

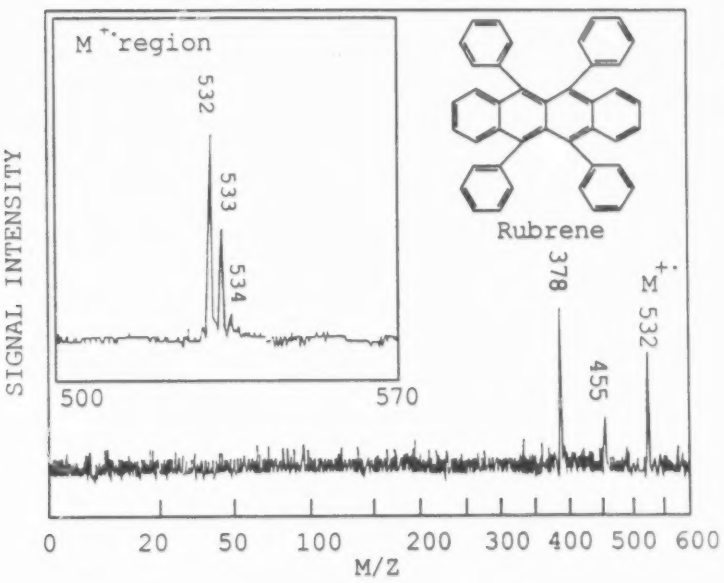

Figure 4.2 Mass spectrum of rubrene (MW 532) obtained by FAB/SJMPI at 266 nm. The laser ionization power density was ~ $1x10^6$ W/cm^2. The molecular ion region is shown in the insert.

377 arises from the molecular ion by the loss of two benzene radicals with one H migration $(M-154+H)^+$. Note that due to the nonpolar nature of PAHs, their mass spectra are extremely difficult to obtain by direct FAB ionization [80]. Combined with HPLC (for instance, via a continuous-flow FAB probe [81]), this technique seems to be a promising method for the detection of high molecular weight or thermally labile PAHs, which are not currently amenable to GC/MS or direct FAB.

Table 4.1 also lists some dipeptides we have studied with the FAB/SJMPI technique. These peptides were also examined by laser desorption/supersonic jet MPI (LD/SJMPI). The LD/SJMPI study was carried out with a pulsed CO_2 laser (Allmark model 852, A-B lasers Inc., Acton, MA) which generates 10.6 μm IR radiation with a 75-ns initial pulse and 2-μs tailing. The repetition rate of the laser can be adjusted from 0.1 Hz to 15 Hz, although 10 Hz rep-rate is used here. In LD/SJMPI, the FAB gun is replaced by a 1-cm diameter NaCl window in a 2" flange. The IR beam from the CO_2 laser is reflected by copper mirrors protected with gold coating (CVI Laser Corp., Albuquerque, NM) and focused on the sample probe by a germanium plano convex lens (Janos Technology Inc., Townshend, VT).

Figure 4.3 shows the mass spectra of Gly-Trp obtained by FAB/SJMPI (Figure 4.3A) and by LD/SJMPI (Figure 4.3B) along with proposed fragmentation patterns. Interestingly, for some of the dipeptides studied by FAB/SJMPI, as the example shown in Figure 4.3A, the molecular ion peak ($M^{+\cdot}$) is rather small (generally < 20%), but the ion peak at 18 mass units lower (M-18) is the dominant ion in the mass spectrum. Note that small peptides have been previously studied by LD/SJMPI [11,45,60,82,83] and, in some cases, the M-18 peak was also found to be the dominant one (see chapter 6). The M-18 peak was carefully examined [82] and believed to be from the thermal

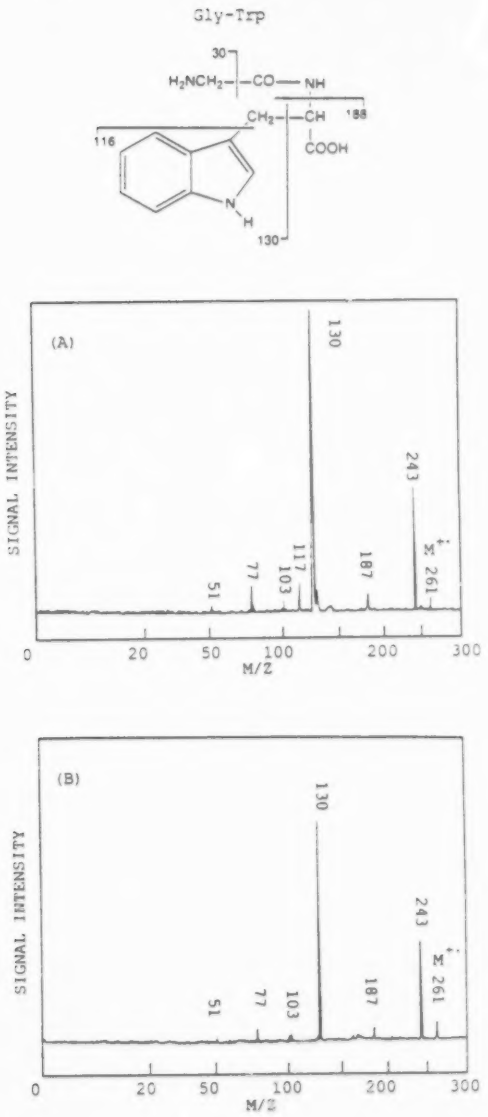

Figure 4.3 Comparsion of MPI mass spectra of Gly-Trp at 266 nm obtained by (A) using the fast atom bombardment method and (B) using the CO_2 laser desorption method for sample introduction into the supersonic jet expansion. The ionization laser power density was about $1x10^6$ W/cm^2.

decomposition product, i.e. cyclodipeptide, during the laser desorption process. This study shows that generation of the M-18 peak is not unique to the IR laser desorption experiment and suggests that the cyclodipeptide is not generated by the IR laser photo dissociation process. However, in LD/SJMPI, the M-18 peak can often be reduced by using a thin sample film and avoiding multiple desorption in the same sample spot [82]. Here, we have found that it is generally more difficult to avoid the M-18 peak in FAB/LDMPI. This probably can be attributed to the fact that the FAB pulse width or the sputtering time (~ 300 ms) in our current system is much longer than the CO_2 laser beam pulse (< 2 μs). Thus, in our current FAB/SJMPI experiments, the thermal decomposition process may compete with the desorption process for some compounds such as dipeptides [84]. Nevertheless, for most compounds listed in Table 4.1, MPI mass spectra from LD and FAB experiments are essentially the same.

Next we have studied the sensitivity of this FAB/SJMPI method. In the past several years, direct desorption mass spectrometry techniques such as LDMS, FABMS, plasma desorption (PD), and secondary ion mass spectrometry (SIMS) have been widely used for the analysis of organic molecules. However, it is believed that the secondary ions generated by these techniques are only a very small fraction (< 10^{-4}) of the total sputtered material [85]. Thus electron ionization [75], chemical ionization [85-87], and multiphoton ionization [34,46,47,88,89] techniques have been employed to post ionize the sputtered neutrals in order to increase the overall sensitivity. To provide an estimate of the sensitivity of this FAB/SJMPI method, a set of standard sample solutions were prepared. Various amounts of sample solution were placed on the 5-mm-diameter sample probe by using a microliter syringe. A higher power was applied to the FAB gun in order to completely desorb the sample in a single pulse. The peak height of the molecular ion peak was recorded and a corresponding plot of the peak

height versus concentration was used to estimate the lower limit of detection. The detection limits at a signal-to-noise ratio of 2 for indole-3-acetic acid (m/z = 175) and triphenylene (m/z = 228) are 26 ng and 21 ng, respectively. Although the detection limits shown here are not nearly as low as the tens of picogram detection limit achieved with LD/SJMPI [59], we believe that a similar detection limit (picogram regime) should be expected when the ionization laser wavelength and supersonic jet cooling are fully optimized.

One of the important aspects of using MPI as an ionization technique for mass spectrometry is its high selectivity. With multiphoton ionization in a supersonic jet, there are at least two ways to improve the selectivity. First of all, a molecule will be efficiently ionized only if the laser wavelength is in resonance with a real intermediate electronic state and the sum of the energy of the photons absorbed exceeds the ionization potential of the molecule. Therefore, MPI is an almost ideal ionization method for the sputtered neutrals produced by FAB. This is because a matrix such as glycerol, which is commonly used in FABMS, does not contribute to the background noise since the glycerol cannot be ionized at 266 nm [16]. Figure 4.4A shows the MPI mass spectrum of 4-acetamidophenol at 266 nm and Figure 4.4B shows the mass spectrum of a Tylenol tablet. The tablet was purchased from a local drug store and contains corn starch and other components according to the label. About 100 μg of a ground-up tablet is mixed with a drop of methanol and the mixture directly placed onto the sample probe. The FAB gun is used to desorb/sputter the sample, the gas-phase neutrals are entrained into a CO_2 jet, and then the neutrals are ionized by 266 nm laser light at a laser power of $1x10^6$ W/cm^2. As Figure 4.4 shows, the mass spectrum of the Tylenol tablet is almost identical to that of 4-acetamidophenol. Other major components such as corn starch are not ionized. This demonstrates that we can

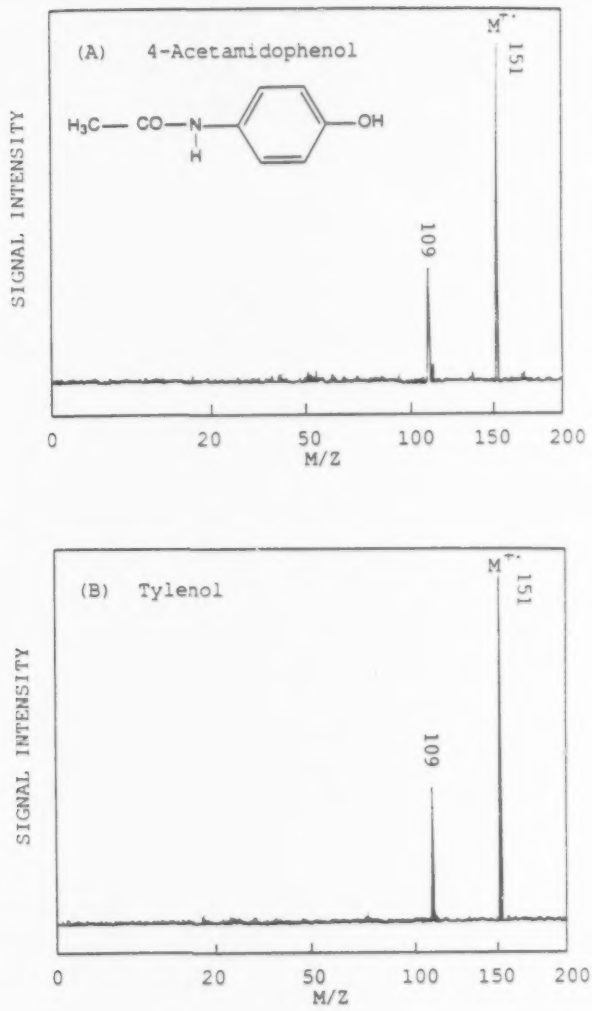

Figure 4.4 Mass spectra of (A) 4-acetamidophenol and (B) Tylenol obtained by using the FAB/SJMPI technique. The ionization laser beam was 266 nm radiation with a power density of ~ 1×10^6 W/cm^2.

selectively ionize the active substance in pharmaceutical dosage forms with very little sample preparation by using FAB/SJMPI.

Another method to enhance the selectivity of this technique is to combine supersonic jet spectroscopy (SJS) with MPIMS. MPIMS combined with SJS has been shown to be a very powerful analytical tool for isomer discrimination and isotope selective detection [10,12,13,90]. More recently, jet-cooled wavelength spectra for biological molecules have also been obtained with the use of laser desorption technique for sample volatilization and the analytical applicability of SJS/MPIMS for the selective detection of biological molecules has been studied [1]. Fast atom bombardment might be an inexpensive and simple alternative for the volatilization and entrainment of thermally labile and nonvolatile molecules into a supersonic jet.

We have also examined the cooling effect by examining the mass resolution in a linear TOFMS [19,34]. In a linear TOFMS, the mass resolution is directly related to the initial kinetic energy distribution of the sample molecules. The energy distribution will be very broad if there is no cooling or only partial cooling for the molecules in the jet. This poor cooling will result in low resolution. By running our system in a linear TOFMS mode, we have found that the mass resolution of molecules such as indole-3-acetic acid with FAB/SJMPI is about 375 at m/z 175. However, the background molecules which are not cooled by the jet give a mass resolution of less than 200. Thus we believe that jet cooling is obtained with the FAB sample entrainment into jet expansions. However, at present, we do not know how cool these molecules are.

Finally, the effect of sample chemical properties on molecular detection in a mixture is examined. The spatial and temporal separation of desorption and ionization processes

in this FAB/SJMPI allows one to uniquely study and control the two individual events. Here we find that, for organic molecules, chemical properties of the sample may play a very important role in the two processes. Figure 4.5 shows the MPI mass spectra of a mixture of indole-3-acetic acid and tryptamine with and without the addition of NaOH or NH_4OH. Figure 4.5A is obtained by using a mixture of indole-3-acetic acid and tryptamine in a 50% methanol / 50% water solvent. Figure 4.5B is the mass spectrum for the same mixture but with the addition of NaOH until the pH > 12. In Figure 4.5C, NH_4OH was used to adjust the pH instead of NaOH. Note that the molecular ion peak for indole-3-acetic acid in Figure 4.5B is absent and no peak corresponding to sodium indole-3-acetate is obtained. The same results are obtained at even higher laser power density although more fragmentation is observed, but no indole-3-acetic acid and / or sodium indole-3-acetate peaks. This might be attributed to the low ionization efficiency of sodium indole-3-acetate. Although the melting point of the organic salt, i.e. sodium indole-3-acetate, is expected to be higher than the indole-3-acetic acid, the desorption of the salt appears to be complete by examining the sample probe after it has been bombarded by FAB. The fact that no peaks were observed from the possible decomposition products (such as indole) leads us to believe that most of the sodium indole-3-acetate molecules are desorbed intact. Note that direct FAB has been used for determination of dissociation constants of weak acids in solution by Caprioli [91]. In his study, sodium salts of a variety of organic acids have also been desorbed intact and detected as $(NaA+H)^+$ and $(NaA+Na)^+$. In addition, the electronic absorption (checked by UV spectra in solution) for sodium indole-3-acetate and indole-3-acetic acid do not differ significantly in terms of absorption bands and absorptivity. These results indicate that sodium indole-3-acetate may not be ionized efficiently by MPI due to its low ionization cross section at 266 nm in the gas phase. To our best knowledge, there is no report on MPI studies of organic salts involving metal cations in the gas

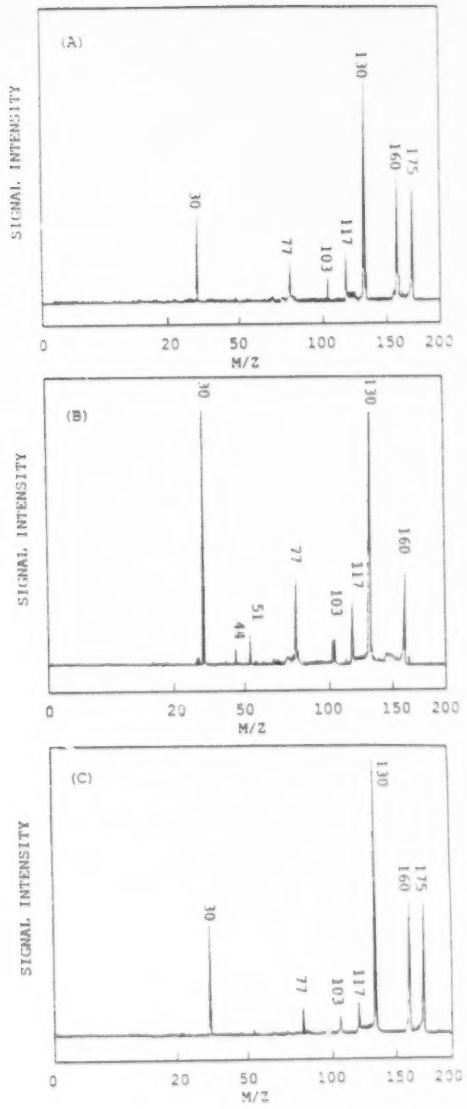

Figure 4.5 MPI mass spectra of a mixture at 266 nm obtained by FAB/SJMPI: (A) tryptamine (MW = 160) and indole-3-acetic acid (MW = 175) ($P \sim 4x10^6$ W/cm^2); (B) tryptamine and indole-3-acetic acid plus NaOH ($P \sim 5x10^6$ W/cm^2); (C) tryptamine and indole-3-acetic acid plus NH_4OH ($P \sim 4x10^6$ W/cm^2).

phase (possibly because most organic salts are unstable upon heating). Now in the case of the ammonium salt, the salt may decompose into indole-3-acetic acid and NH_3 during the FAB desorption process. Similar results are also obtained with other organic acids such as biphenyl phosphoric acid. For analytical applications, this preliminary study indicates that (1) the selective detection of molecules of interest can sometimes be achieved by using simple sample preparation and (2) in the cases where the pH is important, such as buffered biological chemical samples and organic acids, NH_4OH is a better choice for adjusting the pH.

4.4 Conclusion

Fast atom bombardment is a powerful means of desorbing thermally labile biological molecules into the gas phase for analysis by multiphoton ionization mass spectrometry. A variety of biological molecules can be desorbed without significant thermal decomposition. Polycyclic aromatic hydrocarbons can also be studied. At present, the detection limit achieved is typically in the low nanogram regime. The selectivity of this method has also been studied. We have shown that it is possible to use this technique to selectively ionize the active substance in a drug tablet with no sample preparation. We demonstrate that FAB can be used to introduce samples into supersonic jet expansions without affecting the jet cooling. In addition, we have shown that tryptamine can be selectively desorbed from a mixture of indole-3-acetic acid and tryptamine by adding NaOH to the mixture.

Chapter 5

Pulsed Rapid Heating Method for Volatilization of Biological Molecules in Multiphoton Ionization Mass Spectrometry

Part I: Pulsed Rapid Heating for Sample Vaporization

5.1 Introduction

Multiphoton ionization (MPI) mass spectrometry in combination with supersonic jet spectroscopy (SJS) is a powerful technique for chemical analysis [1]. However, in the past, both MPI mass spectrometry and SJS were limited to the study of volatile molecules. In order to extend these two techniques for the study of thermally labile biochemicals, a method for the vaporization of these molecules, without thermal decomposition, must be developed. Thus, pulsed laser desorption (LD) [1,11] and, more recently, fast atom bombardment (FAB) [17] [see chapter 4] have been successfully used for the generation of neutrals from nonvolatile and thermally labile molecules.

Although the mechanisms for the generation of ions and neutrals by LD and FAB are not completely understood, there is some evidence which suggests that neutral formation during LD and FAB can be described by a thermal heating model [92-97]. Thus, in the pulsed LD and FAB/MPI experiments, high energy particles are used to deliver energy to the sample and/or sample substrate. This energy is transferred into heat and vaporizes the molecules coated on the substrate. Clearly, a more straightforward and simple method to volatilize the sample would be direct heating.

However, for the generation of gas phase molecules from thermally labile molecules, the heating rate (or the time taken for energy transfer to the sample molecules for vaporization of intact molecules) is crucial. It is believed [84,98-105] that vaporization, i.e. dissociation of intermolecular bonds, is favored when a high heating rate is used and decomposition, i.e. dissociation of intramolecular bonds, is the dominant process if the heating rate is low. For a given compound, the optimal heating rate in favor of vaporization is currently difficult to measure, and is dependent upon several factors including the sample property (i.e. melting point) and its preparation. However, in general, thermal decomposition is minimized with rapid heating.

Friedman and coworkers [98-100] used a rapid sample heating method to vaporize samples at a heating rate of 12 K/sec for electron impact mass spectrometry. Cotter and Fenselau [101,102] have also used heating rates of > 10 K/sec by inserting a Vespel sample probe directly into a hot ion source block to vaporize biochemicals. Daves and coworkers [84,104,105] used flash desorption to produce gas phase molecules at a heating rate of > 5000 K/sec. These direct heating techniques have been used for the vaporization of biological molecules with some success.

Direct heating methods have several advantages that include (1) low cost (2) simplicity and (3) safe operation compared with pulsed LD and FAB desorption/vaporization techniques. However, one of the major disadvantages is that these methods cannot be used to introduce the sample into the system continuously without re-applying new sample to the probe. Thus, the efficiency and sensitivity of this system suffers. Moreover, it is impossible to perform experiments such as supersonic jet spectroscopy, which requires the sample to be introduced into the system in a continuous or pulsed form for a period of time. Therefore, it is desirable to develop a rapid heating method

with the capability of introducing samples into the system repetitively. It should be noted that even if the sample is thermally stable upon heating, repetitive pulsed heating of samples, compared with continuous heating, can enhance the sample utilization efficiency for pulsed laser ionization in a TOFMS.

In this chapter a pulsed rapid heating method is described for volatilization of thermally labile and nonvolatile molecules for SJ/MPI mass spectrometry. This technique uses a heating probe which consists of an electrically heated plunger driven by a solenoid to desorb the sample in less than 210 μs at a repetition rate of 10 Hz. In part I the design of this heating device is described. Studies on the performance of this technique are then presented. It is demonstrated that this method can be used to vaporize amino acids and dipeptides for SJ/MPI mass spectrometry. The potential applications of this technique for biological molecule detection are discussed. In part II the contact time between the sample and the electrically heated plunger is varied. This allows for studies on the heating nature of the desorption vs decomposition processes.

5.2 Experimental

The time-of-flight mass spectrometer setup has been described in section 1.7 [17-21,58]. In brief, the system consists of an angular reflectron time-of-flight mass spectrometer (R.M. Jordan Co., Grass Valley, CA) mounted vertically in a six-port cross pumped by a 6-in diffusion pump (Varian Associates, Inc., Lexington, MA). A pulsed nozzle (R.M. Jordan Co., Grass Valley, CA) with a 50-μs pulse width is used to form a supersonic jet. CO_2 is used as the expansion gas throughout this work. The jet expands into the acceleration region of the TOF and a laser beam perpendicular to both the jet and flight tube ionizes the sample. No skimmer was used in this study. The 1-meter-long flight tube is differentially pumped by a 4-in. diffusion pump (Varian

Associates, Inc., Lexington, MA). The pressure in the flight tube is usually below $2x10^{-7}$ Torr and the pressure in the ionization region is $< 10^{-6}$ Torr.

The ionization source is a frequency quadrupled Nd:YAG laser (GCR-3, Spectra-Physics, CA) which generates 266 nm radiation with a 7-ns pulse width. The laser is operated at 10 Hz repetition rate. A cylindrical lens is used to focus the laser beam to the mass spectrometer. The focal point is located about 30 mm away from the center of the repeller plate to avoid local excess ionization.

The design of the pulsed rapid heating device is shown in Figure 5.1, along with parts of the experimental setup. The main components of the heating device are the solenoid, the water cooling jacket, and the heated probe. A commercial solenoid (part number: TP6X12; dimension: 1.5" in length, 0.75" in diameter; Guardian Electric, Chicago, Illinois) is used, without any modification, to drive a 4.5" long stainless-steel plunger. The diameter of the plunger is 2.5 mm. A steel base is connected to one end of the plunger so that an electromagnetic force generated inside the solenoid is able to drive the plunger. Two springs are used to hold the plunger so that it can move freely for about 1 cm in a direction either forward to the sample probe or backward to the 1/4" stainless steel rod. In this study, a 1.5-mm diameter thermocoax heating coil (Phillips Electronic Instruments, Norcross, GA) is bent into a U-shape and soldered to the other end of the plunger with the use of silver solder that melts at about 700°C (Americal Platinum and Silver Engelhard Industries, Inc., Iselin, NJ; Brand name: Easy Flow 45). The heating coil is directly used as the tip of the heating probe. The temperature of the heating coil can be kept as high as 500°C, although it is usually held at 250°C for this work. Because the solenoid cannot be operated at high temperatures, a water cooling jacket (0.5" in length and 1" in diameter) constructed of copper is screwed into the

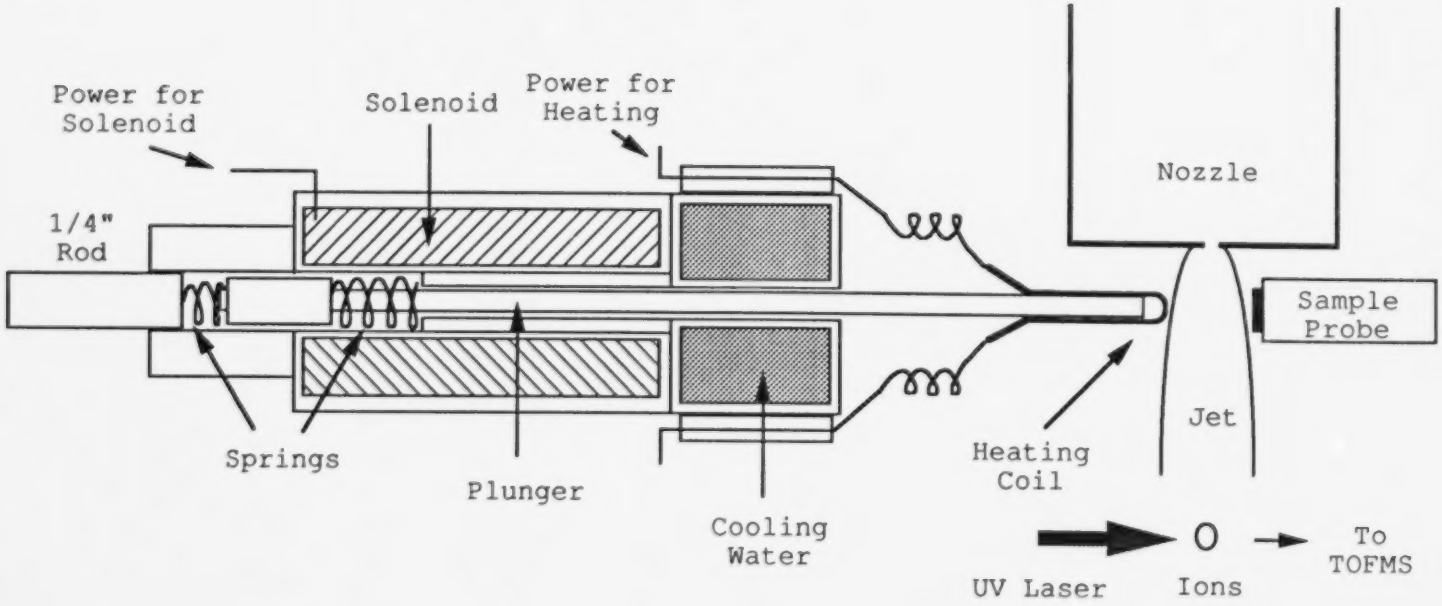

Figure 5.1 Schematic of the pulsed rapid heating probe and part of the experimental setup for multiphoton ionization mass spectrometry and supersonic jet spectroscopy. Drawing is not to scale. The dimensions of the major components are given in the text.

solenoid to isolate the hot probe from the solenoid. We found that the solenoid and part of the plunger remain at the same temperature as that of the cooling water even when the probe is heated above 500°C. The electrical circuit of the power supply used for driving this solenoid is the same as the one used for the solenoid nozzle [106]. This power supply is triggered by a pulse from the Nd:YAG laser and is capable of generating a 400 V pulse with a duration of ~ 35 μs. In this experiment, ~ 170 V pulse is used to drive the solenoid.

The operational principles of this device for sample vaporization can be described as follows. A 10-mm diameter stainless steel sample substrate coated with a sample is inserted into the vacuum chamber and placed near the nozzle orifice. The heating probe is also placed close to the nozzle orifice (see Figure 5.1) through a 2" diameter flange. To ensure that the heating probe and the sample probe do not block the jet expansion, aniline is introduced into the nozzle by mixing it with the CO_2 expanding gas. The molecular ion signal of aniline is monitored during the alignment of both probes. Any signal decrease indicates that the beam is blocked. In this work, the distance between the heating probe and the sample substrate is about 5 mm. When a voltage is applied to the solenoid, the electromagnetic force generated inside the solenoid drives the plunger towards the sample probe; the heating probe makes contact with the sample substrate and vaporization takes place. When the power for the solenoid is turned off, the plunger will be pushed away from the sample substrate by the spring. Because the contact time is very short (see below), the heating is a very localized event, i.e. only the sample in the area in which the heating probe makes a contact is vaporized. By attaching a piece of thermal paper on the sample substrate, we found that the size of the dark spot generated on the paper by the heating probe is about 0.5 mm x 1 mm. By rotating the sample rod to expose a new sample spot to the heating

probe, we can vaporize the sample continuously in a pulsed form in the same manner as in pulsed LD and FAB. The temperature of the heating probe is kept at 250°C for all the compounds studied herein. About 100 μg to 1 mg of sample is generally used and placed onto the sample substrate by either wetting or dissolving the compound in methanol and coating on the surface with the use of a spatula. The sensitivity of the system has not been fully optimized yet. However, the signal intensity of the molecular ion peak in the mass spectrum for the compounds studied is normally more than 5 mV, with a noise level less than 0.2 mV.

The actual sequence of events is controlled by several delay generators. The heating probe is first turned on to vaporize the sample. After the probe returns to its original position, the pulsed nozzle opens to form a supersonic jet, and then the sample is entrained into the jet and carried into the ionization region of the TOFMS where the ionization proceeds. The delay time between the triggering of the solenoid and the opening of the nozzle is optimized to be about 350 μs. After this time delay, the heating probe is fully retracted to its original position before jet expansion takes place.

All chemicals were purchased from Sigma Chemical Co., St. Louis, MO, and used without further purification.

5.3 Results and Discussion

It has been demonstrated that a heating rate in excess of 10^8 K/sec can be achieved with laser desorption by using a pulsed CO_2 laser beam with a pulse width less than 10 μs and a power density in the order of 10^4-10^6 W/cm^2 [43,107]. With this heating rate, thermal decomposition can generally be prevented for modest sized biochemicals. One major objective of the design of this pulsed rapid heating method is to achieve a

high heating rate. Thus, the first question here is, what is the heating rate for this rapid heating method? Although the actual heating time is difficult to determine at present due to a lack of knowledge about the heating process of this method, we have measured the time duration in which the heating probe makes a contact with the sample substrate. This contact time should provide an indication of the heating rate. To measure the contact time, the sample substrate is replaced with a stainless steel plate to which a 12-volt DC is applied. The plate voltage is monitored by a LeCroy digital oscilloscope. When the heating probe (grounded) makes a brief contact with the plate, the voltage is reduced and a trace in a pulsed shape is recorded on the oscilloscope. Figure 5.2 shows the result of this measurement when the solenoid power supply is triggered by the laser. As Figure 5.2 indicates, the contact-time is about 210 μs at FWHM, which is longer than the pulse width from the power supply (~ 35 μs). This indicates that it takes a finite time for the plunger to be moved back and forth by the electromagnetic force and the springs. In this study, the temperature of the heating probe is usually kept at 250°C, thus the heating rate can be as high as 10^6 K/sec if we assume the heating time is approximately the same as the contact time. Thus, the estimated heating rate obtained by this pulsed rapid heating method is much higher than that reported for flash desorption [84,104,105], although it is still lower than that achieved in LD [107].

The use of this method for vaporization of thermally labile biological molecules, studied by using multiphoton ionization mass spectrometry, is illustrated in Figure 5.3. Figure 5.3 shows the soft and hard ionization mass spectra of tryptophan at 266 nm obtained by using this pulsed rapid heating method for sample vaporization. The MPI mass spectra of tryptophan obtained by using the laser desorption sample introduction technique are shown in Figure 5.4 for comparison. Although signal averaging can be performed with this heating method, we find that the reproducibility of the mass

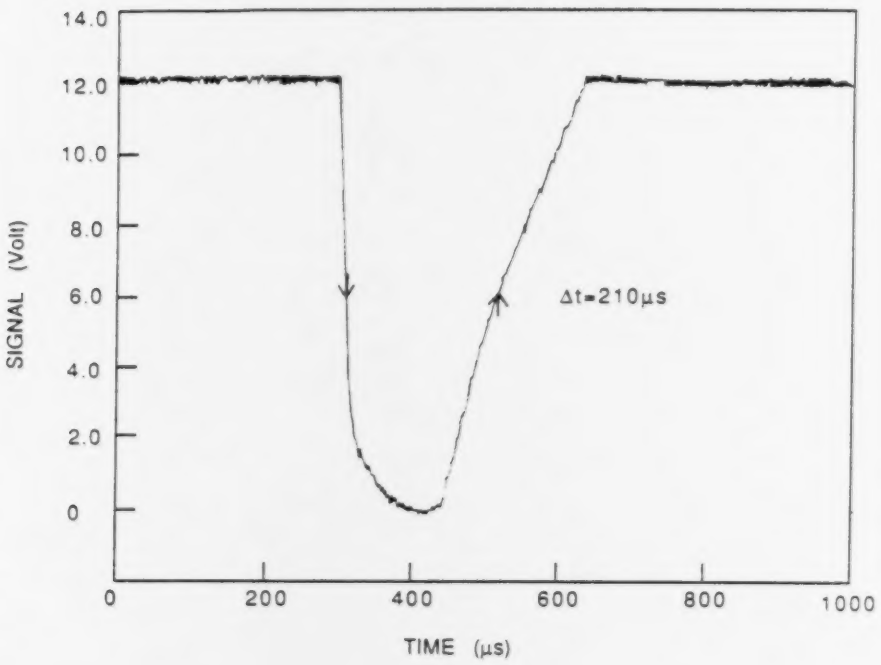

Figure 5.2 The signal output from the measurement of the contact time between the heating probe and the sample substrate.

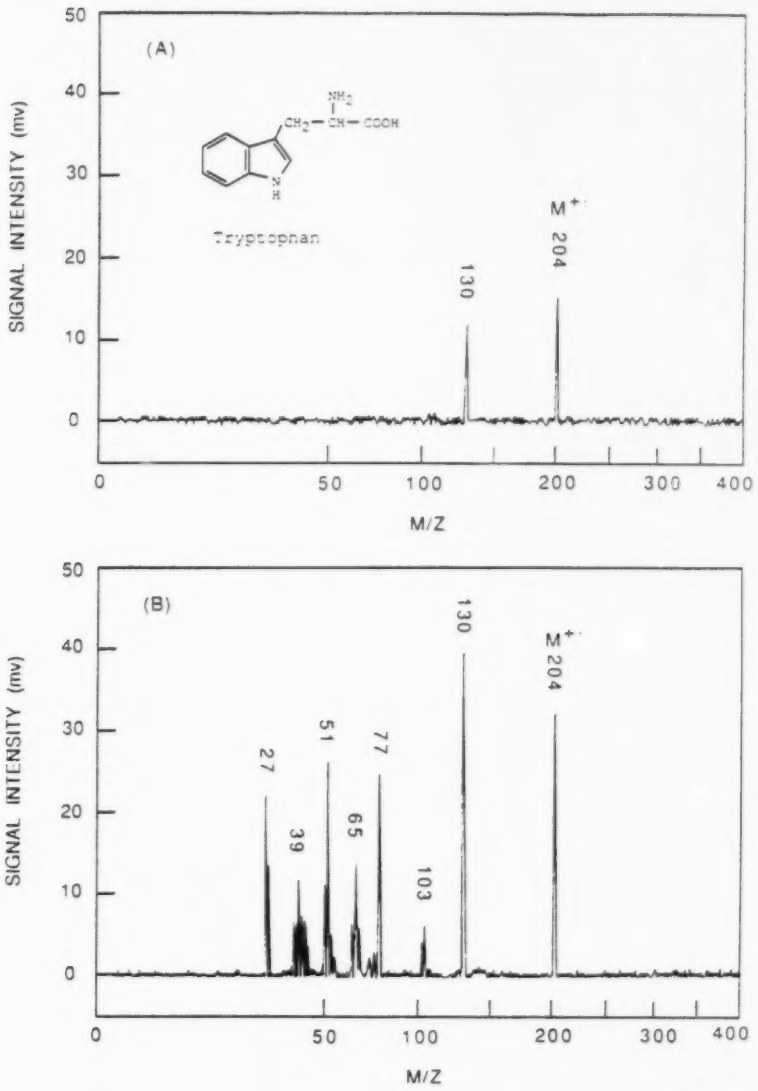

Figure 5.3 Soft and hard MPI mass spectra of tryptophan obtained by using the pulsed rapid heating method for sample vaporization with laser ionization at 266 nm. The ionization laser power densities were (A) $1x10^6$ W/cm^2 and (B) $1x10^7$ W/cm^2.

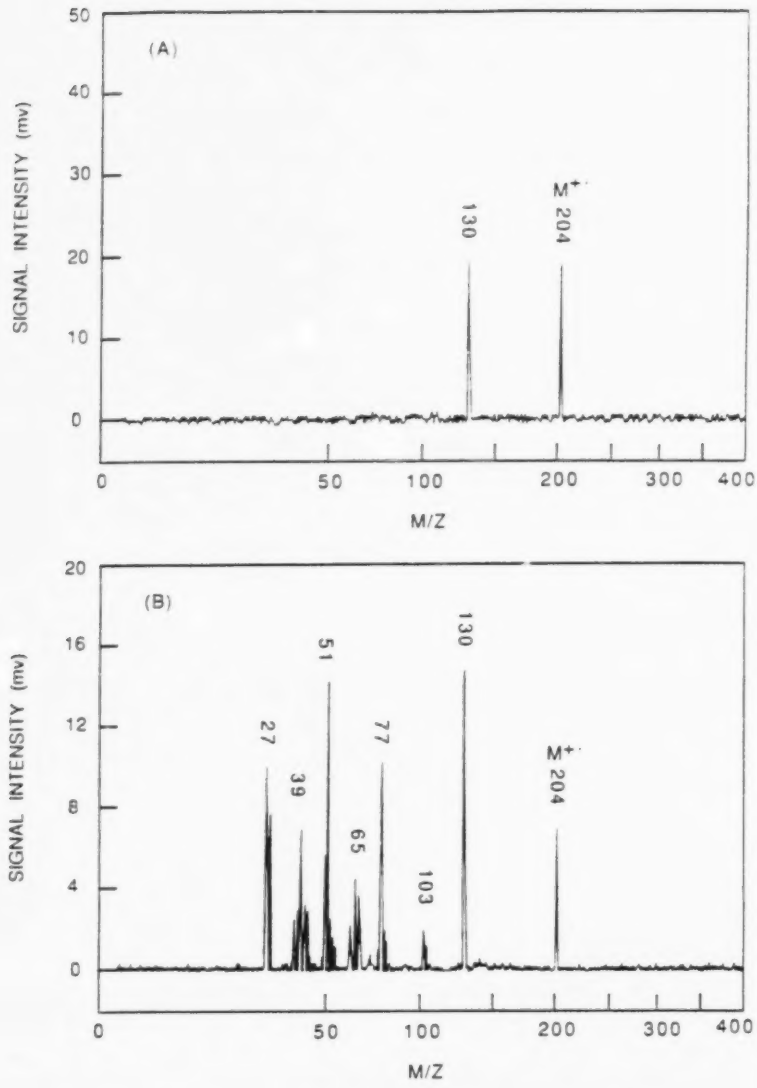

Figure 5.4 Soft and hard MPI mass spectra of tryptophan obtained by using laser desorption with laser ionization at 266 nm. The ionization laser power densities were (A) $1x10^6$ W/cm^2 and (B) $1x10^7$ W/cm^2. The CO_2 laser power density was about $1x10^6$ W/cm^2.

spectral fragmentation pattern from pulse to pulse is excellent. Thus, all spectra are recorded from a single pulse. However, similar to the FAB and LD/MPI experiments, the signal intensity varies from pulse to pulse (± 50 % error). We purchased a rotating sample probe and are experimenting with various sample preparation methods in the hopes of overcoming this intensity variation problem (see chapter 8 concerning the continuous flow probe).

It should be noted that tryptophan is known to be thermally labile and the MPI mass spectrum of tryptophan obtained by conventional heating up to 245°C shows a base peak at m/z 160, which is from the thermally decomposed product, i.e. tryptamine [79]. In this work, in order to demonstrate that it is essential to vaporize biochemicals with a high heating rate to prevent thermal decomposition, we performed the following experiment. Tryptophan is directly deposited onto a direct heating probe which is then placed close to the nozzle. The probe is gradually heated up to ~ 250°C and a mass spectrum is recorded. The MPI mass spectrum obtained is similar to that reported by Levy *et al.* [79] except that the peak at m/z 117 from indole is the base peak along with a strong peak at m/z 160 (tryptamine). The molecular ion peak of tryptophan is small (< 5%). However, as Figures 5.3 and 5.4 show, the mass spectra obtained by LD and this pulsed rapid heating method are essentially identical and no tryptamine or other thermal decomposition products are detected. Note that even with the use of a very high laser power density (1 x 10^7 W/cm^2) for laser ionization, in which case the sensitivity of the MPI technique is better than that under soft ionization conditions, no thermal decomposition products are observed. Mass spectra of the other two aromatic amino acids, tyrosine and phenylalanine, are also obtained with ease when using this heating method for sample vaporization. Figure 5.5 shows the soft ionization mass

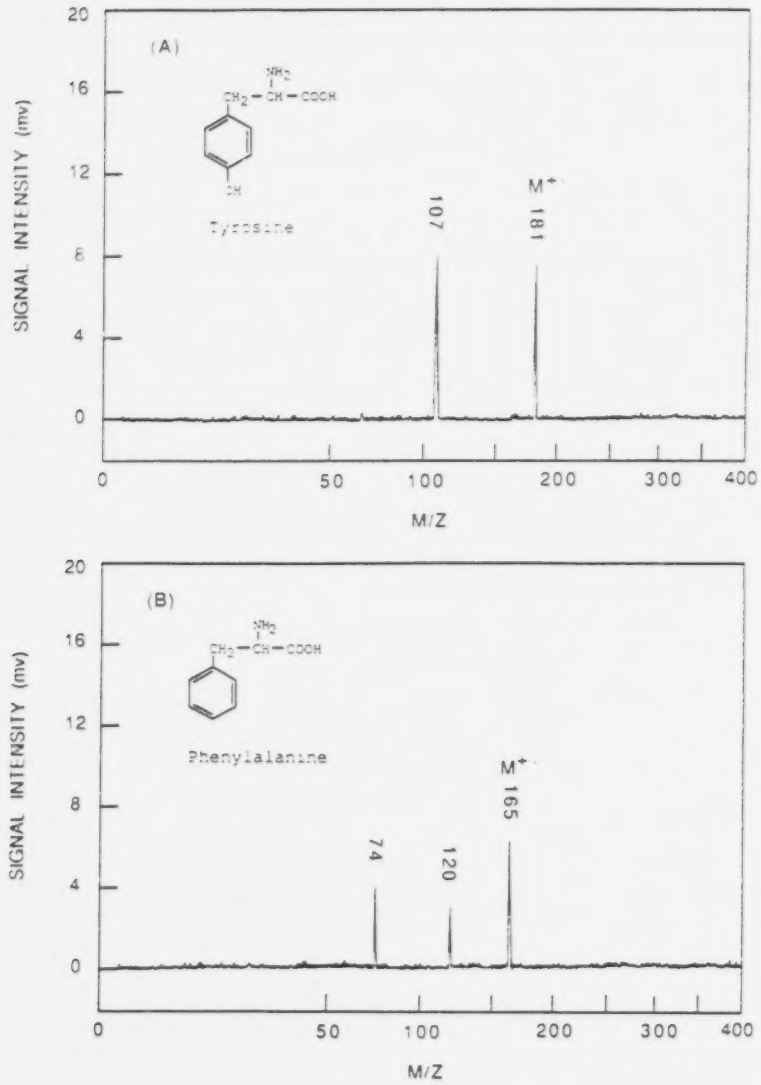

Figure 5.5 Soft ionization mass spectra of (A) tyrosine and (B) phenylalanine obtained by using the pulsed rapid heating method for sample vaporization with laser ionization at 266 nm. The ionization laser power density is about 1×10^6 W/cm^2.

spectra of tyrosine and phenylalanine. Note that strong molecular ion peaks are obtained in each case and no thermally decomposed products are observed.

To investigate the applicability of this technique for the detection of even more fragile molecules, we have studied more than 20 different dipeptides. Typical MPI mass spectra are given in Figure 5.6. Figure 5.6 shows the soft and hard ionization mass spectra of Ala-Tyr obtained by this rapid heating method for sample vaporization with MPI at 266 nm. Presented in Figure 5.7 are the mass spectra of the same dipeptide obtained by LD/MPI. Note that the mass fragmentation patterns shown in Figures 5.6 and 5.7 are almost the same. For all peptides studied, the molecular ion peak is obtained along with a strong peak at M-18. This M-18 peak is generated from the thermal decomposition product during the vaporization. It is also observed in LD and FAB/MPI mass spectrometry [17,82,83]. The thermal decomposition product has been identified in LD/MPI mass spectrometry as a cyclodipeptide [82]. This study provides strong evidence that the generation of neutrals by LD and FAB can be partially explained by the heating model. Moreover, this study, along with FAB/MPI [17], shows that the generation of a M-18 peak is not unique to the LD experiment and suggests that the cyclodipeptide is not generated by the IR laser photo-dissociation process. For the peptides studied, the results obtained by LD or FAB and this method are very similar. These preliminary studies indicate that this pulsed rapid heating method can be a simple alternative for the vaporization of nonvolatile and thermally labile molecules. However, work is needed to demonstrate its analytical applicability for the detection of a wide range of biological molecules, in particular, high molecular weight biochemicals.

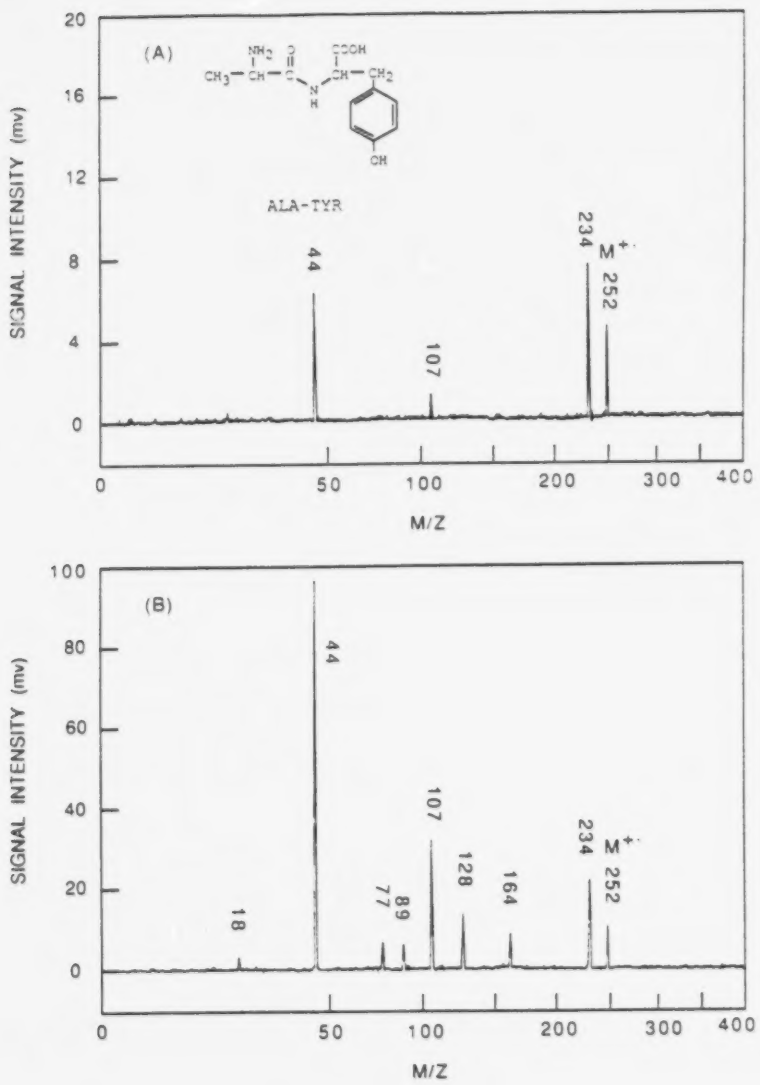

Figure 5.6 Soft and hard MPI mass spectra of Ala-Tyr obtained by using the pulsed rapid heating method for sample vaporization with laser ionization at 266 nm. The experimental parameters are the same as shown in Figure 5.3.

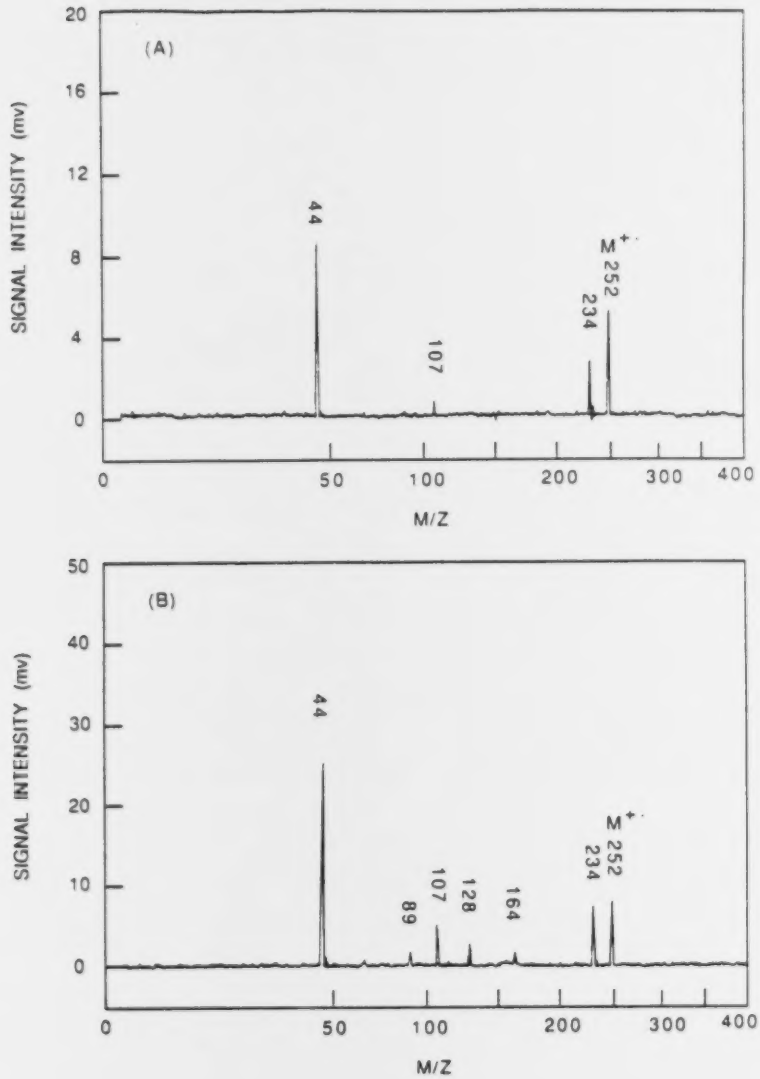

Figure 5.7 Soft and hard MPI mass spectra of Ala-Tyr obtained by using the pulsed CO_2 laser for sample desorption with laser ionization at 266 nm. The experimental parameters are the same as shown in Figure 5.4.

5.4 Conclusion

A pulsed rapid heating method has been successfully developed for vaporization of nonvolatile and thermally labile amino acids and dipeptides. This simple and inexpensive method can be used for vaporization and entrainment of these molecules into a supersonic jet expansion for MPI and SJS studies. This heating method should also prove useful for other techniques which require the formation of neutral molecules. One example is the gas phase UV-Visible absorption spectrophotometric studies of biological molecules (see chapter 7) [22] . For mass spectrometry studies of biochemicals, other ionization techniques such as EI and CI can also be developed for the detection of neutrals generated by this pulsed heating technique. We are now in the process of developing an EI source for our system. We are also exploring the possibility of placing the heating probe directly in the ionization region of the TOFMS for sample vaporization. Note that LD and ion beams have been developed for sample vaporization in the acceleration region of a TOFMS, without the use of a supersonic jet, with MPI post ionization. This has been used for the detection of biochemicals, polycyclic aromatic hydrocarbons, and polymers [88,89,108-110]. However, in these techniques the background due to the secondary ions generated in the desorption process has to be corrected, either by subtracting the background spectrum from the MPI mass spectrum or by using a reflector to reject the directly-desorbed ions in a reflectron TOFMS [88,89,108,109]. On the other hand the PRH technique, presumably generating neutrals for most organic compounds, will not require background correction.

Part II: Pulsed Rapid Heating for Studying Thermal Decomposition vs Vaporization

5.5 Introduction

Sample introduction for nonvolatile and thermally labile molecules for SJS/MPI generally requires vaporization, with no decomposition, for identification and characterization purposes. As discussed in Part I, a pulsed technique is necessary since this causes rapid heating in which molecules desorb into the gas phase before decomposition occurs. Therefore, in order to prevent decomposition, heating has to be quickly performed so as to cause a rapid temperature rise in a very short time frame. A rapid heating rate [84,98-105] translates into fast energy deposition in order to overcome the surface binding forces, yet at the same time not allowing enough time for decomposition to occur due to the accumulation of internal energy.

In this work the effect of different heating rates, both slow and fast, are studied for the desorption vs decomposition of thermally labile amino acids, namely tryptophan and tyrosine. The technique involves the use of an electrically heated plunger driven by a solenoid for sample volatilization, as already described in Part I. The contact time between the heated probe tip and the sample substrate can be varied anywhere from 210 μs to a few seconds. Thus, the current version of this PRH probe yields heating rates from 100 K/s to 10^6 K/s. This allows for variable heating rates for studying biomolecules. The experimental details are discussed in section 5.2.

5.6 Results and Discussion

It is worthwhile to first look at the mass spectra of thermally labile amino acids where heating for sample volatilization is not rapid. In this method the amino acid sample is coated on a wire, and the wire, in turn, is wrapped around a ceramic rod and placed at the end of a direct insertion probe. The heating wire is separated from the rest of the

probe by a copper jacket for water cooling, so as to prevent the vacuum sealant from melting. The highest heating rate attainable by this method is ~ 5 K/s, which is quite slow. Typical mass spectra from the direct heating of tryptophan and tyrosine are shown in Figure 5.8 and the desorption and decomposition are depicted in Schemes 5.1 and 5.2. In the case of tryptophan a small molecular ion peak is seen (< 10%), along with the base peak from a fragment ion (m/z 130). The presence of the thermally decomposed product indole (m/z 117) is unavoidable. Two other decomposition products, methyl indole (m/z 131) and tryptamine (m/z 160), are sometimes observed as well, although their intensities are smaller than indole. In the case of tyrosine, initial direct heating produces the molecular ion and a thermally decomposed product (m/z 137). This is shown in the top mass spectrum of Figure 5.8B. Eventually, the molecular ion decreases in intensity (~ 20%) and a fragment ion (m/z 107) becomes the base peak. A peak at m/z 120 appears, and is a thermally decomposed product with a probable structure shown in Scheme 5.2.

In order to minimize this decomposition from direct heating we next studied the effect of rapid heating on sample introduction. Since the supersonic jet, laser ionization, and TOF mass analysis are all performed in a pulsed manner, it makes sense to also introduce the sample in a pulsed form. A pulsed rapid heating probe is used for this purpose, whereby both the temperature and contact time (between the sample and the heated probe tip) can be varied. In the first case the effect of temperature is studied, while maintaining a constant contact time. This is shown in Figure 5.9 for tryptophan, where the vertical axis represents the percentage of the molecular ion of the major decomposed product, indole, relative to the molecular ion peak of tryptophan. Figure 5.10 is for tyrosine, where the major decomposed product is tyramine. For both amino acids an increase in the temperature of the probe tip generally increases the intensity of

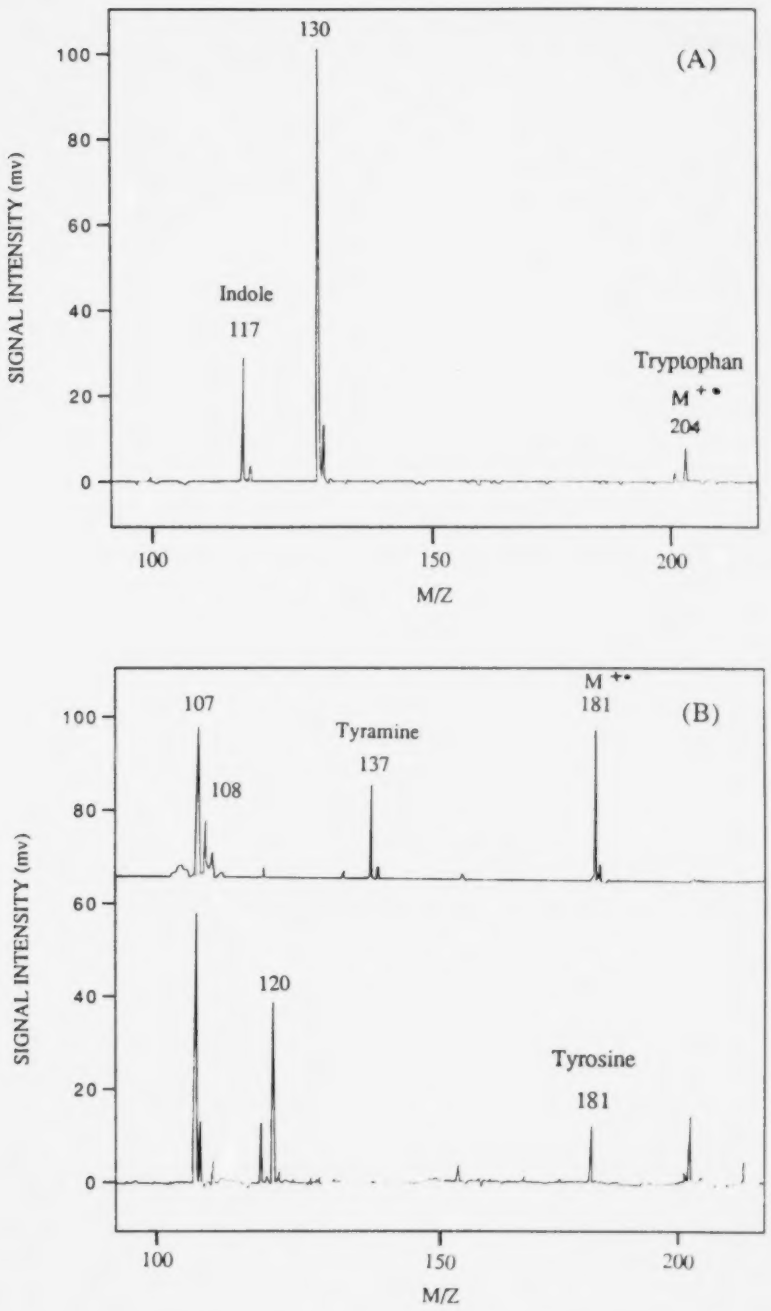

Figure 5.8 Mass spectra resulting from the direct heating of (A) tryptophan and (B) tyrosine (2 spectra shown) at a heating rate of ~ 5 K/s.

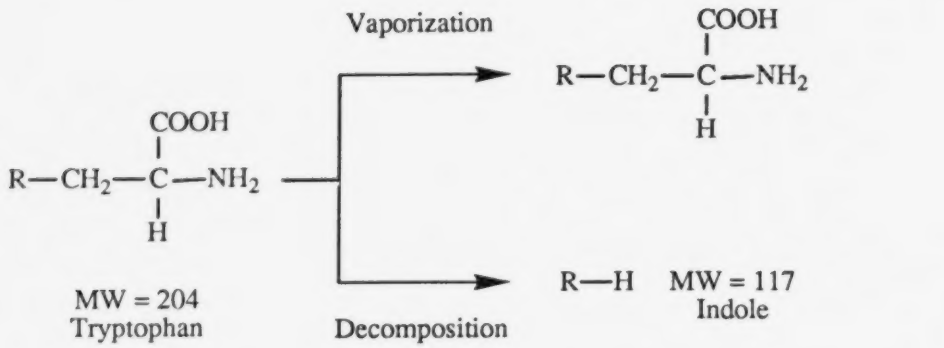

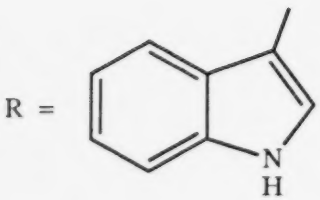

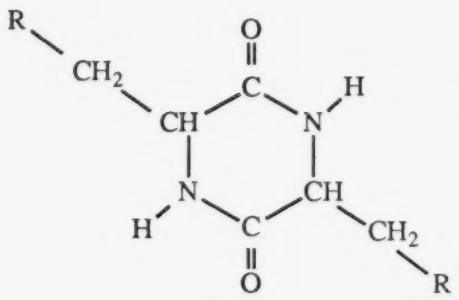

MW = 372 ($2M-2H_2O$)
Cyclic Dimer

Scheme 5.1 The vaporization and decomposition of tryptophan. Vaporization results in the intact tryptophan gas phase molecule, whereas decomposition produces various decomposed species, some of which are shown in the scheme.

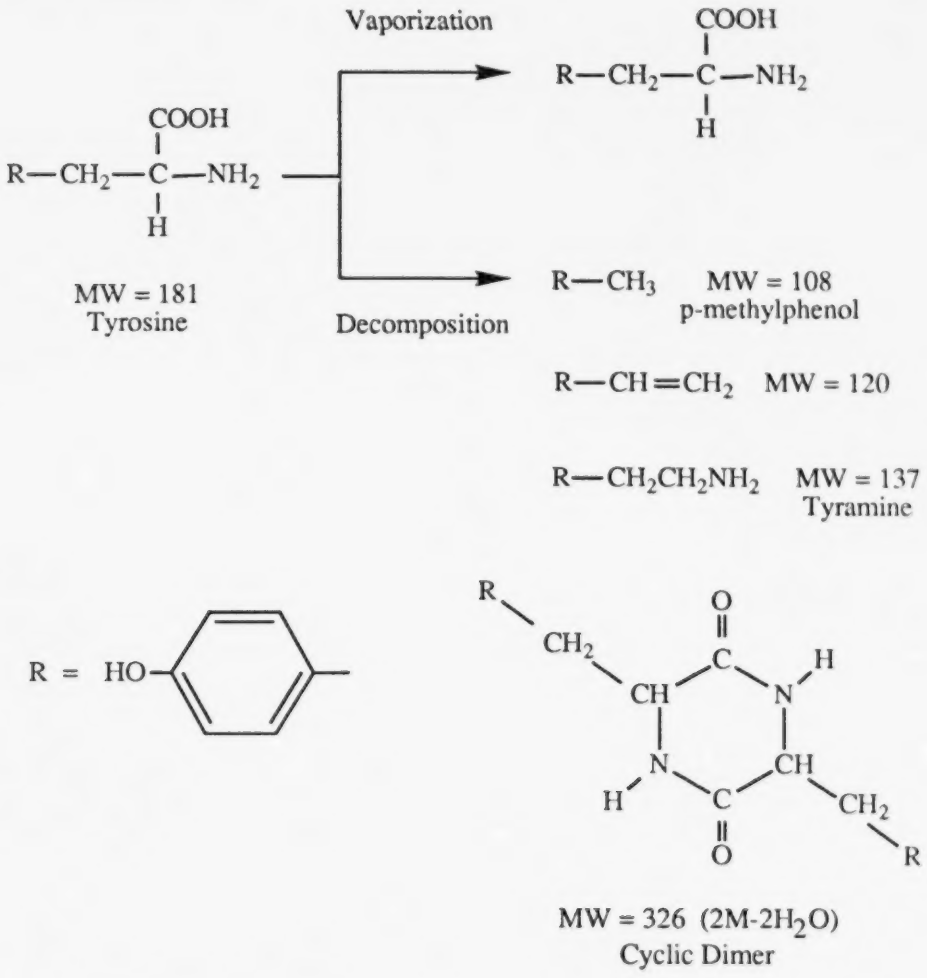

Scheme 5.2 The vaporization and decomposition of tyrosine. Vaporization results in the intact tryosine gas phase molecule, whereas decomposition produces various decomposed species, some of which are shown in the scheme.

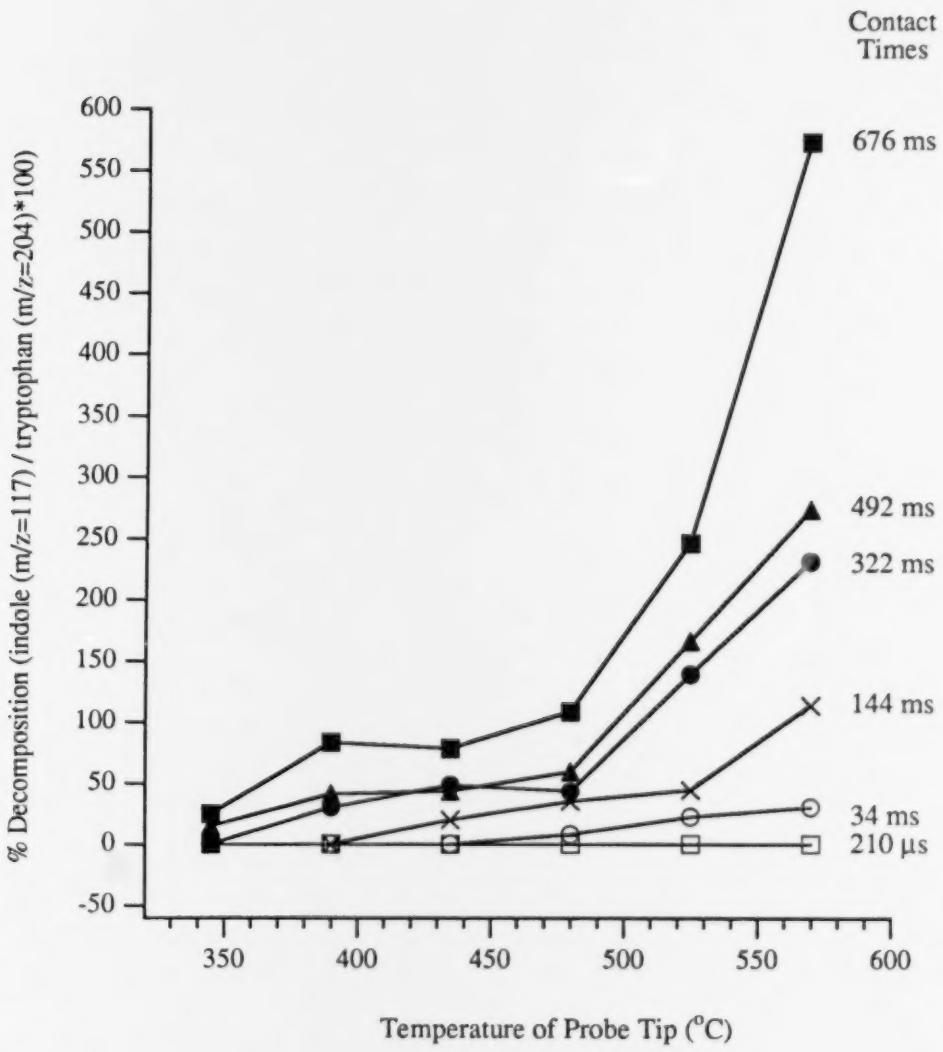

Figure 5.9 % Decomposition of tryptophan vs temperature of the heated probe tip at various constant contact times. The % decomposition is expressed as the percentage of the major decomposed product (indole m/z=117) divided by the intact molecular ion (tryptophan m/z=204) in the mass spectrum.

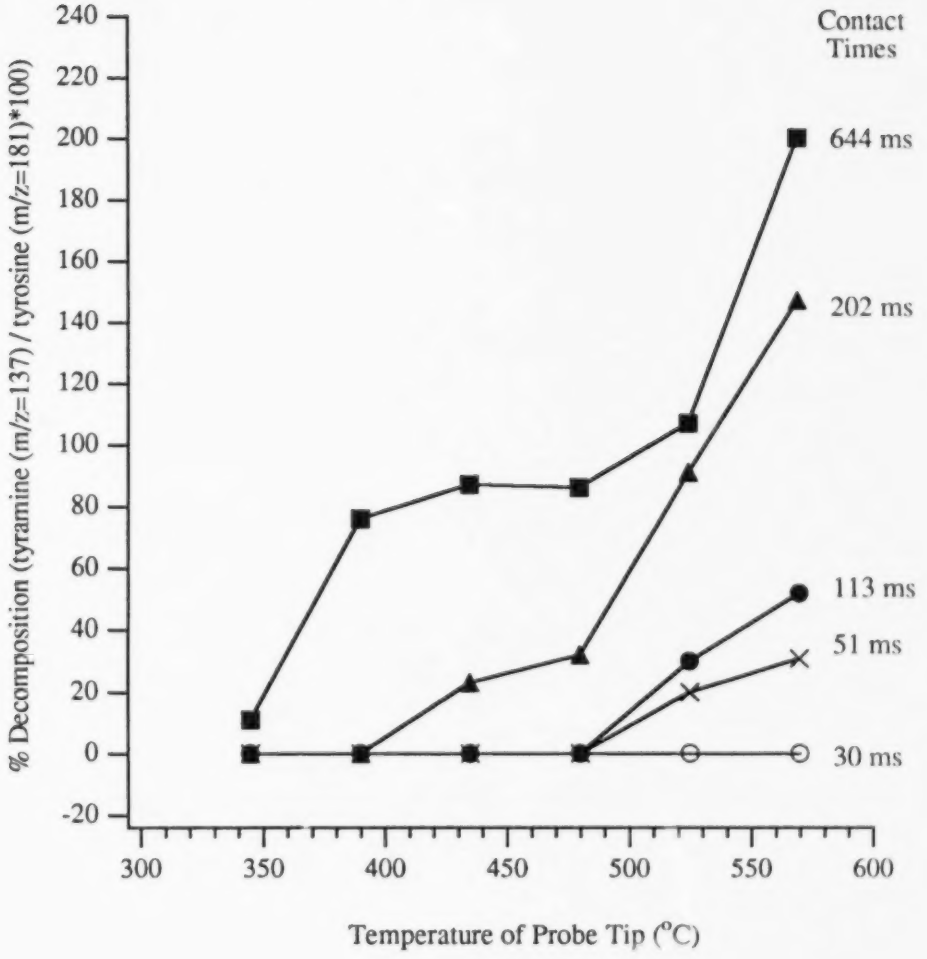

Figure 5.10 % Decomposition of tyrosine vs temperature of the heated probe tip at various constant contact times. The % decomposition is expressed as the percentage of the major decomposed product (tyramine m/z=137) divided by the intact molecular ion (tyrosine m/z=181) in the mass spectrum.

the decomposed products. For tryptophan this is the case when the contact time is > 30 ms, while for tyrosine it is > 40 ms. At a first glance this result seems rather unusual, since an increase in temperature (at a fixed contact time) would result in an increase in the heating rate, thus supposedly minimizing decomposition. However, it is important to note that the increase in the heating rate is not dramatic. For instance, at a fixed contact time of 676 ms for tryptophan, the heating rate increases from 900 K/s to 1250 K/s in Figure 5.9. Other decomposition products start to appear in the mass spectra, as depicted in Schemes 5.1 and 5.2. In the tryptophan case, both tryptamine and a cyclic dimer are generated, in addition to indole. In the tyrosine case, *p*-methylphenol and a cyclic dimer can also be observed, in addition to tyramine. Because decomposition has increased, the molecular ion intensity generally decreases. Consequently, increasing the probe tip temperature in order to increase the heating rate will not be effective.

It is interesting to note that in both Figures 5.9 and 5.10 decomposition can be avoided across the entire temperature range if a very short contact time is used. Although Figure 5.9 shows that a 210 μs contact time will work for tryptophan, a contact time of < 10 ms is probably still sufficient. Similarly, a 30 ms contact time for tyrosine produces no decomposition. Clearly, the contact time between the probe tip and sample substrate plays an important role here and therefore is explored further.

Figure 5.11A illustrates the effect of different contact times between the heated probe tip and tryptophan. Shown is the percent decomposition (indole/tryptophan x 100%) vs contact time at an arbitrarily fixed temperature of 430°C. Virtually identical plots also result in a working temperature range of 370-500°C. In this temperature range decomposition starts to occur when the contact time is > 40 ms. In Figure 5.11B the

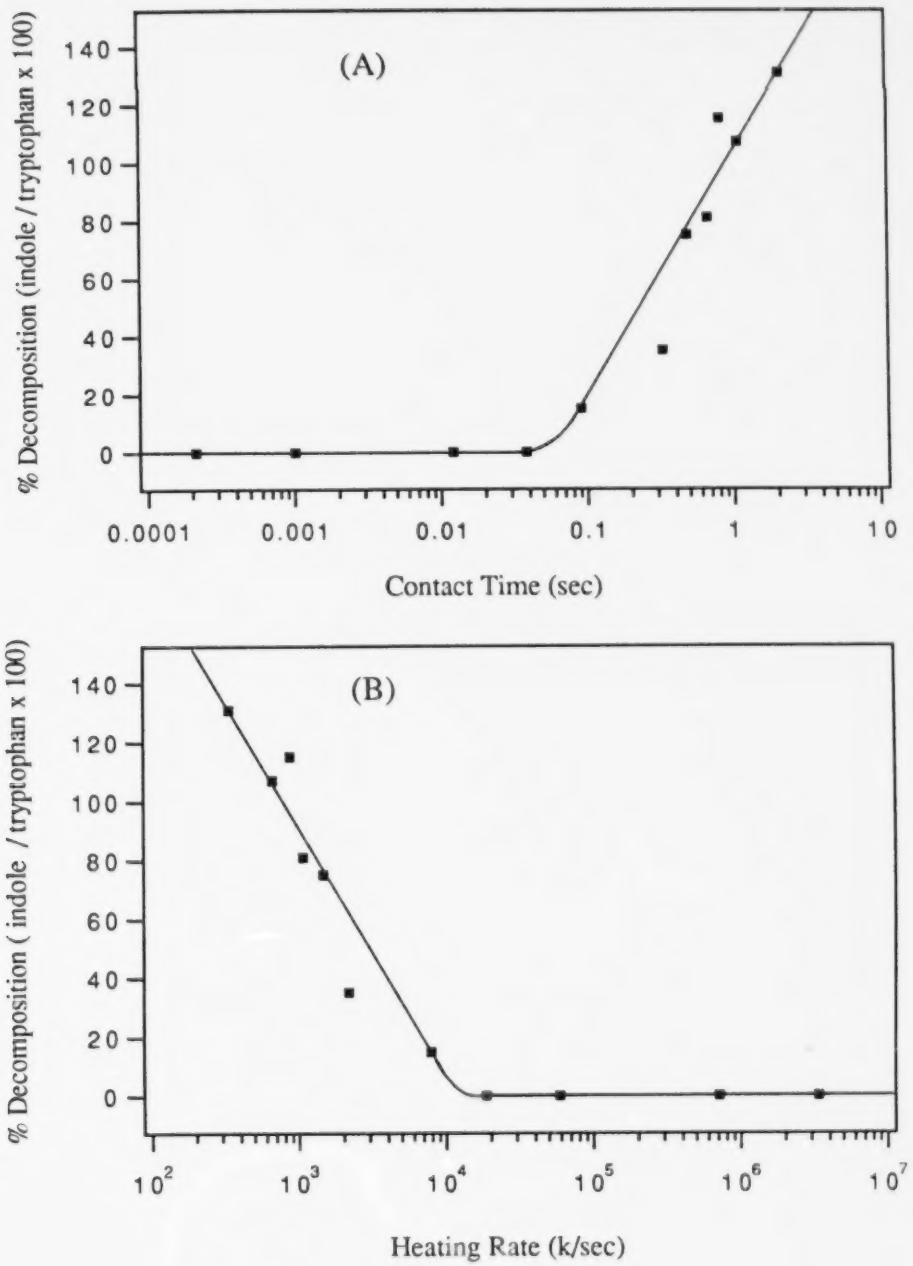

Figure 5.11 % Decomposition of tryptophan vs (A) contact time between the heated probe tip and the sample and (B) heating rate. The % decomposition is expressed as the percentage of the major decomposed product (indole m/z=117) divided by the intact molecular ion (tryptophan m/z=204) in the mass spectrum. The temperature is fixed at 430 C.

horizontal axis has been converted to heating rate (K/s). As Figure 5.11B shows, in order to prevent decomposition a heating rate > 10^4 K/s is required. At this high rate no decomposition products are observed in the mass spectrum. At slower heating rates (< 10^4 K/s) decomposition occurs, and increases steadily as the heating rate becomes lower. The presence of additional decomposed products, namely tryptamine and a cyclic dimer, can be observed at slower heating rates. Eventually, the intensity of the major decomposed products can exceed the intensity of tryptophan (i.e. > 100%). Figure 5.12 shows the results for tyrosine. The decomposed product tyramine starts to appear when the contact time is > 100 ms. Clearly, thermal lability is compound dependent.

The extent of decomposition depends on both the temperature the sample surface experiences and the time taken to transfer the heat energy (i.e. contact time). It is reasonable to say, then, that the rate at which heat is deposited is an important factor [84,98-105]. Shown in Figure 5.13 is the percent decomposition at various heating rates for tryptophan. The temperature of the probe tip and the contact time are simultaneously changed so as to maintain a fixed heating rate. For convenience temperature is shown on the horizontal axis, although contact time could equally well have been plotted. At the slowest heating rate shown (1000 K/s) decomposition is always present, and increases steadily with an increase in both the temperature and contact time (but always at a heating rate of 1000 K/s). At higher heating rates the decomposition begins to decrease. For tryptophan 24 000 K/s is sufficient to eliminate decomposition upto 450°C, but ~ 10% decomposition can still be seen beyond this temperature. Therefore, a heating rate greater than 24 000 K/s is required to completely eliminate decomposition across the entire working temperature range, which corresponds to a contact time of ~ 30 ms. At the highest heating rate shown (300 000

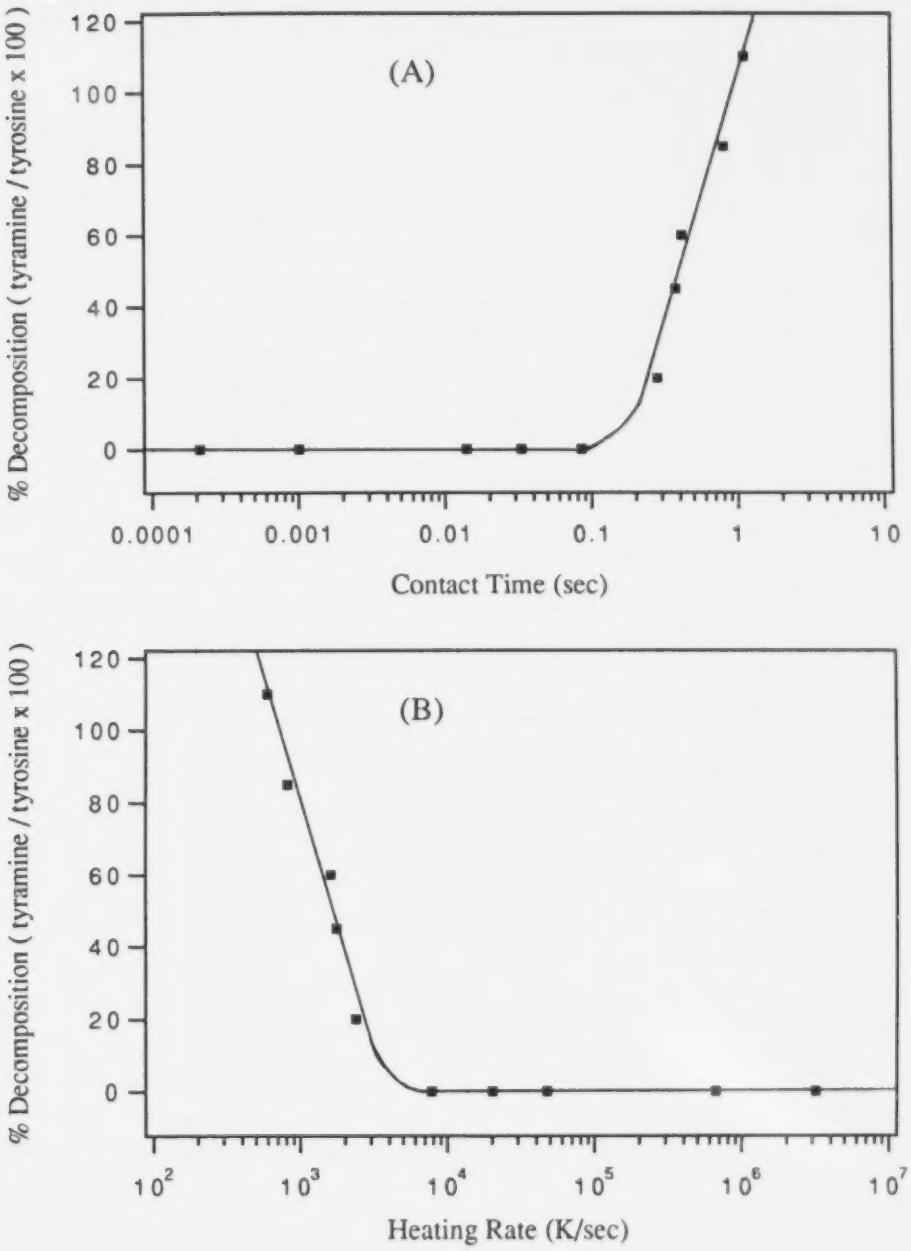

Figure 5.12 % Decomposition of tyrosine vs (A) contact time between the heated probe tip and the sample and (B) heating rate. The % decomposition is expressed as the percentage of the major decomposed product (tyramine m/z=137) divided by the intact molecular ion (tyrosine m/z=181) in the mass spectrum. The temperature is fixed at 390 C.

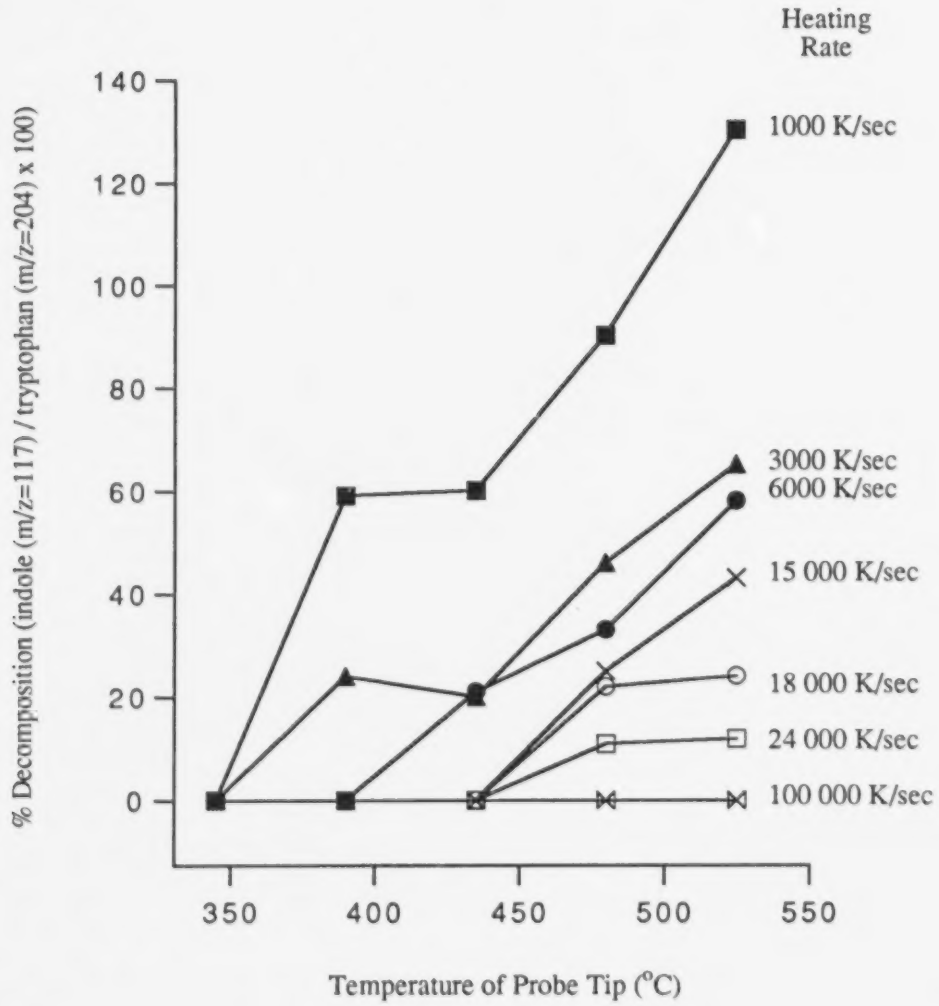

Figure 5.13 % Decomposition of tryptophan at constant heating rates. Both the temperature and contact time are varied so as to maintain a constant heating rate. The % decomposition is expressed as the percentage of the major decomposed product (indole m/z=117) divided by the intact molecular ion (tryptophan m/z=204) in the mass spectrum.

K/s) decomposition is never observed. In Figure 5.14 plots are shown at constant heating rates for tyrosine. The same phenomena as described above is observed, although in this case a heating rate greater than 15 000 K/s is probably sufficient to prevent tyrosine from decomposing.

5.7 Conclusions

1. At a constant contact time, increasing the probe tip temperature in order to increase the heating rate does not work.
2. At a constant heating temperature, a decrease in the contact time decreases the intensity of the decomposed products.
3. High heating rates are necessary to prevent decomposition of thermally labile compounds. This is most easily accomplished by decreasing the contact time.

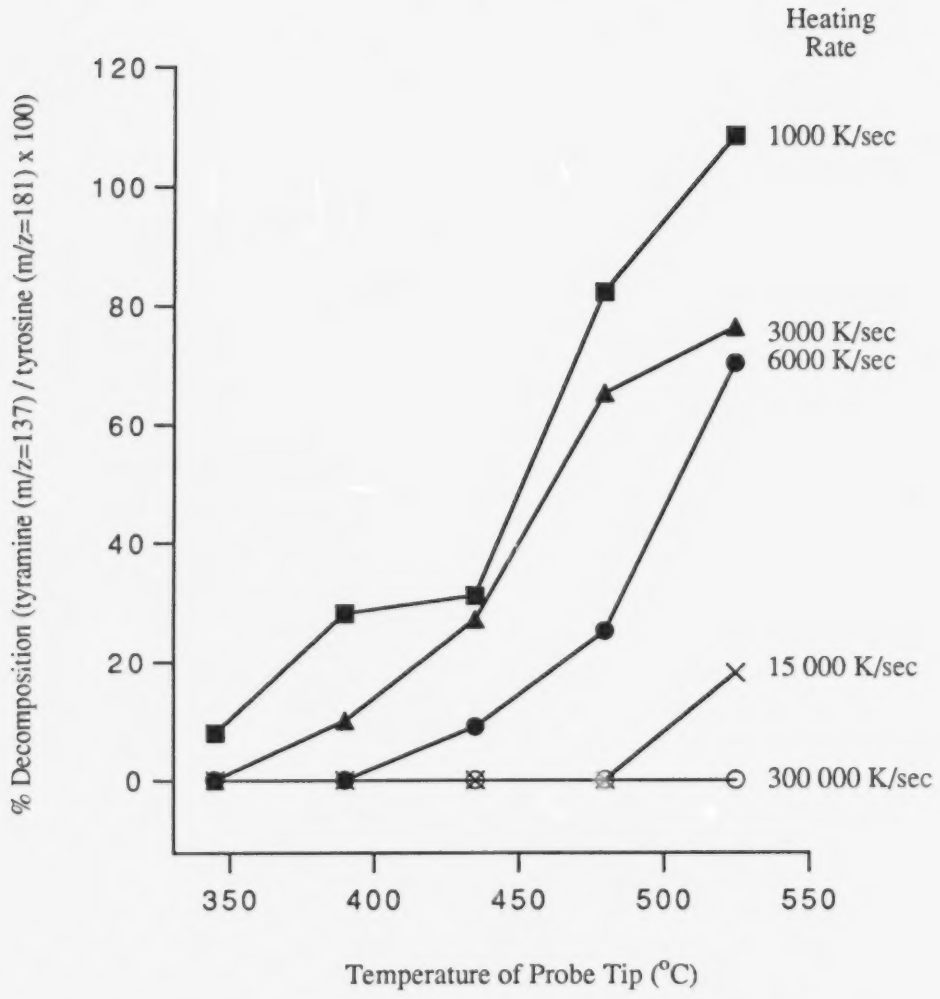

Figure 5.14 % Decomposition of tyrosine at constant heating rates. Both the temperature and contact time are varied so as to maintain a constant heating rate. The % decomposition is expressed as the percentage of the major decomposed product (tyramine m/z=137) divided by the intact molecular ion (tyrosine m/z=181) in the mass spectrum.

Chapter 6

Multiphoton Ionization Study of Water and Ammonia Elimination from Dipeptides with Pulsed Rapid Heating and Laser Desorption for Sample Vaporization

6.1 Introduction

The multiphoton ionization (MPI) technique has been successfully applied to biological molecule studies [1]. In order to volatilize these nonvolatile and thermally labile molecules into the gas phase for MPI, various techniques, including laser desorption (LD) [9,34,46,47], fast atom bombardment (FAB) (see chapter 4) [17] and pulsed rapid heating (PRH) (see chapter 5) [18] have been developed. Among the many biological molecules studied, small peptides, particularly dipeptides, have been extensively investigated by MPI mass spectrometry (MS). Of interest, several research groups have reported the observation of peaks at 17 and/or 18 mass units lower than the molecular ion peak in the mass spectra of dipeptides [9,17,18,45,60,82,111,112]. However, the interpretation of these M-17 and M-18 peaks are still controversial.

Trembreull and Lubman first reported [45] that no molecular ion, but a dominant peak at M-17, is observed in MPI mass spectra of dipeptides such as Phe-Tyr with LD for sample vaporization in a supersonic jet time-of-flight (TOF) mass spectrometer. Beavis et al. also reported MPI mass spectra of dipeptides [111,112]. However, they demonstrated that only the molecular ion is detected at low ionization laser power while the molecular ion along with the M-17 and M-18 peaks can be obtained for dipeptides at high laser power. Later, the M-18 peak was found to be generated from

thermal decomposition during the laser desorption process [60,82,111,112]. Experiments, including the use of Fourier transform infrared (FTIR) spectroscopy, synthesis of cyclodipeptides, and the study of sample matrix and sample preparation effects, revealed that the M-18 peak is from a cyclodipeptide formed by eliminating water from its parent dipeptide during the LD process [60,82]. In contrast, the M-17 peak is not from the thermally decomposed product and is believed to be formed from the molecular ion with the elimination of ammonia, i.e. $(M\text{-}NH_3)^+$ [111,112]. More recently, Zimmerman et al [9] have succeeded in combining MPI with LD in a FTMS and reported that the MPI spectra of some dipeptides such as Trp-Gly also display a dominant peak at M-17. However, from exact mass analysis, it was found that the M-17 peak is from the molecular ion with the loss of hydroxy radical, i.e. $(M\text{-}OH)^+$.

In light of the fact that dipeptides are often used as test compounds for the development of new sample introduction and ionization techniques (see chapters 4-5), the understanding of the fragmentation patterns for these molecules is important for the development of not only LD/MPI but also other techniques involving LD or MPI. In this chapter, we report the MPI mass spectrometric study of dipeptides as well as structurally related amino acid derivatives with the use of laser desorption and the pulsed rapid heating technique for sample vaporization. The objective of this study is to provide further experimental evidence for the origins of the M-17 and M-18 peaks found in the MPI mass spectra of dipeptides.

6.2 Experimental

The experimental setup for supersonic jet multiphoton ionization with laser desorption [17,21,22] and pulsed rapid heating for sample volatilization [18] has been described in section 1.7. In brief, the system consists of an angular reflectron time-of-flight mass

spectrometer (R.M. Jordan Co., Grass Valley, CA) mounted vertically in a six-port cross pumped by a 6-in diffusion pump (Varian Associates, Inc., Lexington, MA). A pulsed nozzle (R.M. Jordan Co., Grass Valley, CA) with a 50-μs pulse width is used to form a supersonic jet. CO_2 is used as the expansion gas throughout this work. The jet expands into the acceleration region of the TOF and a laser beam perpendicular to both the jet and flight tube ionizes the sample. No skimmer was used in this study. The 1-meter-long flight tube is differentially pumped by a 4-in. diffusion pump (Varian Associates, Inc., Lexington, MA). The pressure in the flight tube is usually below $6x10^{-7}$ Torr and the pressure in the ionization region is < 10^{-6} Torr.

A 5-mm or 10-mm diameter sample probe made of machinable Macor ceramic is placed very close to the nozzle orifice. About 100 μg - 1 mg sample is placed on the sample probe directly by either wetting or dissolving the compound in a solvent (i.e. methanol) and coating the surface with a spatula.

For the LD/MPI experiments, a pulsed CO_2 laser (Allmark model 852, A-B lasers Inc., Acton, MA) which generates 10.6 μm IR radiation with a 75-ns initial pulse and 2-μs tailing is used for laser desorption. The laser beam is focused to a ~ 1 mm diameter spot on the sample probe by using a Ge lens [17,18,22]. The laser power density for the desorption is estimated to be $1x10^6$ W/cm^2. In the PRH/MPI work, a heating probe, which consists of an electrically heated plunger driven by a solenoid, is used to make a brief contact with a sample substrate to vaporize the sample in less than 210 μs at a repetition rate of 10 Hz [18]. The gas phase sample molecules are then entrained into the jet and carried into the TOFMS where MPI takes place. The temperature of the probe is kept at 250°C. The estimated heating rate obtained by this PRH method is > 10^6 K/s (see chapter 5).

The ionization source is a frequency quadrupled Nd:YAG laser (GCR-3, Spectra-Physics, CA) which generates 266 nm radiation with a 7-ns pulse width. The laser is normally operated at 10 Hz repetition rate. Most mass spectra are obtained with signal averaging over several laser pulses.

The actual sequence of events is controlled by several delay generators. The CO_2 laser beam or the PRH probe is first turned on to desorb the sample, the pulsed nozzle opens to form a supersonic jet, and then the sample is entrained into the jet and carried into the ionization region of the TOFMS where the ionization proceeds.

All chemicals were purchased from Sigma Chemical Co., St. Louis, MO and used without further purification.

6.3 Results and Discussion

Figure 6.1 shows the LD/MPI mass spectra of Trp-Gly. Here, a relatively thin sample layer is used. Although the sample thickness is unknown, we found that after approximately 10 initial laser desorption pulses, most of the sample in the desorption spot has already vaporized and the ionization signals are approaching zero. Thus, the spectrum shown in Figure 6.1A is the averaged result from the initial 2 laser pulses. Figure 6.1B is the averaged mass spectrum from the third and fourth pulse. The spectrum generated from an additional two pulses in the same sample spot is shown in Figure 6.1C. As Figure 6.1 illustrates, the molecular ion intensity varies from pulse to pulse. By rotating the sample probe, new sample spots can be exposed to the CO_2 laser beam for desorption. It is found that the molecular ion intensity also changes from one sample spot to another. We believe that these signal variations are mainly due to the

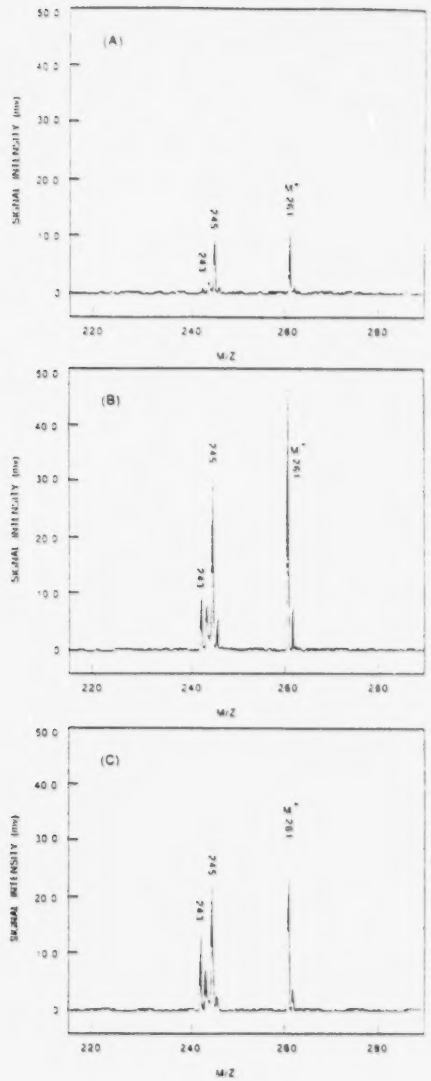

Figure 6.1 MPI mass spectra of Trp-Gly obtained at different laser desorption pulses at the same sample spot: (A) the averaged spectrum from the initial two laser pulses, (B) the averaged spectrum from the third and fourth pulses, and (C) the averaged spectrum from the fifth and sixth pulses. The ionization power density is ~ $2x10^6$ W/cm^2. The CO_2 laser power density is ~ $1x10^6$ W/cm^2.

inhomogeneity of the sample distribution on the substrate surface and the variation of both the ionization and desorption laser powers. We found that the signal intensity variation from spot to spot is about ± 20% for most dipeptides studied. However, the relative intensities between the molecular ion peak and fragments, or the mass fragmentation patterns, do not change significantly from pulse to pulse and spot to spot.

Figure 6.1 also shows that the relative intensity of $M^{+\cdot}$/ $(M-18)^+$ changes from pulse to pulse. This result is consistent with the findings reported by LD/MPI with either a reflectron or a linear TOFMS [60,82,111,112]. It is believed that this M-18 peak is from the cyclodipeptide, a thermally decomposed product generated from the dipeptide with the elimination of water during the laser desorption process [60,82]. In all dipeptides studied, this M-18 peak can sometimes become a dominant peak. Figure 6.2 shows the mass spectrum of Trp-Gly obtained by using a thick sample (~ 0.5 mm in thickness). With the use of a thick sample, over 50 pulses in the same sample spot (multiple desorption) can readily be achieved. In this case, the mass fragmentation patterns from the initial laser pulses are similar to those shown in Figure 6.1. After that, the M-18 peak increases. Figure 6.2 is the resulting mass spectrum from averaging over 50 laser pulses. This result is again consistent with that reported, although different TOF mass spectrometers and laser systems are used [60,82,111,112]. However, the observation of $M-H_2O$ is inconsistent with the LD/MPI result obtained in a FTMS where a dominant peak from protonated $M-H_2O$ was found [9].

It should be noted that, in the FTMS work, a supersonic jet was not used. In an attempt to show the jet effect on the appearance of the M-18 peak in the mass spectrum, a linear TOFMS without the use of a jet is employed. Figure 6.3 shows the mass spectrum of Trp-Gly obtained using the same experimental conditions as in Figure 6.2 except that

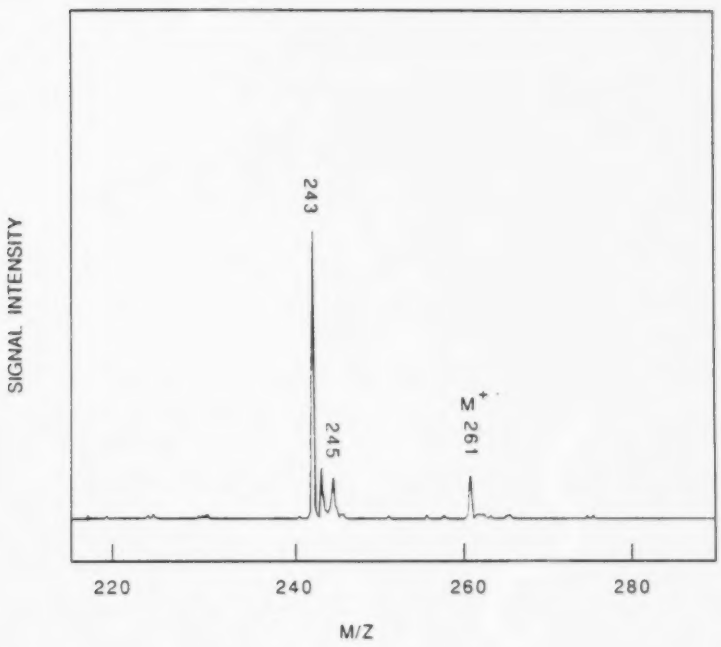

Figure 6.2 LD/MPI mass spectrum of Trp-Gly obtained by averaging over 50 pulses at the same sample spot with the use of a thick sample.

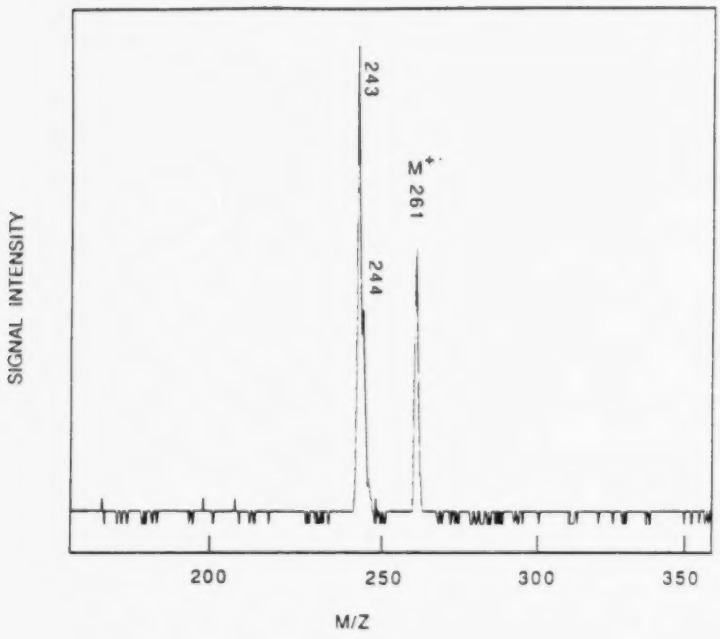

Figure 6.3 LD/MPI mass spectrum of Trp-Gly. The experimental parameters are the same as those used for Figure 6.2 except that no supersonic jet cooling is employed and a linear TOFMS is used.

the sample probe is placed directly between the repeller and the extraction grid of the linear TOFMS. As Figure 6.3 illustrates, the results obtained without the jet are similar to those obtained with the use of a jet. Again, it is found that M-18 can be a dominant peak, providing that multiple desorptions take place in the same spot for a period of time. The absence of the jet does not alter the findings.

Another important fact is that the formation of the M-18 peak is not unique to the MPI experiments with laser desorption for sample vaporization in a TOFMS. This peak is also observed in the FAB/MPI studies of dipeptides (see chapter 4) [17]. In this technique, a pulsed FAB beam, instead of a laser beam, is used to vaporize the sample into a supersonic jet, followed by MPI. More recently, we developed a pulsed rapid heating (PRH) method for sample vaporization (see chapter 5) [18]. We now compare the results of LD/MPI and PRH/MPI from dipeptide studies for a better understanding of the origins of the M-17 and M-18 peaks.

Table 6.1 summarizes the major peaks observed in the mass spectra of dipeptides studied by using PRH/MPI. The summary of the major peaks observed in the mass spectra of these dipeptides studied by LD/MPI is shown in Table 6.2 for comparison. In general, the mass spectra obtained by using PRH/MPI are similar to those obtained by LD/MPI. The major difference is the relative intensity of $M^{+\cdot}$/ $(M-18)^{+}$. The mass spectrum of Trp-Gly, obtained by using PRH/MPI, is shown in Figure 6.4. Note that the intensity of the M-18 peak is higher than those shown in Figure 6.1. In fact, this spectrum is similar to that shown in Figure 6.2. As in LD/MPI, the intensity of the M-18 peak varies from pulse to pulse. Thus, the relative intensity of this peak shown in Table 6.1 is the average value over several different runs. However, unlike in LD/MPI where the M-18 peak can be reduced significantly under some circumstances, this peak

Table 6.1 Summary of the major ions observed in the mass spectra of dipeptides studied by PRH-MPI[a]

Compound	MW	Major ions [m/z (% rel. int.)]
Trp-Gly	261	261(25), 245(16), 244(14), 243(100), 146(9), 130(84)
Gly-Trp	261	261(16), 243(40), 187(8), 130(100)
Trp-Ala	275	275(10), 259(8), 258(11), 257(38), 130(100)
Ala-Trp	275	275(26), 257(61), 187(12), 130(100), 77(14), 44(36)
Tyr-Gly	238	238(27), 222(54), 221(56), 220(100), 136(12), 132(6), 107(36)
Gly-Tyr	238	238(100), 220(100), 107(26)
Tyr-Ala	252	252(12), 236(40), 235(44), 234(100), 146(7), 136(16), 107(30), 44(16)
Ala-Tyr	252	252(89), 234(46), 107(21), 44(100)
Tyr-Leu	294	294(48), 278(76), 277(30), 276(100)
Leu-Tyr	294	294(94), 86(100)
Tyr-Phe	328	328(14), 312(36), 311(50), 310(100), 107(11)
Phe-Tyr	328	328(67), 311(22), 310(100), 120(39)
Phe-Gly	222	222(100), 206(10), 204(22), 120(34)
Gly-Phe	222	222(100)
Phe-Leu	278	278(31), 260(7), 187(17), 120(100)
Leu-Phe	278	278(100), 234(18), 86(16)

[a] The ionization laser beam is 266 nm with a power density of 4×10^6 W/cm^2.

Table 6.2 Summary of the major ions observed in the mass spectra of dipeptides studied by LD-MPI[a]

Compound	MW	Major ions [m/z (% rel. int.)]
Trp-Gly	261	261(99), 245(93), 244(8), 130(100), 117(8)
Gly-Trp	261	261(87), 243(8), 187(47), 170(12), 130(100), 117(8)
Trp-Ala	275	275(100), 259(32), 258(16), 130(81)
Ala-Trp	275	275(100), 257(16), 187(72), 130(65), 44(5)
Tyr-Gly	238	238(17), 222(11), 221(100), 220(3), 136(17), 132(12), 107(4)
Gly-Tyr	238	238(100), 220(6), 164(32), 107(21), 75(25), 30(14)
Tyr-Ala	252	252(51), 236(68), 235(100), 234(28), 14633), 136(26), 107(4), 44(6)
Ala-Tyr	252	252(51), 234(24), 211(27),164(24), 107(12), 44(100)
Tyr-Leu	294	294(41), 278(100), 277(80)
Leu-Tyr	294	294(100), 164(9), 131(9), 86(75)
Tyr-Phe	328	328(59), 312(50), 311(100)
Phe-Tyr	328	328(81), 310(17), 238(15), 222(81), 136(36), 120(100)
Phe-Gly	222	222(30), 206(15), 120(100)
Gly-Phe	222	222(100)
Phe-Leu	278	278(33), 187(17), 120(100)
Leu-Phe	278	278(100), 86(80)

[a] The ionization laser beam is 266 nm with a power density of 4×10^6 W/cm^2.

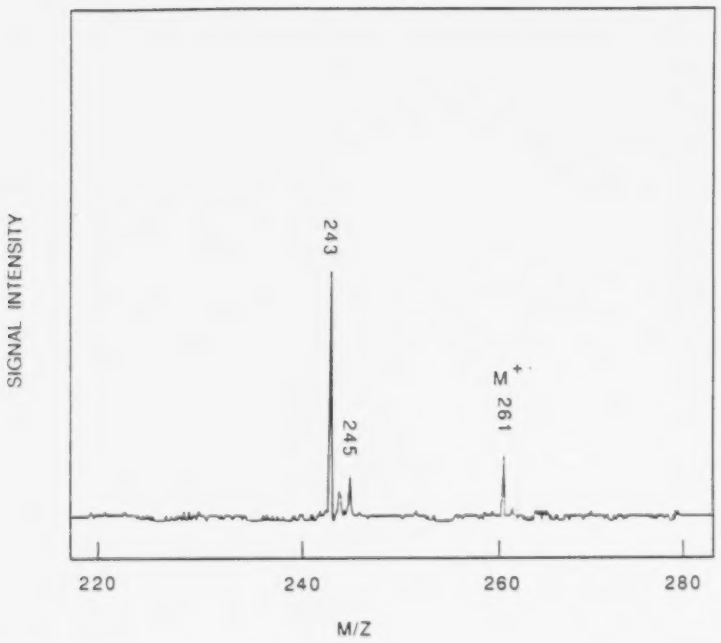

Figure 6.4 MPI mass spectra of Trp-Gly obtained by using the pulsed rapid heating (PRH) method for sample vaporization. The experimental parameters are the same as shown in Figure 6.1A.

is generally observed in PRH/MPI. Compared with the molecular ion peak, this M-18 peak is also very intense, as shown in Figure 6.4 and Table 6.1. Two exceptions are Phe-Leu and Leu-Phe. For these two dipeptides, the M-18 peak is sometimes absent in the MPI mass spectrum. These results again suggest that the M-18 peak is not produced from the molecular ion via MPI fragmentation. Rather, it is from a different species. This is examined more closely below.

The reason for the difficulty in reducing the M-18 peak intensity in PRH/MPI might be attributed to the fact that the heating rate in PRH (~ 10^6 K/s) is lower than that achieved by LD (~ 10^8 K/s) [107]. Furthermore, other non thermal process(es) may also play a role in LD [92,93,113,114]. Thus, in PRH/MPI, the generation of cyclodipeptides by the thermal decomposition process can be a competing process with sample vaporization. The observation of a strong M-18 peak in PRH/MPI, along with the fact that both the appearance and the intensity of the M-18 peak in LD/MPI are not strictly dependent on the CO_2 laser power [60,82], suggests that the cyclodipeptide does not originate from the IR laser beam induced photo dissociation during LD. It should also be noted that the appearance of the M-18 peak is related to the sample vaporization process, not the laser ionization process. Thus, the possibility that the M-18 peak is formed by the UV laser induced photo dissociation in the ionization region followed by MPI can be ruled out. From these experimental results and those reported previously with LD/MPI in a TOFMS, it can be concluded that the M-18 peak formation indeed results from the ionization of the thermally decomposed product, i.e. cyclodipeptide.

It should be noted that Figure 6.1 also shows a strong peak from M-16 along with a peak at M-17. The isotope ratio calculation indicates that this M-17 peak or the M-16

peak is not from the isotope peak of M-18 or M-17, respectively. Note that the M-16 peak is also observed in Figure 6.2. Dipeptides having an N-terminal aromatic group show M-16 and M-17 peaks in the mass spectra, as demonstrated in Tables 6.1 and 6.2. However, these peaks are absent in the mass spectra of dipeptides having a C-terminal aromatic group. The mass spectra shown in Tables 6.1 and 6.2 also reveal that the PRH/MPI technique gives similar results as LD/MPI, which suggests that the M-16 and M-17 peaks are not likely from the IR photo dissociation process during laser desorption. In addition, we found that the relative intensities of these two peaks and the molecular ion peak changes as a function of the ionization laser power. Thus, we can conclude that these two peaks are from the fragments of the molecular ion. It should be noted that, in some cases such as Tyr-Gly, as shown in Table 6.2, the M-17 peak can be larger than the M-16 peak.

Origin of M-17 and M-16: It was first suggested that the M-16 and M-17 peaks are from the molecular ion with the elimination of amino radical and ammonia neutral, respectively [111,112]. However, the recent finding from LD/MPI with a FTMS [9] suggests that the M-17 peak is from the molecular ion minus hydroxy radical. Thus, one can argue that the M-16 peak could be from the protonated M-OH species in the LD/MPI. In order to understand the fragmentation process, we have looked at amino acid derivatives having similar structures as dipeptides as model compounds to study which bond cleavage, i.e. the -CO-OH bond or the >CH-NH_2 bond, occurs more readily.

Table 6.3 summarizes the major peaks observed in the mass spectra of the amino acid derivatives studied using PRH/MPI and LD/MPI. There are several important findings here. First of all, in the cases of tryptophanamide (1) and tyrosinamide (2), both M-17

Table 6.3 Mass spectra of amino acid derivatives studied by PRH/MPI and LD/MPI.*

Compound	Structure	MW	Major Ions [m/z (% rel. int.)] Pulsed Rapid Heating (PRH)	Laser Desorption (LD)
1. DL-Tryptophanamide	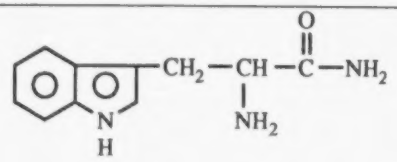	203	203(100), 187(84), 186(29), 130(84)	203(100),187(56),186(8), 130(21)
2. L-Tyrosinamide	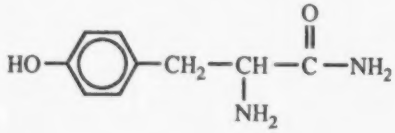	180	180(6), 164(10), 163(100), 136(9), 107(8)	180(5),164(29),163(100)
3. D-Tryptophan Methyl Ester	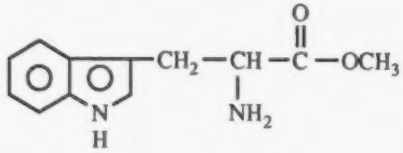	218	218(45), 159(4), 130(100), 103(11), 77(40), 65(21), 51(28)	218(77),159(3),130(100), 103(4), 77(8)
4. L-Tyrosine Methyl Ester	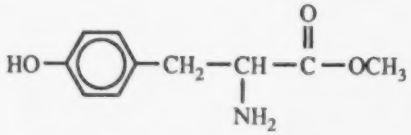	195	195(94), 136(10), 107(100), 88 (56)	195(100),136(8),107(57), 88(32)
5. N-Formyl-DL-Tryptophan	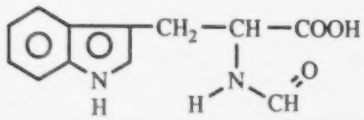	232	232(89), 187(7), 130(100), 117(9), 77(13)	232(100),187(6),130(69), 77(9)

* The ionization laser beam is 266 nm with a power density of 4×10^6 W/cm^2.

Table 6.3 (Continued) Mass spectra of amino acid derivatives studied by PRH/MPI and LD/MPI.

Compound	Structure	MW	Major Ions [m/z (% rel. int.)] Pulsed Rapid Heating (PRH)	Laser Desorption (LD)
6. N-Acetyl-L-Tryptophan	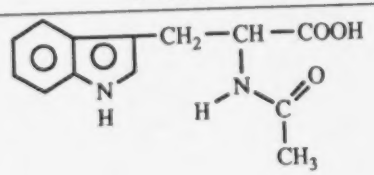	246	246(100), 189(13), 187(15), 130(85)	246(100),189(5),187(11), 130(34)
7. N-Acetyl-L-Tyrosine	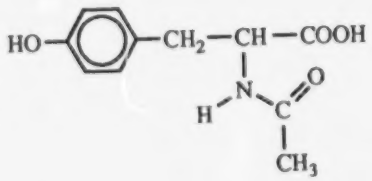	223	223(100), 164(17), 107(33)	223(100),164(58),107(26)
8. N-Acetyl-L-Tryptophan Ethyl Ester	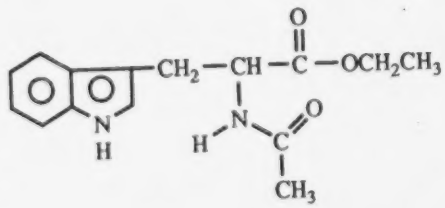	274	274(30), 218(9), 215(7), 130(100), 77(22), 66(13), 65(13), 51(13)	274(100),218(10),21(8), 130(45)
9. N-Acetyl-L-Tyrosine Ethyl Ester	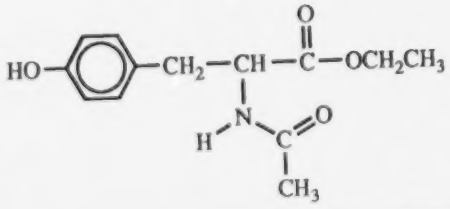	251	251(100), 194(14), 192(25), 107(81)	251(100),194(18),192(29), 107(14)

and M-16 peaks are observed. The M-16 peak can be from the molecular ion with the loss of one of the amino groups. The M-17 peak is from M-NH_3. However, for tryptophan methyl ester (3) and tyrosine methyl ester (4), where the amino group in the amide bond of 1 and 2 is replaced with a methoxy group, no M-17 and M-31 peaks are detected. Since the elimination of the amino radical from the breakage of the amide bond is less energetically favored, compared with the loss of methoxy group from the breakage of the ester bond [115], the failure of observing the M-31 (or M-OCH_3) peak in the mass spectra of 3 and 4 suggests that the loss of the amino group for 1 and 2 is less likely from the amide bond.

For the N-substituted tryptophan and tyrosine derivatives, 5-7, the elimination of the N-substituted group is observed. This group leaves the molecule either as a radical or as a neutral, similar to the fragmentation process observed in compounds 1 and 2 where the M-16 peak is from the loss of the amino radical and the M-17 peak is from the elimination of the ammonia neutral. Thus, for compounds 5-7, no M-17 or M-16 peak is obtained. For compounds 8 and 9, the major fragments are also formed by eliminating the N-substituted group from the molecular ion. No peaks corresponding to the loss of OCH_2CH_3 are detected. This again suggests that the process of the ester bond breakage is energetically less favored than the loss of the N-substituted group.

Scheme 6.1 shows the proposed MPI fragmentation pattern for these substituted amino acids. From the study of the mass spectra of the amino acid derivatives 1-9 and from the structural comparison between these compounds and the dipeptides, the fragmentation process for dipeptides having a N-terminal aromatic group is proposed in Scheme 6.2. The experimental evidence from this study supports the view by Beavis et al [111,112], i.e. the M-16 and M-17 peaks observed in the MPI mass spectra of

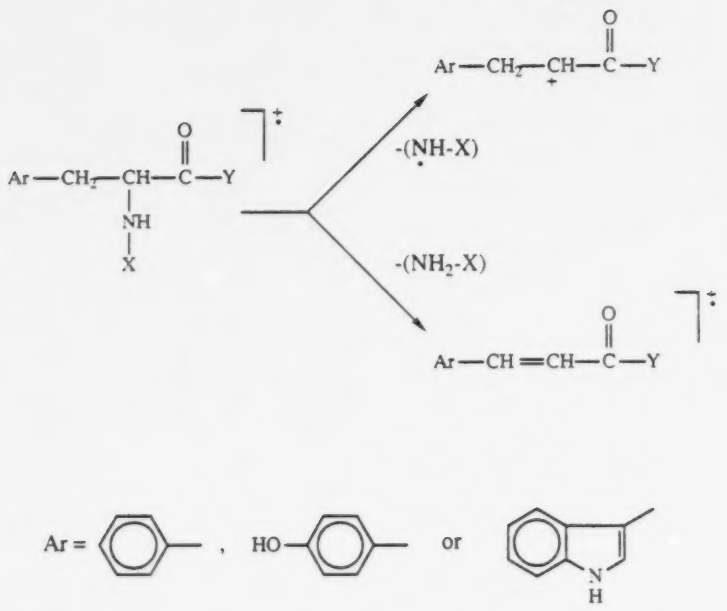

Scheme 6.1 Proposed MPI fragmentation pattern for substituted aromatic amino acids.

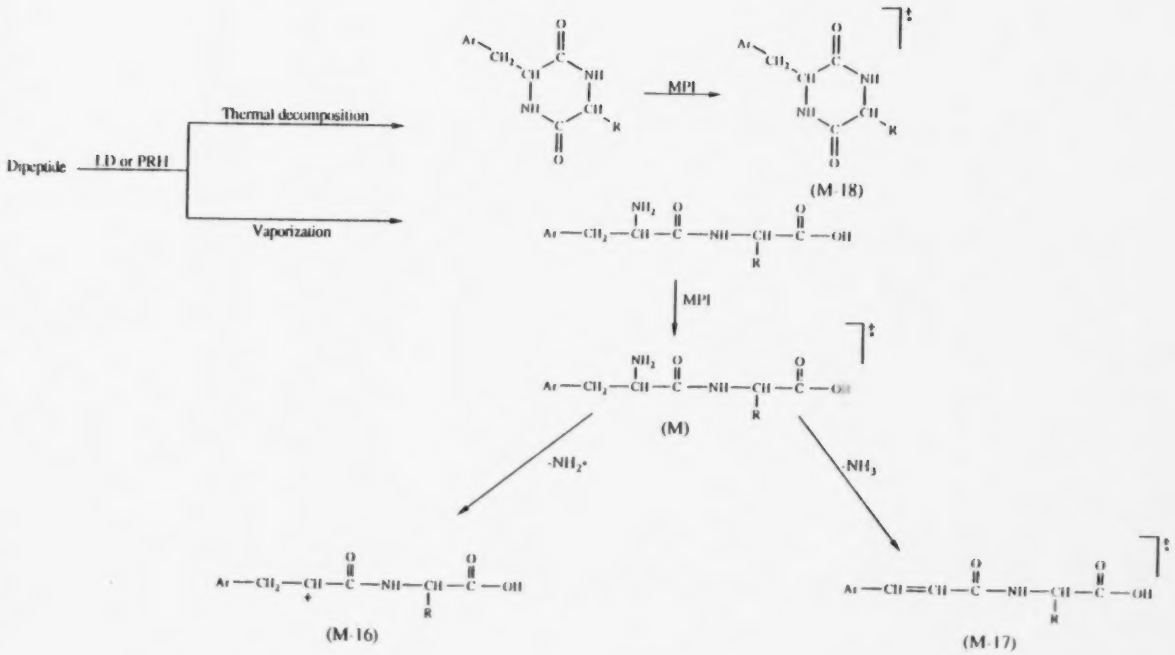

Scheme 6.2 Fragmentation process for dipeptides having an N-terminal aromatic group.

dipeptides originate from the loss of M-NH_2 and M-NH_3, respectively. The fact that the M-17 ion can form a stable resonant structure with the aromatic group can be used to explain why the M-16 and M-17 peaks are observed in the dipeptides having a N-terminal aromatic group, but not in the dipeptides having a C-terminal aromatic group.

6.4 Conclusion

The origins of the peaks at 17 and 18 mass units lower than the molecular ion peak, often found in the multiphoton ionization mass spectra of dipeptides, have been investigated. Two major processes in the interpretation of the MPI mass spectra of dipeptides can be identified (see Scheme 6.2). One is the thermal decomposition process, from which a M-18 peak is observed. This peak is not from the molecular ion of the dipeptide. It is from the MPI of the thermally decomposed product, cyclodipeptide, generated during the sample vaporization process. The other important process is the elimination of an amino radical or ammonia neutral from the molecular ion of the dipeptide having a N-terminal aromatic group. This fragmentation process gives rise to the M-17 and M-16 peaks. For dipeptides having a C-terminal aromatic group, the M-17 and M-16 peaks are normally not detected. In all dipeptides studied, the M-18 peak can be detected in the LD/MPI experiment if a thick sample is used and multiple desorption in the same sample spot takes place. For the FTMS work, the M-17 ion peak is also observed, although it is proposed to be from the molecular ion with the loss of a hydroxy radical [9]. This M-17 ion is proposed to be the protonated cyclodipeptide. This result is clearly different from that reported here and by others [111,112] in which LD/MPI experiments were carried out in a TOFMS.

The reason for the difference is unknown. However, one explanation could be that, in the FTMS work, the thermally decomposed cyclodipeptide is initially formed during

the LD process and then ionized by MPI. This cyclodipeptide radical cation then collides with the remaining neutrals in the resonance cell to form the protonated cyclodipeptide. However, in the TOFMS experiments, a protonated molecular ion is normally not detected [17,18,45,60,82,111,112]. The reason for not observing the protonated species in the TOFMS is that the residence time of the ions in the ionization region where ions and neutrals are both present is very short (< 10 ns). Thus, even if a collision does take place, it will not form a protonated species in the given time frame. However, in FTMS, the ion residence time in the cell is much longer. Thus, protonation could take place via collisions between the ions generated by MPI and the neutrals in the cell.

Chapter 7

Measurement of Gas-Phase Ultraviolet-Visible Absorption Spectra of Thermally Labile Molecules with a Pulsed Rapid Heating Technique for Sample Vaporization

7.1 Introduction

In chapters 5-6 it was successfully demonstrated that the pulsed rapid heating (PRH) technique can be used for the vaporization and entrainment of nonvolatile and thermally labile molecules into a supersonic jet (SJ) expansion for multiphoton ionization (MPI) studies [18]. As an application of the PRH probe for sample vaporization, this chapter deals with PRH for neutral generation at atmospheric pressure [22]. More specifically, it describes a study of the gas phase UV-Visible absorption spectra of biological molecules.

Gas-phase UV-visible spectra have proven useful in areas such as the study of electronic transitions in molecules with relatively higher resolution compared to solution or solid state studies [116]. The absorption spectrum can also provide valuable information for the selection of optimal wavelengths for laser-based detection methods such as multiphoton ionization mass spectrometry [117] and laser-induced fluorescence gas-phase spectroscopy [118,119]. Among the laser-based detection methods, supersonic jet spectroscopy (SJS) [10,120] is a powerful technique for chemical analysis such as isomer identification and molecular structural analysis. Recently,

laser-induced fluorescence and multiphoton ionization jet spectroscopy have been extended to the study of biological molecules [43,59,79,117].

In SJ spectroscopy, in order to obtain a jet-cooled spectrum, some prior knowledge of the general absorption spectrum of the sample molecules in the UV-visible region in the gas phase is generally required to locate the original transitions. For volatile and thermally stable molecules, gas-phase spectra can be obtained by heating the sample in a gas cell in a spectrophotometer. However, for thermally labile biochemicals, conventional heating cannot be applied since decomposition will occur upon heating before a spectrum can be obtained (see chapter 5, Part II). Although solution phase spectra for these molecules can be obtained, the spectra are usually different from the gas-phase spectra. This is particularly true for biological molecules, which often possess functional groups such as OH and COOH. The solvent and pH shifts of the absorbance peaks for these molecules can be quite large. In some cases, over 10 nm shifts are observed [121]. Such shifts clearly cause some problems in locating the origin transition in high resolution spectroscopy in light of the fact that the laser beam is monochromatic and wavelength resolution is very high (i.e. < 0.02 nm for SJS). Thus, methods for obtaining UV spectra in the gas phase are needed. Li and Lubman developed a pulsed laser desorption method for sample volatilization in a diode array spectrophotometer for the measurement of gas-phase UV spectra of biological molecules [121]. In their technique, a pulsed CO_2 laser was used for vaporizing biochemicals at atmospheric pressure. Gas-phase UV spectra for a variety of biochemicals were obtained and studied. These spectra proved extremely valuable for locating the origin transitions or 0-0 transitions in SJS for tyrosine-related molecules, indoles, and catecholamines [43,59].

In this chapter, a simple and inexpensive alternative method for obtaining gas-phase UV-visible spectra of biochemicals is described. It is demonstrated that the PRH technique, producing a heating rate ~ 10^6 K/sec [18], can be used to vaporize intact biochemicals at atmospheric pressure without significant thermal decomposition. It is shown that UV spectra of biochemicals such as tyrosine, Dopa, norepinephrine, and tryptophan can be obtained with this experimental setup. It is our hope that this simple method of obtaining gas phase UV-vis spectra of thermally labile molecules can be readily adapted by investigators interested in the studies of these molecules by high resolution laser spectroscopy.

7.2 Experimental

Figure 7.1 shows the experimental setup for the measurement of gas-phase UV-vis absorption spectrum with a pulsed rapid heating method for sample vaporization. A commercial UV-vis photo diode array spectrophotometer (Hewlett-Packard 8450A) is employed to detect the gas-phase species. The PRH probe has been described in chapter 5. Briefly, it consists of a solenoid, a heating probe, and a water cooling jacket. A solenoid is used to drive a long stainless-steel plunger. A steel base is connected to one end of the plunger so that an electromagnetic force generated inside the solenoid is able to drive the plunger. Two springs are used to hold the plunger so that it can move freely for about 1 cm in either direction. In this study, a 1.5-mm diameter thermocoax heating coil is bent into a U-shape and silver-soldered to the other end of the plunger. The heating coil is directly used as the tip of the heating probe. Because the solenoid cannot be operated at high temperatures, a water cooling jacket constructed of copper is screwed into the solenoid to isolate the hot probe from the solenoid. The electrical circuit of the power supply used for driving this solenoid is the same as the one used for the solenoid nozzle [106]. This power supply is triggered by a pulse from a pulse

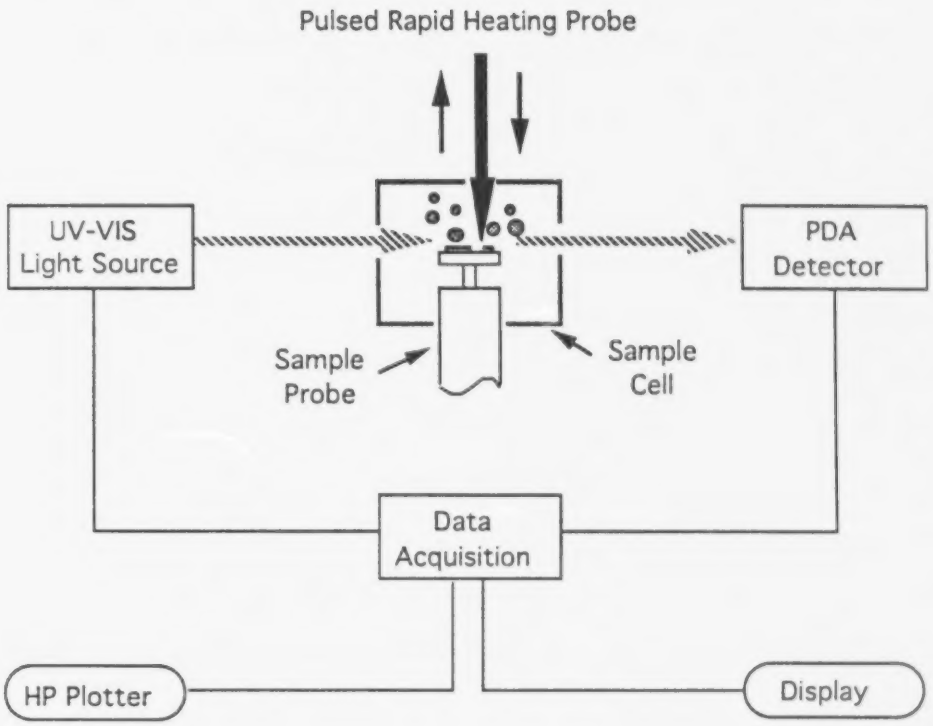

Figure 7.1 Schematic diagram of the experimental setup.

generator and is capable of generating a 400 V pulse with a duration of ~ 35 μs. In this experiment, an ~ 170 V pulse is used to drive the solenoid.

The vaporization process is performed under normal atmospheric conditions. The PRH probe vaporizes the sample, which is coated on a 10-mm diameter ceramic probe, generating a plume of vapor. The light beam from the spectrophotometer is positioned about 1 mm above the PRH probe so as to intersect the maximum amount of vapor without blocking the light beam from the probe. The entire absorption spectrum in the UV-vis region is obtained within 1 second. The actual sample cell used to concentrate the sample plume is constructed of round glass (4-cm length x 1-cm diameter) with four circular holes (see Figure 7.1). The sample holder and the PRH probe are placed ~ 8 mm apart. The contact time between the sample and the probe is ~ 210 μs, producing a heating rate ~ 10^6 K/sec, as reported previously in chapter 5.

About 1 mg of sample is placed onto the ceramic probe by either wetting or dissolving the compound in methanol and coating on the surface with a spatula. A fresh sample is always available for vaporization by simply rotating the sample probe. The PRH probe is operated at 1 Hz to allow the spectrophotometer to record and store the entire spectrum in 1 second. Up to 25 spectra can be stored in the CPU of the spectrophotometer in each run. The temperature of the heating probe is optimized for each sample. Depending upon the melting point of the sample, the temperature is generally in the range of 150-300°C. Since no significant absorptions are present in the visible region for the compounds studied herein, the data is acquired in the UV region only.

In order to study the heating process, we analyzed the sample vapors generated at atmospheric pressure by the PRH technique and by conventional direct heating. In order to collect the sample vapors, a liquid-nitrogen cooled stainless steel sample probe was placed near the vaporization region. The gas phase sample molecules were then condensed on the probe. In order to determine the composition of the condensed vapors we used laser desorption / supersonic jet multiphoton ionization (LD/SJMPI) mass spectrometry. The sample probe was inserted into the vacuum chamber of the LD/SJMPI mass spectrometer for CO_2 laser desorption with 266-nm laser ionization. This mass spectrometer is the same one used in the FAB and PRH work and has been described in detail in section 1.7 [17-19,58].

The slow direct heating method employed in this work is performed by wrapping a quartz cell with several turns of a coaxial heating wire. The sample is put inside the quartz cell, which is then placed in the light path of the spectrophotometer, and the quartz cell is slowly heated. The heating rate is estimated to be ~ 2 °C/sec. Again, for the analysis of the sample vapor, the vapor is collected at the top of the quartz cell using the procedure outlined above, and analyzed by LD/SJMPI.

All chemicals were purchased from Sigma Chemical Co., St. Louis, MO, and used without further purification.

7.3 Results and Discussion

As shown in earlier studies (chapters 5-6), the PRH method is capable of generating intact molecules without significant thermal decomposition in the vacuum for MPI mass spectrometry [18]. The PRH method described herein generates gas phase molecules at atmospheric pressure, similar to laser desorption with a spectrophotometer

for obtaining gas phase UV spectra [121]. Figure 7.2 shows the gas phase UV spectra of tyrosine, Dopa, norepinephrine, and tryptophan obtained by the pulsed rapid heating technique. These spectra are virtually identical to laser desorption results obtained previously [121], as was the case for other compounds studied. These results suggest that the PRH technique is an attractive, inexpensive method compared to laser desorption for obtaining gas phase spectra for thermally labile or high melting point compounds.

However, the similarity between the UV spectra obtained by LD and PRH does not rule out the possibility that thermally decomposed products may be generated by both techniques. Moreover, we found that the UV spectrum of tryptophan obtained by the PRH method is similar to that obtained by the slow heating method, yet it is well known that tryptophan is thermally labile [79,121]. Thus, the next question we have to address is whether we are indeed generating gas phase neutral species, thermally decomposed products, or both by the PRH method. Here, a laser desorption/supersonic jet multiphoton ionization mass spectrometer is used to address this question. Figures 7.3A and 7.3B show the LD/SJMPI mass spectra of pure tryptophan and the sample collected from the vapor generated by the PRH method. As Figures 7.3A and 7.3B indicate, the two mass spectra are essentially identical, with a strong molecular ion peak and a major fragment ion at m/z 130. Note that the relative peak intensity between m/z 130 and m/z 204 is strongly dependent on the laser power density and the laser wavelength [79,122]. The peak at m/z 130 is not detected at the optimal wavelength of 286 nm with low laser power [122]. These results indicate that the fragment ion at m/z 130 is a photo fragment and not a thermal decomposition product. Figure 7.3C shows the mass spectrum of the sample collected from the vapor generated with the conventional slow-heating technique. Figure 7.3C illustrates that tryptophan

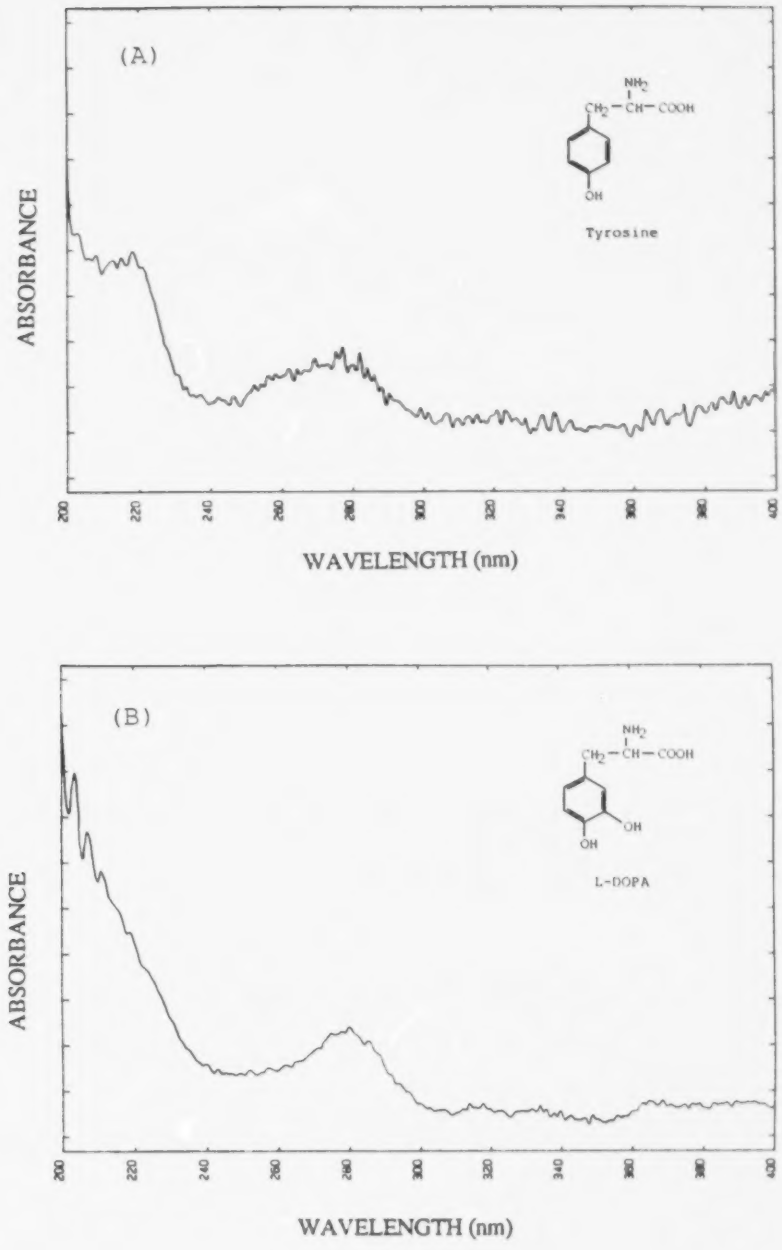

Figure 7.2 Gas-phase UV spectra of (A) tyrosine and (B) Dopa obtained by using the pulsed rapid heating method for sample volatilization in a diode array spectrophotometer.

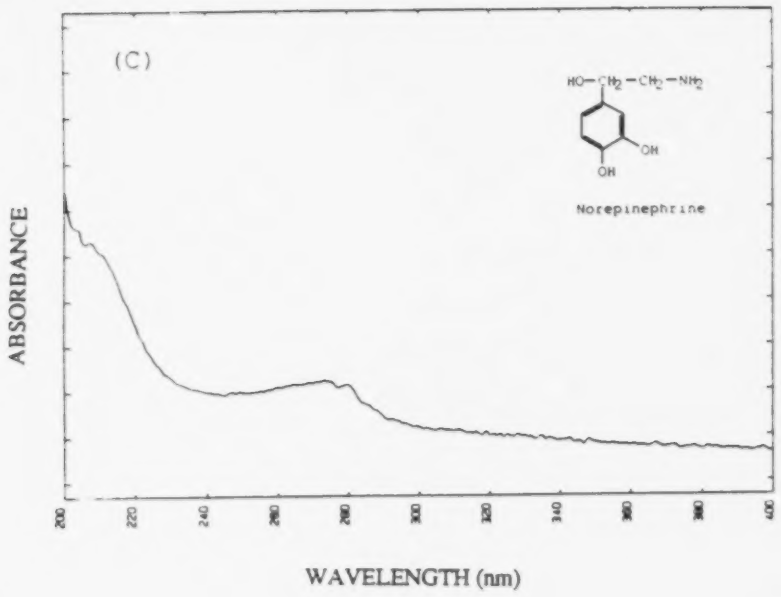

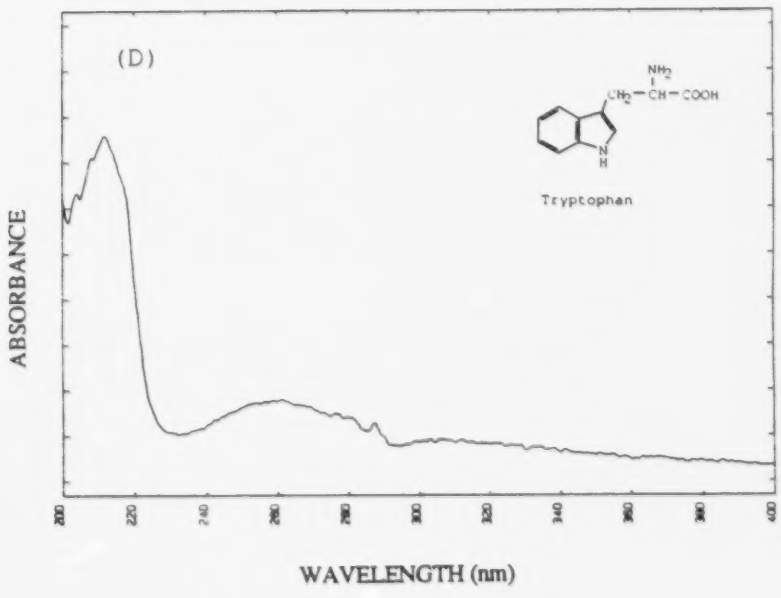

Figure 7.2 (Continued) Gas-phase UV spectra of (C) norepinephrine and (D) tryptophan obtained by using the pulsed rapid heating method for sample volatilization in a diode array spectrophotometer.

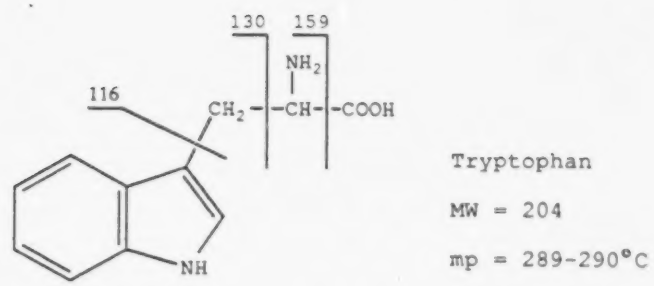

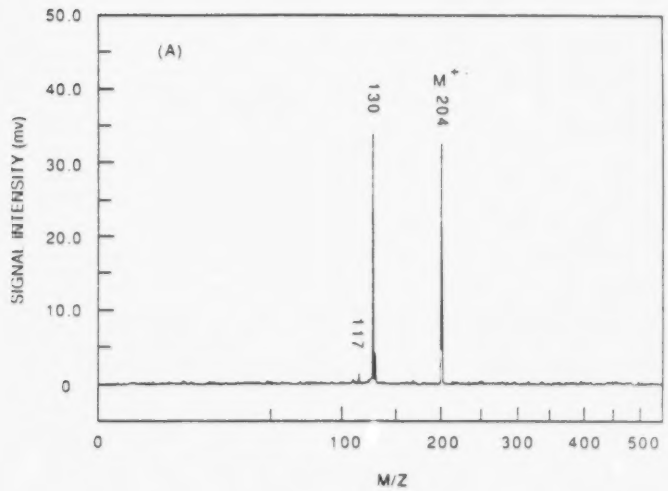

Figure 7.3 (A) MPI mass spectrum of pure tryptophan (MW = 204). The spectrum is obtained by using laser desorption/supersonic jet multiphoton ionization mass spectrometry. The ionization laser beam is 266 nm with a power density of about $1x10^6$ W/cm^2. The power density of the CO_2 desorption laser is about $1x10^6$ W/cm^2.

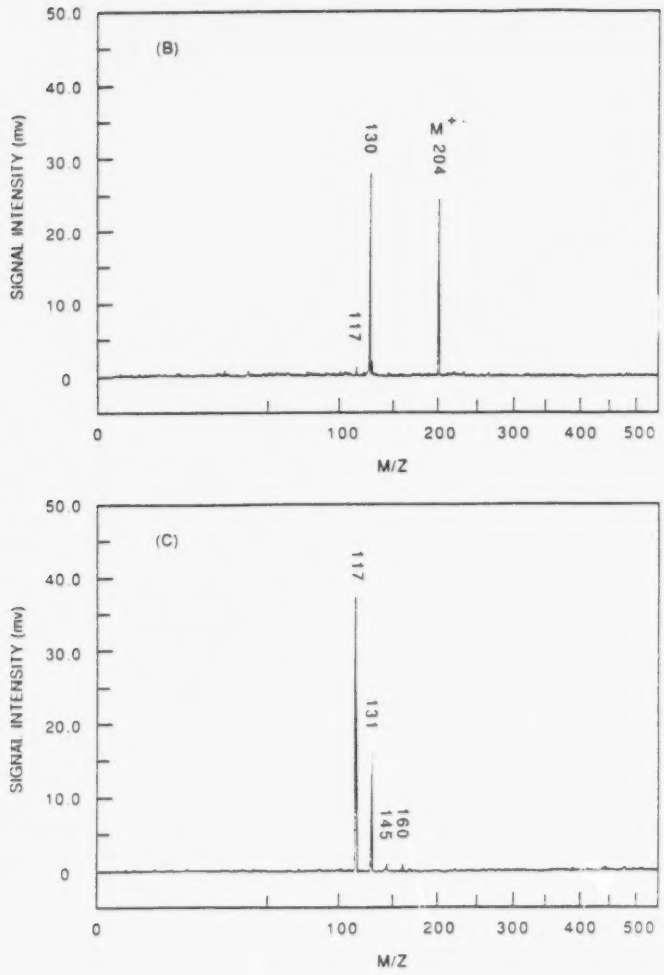

Figure 7.3 MPI mass spectra of (B) the sample collected from the condensed vapor after tryptophan is volatilized in the atmosphere by using the pulsed rapid heating method and (C) the sample collected from the condensed vapor after tryptophan is volatilized by using the slow heating method. The spectra are obtained by using laser desorption/supersonic jet multiphoton ionization mass spectrometry. The ionization laser beam is 266 nm with a power density of about $1x10^6$ W/cm^2. The power density of the CO_2 desorption laser is about $1x10^6$ W/cm^2.

readily decomposes into tryptamine (m/z 160), 3-methyl-indole (m/z 131), and indole (m/z 117) if a slow heating rate is used (~ 2°C/sec). It should be noted that the gas phase spectra for these indole-related molecules are very similar. Thus, in this case, it is difficult to observe in the UV spectrum whether thermal decomposition is taking place during the vaporization process. However, the mass spectrometric study suggests that we are generating neutral gas phase tryptophan species in the pulsed rapid heating process even under atmospheric pressure, since vaporization is clearly favored over decomposition at the faster heating rate [99,102,105] (see chapter 5, part II).

Another class of compounds we have studied are aromatic acids such as amino- and / or hydroxy- substituted benzoic acids. Many of these molecules are biologically significant. For example, a number of metabolites of catecholamines are aromatic acids [123]. These molecules are generally believed to be thermally very labile [123]. Indeed, we found that the UV spectra of the aromatic acids obtained by the PRH method are completely different from those obtained by the slow heating method. Figure 7.4 shows the UV spectra of 3-amino-4-hydroxybenzoic acid in the gas phase with the use of the PRH method for sample vaporization and in methanol solvent. The absorption contours for these two spectra are essentially identical, although the spectrum in methanol is shifted slightly to longer wavelengths. Figure 7.5A shows the UV spectrum of the same compound obtained by the slow heating method. Note that this spectrum is different from that shown in Figure 7.4A, which indicates that structurally different molecules are generated during these two heating processes. To analyze the molecules, the UV spectra of 2-aminophenol in the gas phase and in methanol solvent are obtained and shown in Figures 7.5B and 7.5C, respectively. The spectrum of 2-aminophenol (Figure 7.5B) is almost the same as that shown in Figure 7.5A. This result suggests that thermal decomposition is taking place during the slow

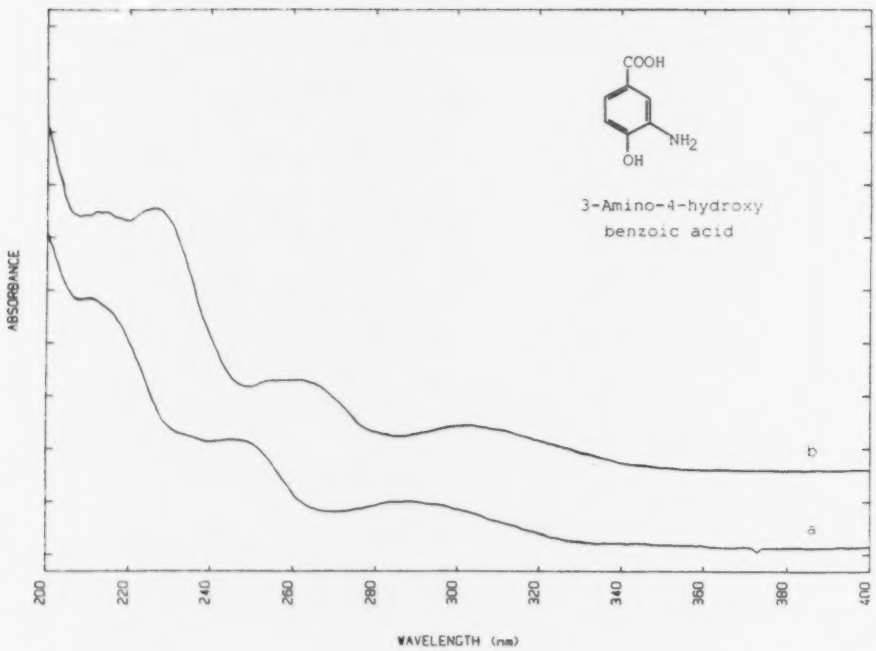

Figure 7.4 UV spectra of 3-amino-4-hydroxybenzoic acid in (a) the gas phase obtained by the PRH method and (b) methanol solvent.

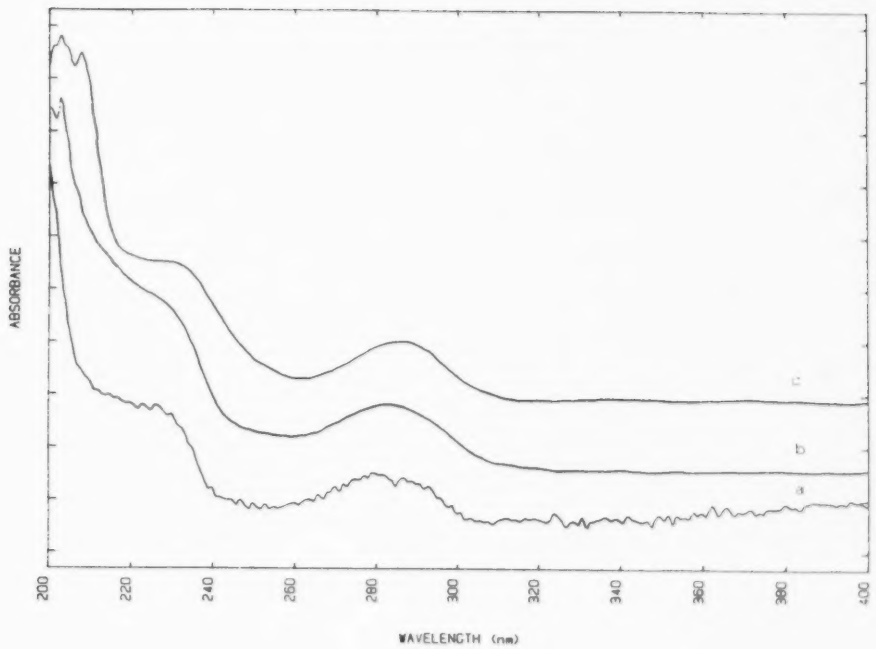

Figure 7.5 UV spectra of (a) 3-amino-4-hydroxybenzoic acid in the gas phase obtained by the slow heating method (b) 2-aminophenol in the gas phase obtained by the PRH method and (c) 2-aminophenol in methanol solvent.

heating of 3-amino-4-hydroxybenzoic acid and one of the major decomposed products might be 2-aminophenol.

To further confirm that slow thermal heating of 3-amino-4-hydroxybenzoic acid produces significant amounts of 2-aminophenol, LD/SJMPI mass spectrometry is again employed to determine the vapor species generated by slow heating and the PRH method. The mass spectra are shown in Figures 7.6 and 7.7. Figure 7.6 shows that the pulsed rapid heating technique produces only 3-amino-4-hydroxybenzoic acid in the gas phase with no thermal decomposition products. Figure 7.7 shows that with slow heating only the decomposed product, 2-aminophenol (m/z 109), is observed in the gas phase. This study indicates that a mass spectrometer with the capability of detecting thermally labile molecules is useful for the determination of thermally decomposed products. However, a simple UV-vis spectrophotometer can still provide some information on whether there is any thermal decomposition during the heating process if the spectrum for the decomposed product is different from that of the intact molecule. More importantly, this study suggests that the PRH method is capable of generating gas-phase molecules under atmospheric pressure conditions for the measurement of UV-vis spectra of these very labile compounds.

7.4 Conclusion

A pulsed rapid heating method has been developed as a means of vaporizing thermally labile biochemicals in a diode-array spectrophotometer for the measurement of gas-phase UV-visible spectra. We have shown that this PRH technique with a heating rate of ~ 10^6 K/sec can vaporize the sample molecules intact at atmospheric pressure without thermal decomposition. Multiphoton ionization mass spectrometry is employed for the identification of intact molecules and any thermally decomposed

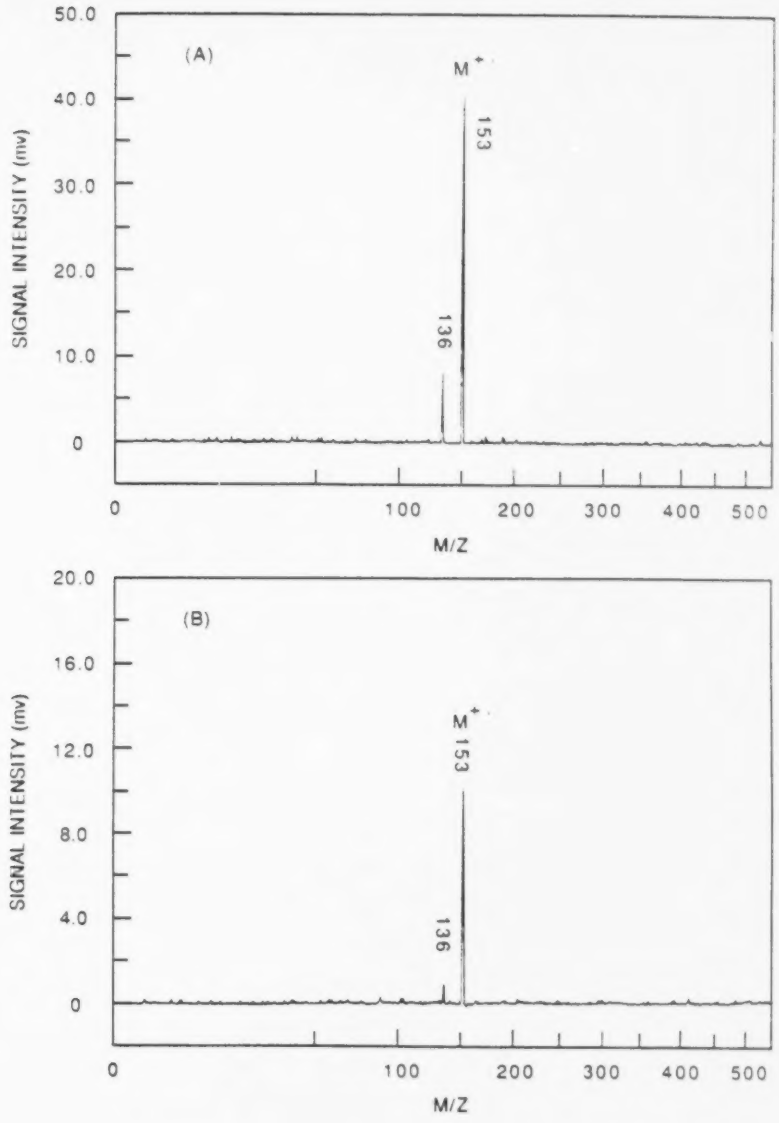

Figure 7.6 MPI mass spectra of (A) pure solid sample of 3-amino-4-hydroxybenzoic acid (MW = 153) and (B) the sample collected from the condensed vapor after 3-amino-4-hydroxybenzoic acid is volatilized in the atmosphere by using the PRH method. The experimental parameters are the same as shown in Figure 7.3.

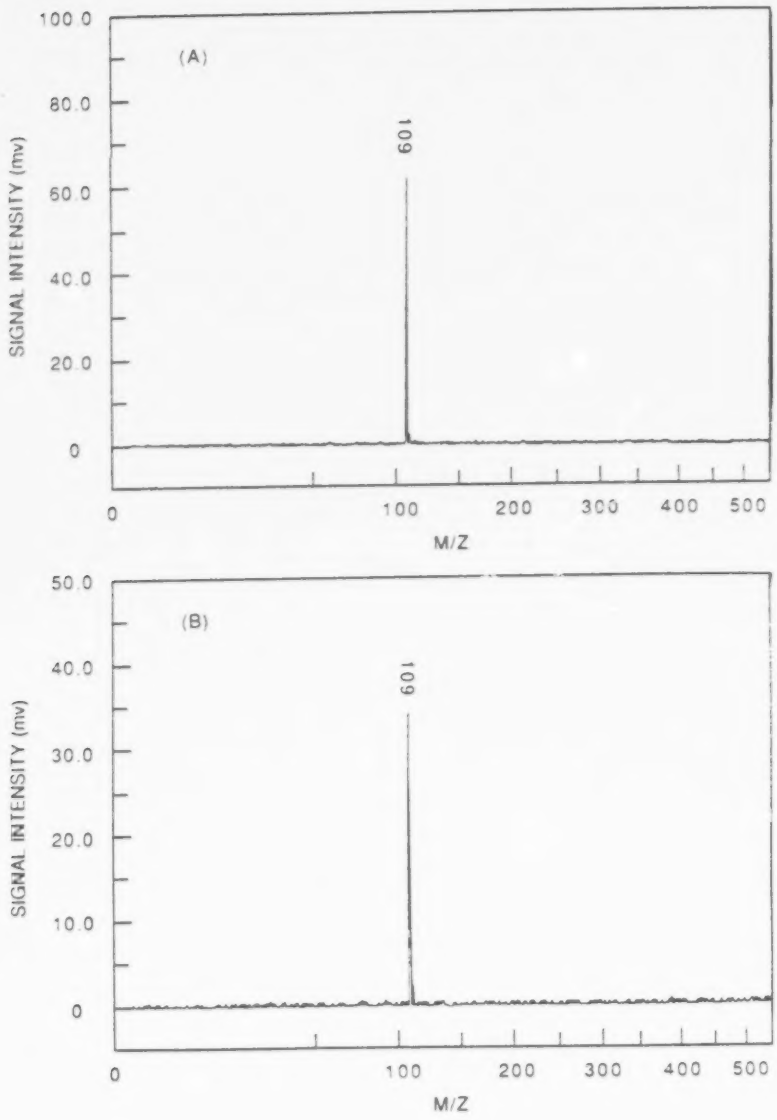

Figure 7.7 MPI mass spectra of (A) the pure solid sample of 2-aminophenol (MW=109) and (B) the sample collected from the condensed vapor after 3-amino-4-hydroxybenzoic acid is volatilized in the atmosphere by using the slow heating method. The experimental parameters are the same as shown in Figure 7.3.

products that may be generated during the PRH process. Using 3-amino-4-hydroxybenzoic acid as a test compound, it is found that thermal decomposition is observed with a conventional direct heating method (heating rate ~ 2 K/sec), whereas sample molecules are vaporized intact with the PRH technique.

Chapter 8

Molecular Cooling and Supersonic Jet Formation in Laser Desorption

8.1 Introduction

Laser desorption (LD) is a powerful method for the generation of ions and neutrals [1,3,46,47,56,124-129]. In particular, matrix-assisted laser desorption ionization (MALDI) has become an increasingly important technique for ion generation in mass spectrometry [3,56,124-129]. As discussed in chapter 1, the technique involves mixing a proper matrix with samples such as peptides and proteins on a substrate, followed by laser desorption. In a time-of-flight mass spectrometer, molecular ions can be observed with little fragmentation even for proteins as large as 300,000 Da [3,56,124-129]. Apparently, although a large amount of energy is implanted to the sample and the sample substrate, these fragile biopolymers can still survive the desorption process. It is also known that the addition of a proper matrix to a sample facilitates the generation of intact neutral molecules by LD.

At present, though, the mechanism for LD is not well understood [130-138]. In studying LD, it is perhaps advantageous to separate the LD process into two temporal events. The first event is the interaction between the laser beam and the sample and/or the sample substrate. The second event is gas expansion after the interaction. Because most experimental measurements are performed after the molecules have expanded a finite distance, it is important to characterize the expansion process well so that any theoretical treatment or experimental measurement of the initial interaction (see chapter

5, Part II) can account for its contribution. This work is directed towards the study of the gas expansion process in laser desorption.

Recently, several groups have argued that molecular cooling during the expansion after the laser impact reduces the probability of thermal degradation of sample molecules [56,128,133-138]. In this work, we have designed an experiment to provide information concerning the internal energies of the desorbed molecules in LD. The experiment involves the use of resonant two-photon ionization (R2PI) spectroscopy [10,139] to examine the molecular population distribution among the internal states of the molecules generated from the desorption process. The key for success of studying the organic molecules spectroscopically is to develop a sample introduction system so that a stable, repetitive desorption event can take place over an extended period sufficient to allow a spectrum to be recorded. We note that Lustig and Lubman [140] have developed a flow probe to deliver samples from a capillary tube to the probe face for repetitive laser desorption. In their technique, neutrals generated by LD are entrained into a supersonic jet and carried into the ionization region of a time-of-flight mass spectrometer (TOFMS), where multiphoton ionization mass spectra are obtained. In this work, a continuous-flow probe is developed to deliver sample and matrix through a capillary tube and onto a stainless steel frit, upon which laser desorption is carried out. The sample molecules expand directly, without a carrier jet, into the acceleration region of a TOFMS, where R2PI is performed with a tunable dye laser. By monitoring the molecular ion intensity of the sample as a function of the ionizing wavelength, a wavelength spectrum is recorded.

In this chapter, we demonstrate that sample molecules, at least for the model compounds studied herein, can be internally cooled during the laser desorption process.

It is found that vibrational temperatures of the small molecules can be significantly lower than room temperature or the temperature of the sample surface. In addition, for the study of molecular cooling for large molecules, a mixture of a high molecular weight biochemical and a probe molecule is used for desorption, and the R2PI spectra of the probe molecule is then examined. The experimental results suggest that the large molecules are cooled during the expansion in LD. This work therefore provides strong evidence supporting the supersonic jet model. It is believed that the matrix species form a jet during LD and provide cooling for the sample molecules. In this work, studies of the parameters affecting the supersonic jet expansion are also reported.

8.2 Experimental

Figure 8.1 shows the schematic of the experimental set-up used for R2PI-MALDI studies. The reflectron time-of-flight mass spectrometer has been described in section 1.7 [17-22,58]. The pressure in the detection region is usually below 1×10^{-5} Torr during operation.

The design concept of the flow probe is, in some aspects, similar to the frit-type probe used in continuous-flow fast atom bombardment mass spectrometry (CF-FABMS) [141]. A silica capillary tube (75 μm i.d., 363 μm o.d., ~ 1 m long) (Polymicro Technologies, Phoenix, AZ) is inserted into a 1.27-cm o.d. and 0.635-cm i.d. stainless steel tube and extends to the probe tip (see Figure 8.1). For electric insulation, the top section of the probe (~ 7.62 cm long) is made of Vespel. The probe tip (5-mm o.d., 1-mm i.d., and ~ 5 mm long), also constructed of Vespel, is then screwed onto this insulator. A septum is placed in between the probe tip and the insulator for vacuum sealing. The capillary tube punctures through this septum and is placed about 1 mm away from the surface of the tip. A 1.55-mm hole is drilled in the center of the tip face

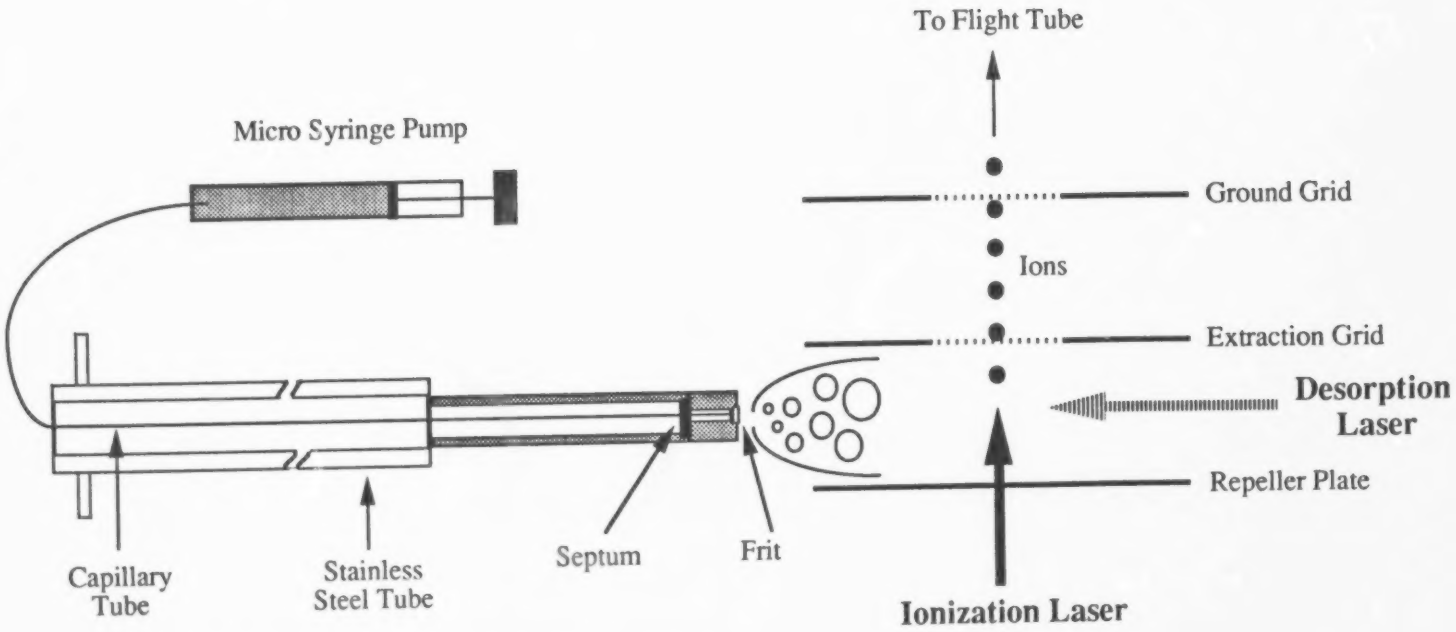

Figure 8.1 Schematic of the continuous flow probe and ionization region of the reflectron time-of-flight mass spectrometer used for resonant two-photon ionization spectroscopic studies of the laser desorption process.

to a depth of 1 mm for housing the stainless steel frit (1.59-mm o.d. and 0.794 mm thick) (Chromatographic Specialties Ltd., Brockville, Ont.). The frit is pushed into the hole to make a direct contact with the end of the capillary tube. The flow probe is inserted into the TOFMS via a custom-made solid probe lock (Whitey Co., ball valve SS-63TSW12T).

In this experiment, a micro syringe pump (Orion Research Inc., Boston, MA) continuously introduces the sample and the matrix onto the frit probe surface. The flow rate is in the range of 2-5 μL/min. Samples are prepared by dissolving the analyte in a water/glycerol mixture to produce a solution in the concentration range of 1-5 mM. The glycerol content is varied from 0-50%. The probe temperature is estimated to be between 5-10°C, depending on the percentage of glycerol used in the solution. It is found that this continuous flow sample introduction technique can provide excellent long term signal stability (less than ± 5% signal variation) which is the key for performing R2PI studies. Moreover, relatively volatile matrices such as water (see Results below) can be used. This is because a dynamic equilibrium between the liquid flow and the vacuum pumping is established in the flow probe. This equilibrium is affected by the flow rate, matrix volatility, and the local pumping speed. Higher flow rate and lower vacuum pumping speed favor retardation of the volatile matrix on the probe.

For laser desorption, a pulsed CO_2 laser (Allmark Model 852, A-B Lasers Inc., Acton, MA) which generates 10.6-μm IR radiation with a 75 ns initial pulse and < 1-μs tailing is used. The repetition rate of this laser can be adjusted from 0.1-15 Hz, although 3 Hz is generally used in this work. The IR laser beam is reflected by copper mirrors protected with a gold coating (CVI Laser Corp., Albuquerque, NM) and focused onto

the sample probe by a germanium plano convex lens (Janos Technology Inc., Townshend, VT). The pulsed neutral sample beam generated from LD expands into the acceleration region of the TOFMS and a UV laser beam perpendicular to the sample probe and the CO_2 beam ionizes the neutrals (see Figure 8.1). The ionization laser beam is from a dye laser (Lumonics HD 500, Ottawa, Ont.) pumped by a Nd:YAG laser (Spectra-Physics GCR-3, Mountain View, CA). Tunable UV radiation is generated by frequency doubling the output of the dye laser (Lumonics HyperTrak-1000). The laser beam is then focused with a convex lens (focal length 30 cm) to a 1-mm diameter spot. The ions produced by the laser are extracted to the flight tube of the TOFMS and detected by a microchannel plate detector.

A digital delay generator is used to control the delay time between the two lasers. The CO_2 laser is first turned on, followed by the ionization laser pulse. The ionization laser power is adjusted for each compound to ensure that only the molecular ion peak is detected in the mass spectrum (soft ionization). The transient signal or the mass spectrum is recorded by a LeCroy 9400A digital oscilloscope. For generating the R2PI spectrum, the molecular ion intensity is monitored with a boxcar integrator as a function of the ionization laser wavelength and recorded on a strip chart recorder.

8.3 Results and Discussion

Evidence of Molecular Cooling: Figure 8.2A shows the room temperature R2PI spectrum of benzimidazole in the vicinity of its origin 0-0 transition (i.e. the transition from the zero vibrational state of the ground electronic state to the zero vibrational state of the excited electronic state). This spectrum was obtained by directly inserting a relatively large quantity of sample (~ 1 mg) on a standard solid probe into the vacuum chamber without performing LD. Benzimidazole (mp 172-174°C) produces sufficient

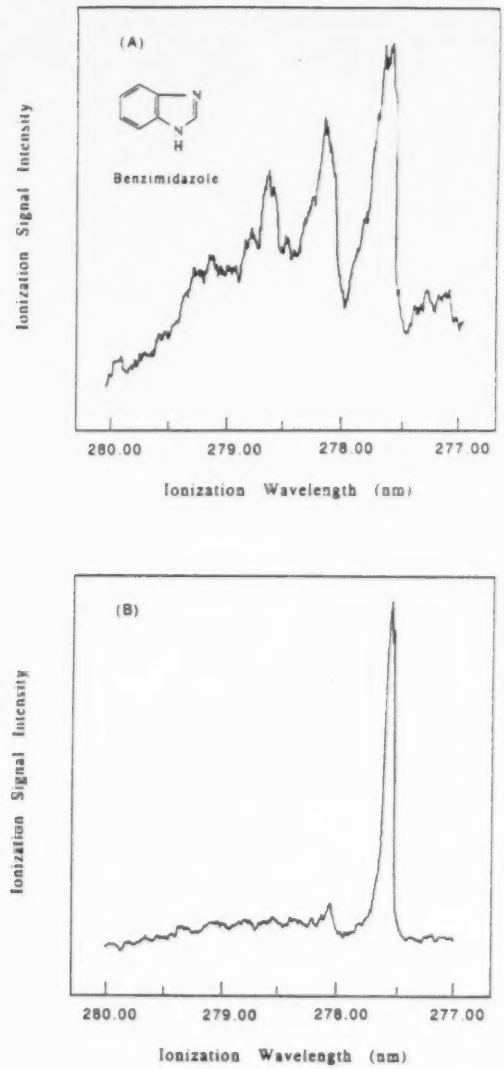

Figure 8.2 R2PI spectra of benzimidazole molecular ion obtained from (A) background molecules at room temperature and (B) molecules generated by using LD with a 7.0 cm expansion distance.

vapor in the vacuum to yield a useful spectrum. Thus, a room temperature R2PI spectrum can be obtained from these background molecules. Figure 8.2B is the R2PI spectrum of the same compound obtained by using LD for neutral generation, with a 7-cm distance between the flow-probe tip and the ionization laser beam. The background signals are negligible compared with the desorption/ionization signals. There are several important features shown in these two spectra. In Figure 8.2A the 0-0 origin band (277.57 nm) is observed along with two comparable vibrational hot bands (278.10 nm and 278.63 nm), corresponding to 1-0 and 2-0 transitions, respectively, with a vibrational spacing ~ 69 cm^{-1}. Clearly, any decrease in the internal energy of this molecule will result in the intensity reduction of these hot bands in the R2PI spectrum. Thus, this molecule should serve as an excellent model to examine the molecular cooling process in LD. Figure 8.2B shows the origin band along with one weak hot band at 278.10 nm. The origin band has been greatly intensified and become much sharper, which indicates that good rotational cooling has been obtained for benzimidazole.

The vibrational temperature of the molecule can be estimated from population distribution among the internal states [142-144]. It is found that the vibrational temperature of the molecules, in the case of Figure 8.2B, is about 46 K for the vibrational mode associated with the hot bands shown. The rotational temperature is, at present, unable to be derived due to the lack of spectral resolution in revealing the individual rotational states. Nevertheless, from the comparison of origin band peak widths in the spectra shown in Figure 8.2A and 8.2B, one would expect that it should be much lower than room temperature. Indeed, the spectrum shown in Figure 8.2B is comparable with that obtained by using a nozzle source [106]. This study indicates that

significant internal molecular cooling may have occurred in the laser desorption process.

Several other molecules such as hydroquinone, resorcinol, carbazole, and indole-3-acetic acid, whose cooling spectra are known from jet experiments with a nozzle source [10,43,59,79,139,145,146], have also been studied. By comparing the room temperature spectra with the spectra obtained from LD, it is found that internal molecular cooling can also be observed for these small molecules.

Parameters Affecting Molecular Cooling: There are several experimental parameters found to affect molecular cooling during gas expansion in LD. First, we find that the cooling is matrix dependent. Here, glycerol is used as the matrix for continuous sample introduction. Glycerol is known to be a good matrix for IR laser desorption [43]. Figure 8.3 shows a series of R2PI spectra of benzimidazole obtained under the same experimental conditions except with varying glycerol concentrations. The expansion distance is fixed at 6.5 cm. As Figure 8.3 illustrates, the cooling effect decreases as the concentration of glycerol increases. Best cooling is obtained when pure water is used. From the nozzle experiment with a seeded molecular beam, it is known that water vapor can be used as the expansion gas to provide good molecular cooling [147]. Water is smaller in size and has fewer internal degrees of freedom than glycerol. It can be cooled more effectively in the jet. Hence, it will absorb more energy from the seeded molecules, resulting in lower internal temperatures. In this LD work, it appears that the water molecules also serve as an expansion gas to absorb some internal energy from the seeded sample molecules.

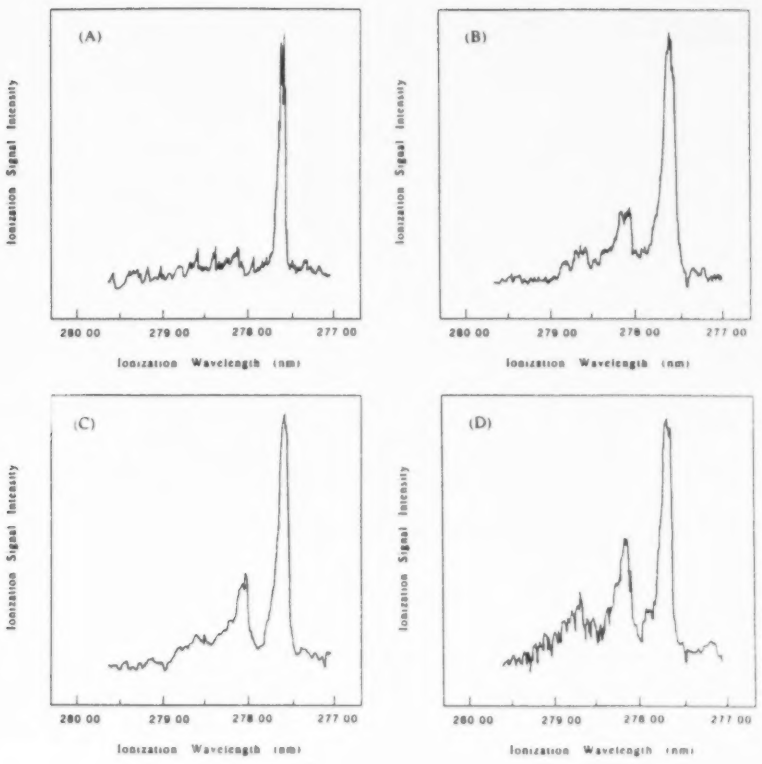

Figure 8.3 R2PI spectra of benzimidazole with LD and varying glycerol percentages: (A) 0% (B) 10% (C) 20% and (D) 50%. The sample expansion distance is fixed at 6.5 cm.

It is worth noting that when the water content increases the pulse-to-pulse reproducibility decreases, resulting in lower signal to noise ratios in the wavelength spectrum. This is due to flow instability caused by a decrease in flow viscosity, similar to that observed in CF-FABMS [141]. In general, a 5-20% glycerol content provides an optimal combination of cooling and signal stability. Addition of a small percentage (< 10%) of other volatile solvents such as methanol or acetonitrile to this mixture does not alter the cooling and the signal stability significantly. However, if more than 50% of these volatile solvents are used, the signal becomes unstable and efficient molecular cooling is difficult to obtain.

The extent of the molecular cooling is also dependent upon the sample expansion distance. Figure 8.4 shows various R2PI spectra of benzimidazole as a function of the distance between the sample probe tip and the ionization laser beam. Clearly, as the expansion distance is increased, the intensities of the hot bands decrease. It is interesting to note that the spectrum at a distance of 4.0 cm (Figure 8.4A) is very similar to the R2PI spectrum of the sample at room temperature (Figure 8.2A). No spectra are shown for expansion distances less than 4 cm. This is because when the distance is shorter than 4 cm, the signal becomes unstable (± 20%). Although the exact threshold distance is compound and matrix dependent, it is normally in the region of 3.5 to 4.5 cm (i.e. 1.5 to 2.5 cm away from the edge of the acceleration plates).

One possible cause of this threshold behavior might be the presence of charged species generated from the desorption laser, which could interfere with the electric field (i.e. via space charging) within the ionization region of the TOFMS. This interference would become severe when the probe is placed close to or inside the acceleration region. However, we find that, by moving the probe to the center of the extraction grid

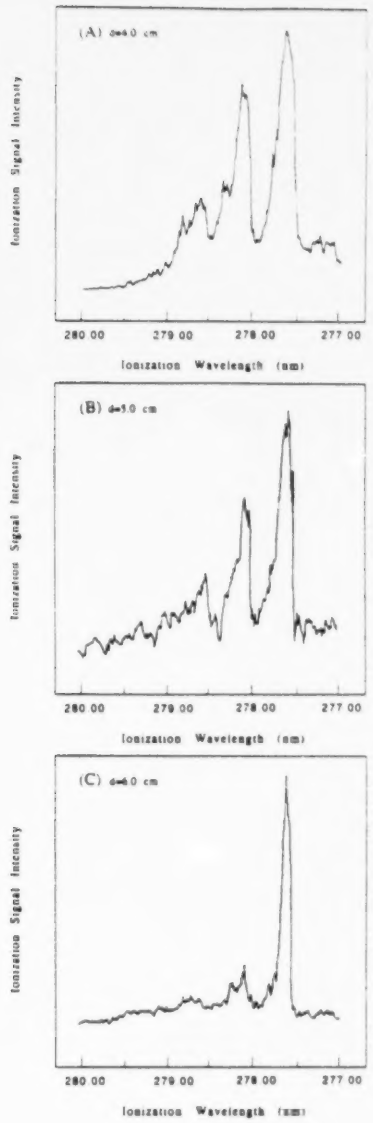

Figure 8.4 R2PI spectra of benzimidazole with LD and varying sample expansion distances: (A) 4.0 cm (B) 5.0 cm and (C) 6.0 cm. The solution sample contains 5% glycerol.

and operating the CO_2 laser only, no ions are detected. This indicates that the signal instability is not from charged species interfering with the electric field. The desorption laser under the experimental conditions used appears to act mainly for the generation of neutrals.

A possible explanation for the threshold behavior of the signal stability is the molecular scattering of the gas jet caused by the acceleration plates. It appears that the initial molecular density of the jet formed by laser desorption is quite high. Unless the jet has expanded a finite distance and the density has been reduced, molecular scattering can take place and interfere with the jet expansion. Note that molecular scattering can also cause interference in the molecular beam experiments with a nozzle source [40]. Scattering can be a major problem there, particularly when a free flow region has not been established. Often a skimmer is used to transmit only the center portion of the beam to the ionization region of the mass spectrometer. In any case, from the results shown in Figure 8.4, one would expect that with a short expansion distance (i.e. less than 4 cm), the sample molecules are not effectively cooled below room temperature. However, when the expansion distance increases from 4 to 6 cm, the vibrational temperature drops from room temperature to less than 57 K. This indicates that jet expansion reduces the internal energy quite effectively.

Velocity Distributions: In the experimental configuration described here, the velocity distribution of the molecules can be readily deduced by measuring the time-of-flight or time-of-arrival (TOA) profile of the samples at a fixed expansion distance [46,137,148-151]. Furthermore, the state-selective ionization method used here can provide unique information on the molecular distribution in a sample pulse generated from the laser desorption process.

Figure 8.5A shows the TOA profile for benzimidazole at an expansion distance of 6 cm. It is obtained by monitoring the molecular ion intensity with the ionization laser wavelength at 277.57 nm as a function of the delay time between the desorption laser and the ionization laser. A different profile is obtained when the ionization laser wavelength is set at 278.10 nm, corresponding to a hot band transition. This profile is shown in Figure 8.5B. The ionization wavelength dependence of the TOA profile is due to the fact that the ion intensity, which is used for plotting the profile, is dependent on the number of neutral molecules available in a particular state to be monitored. Figure 8.5 suggests that different state distributions or molecular cooling are obtained at different regions of the sample profile. This is further confirmed by examining the R2PI spectra of benzimidazole at various positions of the TOA profile. These spectra are shown in Figure 8.6.

Figure 8.6 also illustrates that optimal cooling is achieved at the front portion of the sample pulse. This result is similar to that observed in the jet experiment with a pulsed nozzle source [58] where the front portion of the molecules with a highly directed mass flow are internally cooled more effectively. The tail of the sample pulse consists of some molecular random motions due to background scattering and/or other scattering processes from various sources. The scattering processes tend to block some molecules moving in the jet expansion direction [58]. As a result, the cold molecules are moving faster than the hot molecules. The 277.57-nm TOA profile shown in Figure 8.5A, consisting of a large portion of cold molecules, has a most probable velocity of 7.5 x 10^4 cm/s. In contrast, the 278.10-nm TOA profile, representing mostly hot molecules, has a most probable velocity of 5.9 x 10^4 cm/s. This study indicates that velocity distributions are dependent on molecular cooling. If the extent of the molecular

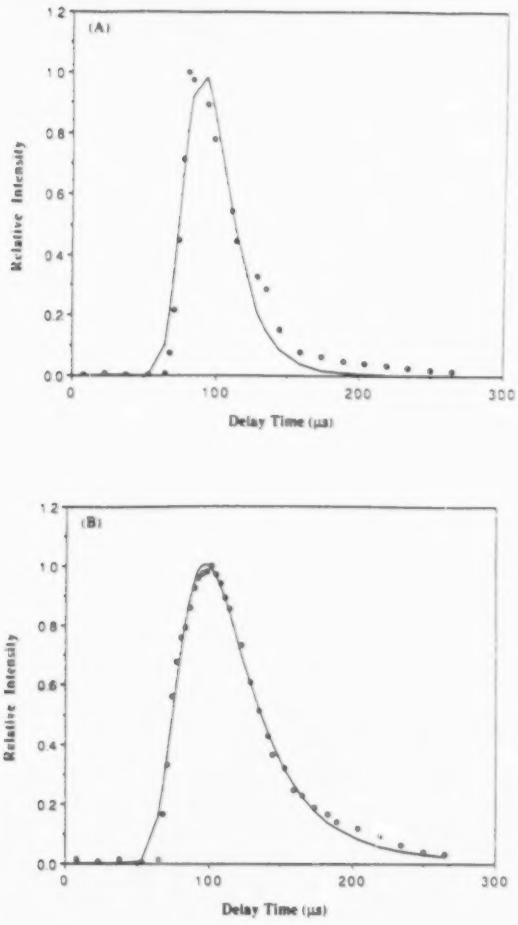

Figure 8.5 Sample pulse profiles of the benzimidazole neutrals generated with LD. These are obtained by monitoring the ionization signal as a function of the time delay between the desorption laser and the ionization laser (at a expansion distance of 6 cm). The ionization laser wavelengths used are (A) 277.57-nm corresponding to the original transition of benzimidazole and (B) 278.10-nm corresponding to the hot band transition. The 278.10-nm profile is scaled about 10 times with respect to the 277.57-nm profile. The solid curve is the best Maxwell-Boltzmann fit.

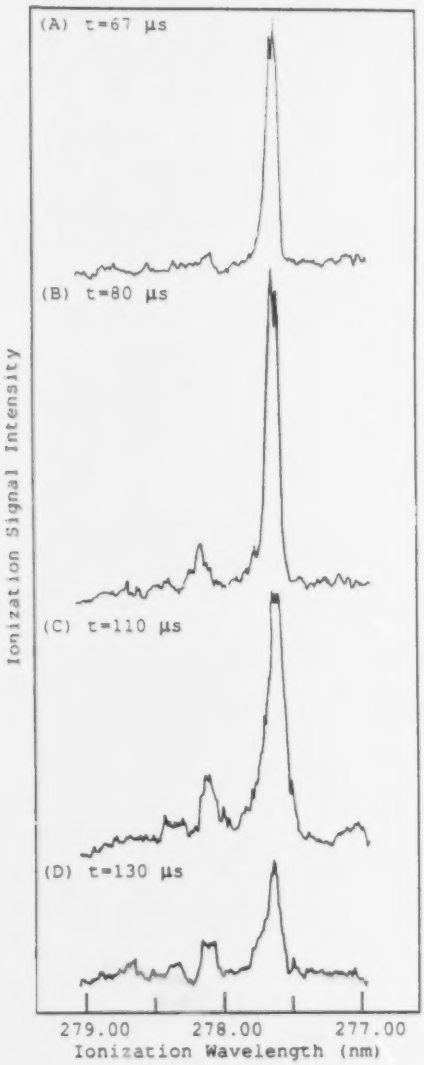

Figure 8.6 R2PI spectra of benzimidazole with LD and different spatial positions of the sample profile shown in figure 8.5. The delay time between the desorption laser and the ionization laser is (A) 67 µs (B) 80 µs (C) 110 µs and (D) 130 µs.

cooling is not substantial, such as in the case where severe molecular scattering occurs during the jet expansion, molecules will move at a lower velocity.

Relation of Internal and Translational Temperatures: The translational temperature of molecules is commonly obtained by fitting TOA data into a Maxwell-Boltzmann distribution [46,137,148-151]. In our system, both the internal temperature and the translational temperature can be obtained, allowing us to examine the relation between these two in the desorption process. We have tried to fit the sample profile data into a modified Maxwell-Boltzmann distribution. The fitting curves are shown in solid lines in Figure 8.5. The translational temperatures derived from the fit are 220 K for the 277.57-nm profile and 450 K for the 278.10-nm-profile. It should be noted that the 277.57-nm sample profile is about 10 times more intense than the 278.10-nm profile. Thus, if no state-selective method is used, the profile obtained will more closely resemble to the 277.57-nm profile and a translational temperature of 220 K would be obtained.

However, as Figure 8.6 indicates, the internal energies of these molecules in the sample pulse cannot be described by using a single temperature. Thus, an averaged internal temperature should be used in order to make a comparison with the translational temperature. This can be estimated by examining the individual internal temperature data from a number of R2PI spectra obtained at various spatial positions of the sample pulse. For the 277.57-nm sample profile shown in Figure 8.5A, the averaged vibrational temperature obtained is estimated to be 66 K. The energy exchange between the translational mode and the vibrational mode of the molecule is incomplete during the expansion.

Note that the 278.10-nm profile is obtained from the relatively hot molecules. These data are a better fit to the Maxwell-Boltzmann distribution than the 277.57-nm profile. In addition, a higher translational temperature for these hot molecules is observed. This illustrates that there is a correlation between the translational temperature and the internal temperature. A lower translational temperature would mean a lower internal temperature.

Molecular Cooling of Large Molecules: While good cooling is observed for small model compounds, we find that it is difficult to observe any significant changes in the spectra of larger molecules such as peptides. This is not totally surprising in light of the fact that the origin transitions of peptides are much more complex [60,152]. Even with a nozzle source, it is difficult to resolve the individual peaks completely. Thus, a broad band is often observed instead of the sharp peaks seen in the spectra of smaller molecules [60]. As a result, for larger molecules, the extent of the cooling obtained in LD is not sufficient to reveal any spectral changes.

While direct probing of the internal temperature of a large molecule is not possible, a set of experiments has been designed to answer the important question, i.e. is there any molecular cooling for large molecules during laser desorption? The experimental design concept can be described as follows. In the conventional supersonic jet experiments with the use of a nozzle source, if a mixture of several components seeded into a carrier gas such as Ar expand to form a jet, molecular cooling for all individual components can be observed [90,118,139,153]. The cooling results from hydrodynamic expansion, where energy transfer processes such as collisional energy relaxation take place among the cooled carrier gas and the seeded sample molecules. The molecular cooling process in the jet reduces the internal temperature of all seeded

sample molecules, although the extent of the cooling, i.e. the ultimate temperature, could be different. In this study, a large spectroscopically unknown sample molecule is mixed with a small probe molecule, such as benzimidazole. The resulting mixture containing excess matrix is subjected to laser desorption, and the probe molecule can be studied in detail by R2PI spectroscopy. The results from this study could provide molecular cooling information for the large sample molecule.

In the first set of experiments, we mix equal moles of benzimidazole with resorcinol and then introduce the mixture to the flow probe. The experiment is performed in the same manner as that used in generating Figure 8.2 where only one component, benzimidazole, is used. The molecular ion peaks of benzimidazole and resorcinol are independently monitored by a gated integrator while the dye laser is scanned, as shown in Figure 8.7. It is found that the spectra obtained for these two compounds from the mixture sample introduction are almost the same as those obtained by introducing one component at a time. Molecular cooling is observed for both compounds.

Next, bradykinin, a small peptide with a molecular weight of 1060, is mixed with benzimidazole in a water/glycerol matrix. The final concentrations for the small peptide and the probe molecule are the same, i.e. ~ 8 x 10^{-4} M. When the mixture is desorbed, followed by laser ionization in the wavelength region of 277-283 nm, only the molecular ion peak of benzimidazole is observed in the mass spectrum and no ion peaks from bradykinin are obtained. However, after several hours of running, no evidence of accumulation of solid samples on the frit probe is found, indicating that the sample molecules are indeed being desorbed by the IR beam. By monitoring the molecular ion intensity of benzimidazole while the dye laser is scanned, an R2PI spectrum is obtained for benzimidazole, as shown in Figure 8.8. It is found that the

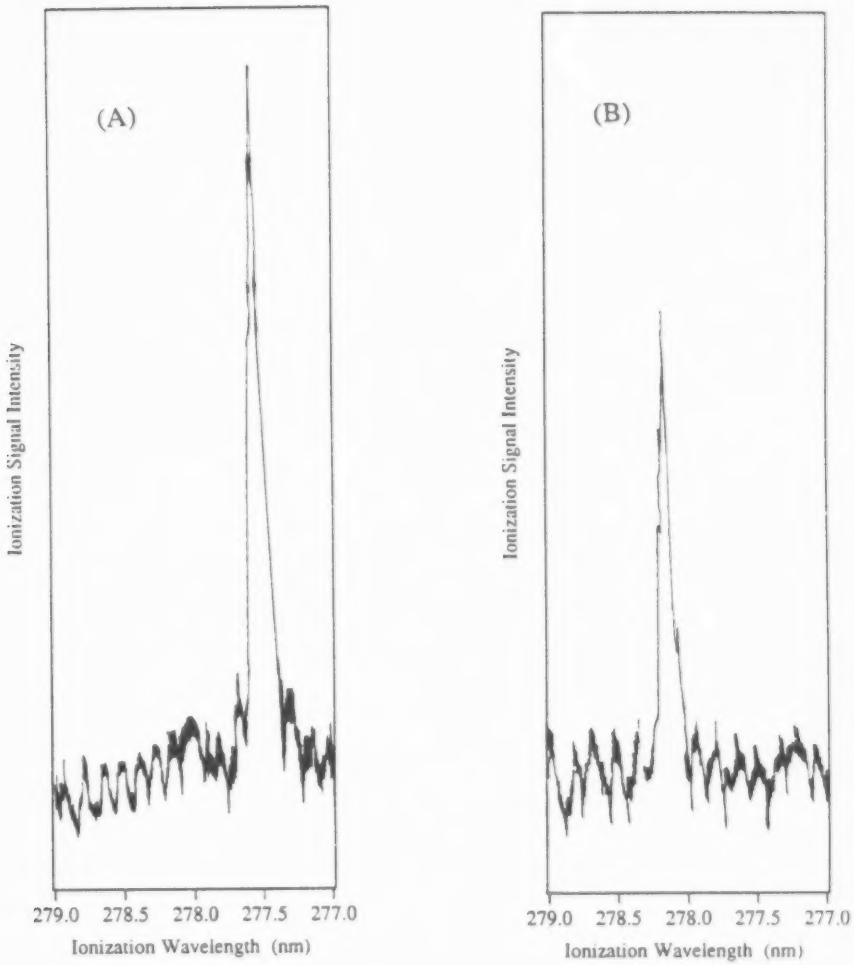

Figure 8.7 R2PI spectra of a benzimidazole and resorcinol mixture (1 x 10^{-3} M each). The molecular ion peaks of (A) benzimidazole and (B) resorcinol are independently monitored by a gated integrator while the dye laser is scanned. Molecular cooling is observed for both compounds.

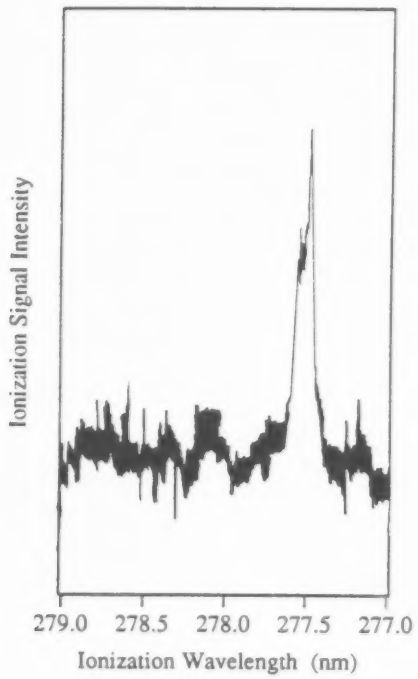

Figure 8.8 R2PI spectra of a benzimidazole and bradykinin (MW = 1060) mixture (8×10^{-4} M each). The molecular ion peak of benzimidazole is monitored by a gated integrator while the dye laser is scanned. Molecular cooling is observed for benzimidazole in the presence of bradykinin.

spectrum is almost the same as that shown in Figure 8.2 when a 7.0 cm expansion distance is used. Cooling dependence on the expansion distance such as that shown in Figure 8.4 is also observed. In addition, by changing the time delay between the desorption laser and the ionization laser to probe different spatial regions of the sample pulse, similar results as shown in Figure 8.6 are obtained.

We have also performed experiments and obtained similar results on a mixture of insulin (MW 5733) and benzimidazole. Moreover, by mixing three components, namely, insulin, benzimidazole, and resorcinol, in a water/glycerol matrix, we can obtain cooling spectra for both benzimidazole and resorcinol.

The above findings indicate that the addition of a small amount of relatively large molecules to the matrix does not alter the molecular cooling of the probe molecules. Since this cooling is the result of extensive energy exchange between the probe molecules and the matrix species, and the large molecules such as bradykinin and insulin are also implanted in this cloud of cold species, molecular cooling of the large molecules should be expected during the laser desorption and jet formation processes.

It should be noted that the present work emphasizes studies of the jet expansion of neutrals in LD. However, the results shown above on neutrals also lead us to the following speculations on ion cooling in LD. It is known that ionic species can be cooled quite effectively by a neutral beam formed by a nozzle [154,155]. Because of the similarity of the nozzle jet and the matrix jet for molecular cooling, one would expect that any ions produced by the desorption laser and entrained into the matrix jet should also be cooled, providing ions are expanded in a field-free region. However, in matrix-assisted laser desorption ionization, ions are often generated inside an electric

field. The presence of the field may change the velocities of the ions. But the effect on neutral jet formation would be minimal because neutral molecules are produced in greater abundance than ions in LD. There is some experimental evidence [156] which suggests that collisions between ions and neutrals do take place in the presence of a high electric field. Since the neutrals are cold molecules, it is conceivable that the ions may be cooled during the ion extraction step through massive collisions among the ions and neutrals. Clearly, a systematic study is needed to fully elucidate the expansion process of ions generated by LD. We believe that the method described here can be extended to expansion studies of ionic and radial species. By monitoring the ionic species or radicals spectroscopically [154,155], information on the processes of ion expansion during LD could be obtained.

8.4 Conclusion

We have designed a system to study the molecular properties of neutrals generated by laser desorption. Using a continuous flow sample probe, problems such as signal instability and multiple desorption in the same sample spot are avoided. We have demonstrated that internal molecular cooling is obtained in the desorption process. This cooling may play an important role in preventing the sample from thermal decomposition.

We have also examined the experimental parameters affecting molecular cooling during jet expansion in LD. It was found that the characteristics of jet expansion in LD are quite similar to those generated with a pulsed nozzle source. Firstly, in molecular beam experiments with a nozzle source, cooling is related to the properties of the carrier gas. In LD, it was shown that cooling was matrix dependent. Matrix molecules with fewer internal degrees of freedom provide better cooling. Secondly, in a nozzle

experiment, the extent of cooling is related to the expansion distance. Until a free-flow region is reached, better cooling is observed as the molecules were probed further away from the nozzle orifice. In LD, a similar phenomena was observed. If an adequate expansion was achieved after desorption, very low vibrational temperatures of the sample molecules was observed. Thirdly, it was found that cold molecules have a different spatial distribution compared to hot molecules in LD. Cold molecules were found at the front of the sample pulse and hot molecules in the tail, similar to the sample pulse from a pulsed nozzle source. This indicates that the velocity or kinetic energy distribution is dependent upon molecular cooling. The hot molecules have lower translational velocities than the cold molecules. Finally, for the molecular cooling study of large molecules, a mixture of a high molecular weight compound and a probe molecule was used. The R2PI spectra of the probe molecule revealed that large molecules are also cooled during expansion in LD.

In summary, although there are several models, including a thermal model and a shock wave model, being proposed to describe the initial laser desorption process, it appears that a supersonic jet model can be used to characterize the gas expansion process. In MALDI, the intact matrix molecules and/or their decomposition products generated by the desorption laser may serve as an expansion gas to form a jet. Samples are entrained into this jet. Since the matrix molecules are internally cold, collisions between the sample and the matrix molecules during expansion provide for extensive energy transfer from the sample molecules to the matrix molecules. In essence, the matrix molecules seem to play the same role as the carrier gas in a jet experiment with a nozzle source.

Chapter 9

Subpicomole Detection of Large Peptides with Continuous-Flow Matrix-Assisted Laser Desorption Ionization Mass Spectrometry

9.1 Introduction

Matrix-assisted laser desorption ionization (MALDI) is a very powerful technique for the generation of ions from large biochemicals [3,56,124-129]. As described in section 1.6, MALDI involves mixing a proper matrix with the sample on a substrate, followed by laser desorption. The technique provides femtomole sensitivity for a wide range of biopolymers. Mass measurement accuracy of better than ± 0.01% has been demonstrated with time-of-flight (TOF) mass spectrometers [56]. MALDI has recently been extended to other types of mass spectrometers [157-160] and, with these mass analyzers, much improved mass resolution has been demonstrated [157-159]. It has also been shown that, without extensive sample clean-up and preparation, good quality mass spectra can be obtained from a sample containing salts and buffers [125-127,161]. Combined with the simplicity of its operation, MALDI has become a very useful tool for biochemical analysis.

Currently, MALDI is performed from a solid insertion probe. A desired feature of the technique would be to desorb and ionize molecules directly from a solution. This would provide an opportunity to use MALDI to study the chemistry of a biological system, such as the monitoring of an enzymatic reaction in a solution, without perturbing its environment. It would also open a new venue to interface MALDI with

various solution-based separation methods such as liquid chromatography (LC) and capillary zone electrophoresis (CZE) for on-line detection and quantitation. For many biological chemical separations, buffers and salts are routinely used. Because of its high tolerance towards salts and buffers, LC/MS or CZE/MS based on MALDI would conceivably require minimum changes in separation conditions.

Recently, our research group demonstrated the feasibility of introducing solution samples directly into a TOF mass spectrometer for MALDI [162]. It involved the use of a continuous flow probe to deliver sample and matrix through a capillary tube and onto a stainless steel frit, upon which laser desorption/ionization was carried out. With this continuous-flow matrix-assisted laser desorption ionization (CF-MALDI) technique [162], it was shown that flow injection analysis could be performed with a liquid matrix, namely 3-nitrobenzyl alcohol. The actual setup closely resembled a LC/MS experiment, but without a column, to obtain mass spectra of small peptides and flow-injection ion profiles with sample injections in the 100 picomole region. It was anticipated that with further modifications, both in the design of the flow probe as well as in the optimization of the TOF mass spectrometer, the sensitivity of the CF-MALDI technique could be enhanced.

In this chapter the design of a new flow probe is described [25]. Improved performance for CF-MALDI in terms of sensitivity, signal stability, and mass resolution is demonstrated. It is shown that, with the new probe, it is now possible to perform flow injection analysis of large peptides with molecular weights above 10,000 with CF-MALDI and to obtain flow injection ion profiles in the subpicomole region. The new flow probe continuously delivers the liquid matrix (dissolved in a solvent mixture) through a capillary tube and onto a small, polyimide Kapton surface (DuPont Co.)

without the use of any frit. An injector placed between the syringe pump and the probe allows for the on-line injection of large peptides and protein samples. The results obtained with this new probe demonstrate that CF-MALDI is a promising and potentially very useful technique for the on-line detection of large biochemicals from solutions.

9.2 Experimental

Probe Design Consideration: In MALDI, a small amount of sample in the picomole to femtomole region, loaded onto a solid probe, often yields a mass spectrum with a good signal-to-noise ratio (static MALDI). The detection limit achieved with the MALDI technique depends on several factors including ionization efficiency, detection efficiency, and the sample loading procedure. From a technical point of view, the major difference between static MALDI and dynamic MALDI (or CF-MALDI) is the sample loading procedure. In both cases only a small area of the sample is subject to laser desorption, since the laser beam is normally focused onto a spot size of less than 500 μm in diameter. Thus, the question of how one loads the sample into a small, confined area on the probe becomes important in determining the overall detection limit of a MALDI system. In CF-MALDI, the sample is either injected or dissolved into a carrier solvent containing 3-nitrobenzyl alcohol, and flows continuously over the probe surface. Consequently, it is expected that the detection limit of the CF-MALDI method is affected by the probe surface area onto which the solution diffuses. Diffusion of the sample solution onto a large area on the probe surface would result in a high detection limit. Other parameters may also play a role in determining the overall sensitivity, such as the degree of sample adsorption onto the capillary tube or to other parts of the probe with which the sample solution makes direct contact.

In order to obtain better detection sensitivity with CF-MALDI it is necessary to increase the ratio between the area of the sample being desorbed and the total area of the sample diffused on the probe. There are two major ways of achieving this goal. Firstly, an increase in the laser beam size would allow a larger sample area to be desorbed. However, we found that an increase in the beam size above 0.5 mm in diameter does not enhance the signal intensity significantly [162]. This interesting finding is carefully being studied to determine whether it is an intrinsic feature of the MALDI technique with a 3-nitrobenzyl alcohol liquid matrix or if it is merely caused by certain experimental conditions. Secondly, the above mentioned ratio could be increased by decreasing the sample probe area. This would allow the sample to flow in a more confined region on the probe surface. The new flow probe described below is geared towards this latter strategy. In addition, the stainless steel frit used in our previous design [162] has been eliminated.

Design of the New Probe: Figure 9.1 shows the design of the new flow probe. A silica capillary tube (101-μm i.d., 370-μm o.d., 38 cm long) (Polymicro Technologies, Phoenix, AZ) is inserted into a 1.27-cm o.d. and 0.635-cm i.d. stainless steel tube and extends from the injector to the probe tip. For electrical insulation the end section of the probe is made of Vespel (~ 2.5-cm long, 2.8-mm o.d. diameter). At the Vespel tip a piece of Kapton (2.8-mm diameter), with a small hole pierced through the center, is mounted. The use of the Kapton sheet improves the flow stability, possibly due to the improvement of surface properties such as the surface flatness over the Vespel material. The capillary tube protrudes through the hole in the Kapton and is placed no more than 1 mm above the surface. The hole will allow the capillary to slide back and forth but it is not big enough to allow back flow of the liquid. A piece of filter paper is wrapped several times around the probe tip to absorb the excess liquid. The flow probe is

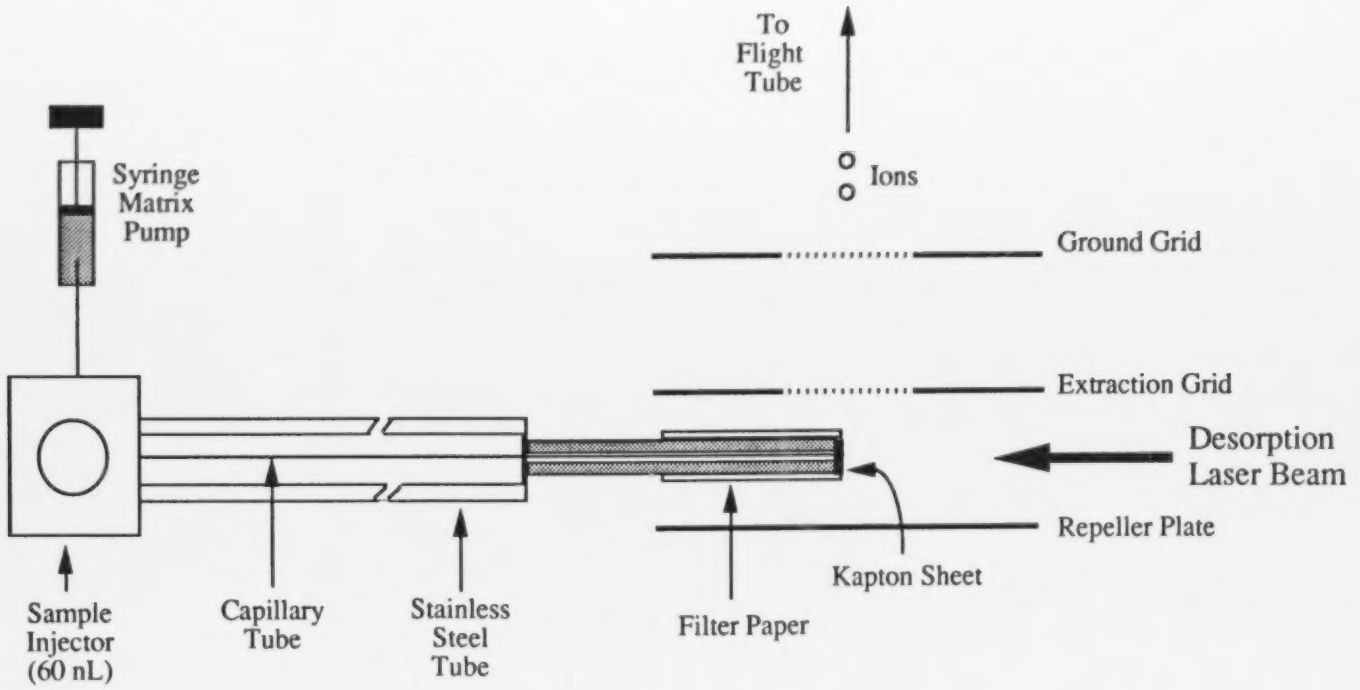

Figure 9.1 Schematic of the flow probe used for continuous-flow matrix-assisted laser desorption ionization. Drawing is not to scale. The dimensions of the major components are given in the text.

conveniently inserted into the TOF mass spectrometer between the repeller and extraction plates via a custom-built solid probe lock (Whitey Co., ball valve SS-63TSW12T).

Sample Preparation: All chemicals were purchased either from Sigma or Aldrich. The carrier solvent consists of a mixture of 25% of 0.1% trifluoroacetic acid (TFA), 25% of 95% ethanol, 30 - 35% ethanediol, and 15 - 20 % 3-nitrobenzyl alcohol (all by volume). Trypsinogen ($6x10^{-6}$ M, MW ~ 24, 000) is also added as an internal standard to the carrier solvent (see below). This entire mixture is filtered through a 0.5 μm PTFE membrane filter and degassed by bubbling helium for 3 minutes. It is continuously introduced onto the tip of the probe surface at a flow rate of 6 μL/min with a micro syringe pump (Orion Research Inc., Boston, MA). A 60-nL sample injector (Valco Instruments Co., Houston, TX) is placed in between the pump and flow probe to perform flow injection analysis. A point heater made of a Nichrome 60 heating coil (Pelican Wire Co., Naples, FL) is placed perpendicular to both the probe and the flight tube to provide gentle heating to the flowing liquid. The distance between the heater and probe is about 2 cm. The temperature of the point heater is about 120°C in the vacuum, although the actual temperature at the probe tip is unknown.

Time-of-Flight Mass Spectrometry: A reflectron time-of-flight mass spectrometer (R.M. Jordan Co., Grass Valley, CA) is used for the CF-MALDI experiments reported here. This angular reflectron system [17-22] has been described in section 1.7. In brief, the ionization region of the TOF consists of a repeller and an extraction grid. Immediately after ionization, ions will be repelled by the repeller plate and drawn through the extraction grid. A set of Einzel lenses placed just above the

extraction grid can be used for focusing the ions. A pair of deflection plates, i.e. the ion deflector, is placed above the Einzel lenses to control the trajectory of ions traveling towards the detector. In addition, a 600 V pulse is applied to one of the deflection plates in order to reject low mass ions. This is important in CF-MALDI in order to reduce ion detection saturation caused by a large number of low mass ions originating from the 3-NBA matrix solution. The microchannel plate detector takes on the order of milliseconds to recover after being activated by incoming ions [57]. Since a complete mass spectrum takes about 150 μs to record it is necessary to deflect the low mass ions, otherwise the high mass ions of interest will not be effectively detected.

Our system consists of two ion detectors. One is placed behind the reflecting field or the reflector which is at the end of the flight tube. In this configuration this system will function the same as a linear TOF mass spectrometer when the reflecting field is turned off. When the field is on, ions will be reflected to the other detector, which is placed at the other end of the flight tube near the extraction grid. The reflector can withstand up to 5 kV reflecting voltage. Thus, the present design of the reflector is suitable for reflecting relatively low mass ions. However, for ions with molecular weights above 10,000 it is generally found that a voltage higher than 5 kV is required to achieve good detection sensitivity. Therefore, in this study, the reflectron system is operated in a linear mode.

Laser Desorption: A frequency quadrupled Nd:YAG laser (GCR-3, Spectra-Physics, CA) which generates 266 nm radiation is used for performing MALDI. The laser is operated at 10 Hz repetition rate. A convex lens (300 mm focal length) is used to focus the laser beam to a ~ 0.5 mm diameter spot on the flow probe. The spot size is estimated by examining the dark image created on a thermal-sensitive paper, which is

placed on the probe using double sided tape, after the paper has been briefly exposed to the laser beam.

Data Processing: The mass spectrum generated by the laser desorption process is recorded with a LeCroy 9400A digital oscilloscope. The analog signal is preamplified 25X before being fed into the oscilloscope. Data produced on the oscilloscope are then transferred in real time to a PC via GPIB. The data transfer and data analysis software was developed in house. The data system is capable of transferring and storing transients up to 20k data points at a repetition rate of greater than 10 Hz from the oscilloscope to the PC via GPIB. After storing all the mass spectra in the PC, either a selective ion or a total ion chromatogram can be established. The display and storage of a mass spectrum of interest can readily be done by moving the cursor along the chromatogram to the point where the mass spectrum is desired. Both the mass spectrum and the chromatogram can be saved into a text disk file for use by other commercial software packages for further processing such as mass spectral averaging.

This simple and readily adaptable data system is adequate and useful for many operations in laser work where relatively higher repetition rates are required. We recently demonstrated the recording and construction of ion chromatograms in LC/TOFMS with a pulsed sample introduction (PSI) interface [24] and CF-MALDI [25]. In addition, we showed that the data system cannot only replace the traditional boxcar integrator for signal monitoring, but also provide multiple ion monitoring for recording wavelength spectra in laser ionization spectroscopy [24].

Data System Hardware: A one meter cable connects the LeCroy's GPIB port to the National Instruments model AT-GPIB board inside a PC. The board has a transfer

speed of 1 MByte/sec. The PC is a generic 486DX33 machine with a 210 MByte hard drive, 4 MBytes of RAM, a mouse, and a high resolution color monitor.

Data System Software: The application is written in Microsoft Quick C version 2.01 and linked with the LabWindows version 2.2.1 libraries from National Instruments. The LabWindows software was chosen mainly because its graphical user interface is easy to configure and has many built in functions. Although a driver for the LeCroy oscilloscope is in the LabWindows instrumental driver library, it is too slow (2 Hz maximum transfer rate for 20 Kbytes transients) for our work. A high speed oscilloscope driver was developed and written in C that uses several strategies (see below) to attain higher transfer speed.

The main goal, in terms of acquiring mass spectral data, was to achieve rapid data storage. Several techniques were employed to attain this goal:

1. Software double buffering is developed and used in our software so that the GPIB board can transfer the data from the digitizer to one buffer, while concurrently the contents of the second buffer is transferred to the disc. After the record has been transferred, the buffers are swapped and the sequence repeated. The concurrence of data transfer from the digitizer and simultaneous data storage to the disc means that the limiting speed of record acquisition is attributed to the rate-determining step.
2. The seek times for the disc are largely eliminated by buffering the data sent to the disc drive by a cache controller card. This allows data to fill the buffer, while at the same time the heads seek the next track and the disc spins to the correct sector.
3. Delays associated with the oscilloscope limit the acquisition speed for small size records (i.e. record length < 2 Kbyte). These delays are reduced by using single-

character commands to control the oscilloscope to shorten the set-up time. For larger size records, the data transfer rate from the LeCroy to the computer limits the acquisition speed.

4. A further speed increase for all record sizes is possible by disabling the display on the LeCroy's front panel. In this manner, LeCroy's internal processor can be freed to deal only with the acquisition and transfer of data, and thus does not have to calculate display information. However, the present version of the software does not allow the mass spectrum to be displayed on the computer screen during the experiment. Nevertheless, the screen can be turned on during the run to continuously observe the mass spectrum. Compared with the screen-off mode, running the experiment in the screen-on mode reduces the transfer speed by at least a factor of 2.

9.3 Results and Discussion

Detection of Large Peptides and Sensitivity: With the new flow probe for performing CF-MALDI experiments, it is found that mass spectra and flow injection ion profiles of peptides and proteins with molecular weights exceeding 10,000 can be obtained. Figure 9.2 shows the mass spectrum of lysozyme, a protein with a molecular weight of about 14,300, obtained by using flow injection CF-MALDI with a total sample injection of 2 picomoles. At this low concentration, a singularly charged molecular ion peak is observed. This is also true for many other peptides studied by CF-MALDI with a 3-NBA liquid matrix. No fragmentation from the parent ion is observed. In the low mass range up to m/z ~ 1000 the large signal is mainly from the matrix molecules. The peak at m/z ~ 24,000 is from trypsinogen. Trypsinogen is added to the carrier solution as a standard which continuously flows onto the probe. The use of the standard assists the initial optimization of the flow conditions. During

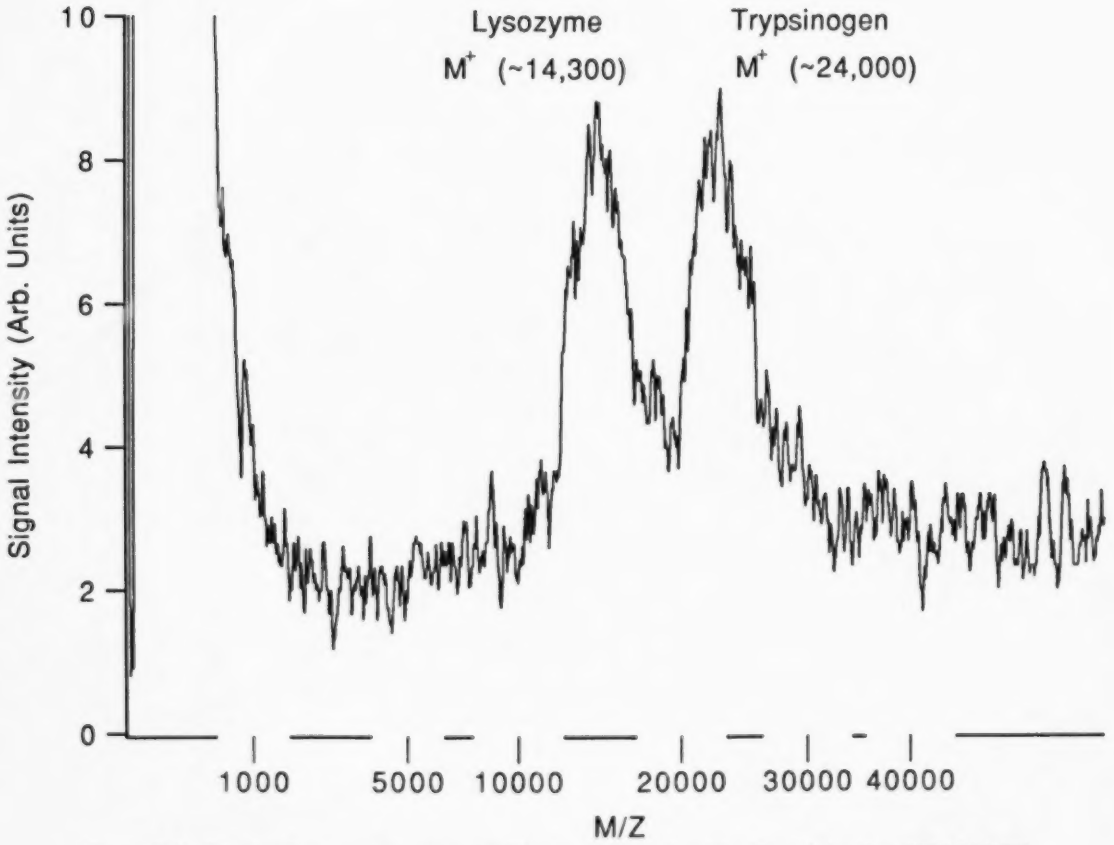

Figure 9.2 Single-shot mass spectrum of lysozyme obtained by flow injection CF-MALDI. The total sample injection is 2 picomoles. Trypsinogen (6×10^{-6} M) is added to the mobile phase and is continuously introduced into the probe for the purpose of optimizing the flow conditions.

the course of the experiment, the molecular ion signal of trypsinogen is carefully monitored to ensure that experimental conditions such as laser power are not significantly changed. This is important in the cases where reproducible results are essential, such as in flow injection quantitative work. A standard is chosen such that its molecular ion peak does not overlap with the molecular ion of the sample. It should be noted that if only a mass spectrum is desired then a standard is not necessary.

With an injection of 2 picomoles of the sample, it is found that, with a laser operating at 10 Hz, more than 500 mass spectra can be obtained. Thus, a flow injection ion profile can be obtained by calculating and plotting the peak area of the molecular ion as a function of the elution time. Figure 9.3 shows the ion profile of seven repeated injections of 2 picomoles of lysozyme. The ion profile is obtained by integrating the molecular ion peak area of each mass spectrum collected and summing 10 peak areas to generate one data point in the ion profile. During the construction of the ion profile, only the peak areas are summed and no averaging of mass spectra is performed.

As Figure 9.3 illustrates, the ion signal from one sample injection lasts more than 50 s. The mass spectrum shown in Figure 9.2 is a representative single shot spectrum from the first injection. The arrow in Figure 9.3 indicates the point from which the mass spectrum was obtained. In our data system, to select and save a single shot spectrum, the cursor is moved to the point shown in Figure 9.3. Since each mass spectrum is assigned a record or file number, any record can be viewed by entering or changing the record number near or at the point chosen. Since one point in Figure 9.3 results from the summing of ten individual peak areas, the change of record number to display different individual mass spectra does not necessarily result in a move of the cursor in the ion profile. A representative single shot spectrum is shown here to illustrate the

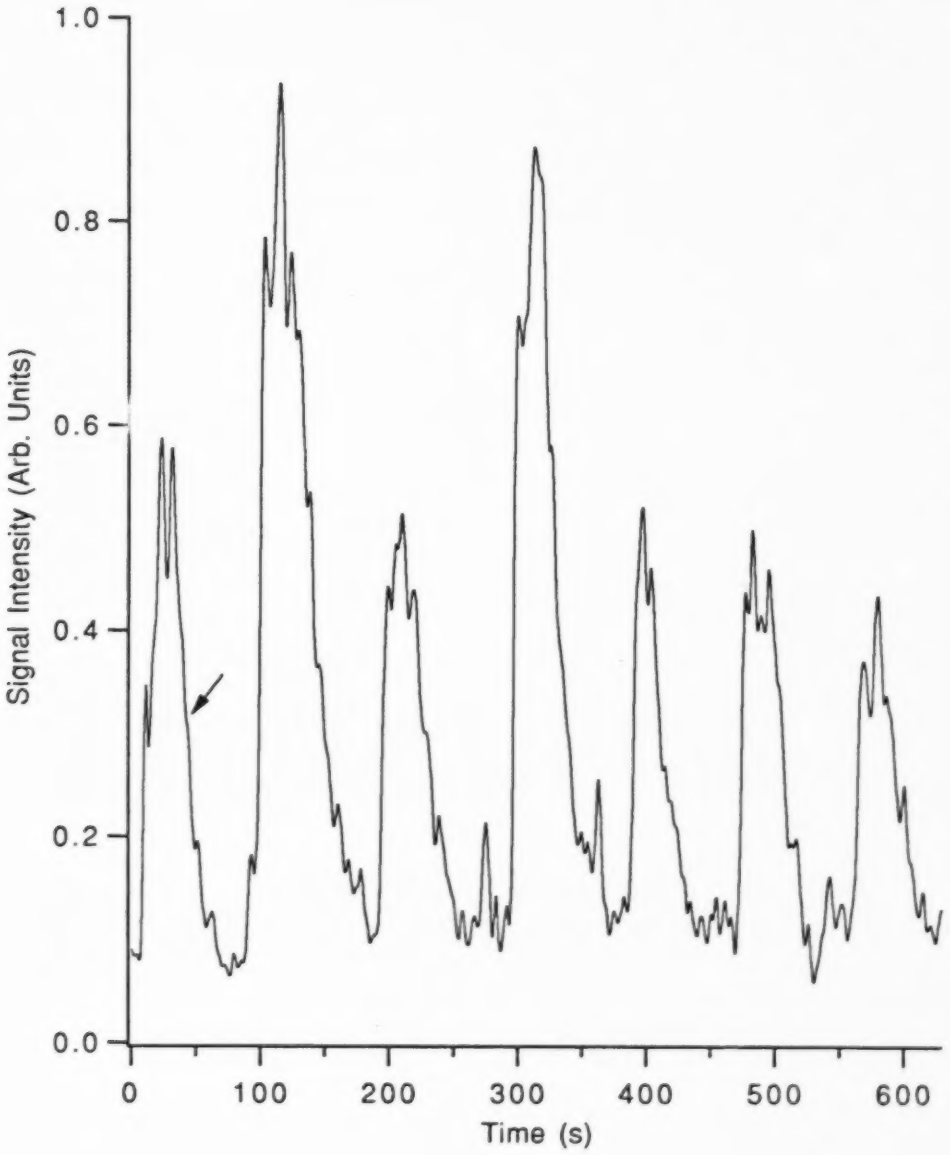

Figure 9.3 Flow injection ion profiles of lysozyme (7 repeat injections; 2 picomoles each).

detection sensitivity of the CF-MALDI method. The exact amount of sample consumed in generating such a spectrum is unknown. However, realizing that over 500 mass spectra with an average peak intensity similar to that shown in Figure 9.2 can be obtained, and only a portion of the sample flowing onto the probe surface is actually being desorbed, much less than 2/500 picomoles or 4 femtomoles of the sample are used for generating one mass spectrum.

Figure 9.4 shows the ion profiles of repeated injections of different amounts of cytochrome c (MW ~ 12,360). These ion profiles display a reasonably good signal-to-noise ratio, which again demonstrates that subpicomole detection of these peptides and proteins is possible with CF-MALDI. A representative single-shot mass spectrum obtained from a total injection of 3 picomoles of cytochrome c is shown in Figure 9.5. The total amount consumed for generating such a spectrum is less than 3/500 picomoles or 6 femtomoles.

Examples of subpicomole detection of peptides with even higher masses are given in Figure 9.6. Figure 9.6 is a representative single-shot mass spectrum of chicken egg albumin with a molecular weight of ~ 44,650 Da. The amount injected is 9 picomoles. Figure 9.7A shows the corresponding flow injection profile. Smoothing the raw data can sometimes result in enhancement of the signal-to-noise ratio, as shown in Figure 9.7B. The smoothing algorithm is derived from Marchand and Marmet [163], and is part of the Igor Software Package (WaveMetrics, Inc.). This smoothing operation, also called Gaussian filtering, convolves the data with normalized coefficients derived from Pascal's triangle.

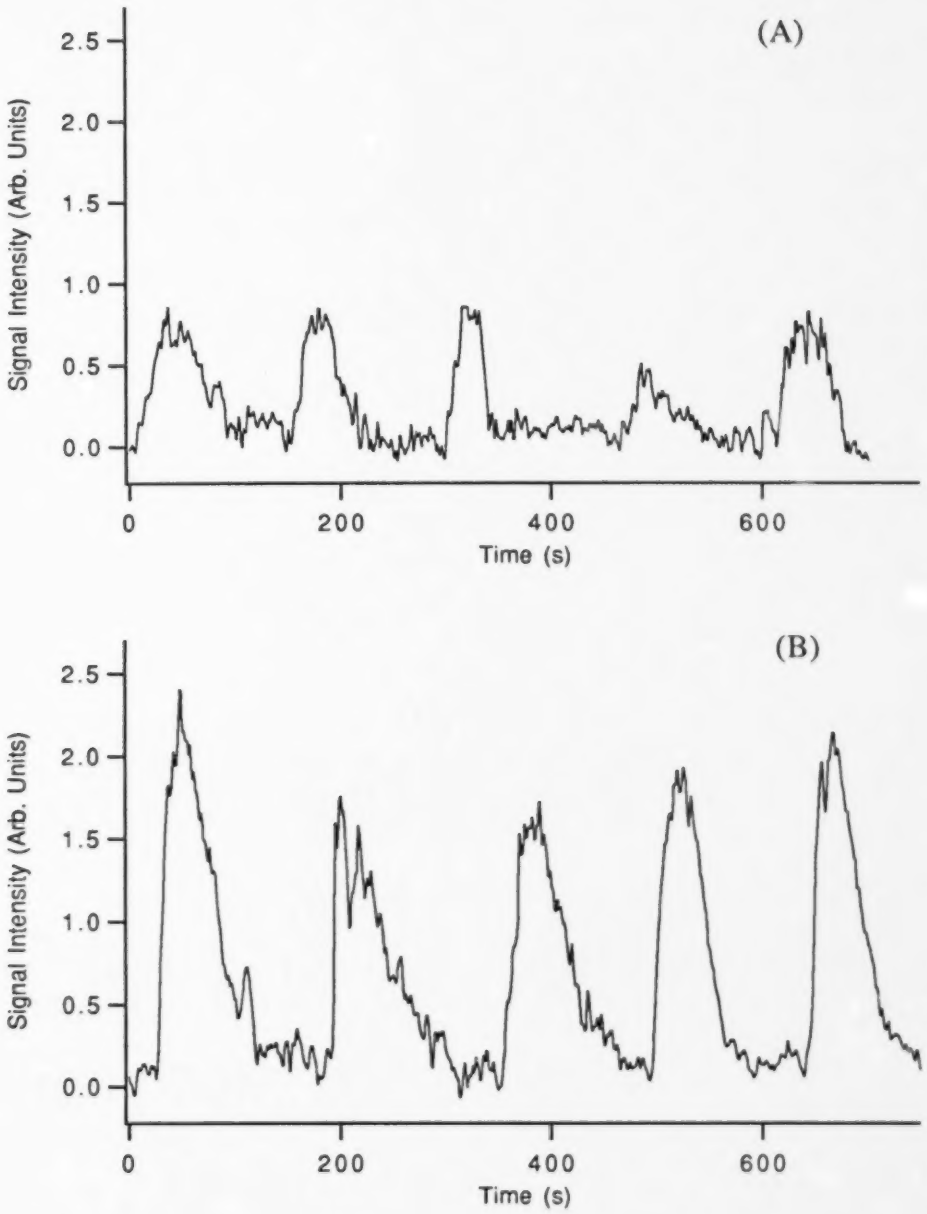

Figure 9.4 Flow injection ion profiles of different amounts of cytochrome c (5 repeat injections)
(A) 3 picomoles and (B) 9 picomoles.

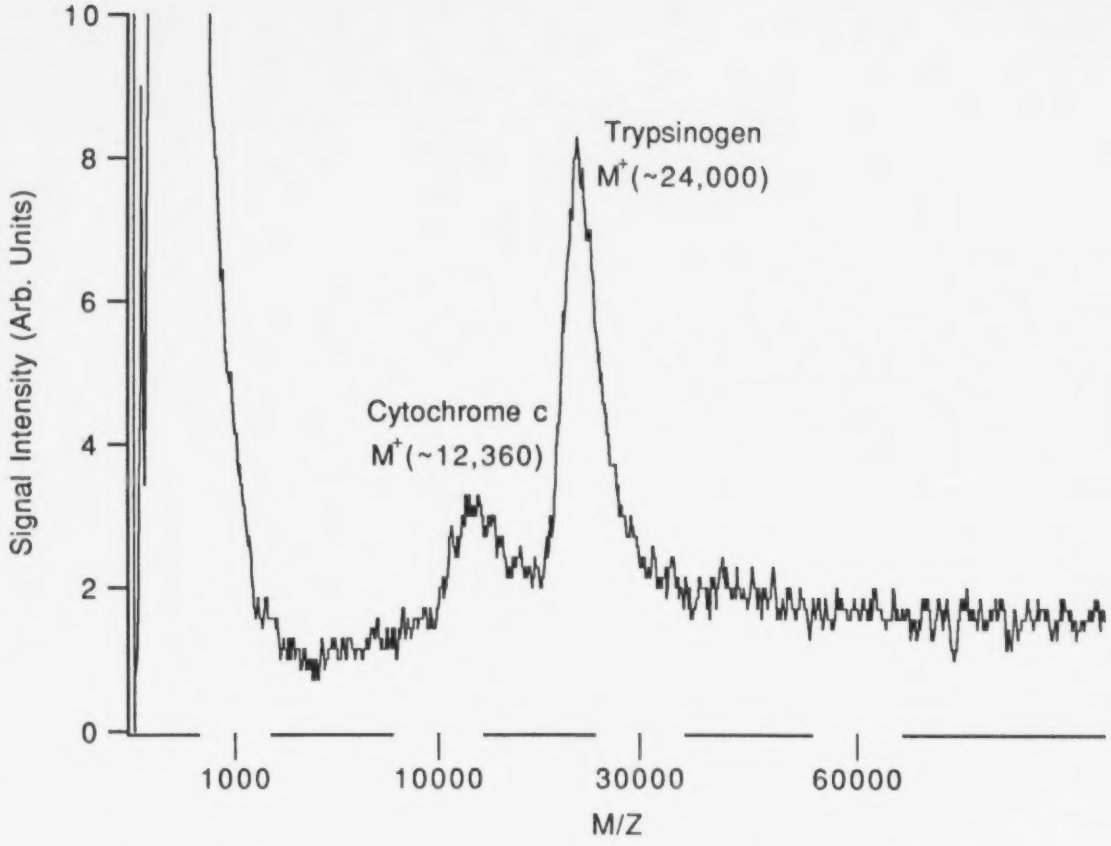

Figure 9.5 Single-shot mass spectrum of cytochrome c obtained by flow injection CF-MALDI (3 picomole injection).

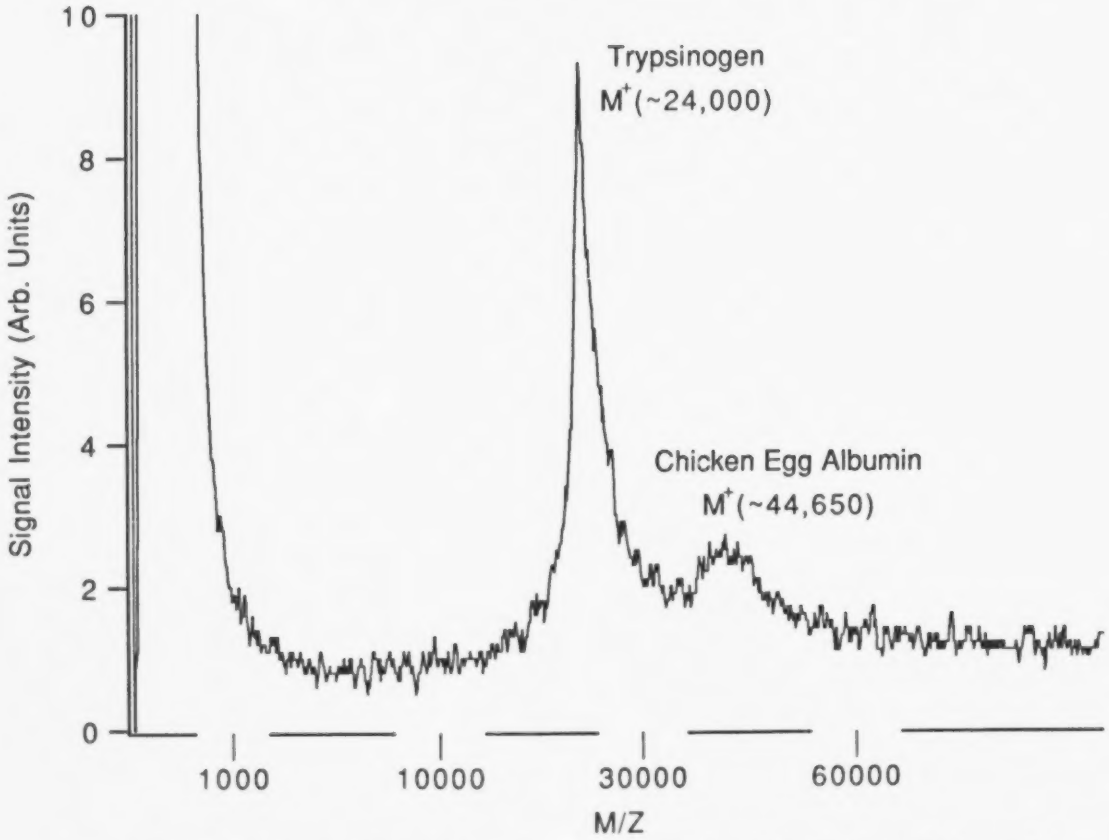

Figure 9.6 Single-shot mass spectrum of chicken egg albumin from a 9 picomole injection. The experimental conditions are similar to those shown in figure 9.4

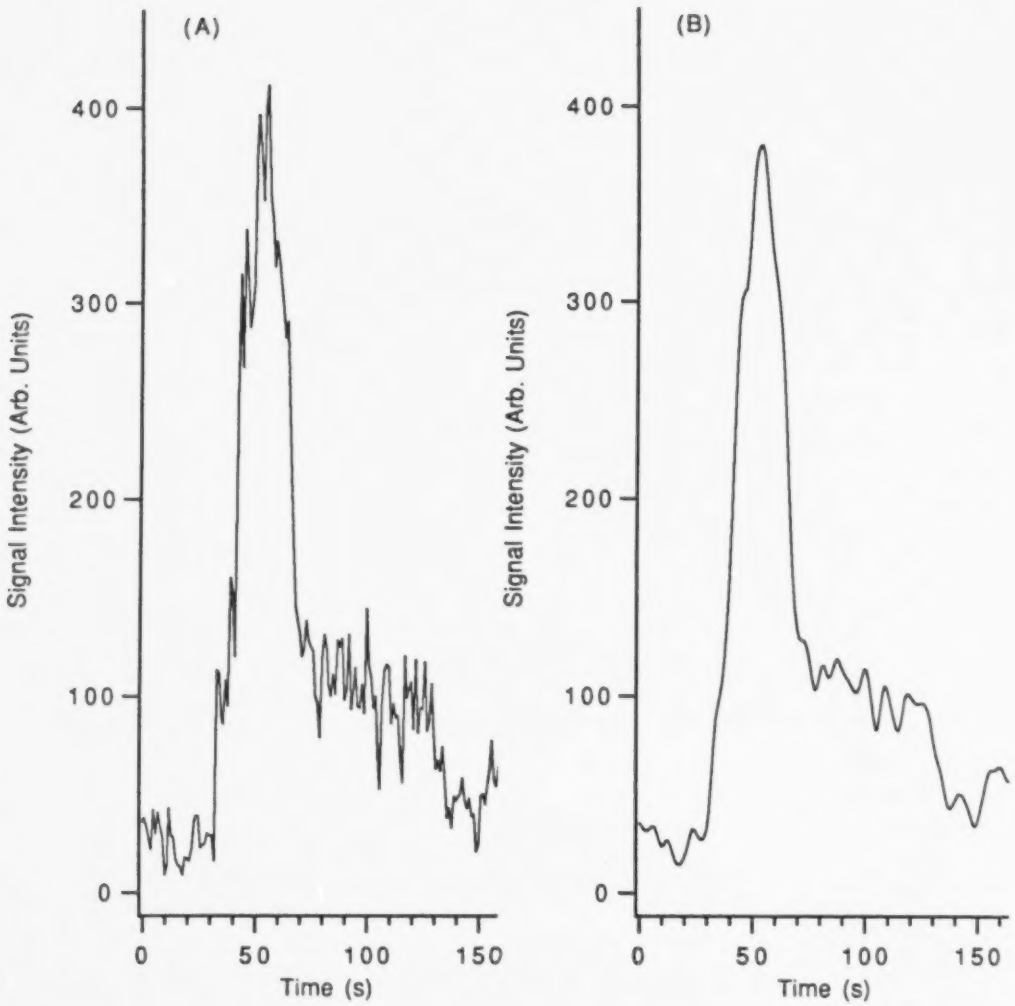

Figure 9.7 (A) Unsmoothed and (B) smoothed flow injection ion profiles of chicken egg albumin (9 picomole injection).

Signal Stability and Quantitation: With CF-MALDI, flow injection experiments can be performed as illustrated in Figures 9.3, 9.4, and 9.7. The peak areas can sometimes be quite reproducible, as shown in Figure 9.4B. The relative standard deviation (RSD) in this case is about 1.5%. However, in general, the average RSD is in the range of 10-20%. As Figures 9.3 and 9.4 illustrate, there are some variations in both the peak intensities and the peak areas in the ion profiles. Although other factors such as variation in injection volume and sample loss due to adsorption of sample molecules on the capillary tube and/or other parts may contribute to these variations, one major parameter which, we believe, plays an important role here is the flow conditions. With the aid of a video camera and a video monitor, we took a close look at the flow on the probe face. We observed some irregular flow patterns on the probe face from time to time. Notably, it was found that the liquid from the capillary tube did not necessarily flow in a defined area. Some local disturbances, perhaps from the solvent evaporation process, were observed.

It is clear that a detailed study is necessary to identify and understand factors that affect the flow stability. At this stage, some preliminary observations on flow stability are worth noting. Firstly, the amount of 3-NBA used in preparing the solution is important. A solution containing 5-20% 3-NBA gives a relatively stable flow. Secondly, high flow rates often result in narrower peaks in the flow injection experiments. Unfortunately, high flow rates also decrease the flow stability. In addition, high flow rates also tend to increase the frequency of replacing the filter paper wrapped around the probe. But, even at a flow rate of 6 μL/min, a fresh filter can last for more than 3 hours. Thirdly, during several hours of daily operation very stable signals can be obtained, although the stable period is sometimes unpredictable. This can actually be seen in Figure 9.3. The 5th, 6th, and 7th injection give reasonably good reproducible

peak areas. Yet, the second and forth injections generate two peaks with areas larger than the other five injections. This is also the case for other flow injection experiments we have performed with this probe. This finding does indicate that highly reproducible results should be possible if the CF-MALDI process were well understood and controlled. In particular, flow conditions and other factors necessary for achieving stable signals must be identified (see chapter 11).

With the new probe, as Figure 9.4 shows, concentration dependence of the signal intensity can be observed. A plot of total sample injected as a function of peak area for this compound is shown in Figure 9.8. An order of magnitude of linear response is obtained. At higher concentrations signal saturation is observed. While the precision of the method needs to be improved further by optimizing the flow conditions as discussed above, this preliminary result does indicate that CF-MALDI has the potential to become an important tool for the quantitation of peptides and proteins.

Mass Resolution: Although the present design of the flow probe does improve the detection sensitivity and extend the applicability of the CF-MALDI to large peptides, it does not enhance the mass resolution. Some preliminary observations on mass resolution are worth noting here. In most reported MALDI work, the ions generated by the laser expand in a direction parallel to the electric field (parallel extraction). All the laser-induced ions experience the same electric field. In this manner, one can reduce the initial spatial distribution of the ions to improve mass resolution. However, in our experimental setup for CF-MALDI, the ions expand in a direction perpendicular to the electric field (orthogonal extraction) with constant voltages applied to the repeller and extraction grid. This configuration allows us to flow the liquid into the ionization region of the TOF without electric breakdown. However, with this configuration, even

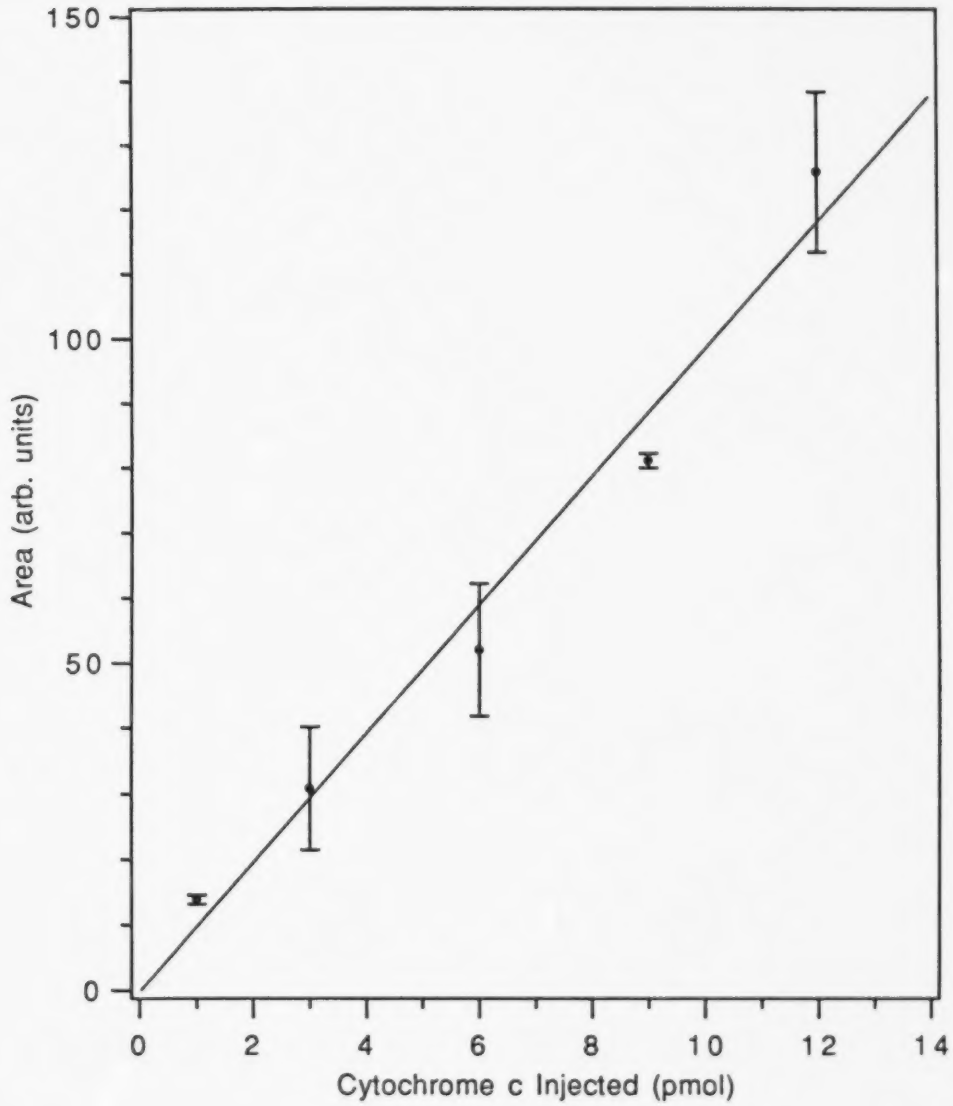

Figure 9.8 Ion profile peak areas as a function of the amount injected for cytochrome c. Error bars are ± 1 standard deviation from 5 repeat injections.

using a very small laser beam size, one would expect some ion spatial distribution, which would result in poor mass resolution. It should be noted that orthogonal ion extraction has been reported previously by Spengler and Cotter [129]. In their work, the ions are extracted by a delayed voltage pulse applied to the acceleration plates. Our results on large peptides appear to have similar mass resolution to those reported by Spengler and Cotter [129], although different matrices are used.

We also find that the resolution obtained with CF-MALDI is not degraded when compared with static MALDI with a 3-NBA matrix. In general, the mass resolution ($t/(2\partial t)$, where t is the flight time and ∂t is the peak width at FWHM) obtained with an orthogonal ion extraction in a linear TOF in both static and CF-MALDI is in the range of 5-20. By comparing with the typical mass resolution reported in the literature [3,56,124-129,164,165], we note that there is a factor of 5-15 times reduction in mass resolution with the orthogonal configuration we are using.

We recently constructed a new test chamber that allows us to perform both parallel and orthogonal ion extraction. With this new apparatus, we can directly compare the performance between these two configurations for ion extraction. We are currently investigating the possibility of using parallel ion extraction configuration for CF-MALDI. Recent results from this new mass spectrometer are presented in chapter 11 [26].

While the orthogonal ion extraction configuration seems to provide poor resolution due to the broad spatial distribution of the ions, another well known factor affecting the mass resolution is the initial kinetic energy distribution of the ions produced by the laser. In an attempt to increase the mass resolution by reducing the initial energy

distribution, we have performed some CF-MALDI experiments by operating the TOF system in a reflectron mode. As discussed in the experimental section, our reflectron TOF system cannot be operated at high voltages. But with low acceleration voltages (< 5 kV), we are able to detect ions from small peptides with molecular weights less than 3000. Figure 9.9A shows the mass spectrum of bacitracin in the molecular ion region obtained in a linear TOF by continuously flowing the sample to the probe, followed by laser desorption. Figure 9.9B shows the mass spectrum obtained with the reflectron system. All experimental conditions are similar to those used for large peptides. However, a higher sample concentration is used due to the sensitivity reduction associated with low acceleration voltages. It is clear that the reflectron provides much better mass resolution. Figure 9.9B reveals that the broad peak observed in the linear spectrum actually consists of several peaks.

As Figure 9.9B shows, the reflectron system does improve mass resolution for performing CF-MALDI, even with the orthogonal ion extraction configuration. For small peptides, we find that mass resolution above 100 with our reflectron system can be obtained. However, whether or not this holds true for high mass ion detection is unknown at present. Installation of a high voltage reflector to one of our linear TOFs is planned in order to examine the performance of CF-MALDI in a reflectron mode for high mass ion detection.

The above mentioned results indicate that a major challenge in the future development of CF-MALDI in a TOF system is to overcome the poor mass resolution associated with the current setup. Several areas need to be improved for circumventing this problem. These include the use of a reflector, the optimization of the ion extraction configuration, a study of other liquid matrices, and the optimization of the solution

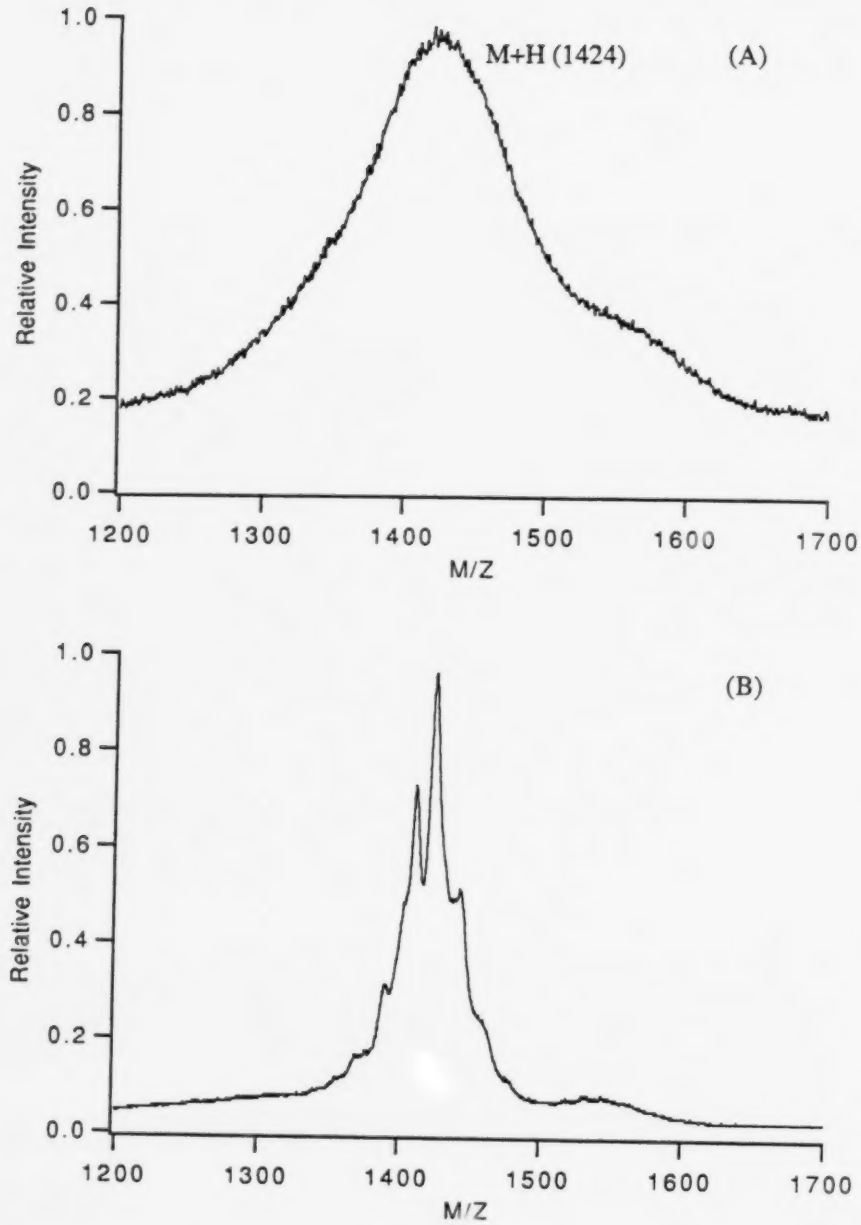

Figure 9.9 (A) Linear and (B) reflectron TOF Mass Spectra of bacitracin under CF-MALDI conditions. The molecular ion region is shown. The flow conditions are the same as those shown in Figure 9.2.

composition (see chapter 11). It should also be noted that the extension of the CF-MALDI method to other types of mass spectrometers [157-160] might be very useful and worthwhile for improving the mass resolution as well as for MS/MS work.

3-NBA Matrix and Mixture Analysis: It is worth commenting on the applicability of 3-NBA as a matrix for peptide detection. In CF-MALDI, the matrix choice is very limited at present. In fact, we find that only 3-NBA works well with our current experimental setup. Although 3-NBA is not being widely used, there are several reports of using it for static MALDI experiments [3,166-169]. We have examined about 50 different peptides and proteins including 24 synthetic peptides with molecular weights up to 67,000. We have not had any major problems for detecting signals from all these compounds with the use of 3-NBA as a matrix, except for pepsin. A mass spectrum of pepsin cannot be obtained with 3-NBA in both static and CF modes. This is consistent with the results reported by Zhao et al [167] where 3-NBA was also used as a matrix in a fibrous substrate. Why a mass spectrum for pepsin cannot be obtained with 3-NBA is unknown at present. Clearly the general applicability of 3-NBA as a matrix for CF-MALDI needs to be investigated further, particularly if the technique is to be extended to other types of biomolecules besides peptides.

MALDI is well suited for the direct study of simple mixtures. Figure 9.10A shows the mass spectrum of a 1 μL solution containing 8 picomoles of lysozyme, 6.5 picomoles of ß-lactoglobulin, and 6 picomoles of trypsinogen, mixed with 1 μL 3-NBA matrix. The mass spectrum obtained with CF-MALDI is shown in Figure 9.10B. This mixture was chosen because it was reported that the addition of pepsin to the mixture reduces the ion signals of these three proteins. We did not observe this ion suppression

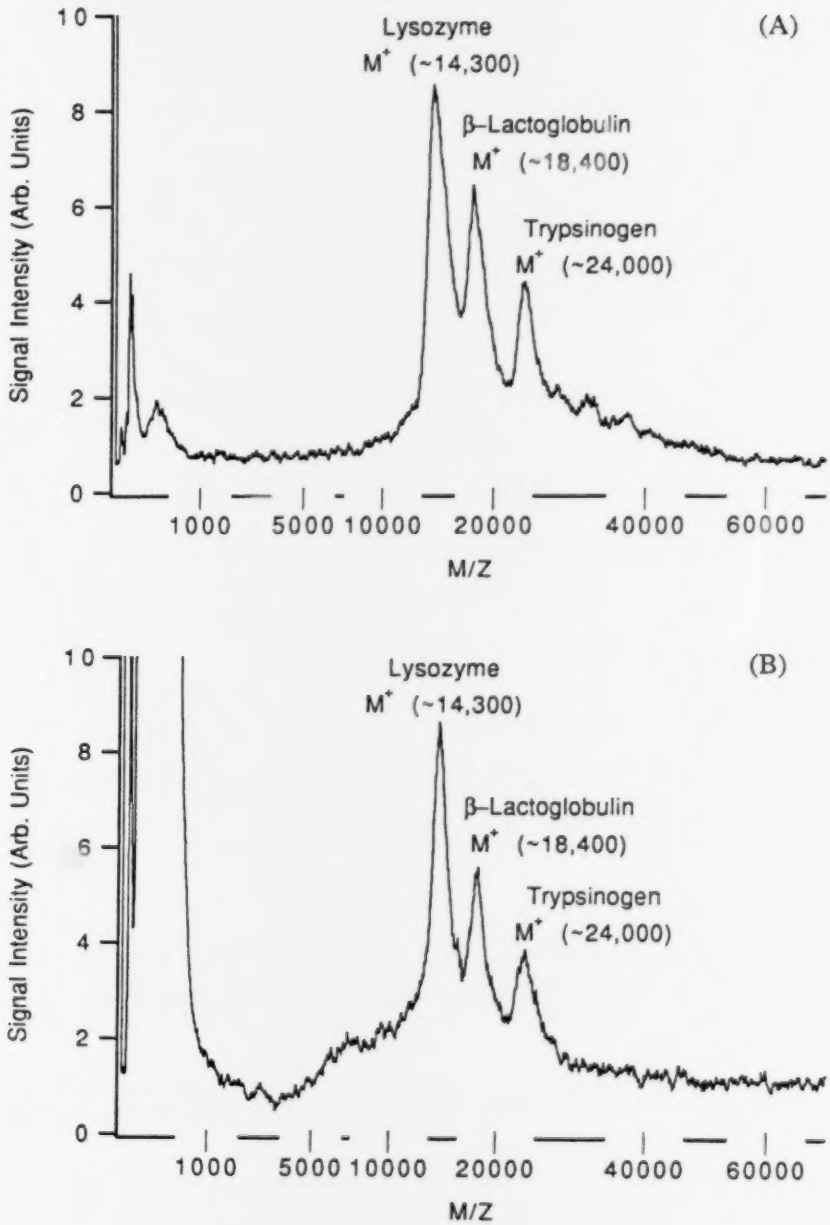

Figure 9.10 (A) Static MALDI and (B) CF-MALDI mass spectra of a mixture of three proteins: lysozyme, b-lactoglobulin, and trypsinogen. The matrix is 3-NBA.

phenomenon in our system with both static MALDI and CF-MALDI. This is not surprising though in light of the fact that the experimental conditions can affect the extent of ion suppression. It is known [161] that by choosing a proper matrix and optimizing the laser conditions as well as the sample preparation procedures, ion suppression effect can sometimes be reduced, although it would become more difficult when the mixture becomes more complex. However, it should be noted that in CF-MALDI with a liquid matrix, another possible complication could arise from the hydrophobicity of a peptide. It is known that in fast atom bombardment where a liquid matrix is used, hydrophobicity of a peptide plays an important role on the ion detection [170]. Whether this is also true in MALDI with the use of liquid matrices such as 3-NBA, and, if so, to what extent hydrophobicity would affect the ion suppression, needs to be investigated in the future. In any case, it is clear that combining a solution-based separation method with MALDI for mixture analysis would reduce or eliminate the ion suppression problem. This forms the basis for chapter 10.

Fritted and Fritless Probes: The current design of the flow probe does not use a frit. On the performance of this flow probe and the frit-type probe reported previously [162], a direct comparison is difficult, at present. However, our work to date indicates there are some differences in performance between these two probes. It was found that the frit probe provided somewhat better flow stability. It was relatively easy to obtain reproducible results. This was particularly true in the initial development of the CF-MALDI technique. However, after we gained more knowledge on the operation of the fritless probe reported here, we now do not see much advantage in using a frit to obtain a stable flow. It seems that it is more difficult to perform flow injection analysis for large peptides with the frit probe. Occasionally, the frit needs to be replaced with a new unit, indicating that adsorption of samples and/or other species on the frit occurs.

There are perhaps two main advantages of using a fritless probe such as the one reported here. One is the possibility of reducing the probe surface size without much difficulty in machining. The second one is the possibility of directing the flow to a confined and, hopefully, smaller region on the probe without much diffusion. Diffusion is normally found in the case of a frit-type probe. Nevertheless, we believe that with our increasing experience with CF-MALDI, a reliable probe should be possible for routine analysis. The current design of the probe shows much promise and, indeed, is used again in the next chapter to couple on-line liquid chromatography with CF-MALDI.

9.4 Conclusion

A new flow probe has been developed to provide improved performance for CF-MALDI. Based on our initial studies with the new flow probe, some important features of CF-MALDI with regard to sensitivity, signal stability, and mass resolution can be summarized as follows. First of all, CF-MALDI can provide sensitive detection for large peptides and proteins. With a total sample injection in the low picomole region, a flow injection ion profile with a good signal-to-noise ratio can be obtained. For a single-shot mass spectrum, the total amount of sample consumed is estimated to be several femtomoles. Secondly, stable flow can be obtained with the new probe as demonstrated with the flow injection experiments. Results from the signal concentration dependence study indicates that a linear response of one order of magnitude can be obtained. Thirdly, the orthogonal ion extraction configuration used for CF-MALDI seems to provide relatively poor mass resolution. However, much improved resolution is obtained with the use of a reflectron TOF system, at least for small peptides. Finally, on the use of 3-NBA as a matrix for CF-MALDI, results indicate that 3-NBA can be used for ion generation for a variety of peptides and

proteins. However, in the case of pepsin, a MALDI spectrum cannot be obtained. Clearly, its applicability still needs to be investigated further. Moreover, searching for new matrices for CF-MALDI applications appears to be a worthy endeavor.

Chapter 10

Interfacing On-Line Conventional or Packed Capillary Liquid Chromatography with Continuous-Flow Matrix-Assisted Laser Desorption Ionization for the Analysis of Proteins

10.1 Introduction

Matrix-assisted laser desorption ionization (MALDI) has become an extremely important mass spectrometric technique for high molecular weight determination of biomolecules. As discussed in section 1.6, a small matrix molecule is mixed with the sample on a substrate, and the solvent is allowed to evaporate before laser desorption/ionization is performed. The resulting ions are usually detected with a time-of-flight mass spectrometer. However, due to the strict sample preparation procedure, a major disadvantage of MALDI is the difficulty in interfacing it to various solution-based separation methods, such as liquid chromatography (LC) and capillary zone electrophoresis (CZE), for on-line complex mixture analysis.

There are a number of benefits that could be achieved in combining on-line chromatography with MALDI:

1. Sample throughput can be increased due to ease of automation.
2. Ion suppression can be reduced. More specifically, in some unfavorable cases a signal for compound X might not be observed due to the presence of compound Y. Chromatography would, in principle, remove this ion suppression if compounds X and Y were separated before the mass spectral analysis.

3. Quantitation can be easily performed using any one of the standard well-known analytical methodologies: calibration curve, standard addition, or internal standardization.
4. Mass spectral quality can be improved by removing interferents with on-line sample clean up.
5. The LC separation stage can be used to select the analyte of interest for generating fragment ions in a collision cell (tandem TOFMS).

Several interfaces for combining LC and CZE with MALDI have been reported. Russell and coworkers developed a technique for producing aerosols from protein solutions [171,172]. Samples are continuously introduced into a TOFMS at 1 mL/min, although the detection sensitivity at present is about 100 nmol with a mass resolution of 5-10. Recently, we demonstrated the feasibility of introducing solution samples directly (no aerosol formation) into a time-of-flight (TOF) mass spectrometer (MS) [162]. It involved the use of a continuous flow (CF) probe to deliver sample and matrix through a capillary tube and onto a stainless steel frit, upon which laser desorption/ionization was carried out. With this continuous-flow MALDI technique, it was shown that flow injection analysis could be performed with a liquid matrix. The actual setup closely resembled a LC/MS experiment, but without a column, to obtain mass spectra of small peptides and flow-injection ion profiles with sample injections in the 100 picomole region. In chapter 9, we described a new flow probe and successfully demonstrated flow injection analysis of large peptides with molecular weights above 10,000 [25]. Flow injection ion profiles of these biomolecules could be obtained with a total sample injection of less than 10 picomoles. For a single-shot mass spectrum, the total amount of sample consumed was estimated to be less than

several femtomoles. In addition, a sensitivity curve exhibiting a linear response of one order of magnitude in the low picomole region could be obtained.

In this chapter we report the development of an on-line post-column matrix addition method to interface a conventional or capillary LC system to CF-MALDI for detection of high molecular weight biochemicals [27]. The interface consists of a three port mixing tee, similar to that employed in continuous-flow fast atom bombardment (CF-FAB) for coupling LC [173,174] or capillary zone electrophoresis (CZE) [174-176]. The effluent from the liquid chromatography system is connected to one port of the mixing tee. The second port is connected to a syringe pump which continuously feeds in the MALDI liquid matrix, 3-nitrobenzyl alcohol (3-NBA), in a diluted form. In this manner the LC effluent is allowed to mix with the liquid matrix. The resulting mixture flows out of the third port and through a flow probe for CF-MALDI with a linear TOFMS. Since no matrix is added to the elution solvent, there is no need to change the LC separation process. In addition, flow rates for LC separation and matrix introduction can be independently changed and optimized for speed and ion detection sensitivity. In this chapter, the design of this LC/MALDI/TOFMS system will first be described. It is shown that the mixing tee does not introduce a significant amount of dead volume to the LC separation stage. Secondly, it will be demonstrated that low picomole separation of peptides and proteins can be performed and detected with LC/MALDI/TOFMS.

10.2 Experimental

CF-MALDI with no LC column

A syringe pump (Harvard Apparatus, Model 11) containing 0.1% trifluoroacetic acid (TFA) and a 60 nL injector, but no LC column, together served as the sample

introduction system, as shown in Figure 10.1. A second syringe pump (Sage Instruments Model 240) contained the liquid MALDI matrix 3-NBA. Both pumps are connected to the 3-port mixing tee. In this manner, the injected sample mixes with the matrix while being carried in the flow probe for MALDI.

Conventional HPLC with CF-MALDI

Gradient separations in liquid chromatography with post-column matrix addition were performed with a Shimadzu LC-600 dual pump system. Figure 10.2 shows the overall schematic of the LC system. A flow rate of 0.5 mL/min was used on the LC column (C18 peptide & protein column, 2.1 mm ID X 25 cm). Pump A contained 0.1% TFA, while pump B consisted of 90:10 acetonitrile:water containing 0.1% TFA. A gradient was performed from an initial 40% pump B to 65% pump B in 5 minutes. From 5 to 8 minutes the gradient was increased to 70%, and subsequently held there. A Rheodyne Model 7125 injection valve with a 20 μL internal loop was used for sample injection. In order to achieve a sample flow rate of 1-5 μL/min prior to matrix addition, the LC effluent was split by a tee using two metering valves connected in parallel. This combination of a fine and coarse metering valve gave reproducible and fine flow rate control of the LC effluent entering the mixing tee. A detailed schematic diagram of the mixing tee is shown in Figure 10.3. The LC effluent (2-4 μL/min) was directed towards the flow probe as a result of the coaxial sheath flow produced by the 3-NBA matrix solution (5 μL/min). This matrix solution was pumped by a syringe pump (Harvard Apparatus, Model 11). The combined flow entered a fused silica capillary tubing (100 μm ID x 360 μm OD X 45 cm), which carries the LC effluent and 3-NBA matrix to the tip surface of the flow probe, at which point MALDI was carried out.

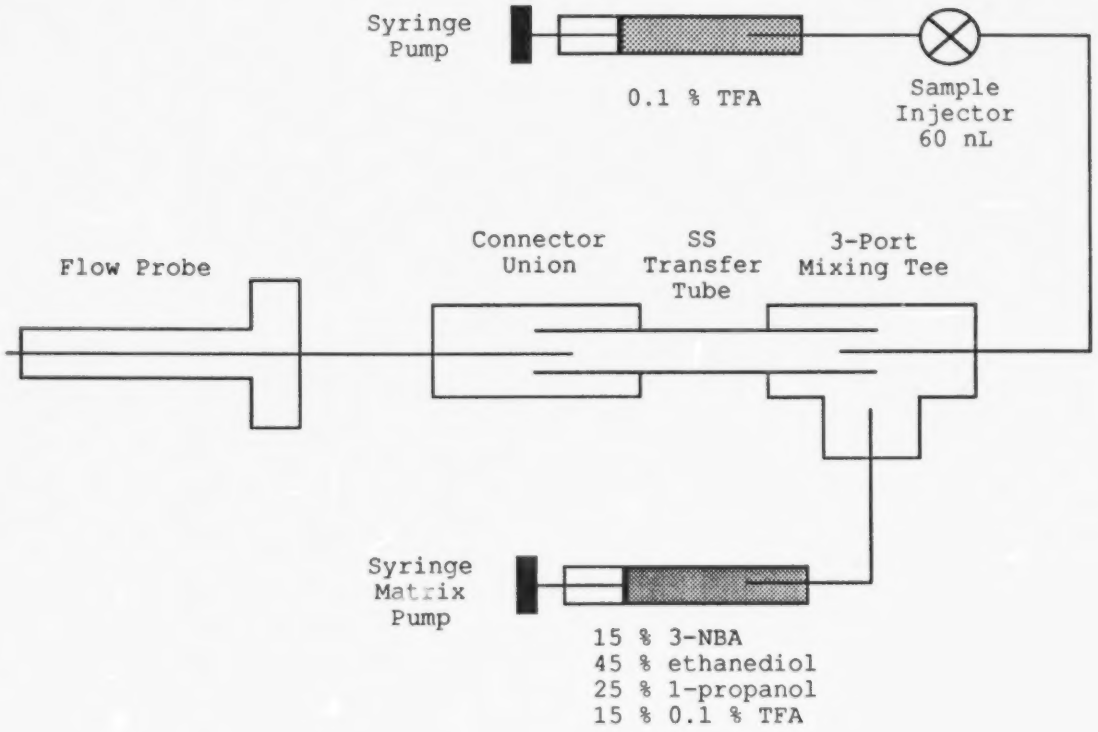

Figure 10.1 Schematic of CF-MALDI with post-matrix addition (no LC column). Drawing is not to scale.

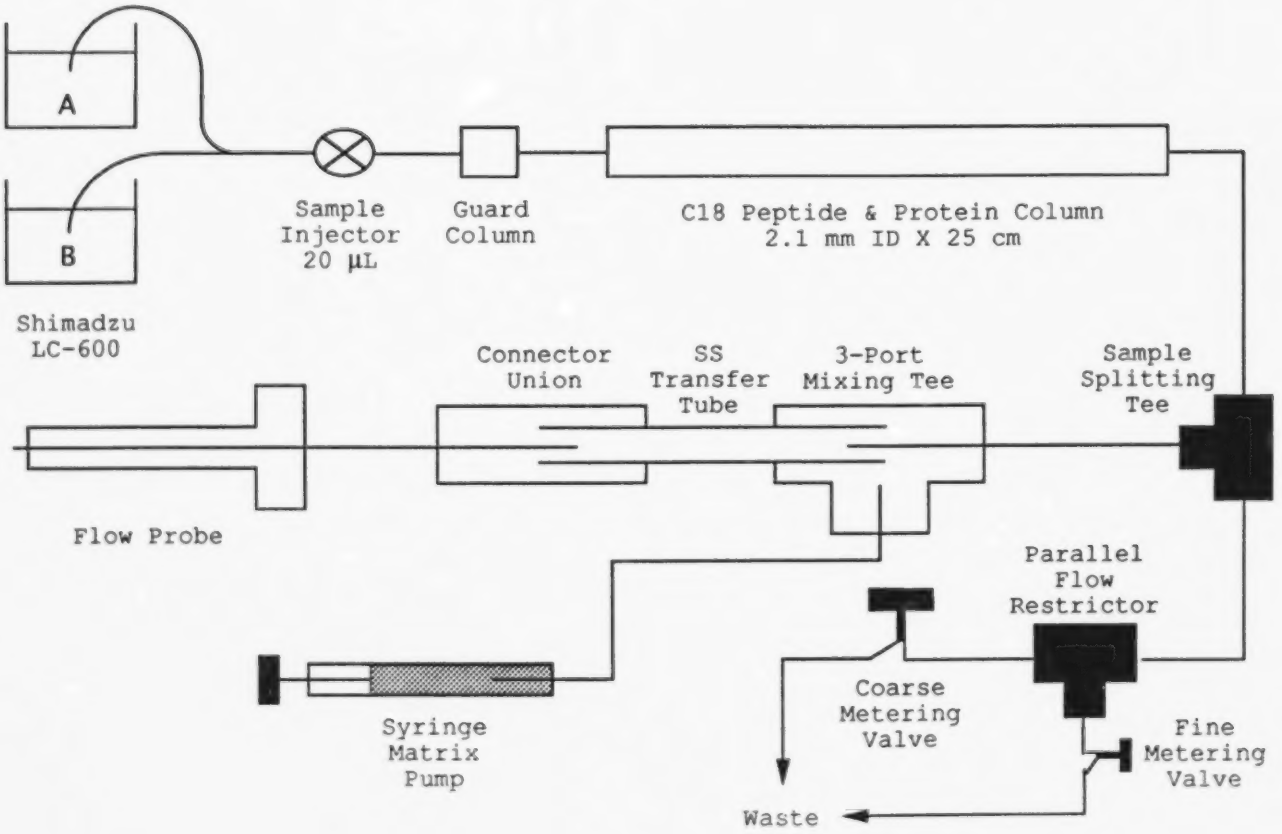

Figure 10.2 Schematic of the Conventional Full-Bore (2.1-mm ID column) LC/MALDI system. Drawing is not to scale.

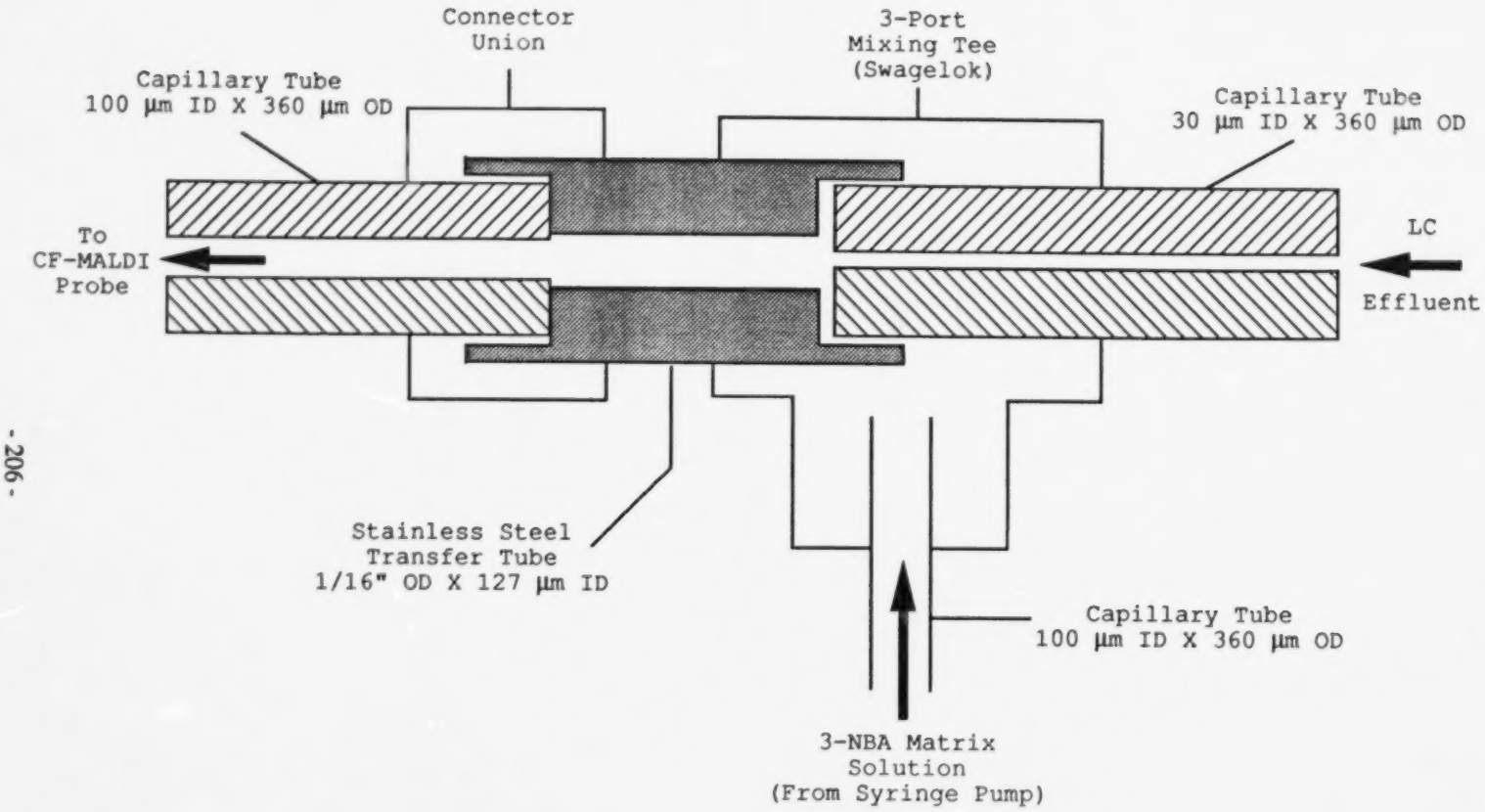

Figure 10.3 Details of the 3-port mixing tee for CF-MALDI with post-matrix addition. Drawing is not to scale.

Packed Capillary HPLC with CF-MALDI

The LC system used for the packed capillary column employs the above described high flow rate LC, but with no gradient. Isocratic conditions were used through out (40% pump B). A schematic of the packed capillary column setup is shown in Figure 10.4. A home built solvent splitter was used to obtain a flow rate compatible for packed capillary chromatography. The solvent splitter consisted of a tee connected to a parallel combination of a coarse and fine metering valve, allowing a controllable flow rate of 2-10 μL/min for the LC separations. The capillary column (Fusica C18, 5 μm, 300 A, LC Packings, 320 μm ID X 5 cm) was connected directly to a Valco sample injector (60 nL) with finger tight fittings. To perform the mass spectrometry, the end of the capillary column was connected directly to the 3-port mixing tee, as shown in Figure 10.3.

Packed Capillary HPLC with UV Detection

To obtain a UV chromatogram a piece of capillary tubing (50 μm ID X 360 μm OD X 60 cm) was connected to the outlet of the LC capillary column, and the other end of the capillary positioned into a 214 nm UV detector (Waters Quanta 4000 capillary electrophoresis), as shown in Figure 10.5. At a point 7 cm from the capillary end a 1-cm portion of the polyimide coating was burned away with a match to yield a clear quartz surface.

CF-MALDI Time-Of-Flight Mass Spectrometry

The design of the new flow probe, along with the time-of-flight mass spectrometry, has been described in detail in chapter 9. However, the sample preparation procedure was slightly modified. Here, the carrier solvent consisted of 15% of 0.1% trifluoroacetic acid (TFA), 45% ethylene glycol, 25% 1-propanol, and 15% 3-

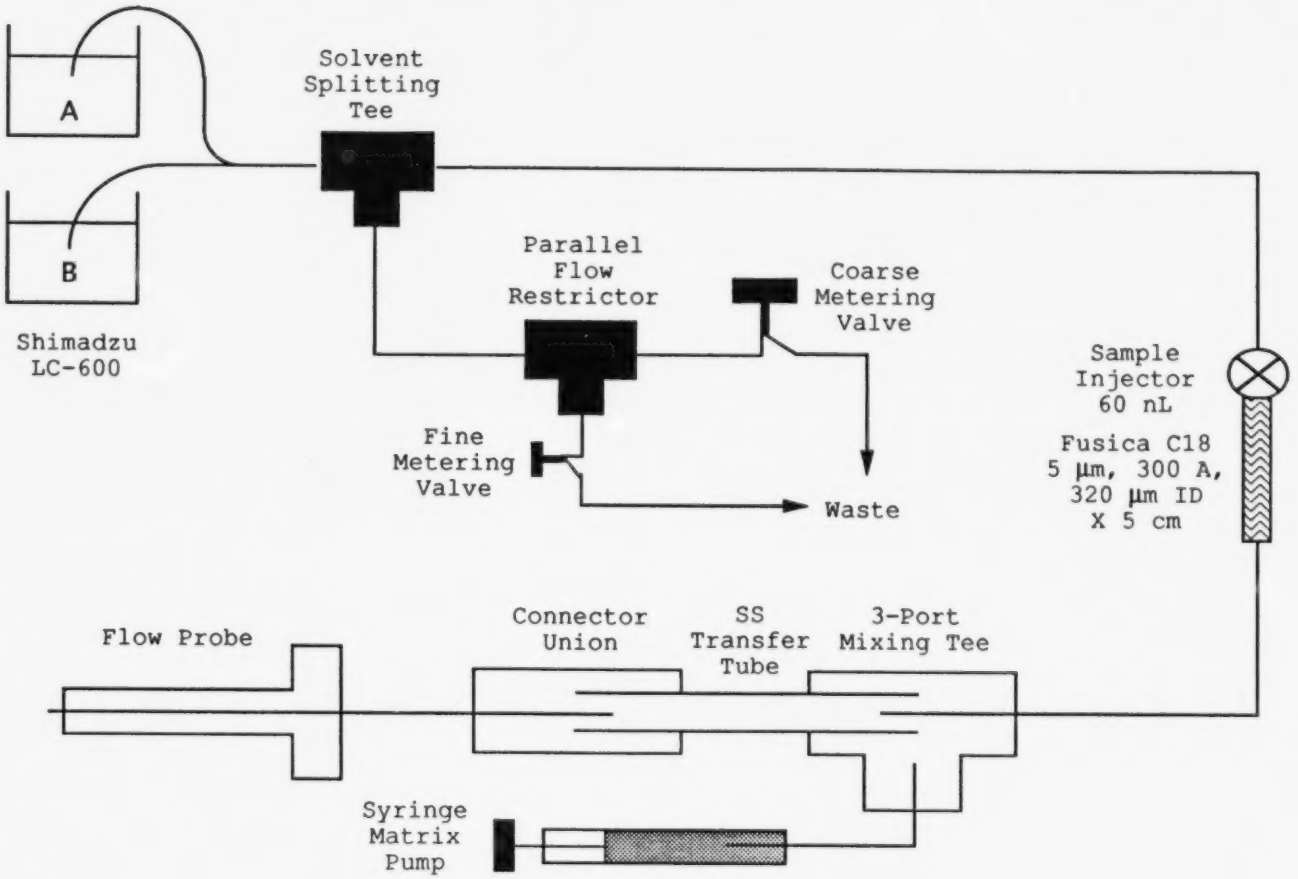

Figure 10.4 Schematic of the packed capillary LC/MALDI system. Drawing is not to scale.

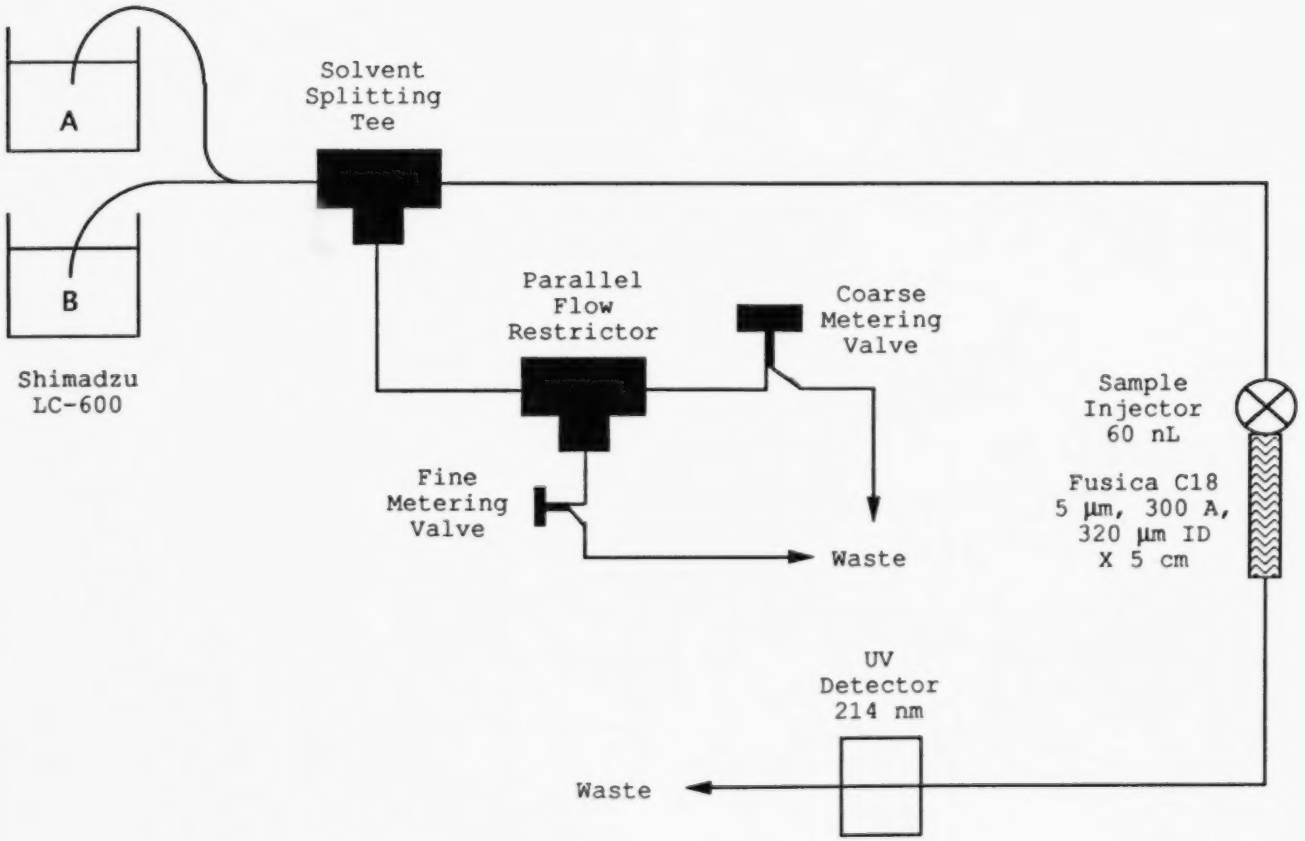

Figure 10.5 Schematic of the packed capillary LC with UV Detection. Drawing is not to scale.

nitrobenzyl alcohol (all by volume). Previous experiments employed ethanol, but it was replaced in this experiment by 1-propanol to take advantage of its higher boiling point.

10.3 Results and Discussion

Experiments were initially performed with no LC column (i.e. flow injection analysis) to examine the performance of the interface design (Figure 10.1). A syringe pump in series with an injector served as the sample introduction system into the 3-port mixing tee. Figure 10.6A and 10.6B show 4 repeat injections of 8 pmol cytochrome c (MW ~ 12380) and 5 repeat injections of 7 pmol lysozyme (MW ~ 14400). The data system used to generate these flow profiles was described in chapter 9. In brief, all mass spectra generated during the sample injection were stored in a PC. Ion chromatograms were generated by integrating the molecular ion peak of the injected sample in each collected mass spectrum and summing 10 peak areas to generate one point in the ion profile. These ion profiles display a reasonably good signal-to-noise ratio. The peak to peak reproducibility varies somewhat, but for the present purpose it is adequate. A comparison between these ion profiles and those obtained without a 3-port mixing tee shows that significant peak broadening does not occur.

Consequently, cytochrome c and lysozyme were chosen as model proteins to evaluate the on-line LC/MALDI/TOFMS system. Figure 10.7A shows a gradient LC/MALDI/TOFMS ion chromatogram of a separated mixture of these 2 proteins on a conventional LC column. A 5 nmol injection of each protein was made, with 0.2% (10 pmol) split to the MS. Ion chromatograms were generated by separately integrating the molecular ion peak of cytochrome c and lysozyme of each mass spectrum collected and summing 10 peak areas to generate one point in the ion profile.

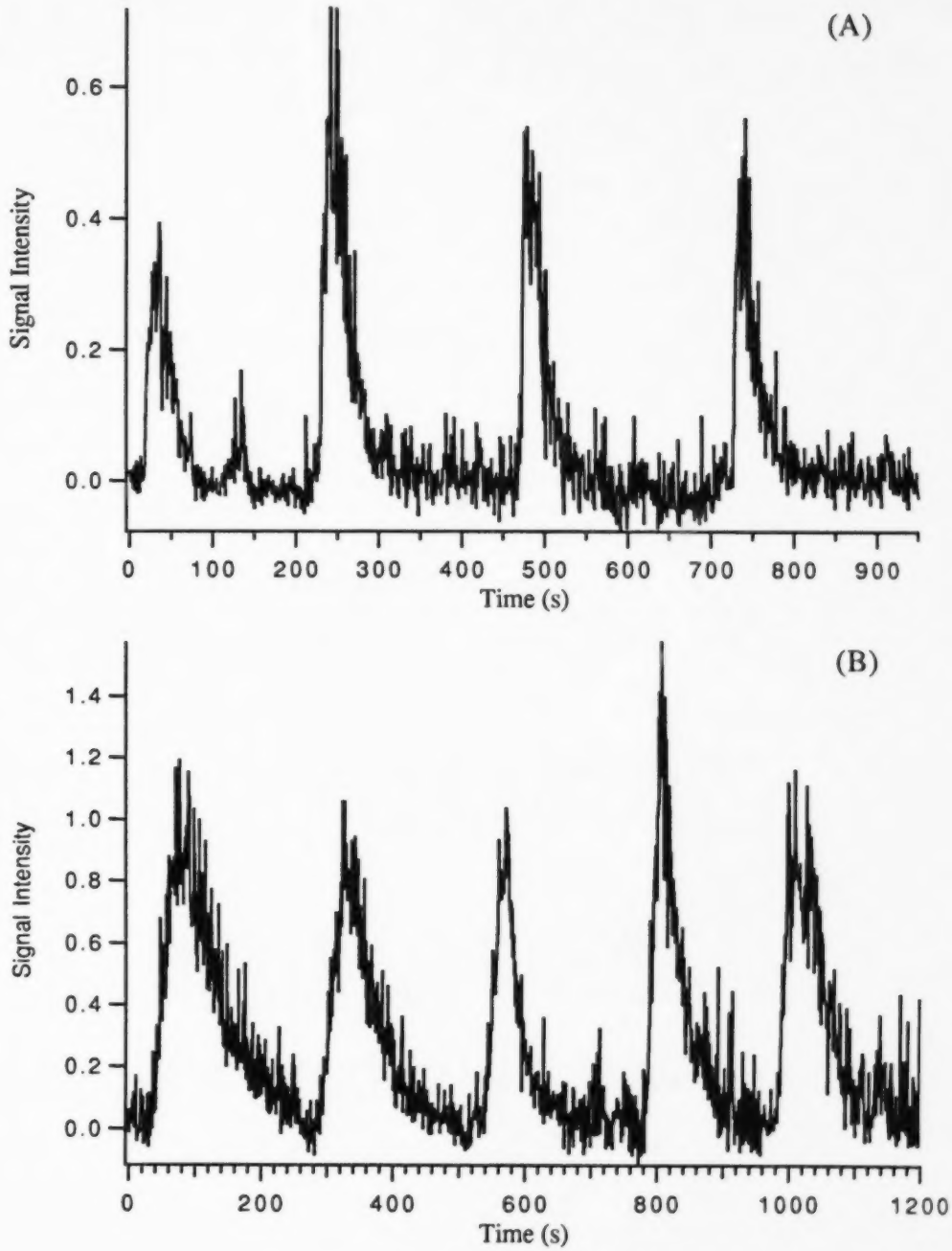

Figure 10.6 CF-MALDI flow injection analysis with post-matrix addition (no LC column) of
(A) 4 repeat injections of cytochrome c (8 pmol each) and
(B) 5 repeat injections of lysozyme (7 pmol each).

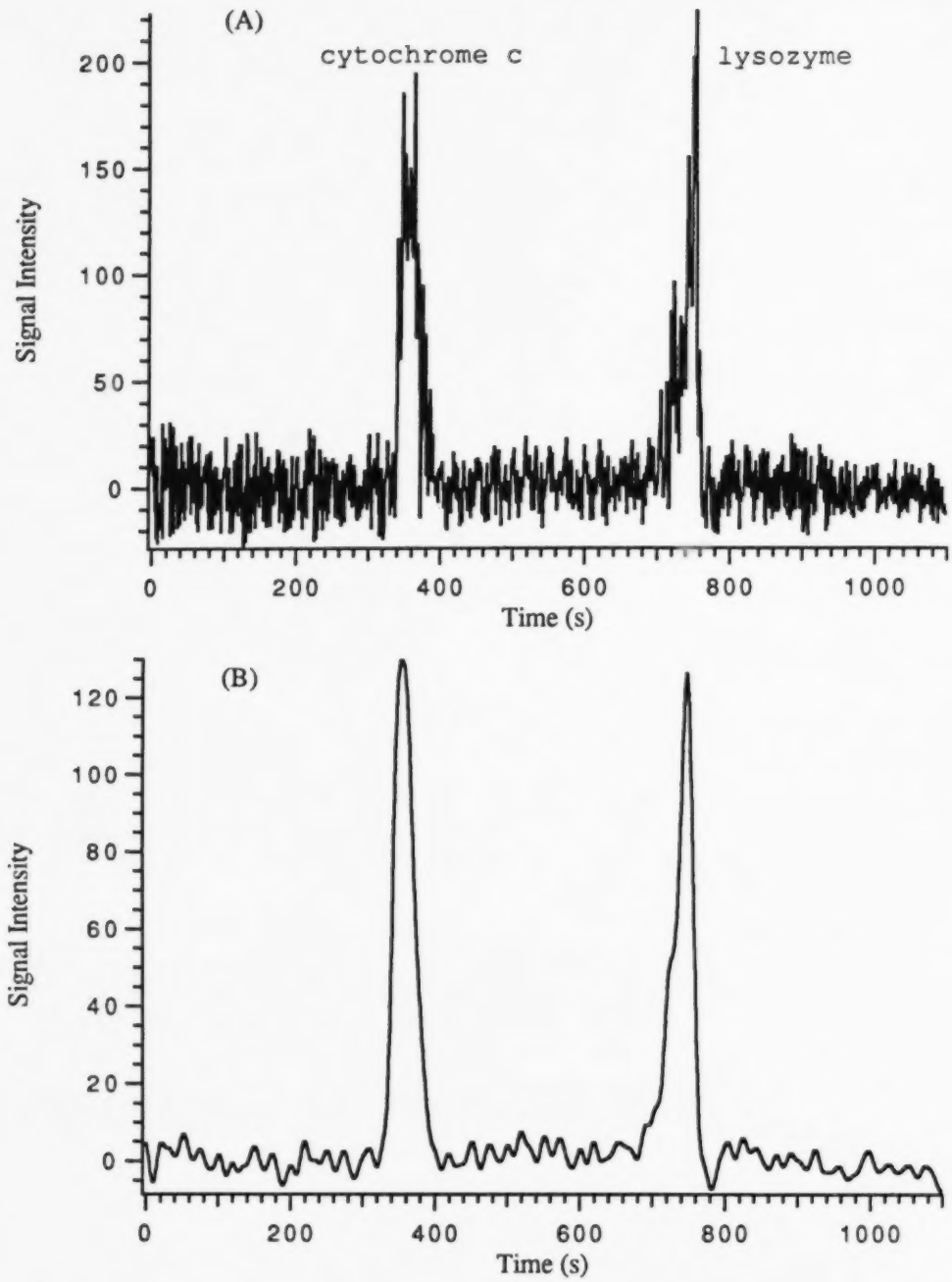

Figure 10.7 On-line gradient separation of cytochrome c and lysozyme with conventional LC and MALDI/TOFMS detection. Chromatograms represent 5 nmol injection each with 0.2% (10 pmol) split to MS.
(A) raw data and (B) smoothed data.

The individual ion chromatograms of cytochrome c and lysozyme were then summed to generate the total ion chromatogram. The two proteins are clearly well separated, exhibiting a FWHM between 25-30 seconds. However, the baseline is quite noisy, even after 10 point averaging. The cause of this noise is most likely due to the flow conditions. With the aid of a video camera and a video monitor, we took a close look at the flow on the probe surface. Indeed, some irregular flow patterns were observed from time to time, thus causing an unstable flow. A local equilibrium among the continuous liquid flow, absorption of the excess liquid by the filter paper, gentle heating with the point heater, and the pumping speed of the vacuum pumps must exist for a stable flow to be achieved. In the present case the flow rate was most likely too high, causing the liquid not to flow in a well defined area. Figure 10.7B shows the same ion chromatogram after data smoothing. The smoothing algorithm is derived from Marchand and Marmet [163], and is part of the Igor Software Package (WaveMetrics, Inc.). This smoothing operation, also called Gaussian filtering, convolves the chromatogram with normalized coefficients derived from Pascal's triangle. For comparison purposes a UV chromatogram of the same mixture is shown in Figure 10.8. However, the UV chromatogram was not obtained on-line with the CF-MALDI results, hence a strict comparison cannot be made. Nevertheless, based on peak shapes and widths, the mixing tee does not introduce a significant amount of peak broadening or distortion to the LC separation.

Figure 10.9A shows a gradient separation of 3 proteins: cytochrome c, lysozyme, and myoglobin. The gradient consisted of 35% to 85% pump B in 20 minutes. Although the signal is quite noisy, again attributed to the flow conditions, it does demonstrate that complex mixture separations are possible with the mixing tee interface. Figure 10.9B shows the same ion chromatogram after data smoothing.

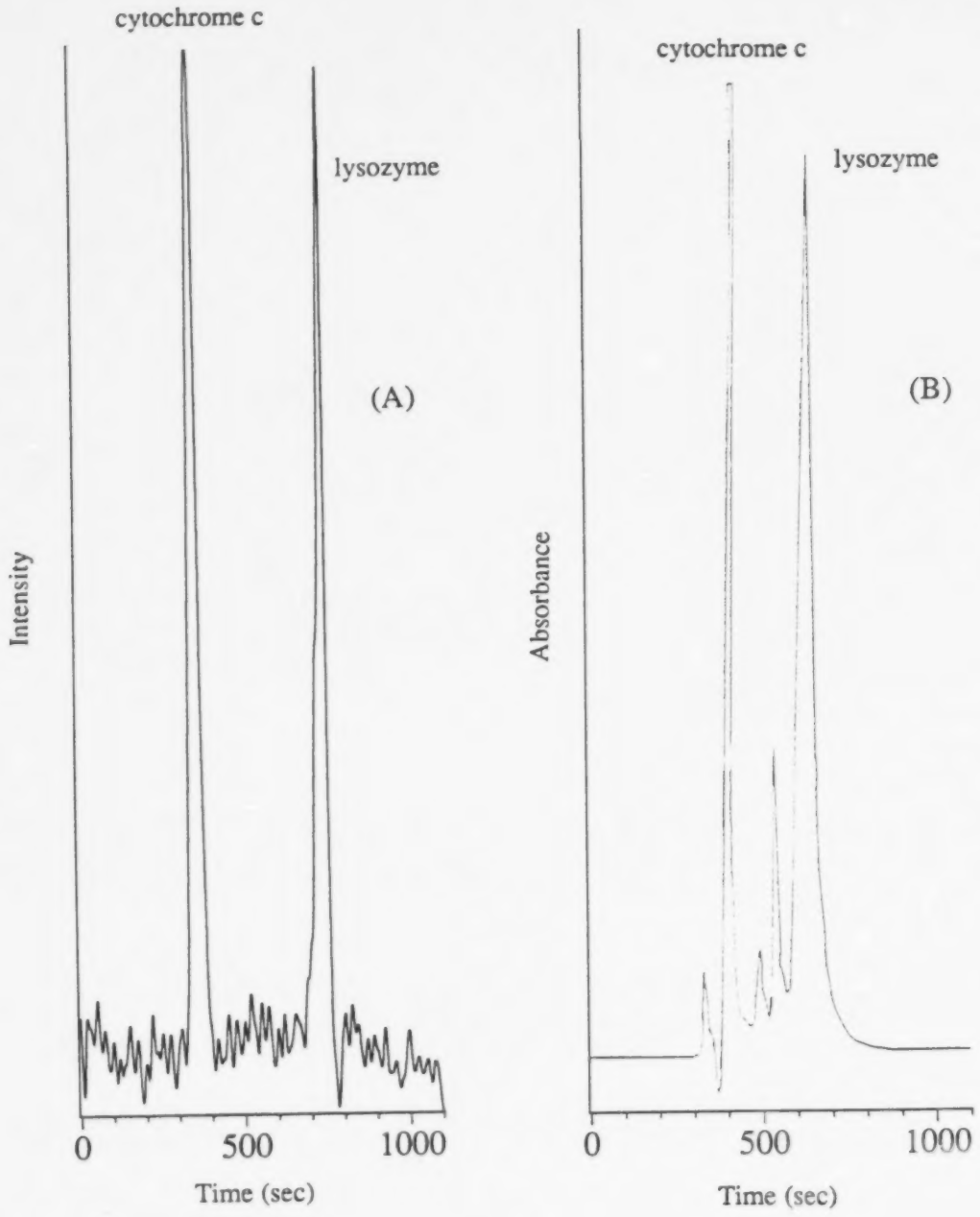

Figure 10.8 Comparison of an on-line gradient LC separation of cytochrome c and lysozyme with (A) MALDI/TOFMS detection and (B) UV detection (242 nm).

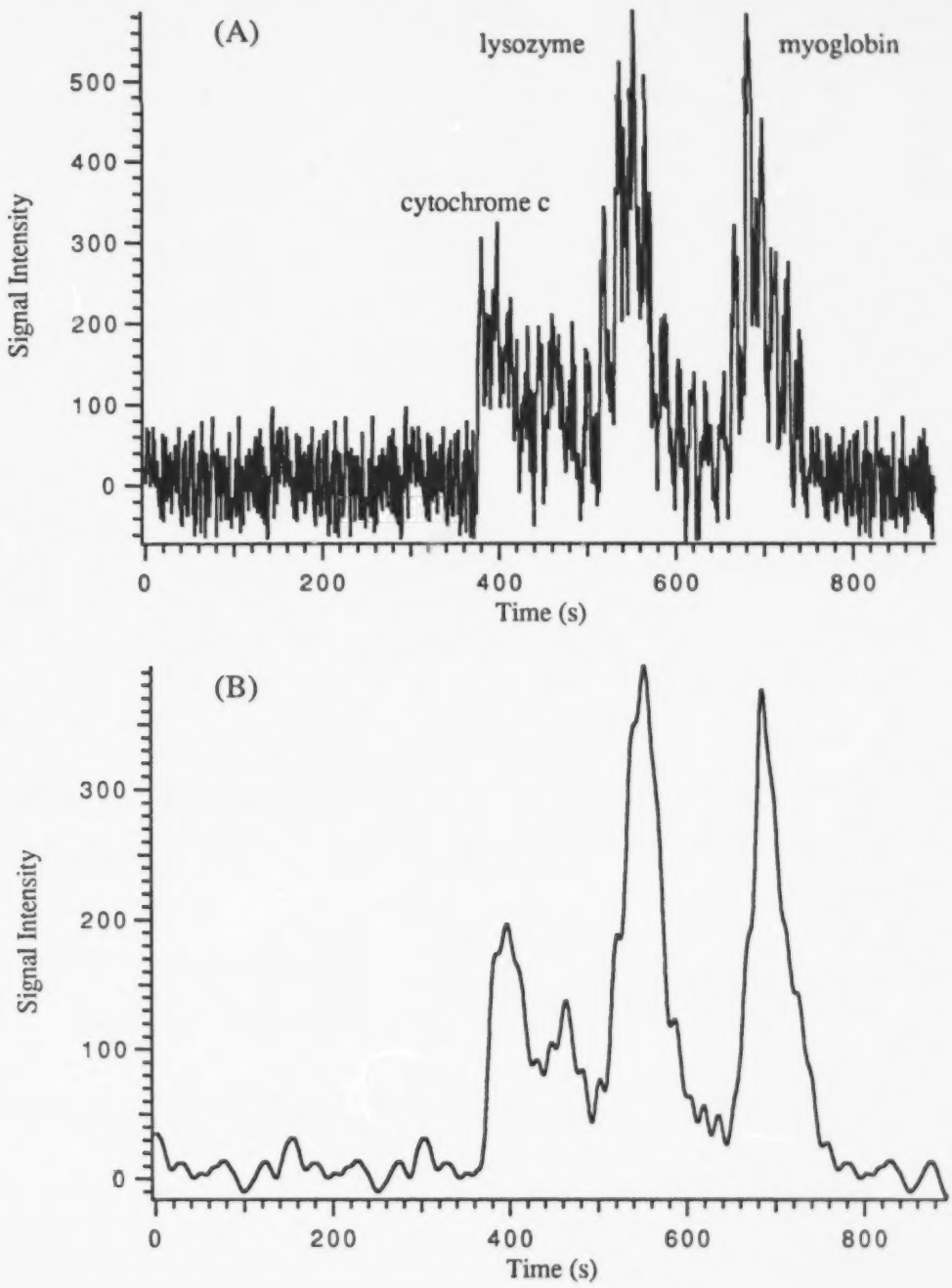

Figure 10.9 On-line gradient separation of cytochrome c, lysozyme, and myoglobin with conventional LC and MALDI/TOFMS detection. Chromatogram represents 5 nmol injection each with 0.2% split to MS. (A) raw data and (B) smoothed data.

The results presented so far have required a high sample split ratio, on the order of 500, in order to avoid overloading the mass spectrometer with excess solvent. We thus explored the possibility of using packed capillary LC/MALDI/TOFMS. With slight modifications the methodology applied to the conventional packed column LC was also applied to the packed capillary column (Figure 10.4). The 3-NBA matrix solution was added to the mixing tee post-column, and the entire sample mixture introduced through the flow probe and onto the probe surface. Figure 10.10A again shows the MALDI/TOFMS ion chromatogram of a separated mixture of cytochrome c (9 pmol) and lysozyme (8 pmol) on a capillary LC column. Figure 10.10B shows the smoothed data. Unlike the previous LC experiment, the entire sample injected onto the column was subjected to mass spectrometric analysis. The two proteins are clearly resolved in the ion chromatogram. For comparison purposes a UV chromatogram of the same mixture is shown in Figure 10.11. As before, the UV chromatogram was not obtained on-line with the CF-MALDI results, hence a strict comparison cannot be made. Nevertheless, based on peak shapes and widths, the mixing tee does not introduce a significant amount of peak broadening or distortion to the LC separation.

Mass Resolution: The mass resolution with the CF-MALDI technique in chapter 9 was poor, between 10-20. Unfortunately, the mass resolution with LC/MALDI/TOFMS has not improved. We believe there are several major reasons for this. Firstly, the ions are extracted in an orthogonal configuration with constant voltages applied to the repeller and extraction grid. This simple design allows us to place the flow probe between these two grids, and consequently flow the liquid into the ionization region of the TOFMS without electric breakdown. However, this will result in some ion spatial distribution and degrade the mass resolution, even with a very small laser beam size. We are currently in the process of performing LC/MALDI in a

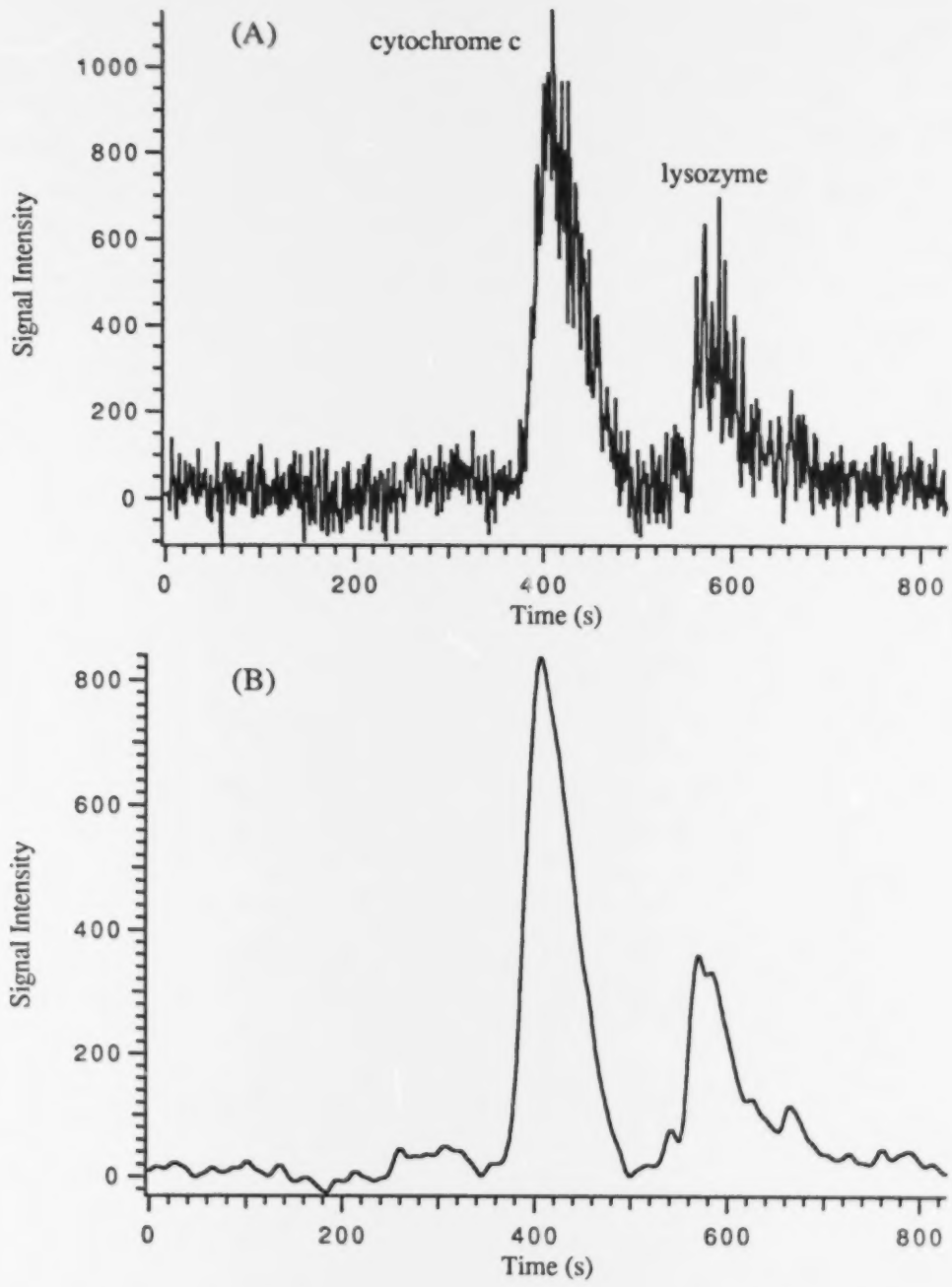

Figure 10.10 On-line isocratic separation of cytochrome c (9 pmol) and lysozyme (8 pmol) with packed capillary LC and MALDI/ TOFMS detection. (A) raw data and (B) smoothed data.

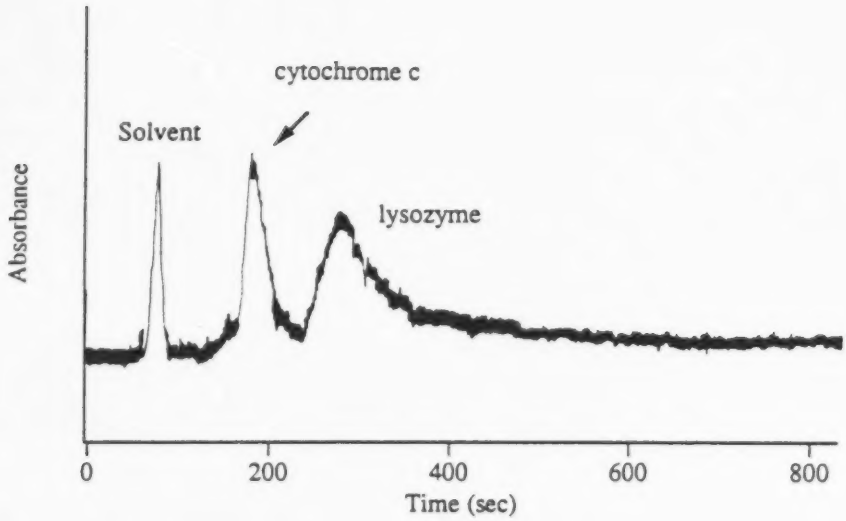

Figure 10.11 Isocratic separation of cytochrome c and lysozyme with a packed capillary LC and 214 nm UV detection.

parallel configuration. The ions generated by the laser will be extracted with an electric field that is parallel to the flight tube. The reduction in the initial spatial distribution of the ions should improve the mass resolution. Improved results with parallel CF-MALDI are presented in chapter 11.

A second factor causing poor mass resolution is the presence of ethylene glycol in the matrix solution. Ethylene glycol, in conjunction will gentle heating from a point heater, prevents the flowing solution from freezing in the vacuum. However, current work in our laboratory indicates that ethylene glycol causes both ion suppression and saturation of the detector due to the large number of low mass background ions [28]. Although the low mass ions are pulsed away from the detector at the beginning of each laser pulse, there is an inherent limit to this degree of ion reduction. The large background in the mass spectra effectively blocks the first 3000 mass units. We have currently designed a new flow probe with direct heating of the probe tip, thus eliminating the use of ethylene glycol, in order to reduce the low mass ions. Again, results with this new design are presented in chapter 11.

Thirdly, the presence of a large number of adduct peaks degrades the mass resolution. Impurities such as sodium and potassium cause a large number of adducts to be formed with the protein samples. Solid matrices for MALDI can usually be used to generate mass spectra virtually free of interfering adducts by carefully controlling the laser power. However, this is usually not the case for the liquid matrix 3-NBA, and more often than not the adduct peaks can be very intense. It becomes more and more difficult to resolve these adduct peaks with increasing molecular weight, eventually resulting in one broad peak encompassing all the adduct complexes. Again, we are currently searching for ways to reduce these adduct peaks with 3-NBA. At the same

time, we plan to add a high voltage ion reflector to improve the instrumental mass resolution, in order to better resolve the adduct peaks. With high mass resolution, adduct formation would only be a problem in the case of high molecular weight proteins.

10.4 Conclusions

1. Low picomole amounts of proteins can be separated and detected with LC/MALDI/TOFMS.
2. The mixing tee interface design does not introduce significant peak broadening or distortion.
3. Flow rates for LC and matrix addition can be independently optimized for speed and ion detection sensitivity.
4. Mass resolution is currently poor for large proteins. But for small peptides, good resolution can be obtained with CF-MALDI (see chapter 11).

Chapter 11

Continuous-Flow Matrix-Assisted Laser Desorption Ionization of Peptides with Parallel Ion Extraction

11.1 Introduction

Chapters 9 and 10 dealt with the coupling of the continuous flow (CF) technique to matrix-assisted laser desorption ionization (MALDI) for the detection of proteins. More specifically, chapter 9 described flow injection analysis to introduce solution samples directly into a time-of-flight mass spectrometer (TOFMS) for MALDI [25]. Chapter 10 dealt with on-line post-column matrix addition to interface liquid chromatography (LC) with CF-MALDI [27]. Although sensitivity was acceptable (low-picomole levels), mass resolution was poor, between 10-20.

There are several reasons why mass resolution may have been poor. Firstly, the laser-induced ions expand in a direction orthogonal to the flight tube, with constant voltages applied to the repeller and extraction grid. However, this will result in some ion spatial distribution and degrade the mass resolution, even with a very small laser beam size. A second factor which may cause poor resolution is the presence of ethylene glycol in the matrix solution. Ethylene glycol, in conjunction will gentle heating from a point heater, prevents the flowing solution from freezing in the vacuum. However, current work in our laboratory indicates that this compound causes ion suppression [28]. When ethylene glycol is present the laser power must be increased in order to detect the analyte. This results in high background signals from the low mass ions,

consequently saturating the detector. Since it takes on the order of milliseconds for the detector to recover [57], large molecular ions are not effectively detected.

In this chapter we describe a new linear mass spectrometer designed to improve the mass resolution for CF-MALDI. The laser-induced ions expand in a direction parallel to the flight tube. Since this reduces the initial spatial distribution of the ions the mass resolution will correspondingly improve. In addition, the continuous flow probe has been modified to allow direct heating of the probe tip, thus eliminating the use of ethylene glycol. The results presented in the chapter are mainly concerned with the mass accuracy and resolution that may be obtained with flow injection CF-MALDI for peptides.

11.2 Experimental

Time-of-Flight Mass Spectrometry. Figure 11.1 illustrates the design of the new linear TOF with parallel ion extraction. There are four gridless acceleration plates spaced by 4.7 mm. The voltages applied to the four acceleration plates are 12.0 kV, 10.5 kV, 8.0 kV, and ground, with the ground plate closest to the flight tube. The CF probe is inserted into the center of the first acceleration plate and held at 12 kV (see below). During operation of the CF probe the vacuum pressure is normally $1x10^{-5}$ Torr in the ionization region and $5x10^{-6}$ Torr in the flight tube. The desorption/ionization laser is a frequency quadrupled Nd:YAG (266 nm) operated at 5 Hz, and strikes the target at 75° to the sample normal.

Flow Probe Design. Figure 11.2 depicts the modified CF-MALDI probe tip. In the previous design the liquid was allowed to flow onto an insulating smooth Kapton (i.e. polyimide) surface, upon which desorption/ionization was carried out. In the new

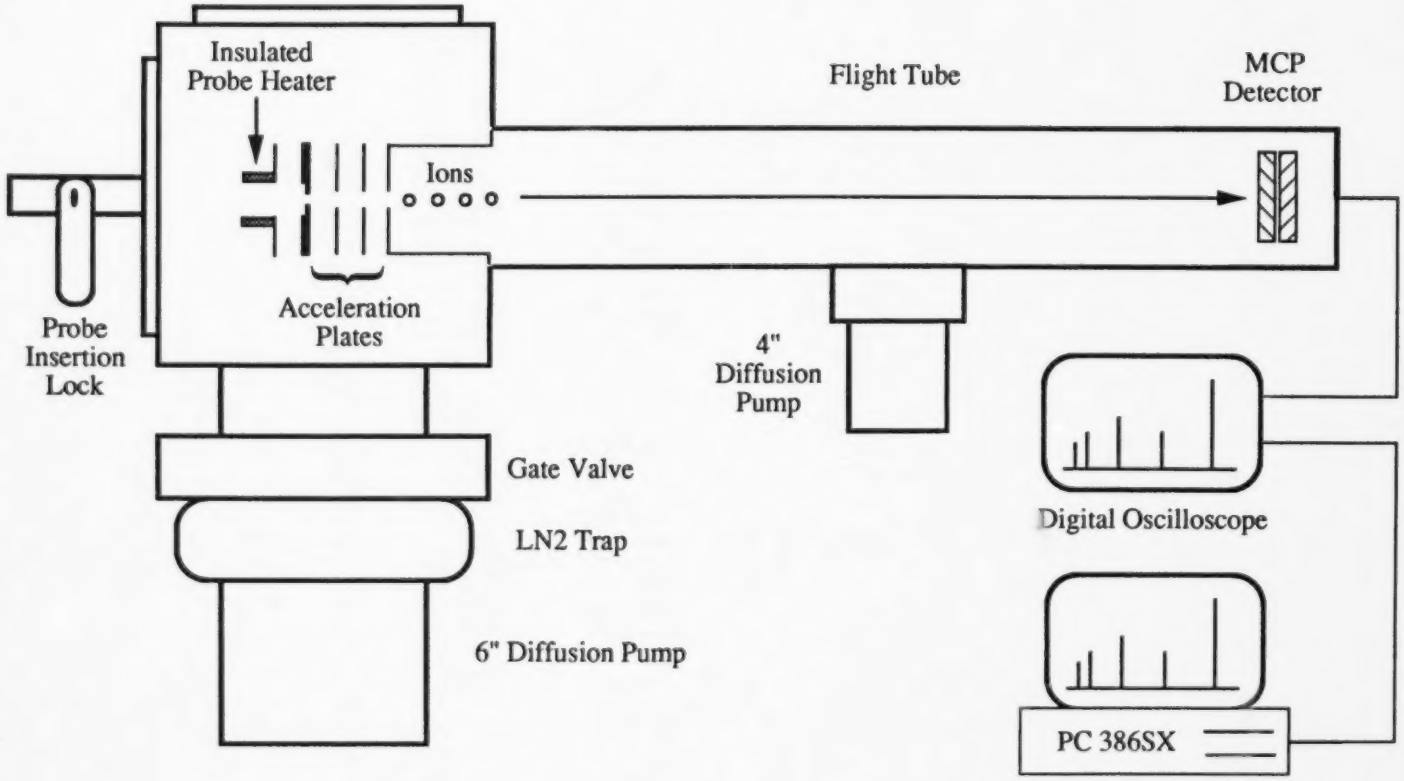

Figure 11.1 Schematic diagram of the new linear time-of-flight mass spectrometer with parallel ion extraction and an electrically insulated probe heater. Drawing is not to scale.

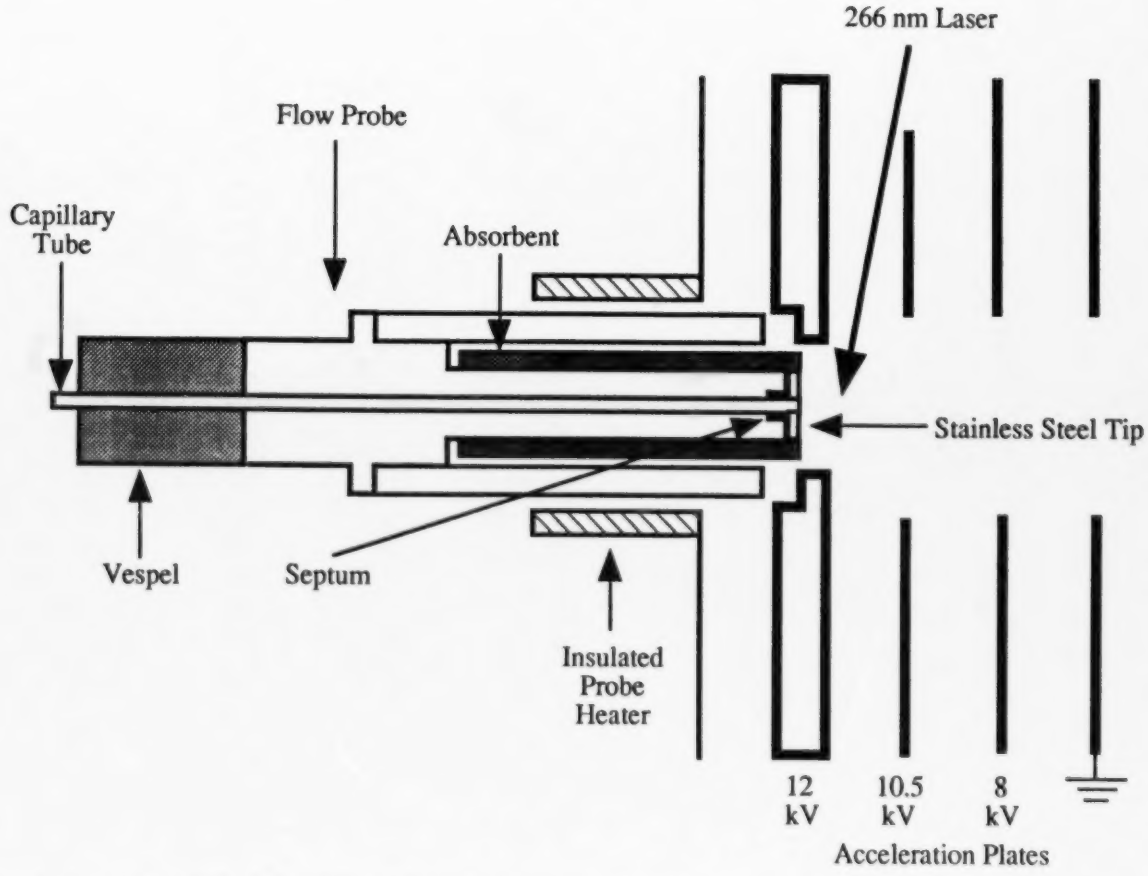

Figure 11.2 CF-MALDI probe tip and the acceleration plates of the time-of-flight mass spectrometer.

design the probe tip is constructed of stainless steel. Once the CF probe is inserted into the mass spectrometer the probe tip makes direct contact with the first acceleration plate. In this manner, the probe tip is floated to the same voltage as the first acceleration plate (i.e. 12 kV).

The probe tip and the flow probe body, both constructed of stainless steel, are electrically insulated from each other with a piece of Vespel, as shown in Figure 11.2. A silica capillary tube (75-μm i.d., 370-μm o.d., 45 cm long) (Polymicro Technologies, Phoenix, AZ) is inserted into the stainless steel tube and extends from the 3-port mixing tee to the probe tip (see below). An absorbent is placed around the probe tip to absorb the excess liquid.

Other major changes include the manner in which the probe tip is heated in order to prevent the flowing solution from freezing in the vacuum. An electrically insulated probe heater is attached behind the first acceleration plate. This allows direct even heating of the entire probe tip (~ 65°C). With this particular modification ethylene glycol is no longer required, hence reducing the production of low mass background ions. Furthermore, it is not necessary to pulse the deflection plates in order to avoid detector saturation [57], as previously explained in chapter 9.

Sample Preparation. Most of the chemicals were purchased either from Sigma or Aldrich. Peptide samples were provided by Synthetic Peptides Inc. at the Univ. of Alberta. A 3-port mixing tee (described in chapter 10) was used for all of the CF-MALDI work. The effluent from the liquid chromatography system (0.4 ml / min) (50% water acidified with trifluoroacetic acid (TFA) and 50% acetonitrile) was split by a home-built solvent splitter before entering the first port of the mixing tee (0.1 to 1.0

μL / min). A 60-nL sample injector (Valco Instruments Co., Houston, TX) was placed in between the LC pumps and the mixing tee to allow for flow injection analysis. Note that on-line chromatographic separations (as described in chapter 10) with this setup will be performed in the near future. The second port is connected to a syringe pump which continuously feeds in the matrix solution at 1.7 μL / min The matrix solution contains (by volume): (a) 70% 3-NBA, (b) 25% 1-propanol and (c) 5% water acidified to pH 2 with TFA, with gramicidin S (4-5 pmol / μL, MW 1142.5) added as a molecular weight marker. The resulting mixture flows out of the third port and is directed towards the flow probe. In this manner, the sample is allowed to mix with the liquid matrix as it travels to the probe tip. All solutions are filtered and degassed.

Flow Stability. Achieving a stable flow is possible over a range of conditions, similiar to the requirements for CF-FAB [141]. Establishing a thin film and stable flow are critical in obtaining good resolution mass spectra. A video camera is used to monitor the liquid flow. Once the CF probe is inserted into the mass spectrometer, a period of 5-10 minutes is required before a stable flow is achieved, again similar to CF-FAB.

11.3 Results

Ion Extraction Considerations. Figure 11.3 illustrates the manner in which the orthogonal versus parallel ion extraction experiments are carried out. In the orthogonal case (Figure 11.3A) the sample probe is conveniently placed between the repeller and extraction grids of the TOF mass spectrometer, thus allowing flow of the liquid into the ionization region without electric breakdown. The laser-induced ions expand perpendicular to the electric field in the acceleration region. However, the problem here is that ions will be created in different regions of the electric field due to the finite

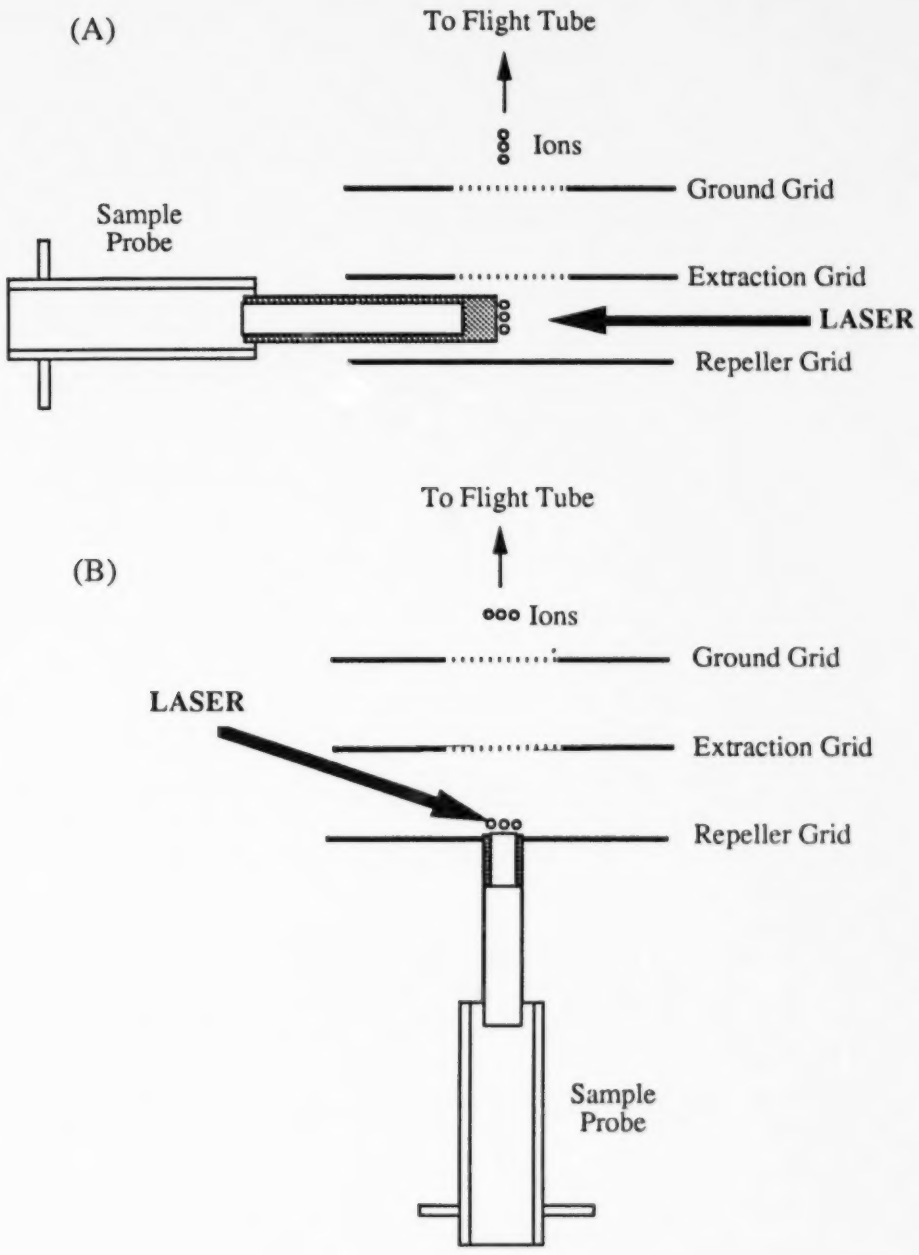

Figure 11.3 (A) Orthogonal and (B) parallel ion extraction for time-of-flight mass spectrometry.

width of the laser beam. Since this results in a spatial distribution of the ions, the resolution will correspondingly decrease. The solution to this problem is to desorb/ionize sample molecules from an isoelectric surface. That is, from a sample plane which experiences the same electric field at any point on the plane. This is known as parallel ion extraction and is shown in Figure 11.3B. The laser-induced ions experience the same electric field as they expand in a direction parallel to the flight tube. Since the spatial distribution of the ions has been reduced an enhancement in resolution is expected.

Experiments were initially performed with static MALDI (i.e. no continuous flow) in order to assess orthogonal versus parallel ion extraction. In static MALDI, the matrix is mixed with the analyte directly on a small probe tip. The mixture is allowed to dry before insertion into the mass spectrometer. Figure 11.4A shows the mass spectrum of bovine insulin ß-chain (7 pmol) with a 3-NBA matrix under orthogonal ion extraction conditions. A single peak is observed with a calculated resolution of 20. Figure 11.4B shows the same sample obtained under parallel ion extraction. A resolution of 72 is observed, along with an order of magnitude less sample required for the mass analysis (0.7 pmol). Clearly, parallel ion extraction is superior in terms of resolution and sensitivity.

CF-MALDI. Figure 11.5 shows a MALDI mass spectrum of bradykinin (9 pmol injection) collected under continuous flow conditions with parallel ion extraction. The resolution is 213 FWHM in this case. The mass resolution observed is generally in the range of 100-200 FWHM for CF-MALDI on our linear TOF for small peptides (MW < 1500 Da). This is a dramatic improvement in resolution compared to the results presented in chapter 9 (resolution 10-20). The resolution and sensitivity are dependent

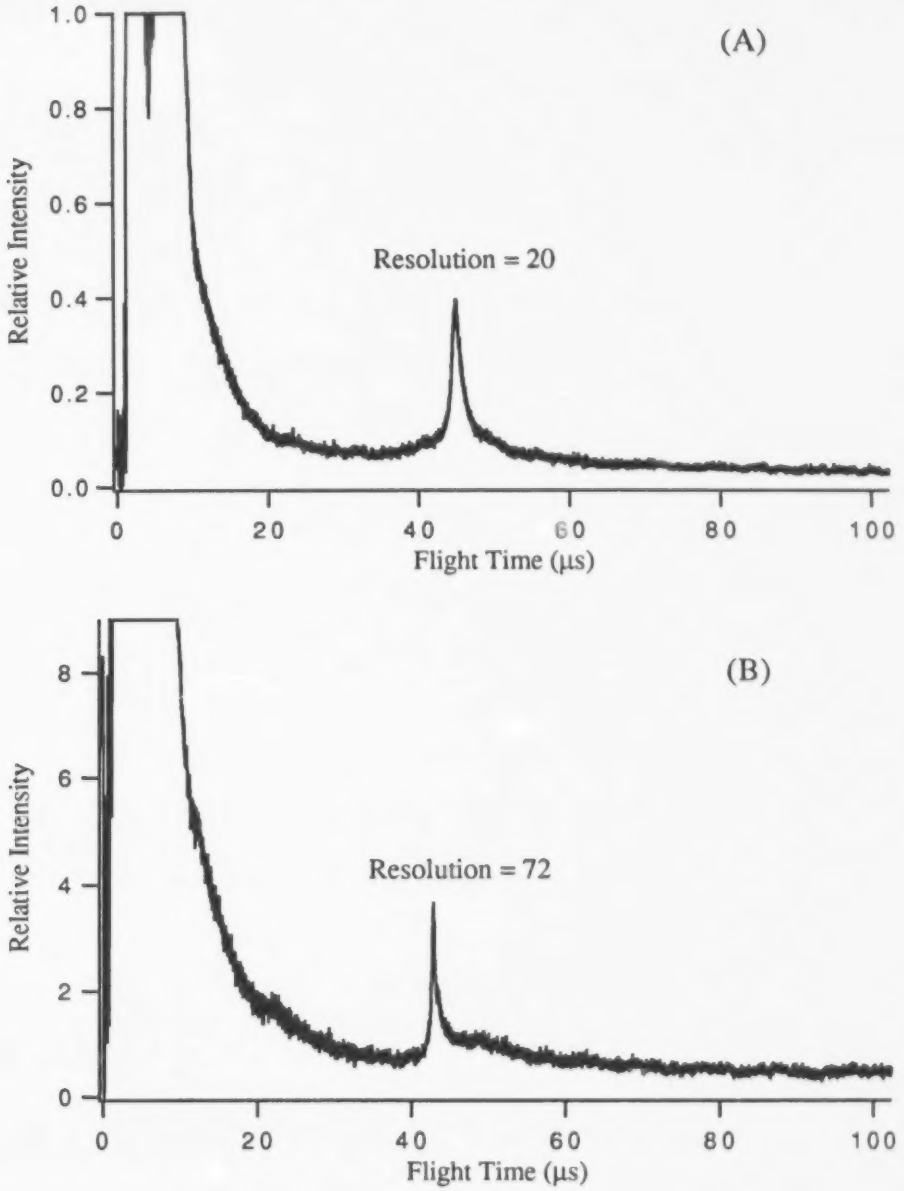

Figure 11.4 Static MALDI mass spectra of (A) bovine insulin ß-chain (7pmol) with 3-NBA (0.5 μL). Sample is desorbed orthogonally to the flight tube. (B) bovine insulin ß-chain (0.7 pmol) with 3-NBA (0.12 μL). Sample is desorbed parallel to the flight tube. Sum of 5 spectra.

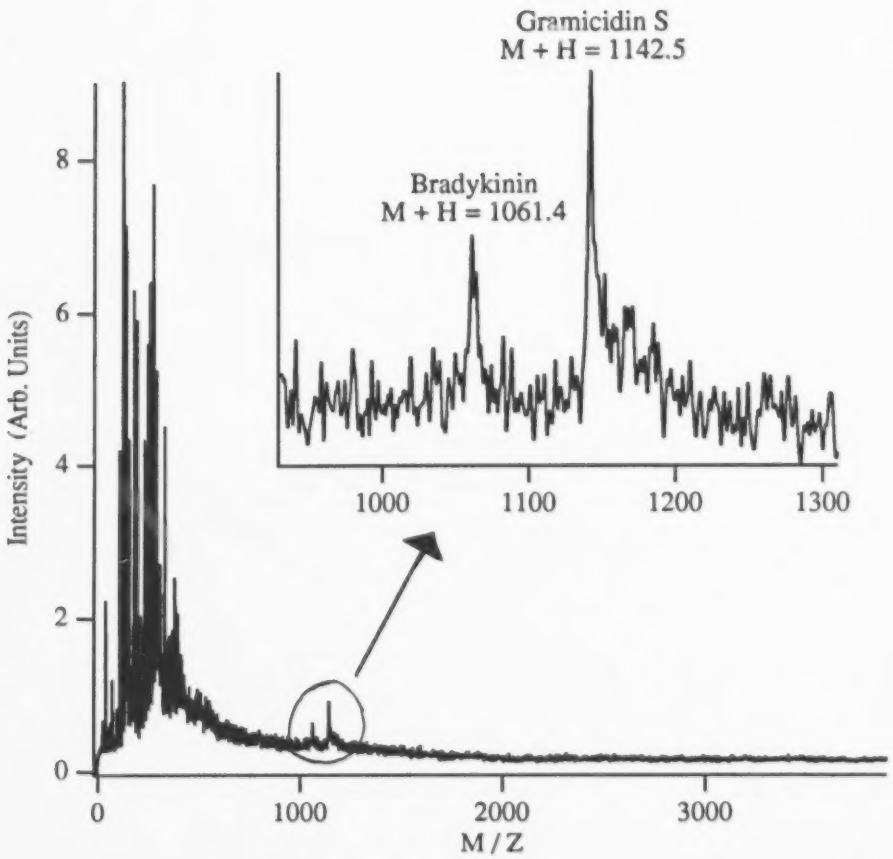

Figure 11.5 CF-MALDI mass spectrum of bradykinin (9 pmol injection) with parallel ion extraction. Gramicidin S acts as an internal mass calibrant present in the matrix solution.

upon the water/acetonitrile flow rates used for the flow injection analysis. As expected high flow rates decrease the sensitivity and resolution, and may cause the liquid flow to become unstable.

Table 11.1 lists the mass accuracy that was observed for a number of peptides using gramicidin S as an internal standard. The CF-MALDI mass accuracy is typically 0.07 % for small peptides (MW < 1500 Da) with crystalline matrices. For comparison purposes, the mass accuracy is typically 0.01% for internally calibrated peptides on a solid insertion probe (i.e. static MALDI) [56,127]. Future improvements to the resolution with the CF probe would likely cause a corresponding increase in mass accuracy.

Limitations. Static MALDI performed on a solid insertion probe with a crystalline matrix yields spectra with a resolution of ~ 500 FWHM, at least for peptides up to ~ 10,000 Da. On the other hand, with 3-NBA as a matrix, spectra with a resolution of ~ 280 FWHM are obtained (for peptides up to 1500 Da). The reason for this discrepancy is that 3-NBA tends to form extensive alkali metal adduct ions (mainly M+Na and M+K). Crystalline MALDI matrices usually yield mass spectra virtually free of interfering adducts if the laser power if carefully controlled. However, this is usually not the case for the liquid matrix 3-NBA, and more often than not the adduct peaks can be very intense. The formation of these adducts becomes increasingly problematic with increasing mass, thus limiting the utility of the liquid matrix. A broad peak is observed for peptides greater than ~ 2000 Da, thus severely limiting mass accuracy assignments.

As discussed in chapter 10, we are currently searching for ways to reduce these adduct peaks with 3-NBA. At the same time, we plan to add a high voltage ion reflector to

TABLE 11.1

Mass Accuracy Observed For Peptides with CF-MALDI

Peptide	Average Mass (Da)		
	Calculated M + H	Measured M + H	Accuracy (%)
Ac-KLEALEA-AM	814.96	815.9	0.12
Ac-TQDEQFIP-AM	1019.10	1019.3	0.02
Bradykinin	1061.23	1061.5	0.03
LYPVKLYPVK	1220.54	1220.0	0.04
Ac-KLEALEAKLEALEA-AM	1569.84	1571.9	0.13

Ac- : N-terminal acetate

AM- : C-terminal amide

improve the instrumental mass resolution, in order to better resolve the adduct peaks. With high mass resolution, adduct formation would only be a problem in the case of high molecular weight biomolecules.

11.4 Conclusions

1. The mass resolution is strongly dependent upon the composition of the matrix solution. In addition, high water flow rates decrease the resolution, sensitivity and flow stability.
2. The mass resolution observed for CF-MALDI is generally in the range of 100-200 on our linear TOF for small peptides (MW < 1500 Da).
3. The mass accuracy for small peptides (MW < 1500 Da) is typically 0.07% for CF-MALDI, compared to 0.01% for crystalline matrices.
4. Compared to crystalline matrices, 3-NBA tends to form extensive alkali metal adduct ions, resulting in a general reduction of mass resolution.

CHAPTER 12

Summary

The main theme of my research has been to develop novel sample introduction techniques for laser ionization mass spectrometry. The development of new and more versatile desorption / ionization sources for both small and large molecules has become one of the most active research areas in mass spectrometry. In laser-induced MPI, molecules can be ionized with high efficiency and mass fragmentation patterns can be readily controlled by adjusting the laser power density and wavelength. With the discovery of matrix-assisted laser desorption ionization (MALDI) in 1987, the mass spectrometric analysis of biopolymers in the molecular mass range between a few thousand to a few hundred thousand Daltons is now possible [3,56].

The first part of this thesis has been mainly focused on the development of SJ spectroscopy and MPI-MS for the study of small biological molecules (MW < 1000). MPI and SJS are generally used for probing gas phase molecules, hence in the past both MPI mass spectrometry and SJS were limited to studies of volatile molecules. In order to extend these two techniques to the study of thermally labile biochemicals, a method for desorption / vaporization without thermal decomposition is required. Laser desorption (LD) has been successfully used to introduce biological molecules into a supersonic jet expansion. However, we were interested in simple alternative methods to introduce thermally labile and nonvolatile molecules into supersonic jets. Methods that have been developed and applied in our labs are pulsed fast atom bombardment (FAB) and pulsed rapid heating (PRH). In the FAB technique fast atoms (Ar or Xe) are

used to desorb sample molecules. In the PRH technique a heating probe consisting of an electrically heated plunger driven by a solenoid is used to desorb the sample in 210 μs. Both FAB and PRH can be used to vaporize amino acids, dipeptides, and polycyclic aromatic hydrocarbons for SJ/MPI mass spectrometry. In addition, the contact time between the sample and the electrically heated plunger could be varied. This allowed for some studies on the heating nature of the desorption vs decomposition processes for tryptophan and tyrosine. In summary, both FAB and PRH are simple and inexpensive methods, comparable in performance to LD.

Other work was also carried out in relation to SJ/MPI mass spectrometry. A method was developed to enhance signal intensity without degradation in both the mass resolution and supersonic jet cooling by using a cylindrical lens instead of a spherical lens. MPI/MS for the difficult isomer discrimination of substituted PAHs, anilines, and phenols was studied. Water and ammonia elimination from labile dipeptides was looked at using PRH and LD. As an application, the PRH technique was used for obtaining gas phase UV-Visible absorption spectra of thermally labile compounds. And finally, in order to have a better understanding of the mechanisms involved in LD, resonant two-photon ionization (R2PI) spectroscopy was used to examine molecular cooling and supersonic jet formation in LD.

In the second part of this thesis large molecules (MW > 1000) were studied with MALDI. MALDI has become an extremely important mass spectrometric technique for the high molecular weight determination of biomolecules. A small matrix molecule is mixed with samples on a substrate, and the solvent is allowed to evaporate before laser desorption / ionization is performed. However, due to the strict sample preparation procedure, a major disadvantage of MALDI is the difficulty in interfacing

to various solution-based separation methods such as liquid chromatography (LC) and capillary zone electrophoresis (CZE) for on-line complex mixture analysis. Consequently, we concentrated our efforts in coupling continuous flow (CF) to MALDI for flow injection analysis of large peptides and proteins. At the same time, a data system was developed for transferring and storing mass spectra at high repetition rates, specifically for CF-MALDI, with the help from Larry Coulson in the chemistry department. In order to further extend CF-MALDI, the coupling of liquid chromatography (LC) to MALDI for the on-line separation and detection of peptides and proteins was carried out. And finally, current research in our laboratory involving LC-MALDI with an improved ion extraction geometry was described.

Most of the earlier work covered in this thesis (chapters 2-8) has been published. Some of the later work on MALDI has either been submitted for publication or will be submitted in the near future. A list of publications and submissions is provided in Table 12.1.

Table 12.1 Publications

Chapter	Publication		
	Authors	Title	Journal
2	A.P.L. Wang, J.Y. Zhang, D.S. Nagra, and L. Li	Signal Enhancement by Using a Planar Laser Beam for Multiphoton Ionization in a Supersonic Jet / Reflectron Time-of-Flight Mass Spectrometer	App. Spectrosc. **1991**, 45, 304.
3	J.Y. Zhang, D.S. Nagra, A.P.L. Wang, and L. Li	On the Capability of Multiphoton Ionization Mass Spectrometry for Isomer Discrimination: Mass Spectra of Positional Isomers of Aromatic Molecules	Int. J. Mass Spectrom. Ion Processes **1991**, 110, 103
4	L. Li, A.M. Hogg, A.P.L. Wang, J.Y. Zhang, and D.S. Nagra	Pulsed Fast Atom Bombardment Sample Desorption with Multiphoton Ionization in a Supersonic Jet / Reflectron Time-of-Flight Spectrometer	Anal. Chem. **1991**, 63, 974.
5	D.S. Nagra, J.Y. Zhang, and L. Li	Pulsed Rapid Heating For Volatization of Amino Acids and Small Peptides in MPI Mass Spectrometry	Anal. Chem. **1991**, 63, 2188.
6	D.S. Nagra, J.Y. Zhang, A.P.L. Wang, and L. Li	Multiphoton Ionization Study of Water and Ammonia Elimination from Dipeptides with Pulsed Rapid Heating and Laser Desorption for Sample Vaporization	Int. J. Mass Spectrom. Ion Processes **1992**, 116, 127.
7	J.Y. Zhang, D.S. Nagra, and L. Li	Measurement of Gas-Phase Ultraviolet-Visible Absorption Spectra of Thermally Labile Molecules with a Pulsed Rapid Heating Technique for Sample Vaporization	Anal. Chem. **1991**, 63, 2995.

Table 12.1

Publications (continued)

Chapter	Publication		
	Authors	Title	Journal
8	J.Y. Zhang, D.S. Nagra, and L. Li	Molecular Cooling and Supersonic Jet Formation in Laser Desorption	Anal. Chem. **1993**, 65, 2812.
9	D.S. Nagra and L. Li	Subpicomole Detection of Large Peptides with Continuous-Flow Matrix-Assisted Laser Desorption Ionization Mass Spectrometry	To be submitted
9	L.D. Coulson, D.S. Nagra, X.G. Guo, R.M. Whittal, and L. Li	A Mass Spectral Recording and Storing System Based on GPIB Data Transfer for Laser Ionization Time-of-Flight Mass Spectrometry	Appl. Spectrosc. In Press.
10	D.S. Nagra and L. Li	Interfacing On-Line Full Bore or Packed Capillary Liquid Chromatography with Continuous-Flow Matrix-Assisted Laser Desorption Ionization for the Analysis of Proteins	To be submitted
11	R.M. Whittal, D.S. Nagra, and L. Li	Optimization of CF-MALDI with an Improved Ion Extraction Geometry	To be submitted

BIBLIOGRAPHY

1. Lubman, D.M.; Li, L. In *Lasers and Mass Spectrometry*; Lubman, D.M., Ed.; Oxford University Press: New York, 1990; Chapter 16, pp. 353-382

2. Lubman, D.M.; Naaman, R.; Zare, R.N. *J. Chem. Phys.* **1980**, *72*, 3034.

3. Karas, M.; Bachmann, D.; Bahr, U.; Hillenkamp, F. *Int. J. Mass Spectrom. Ion Processes* **1987**, *78*, 53.

4. Dobson, R.L.M.; D'Silva, A.P.; Weeks, S.J.; Fassel, V.A. *Anal. Chem.* **1986**, *58*, 2129.

5. Irion, M.P.; Bowers, W.D.; Hunter, R.L.; Rowland, F.S.; R. T. McIver, J. *Chem. Phys. Lett.* **1982**, *93*, 375.

6. Carlin, T.J.; Frieser, B.S. *Anal. Chem.* **1983**, *55*, 571.

7. Sack, T.M.; McCrery, D.A.; Gross, M.L. *Anal. Chem.* **1985**, *57*, 1290.

8. Kuo, C.H.; Beggs, C.G.; Kemper, P.R.; Bowers, M.T.; Leahy, D.J.; Zare, R.N. *Chem. Phys. Lett.* **1989**, *163*, 291.

9. Zimmerman, J.A.; Watson, C.H.; Eyler, J.R. *Anal. Chem.* **1991**, *63*, 361.

10. Hayes, J.M. *Chem. Rev.* **1987**, *87*, 745.

11. Grotemeyer, J.; Schlag, E.W. *Angew. Chem. Int. Ed. Engl.* **1988**, *27*, 447.

12. Tembreull, R.; Lubman, D.M. *Anal. Chem.* **1984**, *56*, 1962.

13. Sin, C.H.; Pang, H.M.; Lubman, D.M.; Zorn, J.C. *Anal. Chem.* **1986**, *58*, 487.

14. Rizzo, T.R.; Park, Y.D.; Peteanu, L.; Levy, D.H. *J. Chem. Phys.* **1985**, *83*, 4819.

15. Cable, J.R.; Tubergen, M.J.; Levy, D.H. *J. Am. Chem. Soc.* **1987**, *109*, 6198.

16. Li, L.; Lubman, D.M. *Appl. Spectrosc.* **1988**, *42*, 418.

17. Li, L.; Hogg, A.M.; Wang, A.P.L.; Zhang, J.Y.; Nagra, D.S. *Anal. Chem.* **1991**, *63*, 974.

18. Nagra, D.S.; Zhang, J.Y.; Li, L. *Anal. Chem.* **1991**, *63*, 2188.

19. Wang, A.P.L.; Zhang, J.Y.; Nagra, D.S.; Li, L. *Appl. Spectrosc.* **1991**, *45*, 304.

20. Zhang, J.Y.; Nagra, D.S.; Wang, A.P.L.; Li, L. *Int. J. Mass Spectrom. Ion Processes* **1991**, *110*, 103.

21. Nagra, D.S.; Zhang, J.Y.; Wang, A.P.L.; Li, L. *Int. J. Mass Spectrom. Ion Processes* **1992**, *116*, 127.

22. Zhang, J.Y.; Nagra, D.S.; Li, L. *Anal. Chem.* **1991**, *63*, 2995.

23. Zhang, J.Y.; Nagra, D.S.; Li, L. *Anal. Chem.* **1993**, *65*, 2812.

24. Coulson, L.D.; Nagra, D.S.; Guo, X.; Whittal, R.M.; Li, L. *Appl. Spectrosc.* **1994**, In Press.

25. Nagra, D.S.; Li, L.; "Design of a New Flow Probe for Continuous-Flow Matrix-Assisted Laser Desorption Ionization," in Proceedings of the 41st ASMS Conference on Mass Spectrometry and Allied Topics; San Francisco, CA, 1993, p. 671.

26. Whittal, R.M.; Nagra, D.S.; Li, L.; "Optimization of Ion Extraction and Ion Detection for Continuous-Flow Matrix-Assisted Laser Desorption," in Proceedings of the 41st ASMS Conference on Mass Spectrometry and Allied Topics; San Francisco, CA, 1993, p. 672.

27. Nagra, D.S.; Li, L.; "LC/TOFMS with Continuous-Flow MALDI," in Proceedings of the 42st ASMS Conference on Mass Spectrometry and Allied Topics; Chicago, May 31-June 4, 1994.

28. Whittal, R.M.; Nagra, D.S.; Li, L.; "Continuous-Flow Matrix-Assisted Laser Desorption Ionization of Peptides," in Proceedings of the 42nd ASMS Conference on Mass Spectrometry and Allied Topics; Chicago, May 31-June 4, 1994.

29. Lubman, D.M. *Anal. Chem.* **1987**, *59*, 31.

30. Dietz, T.G.; Duncan, M.A.; Powers, D.E.; Smalley, R.E. *Chem. Phys. Lett.* **1980**, *70*, 246.

31. Boesl, U.; Neusser, H.J.; Schlag, E.W. *Chem. Phys.* **1981**, *55*, 193.

32. Zandee, L.; Bernstein, R.B. *J. Chem. Phys.* **1979**, *71*, 1359.

33. Lubman, D.M.; Kronick, M.N. *Anal. Chem.* **1982**, *54*, 660.

34. Tembreull, R.; Lubman, D.M. *Anal. Chem.* **1986**, *58*, 1299.

35. Rhodes, G.; Opsal, R.B.; Meek, J.T.; Reilly, J.P. *Anal. Chem.* **1983**, *55*, 280.

36. Reilly, J.P.; Kompa, K.L. *J. Chem. Phys.* **1980**, *73*, 5468.

37. Zandee, L.; Bernstein, R.B.; Lichtin, D.A. *J. Chem. Phys.* **1978**, *69*, 3427.

38. Zandee, L.; Bernstein, R.B. *J. Chem. Phys.* **1979**, *70*, 2574.

39. Boesl, U.; Neusser, H.J.; Schlag, E.W. *J. Chem. Phys.* **1980**, *72*, 4327.

40. *Molecular Beams and Low Density Gas Dynamics* ; Wegener, P.P., Ed.; Marcel Dekker: New York, 1974.

41. Levy, D.H. *Sci. Amer.* **1984**, *250(2)*, 96.

42. Hayes, J.M.; Small, G.J. *Anal. Chem.* **1983**, *55*, 565.

43. Li, L.; Lubman, D.M. *Rev. Sci. Instrum.* **1988**, *59*, 557.

44. Cotter, R.J. *Anal. Chim. Acta* **1987**, *195*, 45.

45. Tembreull, R.; Lubman, D.M. *Anal. Chem.* **1987**, *59*, 1003.

46. Engelke, F.; Hahn, J.H.; Henke, W.; Zare, R.N. *Anal. Chem* **1987**, *59*, 909.

47. Grotemeyer, J.; Boesl, U.; Walter, K.; Schlag, E.W. *Org. Mass Spectrom.* **1986**, *21*, 595.

48. Hager, J.W.; Wallace, S.C. *Anal. Chem.* **1988**, *60*, 5.

49. Skoog, D.A. *Principles of Instrumental Analysis;* 3rd ed.; Saunders College Publishing: Philadelphia, 1985, p. 535.

50. Mamyrin, B.A.; Karataev, V.I.; Schmikk, D.V.; Zagulin, V.A. *Sov. Phys. JEPT (Engl. Trans.)* **1973**, *37*, 45.

51. Lambert, J.B.; Shurvell, H.F.; Lightner, D.; Cooks, R.G. *Introduction to Organic Spectroscopy;* ; Macmillan: New York, 1987, p. 340.

52. Walter, K.; Boesl, U.; Schlag, E.W. *Int. J. Mass Spectrom. Ion Processes* **1986**, *71*, 309.

53. Yang, M.; Reilly, J.P. *Anal. Instrum.* **1987**, *16*, 133.

54. Whitehouse, C.M.; Dreyer, R.N.; Yamashita, M.; Fenn, J.B. *Anal. Chem.* **1985**, *57*, 675.

55. Fenn, J.B.; Mann, M.; Meng, C.K.; Wong, S.F. *Mass Spectrom. Rev.* **1990**, *9*, 37.

56. Hillenkamp, F.; Karas, M.; Beavis, R.C.; Chait, B.T. *Anal. Chem.* **1991**, *63*, 1193.

57. Beavis, R.C.; Chait, B.T. *Methods and Mechanisms for Producing Ions from Large Molecules* **1991**, 227.

58. Wang, A.P.L.; Li, L. *Appl. Spectrosc.* **1991**, *45*, 969.

59. Li, L.; Lubman, D.M. *Anal. Chem.* **1988**, *60*, 2591.

60. Li, L.; Lubman, D.M. *Appl. Spectrosc.* **1989**, *43*, 543.

61. Hudgens, J.W.; Seaver, M.; DeCorpo, J.J. *J. Phys. Chem.* **1981**, *85*, 761.

62. Lubman, D.M. *J. Phys. Chem.* **1981**, *85*, 3752.

63. Mordaunt, D.; Loper, G.; Wessel, J. *J. Phys. Chem.* **1984**, *88*, 5197.

64. Chang, T.C.; Johnston, M.V. *J. Phys. Chem* **1987**, *91*, 884.

65. Parker, D.H.; Bernstein, R.B. *J. Phys. Chem.* **1982**, *86*, 60.

66. Kuhlewind, H.; Neusser, H.J.; Schlag, E.W. *J. Phys. Chem.* **1985**, *89*, 5600.

67. Williams, E.R.; McLafferty, F.W. *J. Am. Soc. Mass Spectrom.* **1990**, *1*, 361.

68. Neusser, H.J. *Int. J. Mass Spectrom. Ion Processes* **1987**, *79*, 151.

69. Pachuta, S.J.; Kenttamaa, H.I.; Sack, T.M.; Cerny, R.L.; Tomer, K.B.; Gross, M.L.; Pachuta, R.R.; Cooks, R.G. *J. Am. Chem. Soc.* **1988**, *110*, 657.

70. Johnson, P.M. *Acc. Chem. Res.* **1980**, *13*, 20.

71. Koplitz, B.D.; McVey, J.K. *J. Chem. Phys.* **1984**, *80*, 2271.

72. Lubman, D.M.; Kronick, M.N. *Anal. Chem.* **1983**, *55*, 867.

73. Barber, M.; Bordoli, R.S.; Elliott, G.J.; Sedgwick, R.D.; Tyler, A.N. *Anal. Chem.* **1982**, *54*, 645.

74. Cotter, R.J. *Anal. Chem.* **1984**, *56*, 2594.

75. Breemen, R.B.V.; Snow, M.; Cotter, R.J. *Int. J. Mass Spectrom. Ion Processes* **1983**, *49*, 35.

76. Hogg, A.M. *Int. J. Mass Spectrom. Ion Phys.* **1983**, *49*, 25.

77. Alexander, A.J.; Hogg, A.M. *Int. J. Mass Spectrom. Ion Processes* **1986**, *69*, 297.

78. Ross, M.M.; Wyatt, J.R.; Colton, R.J.; Campana, J.E. *Int. J. Mass Spectrom. Ion Processes* **1983**, *54*, 237.

79. Rizzo, T.R.; Park, Y.D.; Peteanu, L.A.; Levy, D.H. *J. Chem. Phys.* **1986**, *84*, 2534.

80. *Chemical Analysis of Polycyclic Aromatic Compounds* ; Tuan, V.D., Ed.; John Wiley & Sons, Inc.: New York, 1989.

81. Caprioli, R.M.; Fan, T.; Cottrell, J.S. *Anal. Chem.* **1986**, *58*, 2949.

82. Li, L.; Lubman, D.M. *Rapid Commun. Mass Spectrom.* **1989**, *3*, 12.

83. Beavis, R.C.; Lindner, J.; Grotemeyer, J.; Schlag, E.W. *Chem. Phys. Lett.* **1988**, *146*, 310.

84. Anderson, W.R.; Frick, W.; Daves, G.D. *J. Am. Chem. Soc.* **1978**, *100*, 1974.

85. Freas, R.B.; Ross, M.M.; Campana, J.E. *J. Am. Chem. Soc.* **1985**, *107*, 6195.

86. Cotter, R.J. *Anal. Chem.* **1980**, *52*, 1767.

87. Campana, J.E.; Freas, R.B. *J. Chem. Soc., Chem. Commun.* **1984**, 1414.

88. Winograd, N.; Baxter, J.P.; Kimock, F.M. *Chem. Phys. Lett.* **1982**, *88*, 581.

89. Becker, C.H.; Gillen, K.T. *Anal. Chem.* **1984**, *56*, 1671.

90. Tembreull, R.; Sin, C.H.; Li, P.; Pang, H.M.; Lubman, D.M. *Anal. Chem.* **1985**, *57*, 1186.

91. Caprioli, R.M. *Anal. Chem.* **1983**, *55*, 2387.

92. Zare, R.N.; Levine, R.D. *Chem. Phys. Lett.* **1987**, *136*, 593.

93. Hall, R.B. *J. Phys. Chem.* **1987**, *91*, 1007.

94. Peyl, G.J.Q.v.d.; Isa, K.; Haverkamp, J.; Kistemaker, P.G. *Org. Mass Spectrom.* **1981**, *16*, 416.

95. Hercules, D.M.; Day, R.J.; Balasanmugam, K.; Dang, T.A.; Li, C.P. *Anal. Chem.* **1982**, *54*, 280.

96. Burgess, D.; Jr.; Viswanathan, R.; Hussla, I.; Stair, P.C.; Weitz, E. *J. Chem. Phys.* **1983**, *79*, 5200.

97. Breemen, R.B.V.; Snow, M.; Cotter, R.J. *Int. J. Mass Spectrom. Ion Phys.* **1983**, *49*, 35.

98. Beuhler, R.J.; Flanigan, E.; Greene, L.J.; Friedman, L. *Biochem. Biophys. Res. Commun.* **1972**, *46*, 1082.

99. Beuhler, R.J.; Flanigan, E.; Greene, L.J.; Friedman, L. *J. Am. Chem. Soc.* **1974**, *96*, 3990.

100. Beuhler, R.J.; Flanigan, E.; Greene, L.J.; Friedman, L. *Biochemistry* **1974**, *13*, 5060.

101. Cotter, R.J.; Fenselau, C. *Biomed. Mass Spectrom.* **1979**, *6*, 287.

102. Cotter, R.J. *Anal. Chem.* **1980**, *52*, 1589a.

103. Hansen, G.; Munson, B. *Anal. Chem.* **1978**, *50*, 1130.

104. Anderson, W.R.; Frick, W.; Daves, G.D.; Barofsky, D.F.; Yamaguchi, I.; Chang, D.; Folkers, K.; Rosell, S. *Biochem. Biophys. Res. Commun.* **1977**, *78*, 372.

105. Daves, G.D. *Acc. Chem. Res.* **1979**, *12*, 359.

106. Sin, C.H.; Pang, H.; Lubman, D.M. *Anal. Instrum.* **1988**, *17*, 87.

107. Zenobi, R.; Hahn, J.H.; Zare, R.N. *Chem. Phys. Lett.* **1988**, *150*, 361.

108. Hrubowchak, D.M.; Ervin, M.H.; Winograd, N. *Anal. Chem.* **1991**, *63*, 225.

109. Pallix, J.B.; Schuhle, U.; Becker, C.H.; Huestis, D.L. *Anal. Chem.* **1989**, *61*, 805.

110. Hahn, J.H.; Zenobi, R.; Bada, J.L.; Zare, R.N. *Science* **1988**, *239*, 1523.

111. Beavis, R.C.; Lindner, J.; Grotemeyer, J.; Schlag, E.W. *Z. Naturforsch.* **1988**, *43a*, 1083.

112. Beavis, R.C.; Lindner, J.; Grotemeyer, J.; Schlag, E.W.; "Matrix Effects in IR-Laser Desorption of Neutral Molecules," in 36th ASMS Conference on Mass Spectrometry and Allied Topics; San Francisco, CA, 1988, 530.

113. Sunner, J.; Ikonomou, M.G.; Kebarle, P. *Int. J. Mass Spectrom. Ion Processes* **1988**, *82*, 221.

114. Lindner, B.; Seydel, U. *Anal. Chem.* **1985**, *57*, 895.

115. Silverstein, R.M.; Bassler, G.C.; Morel, T.C. *Spectrometric Identification of Organic Compounds;* ; Wiley: New York, 1981, pp. 28-32.

116. Innes, K.K.; Ross, I.G.; Moomaw, W.R. *J. Mol. Spectrosc.* **1988**, *132*, 492.

117. Lubman, D.M. *Mass Spectrom. Rev.* **1988**, *7*, 535.

118. Stiller, S.W.; Johnston, M.V. *Anal. Chem.* **1987**, *59*, 567.

119. Zare, R.N.; Dadigian, P.J. *Science* **1974**, *185*, 739.

120. Sin, C.H.; Tembreull, R.; Lubman, D.M. *Anal. Chem.* **1984**, *56*, 2776.

121. Li, L.; Lubman, D.M. *Anal. Chem.* **1987**, *59*, 2538.

122. Grotemeyer, J.; Walter, K.; Boesl, U.; Schlag, E.W. *Int. J. Mass Spectrom. Ion Processes* **1987**, *78*, 69.

123. *Quantitative Analysis of Catecholamines and Related Compounds* ; Krstulovic, A.M., Ed.; Wiley: New York, 1986.

124. Tanaka, K.; Waki, H.; Ido, Y.; Akita, S.; Yoshida, Y.; Yoshida, T. *Rapid Commun. Mass Spectrom.* **1988**, *2*, 151.

125. Beavis, R.C.; Chait, B.T. *Rapid Commun. Mass Spectrom.* **1989**, *3*, 233.

126. Beavis, R.C.; Chait, B.T. *Rapid Commun. Mass Spectrom.* **1989**, *3*, 432.

127. Beavis, R.C.; Chait, B.T. *Anal. Chem.* **1990**, *62*, 1836.

128. Nelson, R.W.; Rainbow, M.J.; Lohr, D.E.; Williams, P. *Science* **1989**, *246*, 1585.

129. Spengler, B.; Cotter, R.J. *Anal. Chem.* **1990**, *62*, 793.

130. Ehring, H.; Karas, M.; Hillenkamp, F. *Org. Mass Spectrom.* **1992**, *27*, 472.

131. Gimon, M.E.; Preston, L.M.; Solouki, T.; White, M.A.; Russell, D.H. *Org. Mass Spectrom.* **1992**, *27*, 827.

132. Ens, W.; Mao, Y.; Mayer, F.; Standing, K.G. *Rapid Commun. Mass Spectrom.* **1991**, *5*, 117.

133. Lincoln, K.A.; Covington, M.A. *Int. J. Mass Spectrom. Ion Phys.* **1975**, *16*, 191.

134. Vertes, A.; Levine, R.D. *Chem. Phys. Lett.* **1990**, *171*, 284.

135. Kimbrell, S.M.; Yeung, E.S. *Appl. Spectrosc.* **1991**, *45*, 442.

136. Beavis, R.C.; Chait, B.T. *Chem. Phys. Lett.* **1991**, *181*, 479.

137. Fehre, T.H.; Becker, C.H. *Rapid Commun. Mass Spectrom.* **1991**, *5*, 378.

138. Pan, Y.; Cotter, R.J. *Org. Mass Spectrom.* **1992**, *27*, 3.

139. Lin, S.H.; Fujimura, Y.; Neusser, H.J.; Schlag, E.W. *Multiphoton Spectroscopy of Molecules;* ; Academic Press: New York, 1984.

140. Lustig, D.A.; Lubman, D.M. *Rev. Sci. Instrum.* **1991**, *62*, 957.

141. Caprioli, R.M. In *Continuous-Flow Fast Atom Bombardment Mass Spectrometry*; Caprioli, R.M., Ed.; Wiley: Chichester, 1990; Chapter 1, pp. 1-27.

142. Smalley, R.E.; Wharton, L.; Levy, D.H. *Acc. Chem. Res.* **1977**, *10*, 139.

143. Chou, J.S.; Sumida, D.; Wittig, C. *Chem. Phys. Lett.* **1983**, *100*, 397.

144. McClelland, G.M.; Saenger, K.L.; Valentini, J.J.; Herschbach, D.R. *J. Phys. Chem.* **1979**, *83*, 947.

145. Dunn, T.M.; Tembreull, R.; Lubman, D.M. *Chem. Phys. Lett.* **1985**, *121*, 453.

146. Lubman, D.M.; Li, L.; Dunn, T.M. *J. Phys. Chem.* **1989**, *93*, 3444.

147. Wang, A.P.L.; Li, L. Unpublished Work, University of Alberta, 1992.

148. Nogar, N.S.; Estler, R.C.; Miller, C.M. *Anal. Chem.* **1985**, *57*, 2441.

149. Amirav, A.; Even, U.; Jortner, J. *Chem. Phys.* **1980**, *51*, 31.

150. Kolodney, E.; Amirav, A. *Chem. Phys.* **1983**, *82*, 269.

151. Hansen, S.G. *J. Appl. Phys.* **1989**, *66*, 3329.

152. Cable, J.T.; Tubergen, M.J.; Levy, D.H. *J. Am. Chem. Soc.* **1989**, *111*, 9032.

153. Pepich, B.V.; Kalman, D.A.; Callis, J.B.; Burns, D.H.; Gouterman, M. *Anal. Chem.* **1986**, *58*, 2825.

154. Engelking, P.C. *Chem. Rev.* **1991**, *91*, 399.

155. Miller, T.A. *Science* **1984**, *223*, 545.

156. Ens, W.; Zhou, J.; Schriemer, N.P.; Standing, K.G.; Verentchikov, A.; in Proceedings of the 40th ASMS Conference on Mass Spectrometry and Allied Topics; Washington, DC, May 31-June 5, 1992, 1927.

157. Hill, J.A.; Annan, R.S.; Biemann, K. *Rapid Commun. Mass Spectrom.* **1991**, *5*, 395.

158. Annan, R.S.; Kochling, H.J.; Hill, J.A.; Biemann, K. *Rapid Commun. Mass Spectrom.* **1992**, *6*, 298.

159. Castoro, J.A.; Chiu, R.W.; Monnig, C.A.; Wilkins, C.L. *J. Am. Chem. Soc.* **1992**, *114*, 7571.

160. Chambers, D.M.; Goeringer, D.E.; Mcluckey, S.A.; Glish, G.L. *Anal. Chem.* **1993**, *65*, 14.

161. Karas, M.; Bahr, U.; Giebmann, U. *Mass Spectrom. Rev.* **1991**, *10*, 335.

162. Li, L.; Wang, A.P.L.; Coulson, L.D. *Anal. Chem.* **1993**, *65*, 493.

163. Marchand, P.; Marmet, L. *Rev. Sci. Instrumentation* **1983**, *54*, 1034.

164. Spengler, B.; Kirsch, D.; Kaufmann, R.; Karas, M.; Hillenkamp, F.; Giessmann, U. *Rapid Commun. Mass Spectrom.* **1990**, *4*, 301.

165. Brown, R.S.; Gilfrich, N.L. *Rapid Commun. Mass Spectrom.* **1992**, *6*, 697.

166. Karas, M.; Bahr, U.; Ingendoh, A.; Nordhoff, E.; Stahl, B.; Strupat, K.; Hillendamp, F. *Anal. Chimica Acta* **1990**, *241*, 175.

167. Zhao, S.; Somayajula, K.V.; Sharkey, A.G.; Hercules, d.M.; Hillenkamp, F.; Karas, M.; Ingendoh, A. *Anal. Chem.* **1991**, *63*, 450.

168. Chan, T.W.D.; Colburn, A.W.; Derrick, P.J. *Org. Mass Spectrom.* **1992**, *27*, 53.

169. Cornett, D.S.; Duncan, M.D.; Amster, I.J. *Org. Mass Spectrom.* **1992**, *27*, 831.

170. Caprioli, R.M.; Moore, W.T.; Petrie, G.; Wilson, K. *Int. J. Mass Spectrom. Ion Processes* **1988**, *86*, 187.

171. Murray, K.K.; Russell, D.H. *Anal. Chem.* **1993**, *65*, 2534.

172. Murray, K.K.; Russell, D.H. *J. Am. Soc. Mass Spectrom.* **1994**, *5*, 1.

173. Caprioli, R.M.; Tomer, K. In *Continuous-Flow Fast Atom Bombardment Mass Spectrometry*; Caprioli, R.M., Ed.; Wiley: Chichester, 1990; Chapter 5, pp. 93-120.

174. Deterding, L.J.; Parker, C.E.; Perkins, J.R.; Moseley, M.A.; Jorgenson, J.W.; Tomer, K.B. *J. Chromatogr.* **1991**, *554*, 329.

175. Tomer, K.; Moseley, M.A. In *Continuous-Flow Fast Atom Bombardment Mass Spectrometry*; Caprioli, R.M., Ed.; Wiley: Chichester, 1990; Chapter 6, pp. 121-136.

176. Caprioli, R.M.; Moore, W.T.; Martin, M.; DaGue, B.B.; Wilson, K.; Moring, S. *J. Chromatogr.* **1989**, *480*, 247.